

**DESIGN, SYNTHESIS AND CHARACTERIZATION OF  
ZINC(II)-SELECTIVE RATIOMETRIC FLUORESCENT SENSORS**

A Thesis  
Presented to  
The Academic Faculty

by

Yonggang Wu

In Partial Fulfillment  
of the Requirements for the Degree  
Doctor of Philosophy  
in the  
School of Chemistry and Biochemistry

Georgia Institute of Technology  
December 2007  
Copyright © 2007 by Yonggang Wu

**DESIGN, SYNTHESIS AND CHARACTERIZATION OF  
ZINC(II)-SELECTIVE RATIOMETRIC FLUORESCENT SENSORS**

Approved by

Dr. Christoph J. Fahrni, Advisor  
School of Chemistry and Biochemistry  
*Georgia Institute of Technology*

Dr. Donald F. Doyle  
School of Chemistry and Biochemistry  
*Georgia Institute of Technology*

Dr. Angus P. Wilkinson  
School of Chemistry and Biochemistry  
*Georgia Institute of Technology*

Dr. Z. John Zhang  
School of Chemistry and Biochemistry  
*Georgia Institute of Technology*

Dr. Niren Murthy  
Department of Biomedical Engineering  
*Georgia Institute of Technology*

Date Approved: August 31, 2007

## ACKNOWLEDGEMENTS

I would like to thank Dr. Christoph J. Fahrni for his support during my graduate studies at Georgia Tech. I have learned a great deal from him. I would also thank Reagan McRae for her help on biological experiments, Dr. Maged M. Henary and Dr. Sumalekshmy Sarojini for the work we've done together, Karl Hüttinger, Dr. Jing Li, Dr. John Cody, Dr. Subrata Mandal and Dr. Liuchun Yang and all others who worked in this group.

Most importantly, I would like to thank my family and my wife Baidan for their support.

## TABLE OF CONTENTS

ACKNOWLEDGEMENTS.....	iii
LIST OF TABLES.....	ix
LIST OF FIGURES.....	x
LIST OF SYMBOLS AND ABBREVIATIONS.....	xiii
SUMMARY.....	xv
CHAPTER I INTRODUCTION	
1.1. Zinc in Biology .....	1
1.1.2. Zinc Homeostasis.....	2
1.1.2.1. Zinc Transporters .....	3
1.1.2.2 Metallothioneins (MTs) .....	4
1.1.2.3. Labile Zinc Pools .....	5
1.2. Zinc-Selective Fluorescent Sensors .....	5
1.2.1. First Generation Sensors and Fluorophore Platforms .....	6
1.2.2. Binding Groups.....	9
1.2.3. Ratiometric Sensors .....	11
1.3. Thesis Objective.....	13
1.4. References:.....	15

CHAPTER II ZINC(II)-SELECTIVE RATIO-METRIC FLUORESCENT SENSORS  
BASED ON INHIBITION OF EXCITED-STATE INTRAMOLECULAR PROTON  
TRANSFER

2.1. Introduction.....	25
2.2. Results and Discussion .....	28
2.2.1. Synthesis .....	28
2.2.2. Ground-State Tautomerism .....	28
2.2.3. Protonation Equilibria.....	35
2.2.4. Complexation Studies .....	38
2.2.5. Absorption Spectra.....	40
2.2.6 Emission Spectra.....	40
2.2.7. Apparent Zn <sup>II</sup> Binding Affinities.....	41
2.2.8. Ratiometric Measurements .....	42
2.2.9. Selectivity Towards Zn <sup>II</sup> .....	45
2.3. Conclusion .....	47
2.4. Experimental Section.....	48
2.4.1. Materials and Reagents .....	48
2.4.2. Synthesis .....	48
2.4.3. Steady-state Absorption and Fluorescence Spectroscopy.....	56
2.4.4. Electrode Calibration in Aqueous Solution.....	57
2.4.5. Potentiometry .....	57

2.4.6. Spectrophotometric Titrations.....	58
2.4.7. Complex stability constants .....	58
2.5. References:.....	62

CHAPTER III EXCITED STATE INTRAMOLECULAR PROTON TRANSFER IN  
2-(2'- ARYLSULFONAMIDOPHENYL) BENZIMIDAZOLE DERIVATIVES: THE  
EFFECT OF DONOR AND ACCEPTOR SUBSTITUENTS

3.1. Introduction.....	66
3.2. Results and Discussion .....	68
3.2.1. Synthesis .....	68
3.2.2. Protonation Equilibria.....	70
3.2.3. Ground-State Tautomerism .....	76
3.2.4. Substituent Effects on Photophysical Properties .....	80
3.2.4.1 Effect of Donor Substitution.....	80
3.2.4.2. Effect of Acceptor Substitution.....	84
3.2.4.3. Effect of Donor-Acceptor Double Substitutions.....	85
3.3 Conclusion .....	86
3.4. Experimental Section.....	87
3.4.1. Synthesis .....	87
3.4.2 Structural Assignments on the Basis of 2D $^1\text{H}$ - $^1\text{H}$ COSY experiments.	106
3.4.3. Electrode Calibration in Aqueous Solution.....	106
3.4.4. Spectrophotometric Titrations.....	110

3.4.5. Steady-state Absorption and Fluorescence Spectroscopy .....	110
3.5. References:.....	111

CHAPTER IV EXCITED STATE INTRAMOLECULAR PROTON TRANSFER IN  
2-(2'-ARYLSULFONAMIDOPHENYL)BENZIMIDAZOLE DERIVATIVES:  
INSIGHTS INTO THE ORIGIN OF DONOR SUBSTITUENT-INDUCED EMISSION  
ENERGY SHIFTS

4.1. Introduction.....	113
4.2. Results and Discussion .....	116
4.2.1. Synthesis .....	116
4.2.2. Protonation Equilibria.....	118
4.2.3. UV-vis Spectra .....	119
4.2.4. Fluorescence Spectra .....	121
4.2.5. Solvatochromic Shift Studies.....	122
4.2.5.1. Onsager's Reaction Field Model .....	125
4.2.5.2. Reichardt's $E_T(30)$ Solvent Scale.....	128
4.2.5.3. Kamlet-Abboud-Taft's Solvent Index (KAT) .....	131
4.3. Conclusion .....	136
4.4. Experimental Section.....	136
4.4.1. Synthesis. ....	136
4.4.2. Electrode Calibration in Aqueous Solution.....	142
4.4.3. Spectrophotometric Titrations.....	142

4.4.4. Steady-state Absorption and Fluorescence Spectroscopy .....	142
4.5. References:.....	144
 CHAPTER V EXCITED STATE INTRAMOLECULAR PROTON TRANSFER (ESIPT) IN 2-(2'-SULFONAMIDOPHENYL)BENZIMIDAZOLE DERIVATIVES: IMPACT OF EXTENDED $\pi$ -CONJUGATION	
5.1. Introduction.....	145
5.2. Results and Discussion .....	147
5.2.1. Synthesis .....	147
5.2.2. Protonation Equilibria.....	150
5.2.3. Photophysical Studies in Aqueous Solution. ....	151
5.2.3.1. UV-vis Spectra. ....	151
5.2.3.2. Fluorescence Steady-State Spectra. ....	151
5.2.3.3. Time Resolved Spectroscopy. ....	155
5.2.3.4. Fluorescence Quantum Yield and Brightness. ....	157
5.2.4. Photochemical Studies .....	157
5.3. Conclusions.....	158
5.4. Experimental Section.....	162
5.4.1. Synthesis. ....	162
5.4.2. Steady-state Absorption and Fluorescence Spectroscopy. ....	170
5.4.3. Electrode Calibration in Aqueous Solution.....	170
5.4.4. Determination of pK <sub>a</sub> Values. ....	171
5.4.5. Actinometry.....	171

5.4.6. Determination of Quantum Yield ( $\phi$ ) of Photochemical Reactions.....	171
5.4.7. Time-Resolved Measurements.....	173
5.4.8. 2D Fluorescence Spectra.....	174
5.5. References:.....	174
APPENDIX A: SPECTROSCOPIC DATA .....	176
APPENDIX B: PHOTOCHEMICAL DATA.....	181

## LIST OF TABLES

<b>Table 2-1.</b> Protonation constants and photophysical data for ligands <b>2-6b</b> , <b>2-7b</b> , <b>2-8b</b> , and <b>2-9b</b> in aqueous solution. ....	36
<b>Table 2-2.</b> Protonation constants and photophysical data for ligands <b>2-6b</b> , <b>2-7b</b> , <b>2-8b</b> , and <b>2-9b</b> in aqueous solution. ....	37
<b>Table 3-1.</b> Protonation Constants of Benzimidazole Derivatives <b>3-5a-3-5l</b> in Aqueous Solution .....	72
<b>Table 3-2.</b> Photophysical Data of Benzimidazole Derivatives <b>3-5a-3-5l</b> in Aqueous Solution .....	73
<b>Table 4-1:</b> Protonation Constants and Photophysical Data of Benzimidazole Derivatives <b>4-1b-4-5b</b> in Aqueous Solution.....	112
<b>Table 4-2:</b> Fitted Parameters for the Regression Analysis of the Solvatochromic Peak Fluorescence Emission Shifts According to the $E_T(30)$ Empirical Solvent Model .....	127
<b>Table 4-3:</b> Fitted Parameters for the Multiple Regression Analysis of the Solvatochromic Peak Fluorescence Emission Shifts According to the Kamlet-Abboud-Taft Empirical Solvent Model .....	127
<b>Table 4-4:</b> Experimental and Calculated Vertical Excitation and Emission Energies (eV) for <b>4-1c-4-3c</b> .....	132
<b>Table 4-5:</b> HFCIS/3-21+G(d,p)//INDO-SCI Computed Ground and Excited State Dipole Moments and Their Differences for <b>4-1c-4-3c</b> .....	132
<b>Table 5-1:</b> Protonation Constants and Photophysical Data. ....	142
<b>Table A-1:</b> Selected solvent parameters utilized in the solvatochromic shift analyses in Chapter 4. ....	168
<b>Table A-2:</b> Peak absorption and emission energies of compound <b>4-1a</b> .....	170
<b>Table A-3:</b> Peak absorption and emission energies of compound <b>4-2a</b> .....	170

<b>Table A-4:</b> Peak absorption and emission energies of compound <b>4-3a</b> .....	171
<b>Table A-5:</b> Peak absorption and emission energies of compound <b>4-4a</b> .....	171
<b>Table A-6:</b> Peak absorption and emission energies of compound <b>4-5a</b> .....	172

## LIST OF FIGURES

<b>Figure 2-1.</b> Variable-temperature <sup>1</sup> H NMR spectra of ligand <b>2-7a</b> in CD <sub>3</sub> OD (3 mM). .....	30
<b>Figure 2-2.</b> Potentiometric titration curves for ligands <b>2-6b-2-9b</b> in water .....	31
<b>Figure 2-3.</b> Comparison of the UV-visible absorption (left) and normalized fluorescence emission spectra (right) of the species with protonated and deprotonated sulfonamide nitrogen atom in aqueous solution for ligands a) <b>2-6b</b> , b) <b>2-7b</b> , c) <b>2-8b</b> , and d) <b>2-9b</b> .....	32
<b>Figure 2-4.</b> Calculated species distribution diagrams for ligands a) <b>2-6b</b> , b) <b>2-7b</b> , c) <b>2-8b</b> , and d) <b>2-9b</b> . .....	33
<b>Figure 2-5.</b> UV-visible absorbance (left) and fluorescence emission spectra (right) of ligands a) <b>2-6b</b> , b) <b>2-7b</b> , c) <b>2-8b</b> , and d) <b>2-9b</b> as a function of added Zn <sup>II</sup> .....	38
<b>Figure 2-6.</b> Change of the emission intensity ratio at 400 and 500 nm ( $\lambda_{\text{ex}}=320$ nm) for ligands <b>2-6b-2-9b</b> as a function of free Zn <sup>II</sup> .....	42
<b>Figure 2-7.</b> Emission intensity at 405 nm ( $\lambda_{\text{ex}}=320$ nm) of ligands <b>2-6b</b> , <b>2-8b</b> , and <b>2-9b</b> in response to various metal cations. ....	43
<b>Figure 2-8.</b> Emission intensity ratios at 400 and 500 nm in response to various metal cations: a) 10 $\mu$ M <b>2-6b</b> , all M <sup>2+</sup> 1 mM; b) 10 $\mu$ M <b>2-8b</b> , Ca <sup>II</sup> , Mg <sup>II</sup> 1 mM, all other M <sup>2+</sup> 10 $\mu$ M; c) 10 $\mu$ M solution of <b>2-9b</b> , Ca <sup>II</sup> , Mg <sup>II</sup> 1 mM, all other M <sup>2+</sup> 10 $\mu$ M. ....	45
<b>Figure 3-1.</b> Molecular orbital surfaces of the HOMO and LUMO responsible for the lowest energy transition in the UV-vis spectrum of 2-(2'-tosylaminophenyl)-benzimidazole (TPBI) (CI-ZINDO calculation). ....	67
<b>Figure 3-2.</b> Linear dependence of the sulfonamide acidity ( $\text{p}K_{\text{a1}}$ ) on Hammett's $\sigma$ parameters <sup>3</sup> for monosubstituted fluorophores <b>3-5a</b> , <b>3-5b</b> , <b>3-5d-3-5g</b> , and <b>3-5l</b> .....	71

<b>Figure 3-3.</b> Variable temperature $^1\text{H}$ NMR spectra 5(6)-cyano-substituted benzimidazole derivative <b>3-4i</b> in acetone- $d_6$ (20 mM). .....	76
<b>Figure 3-4.</b> Two-dimensional 500 MHz $^1\text{H}$ - $^1\text{H}$ NOESY spectra of (a) <b>3-4i</b> (left) and (b) <b>3-4k</b> (right) in acetone- $d_6$ at $-80^\circ\text{C}$ . .....	77
<b>Figure 3-5.</b> Effect of donor substituents: deconvoluted UV-vis absorption spectra (left) and fluorescence emission spectra (right) of compounds (a) <b>3-5a</b> , (b) <b>3-5e</b> , (c) <b>3-5f</b> , and (d) <b>3-5k</b> in aqueous solution (0.1 M KCl, $25^\circ\text{C}$ ). .....	80
<b>Figure 3-6.</b> Effect of acceptor substituents: deconvoluted UV-vis absorption spectra (left) and fluorescence emission spectra (right) of compounds (a) <b>3-5b</b> , (b) <b>3-5i</b> , (c) <b>3-5d</b> , and (d) <b>3-5c</b> in aqueous solution (0.1 M KCl, $25^\circ\text{C}$ ). .....	81
<b>Figure 3-7.</b> 2D $^1\text{H}$ - $^1\text{H}$ COSY NMR spectrum of <b>3-4i</b> at $-80^\circ\text{C}$ in acetone- $d_6$ . Top: overview spectrum. Bottom: Connectivity within the central aromatic ring and the benzimidazole moiety of the two tautomeric species is shown to the right. ....	104
<b>Figure 3-8.</b> 2D $^1\text{H}$ - $^1\text{H}$ COSY NMR spectrum of <b>3-4k</b> at $-80^\circ\text{C}$ in acetone- $d_6$ . Top: overview spectrum. Bottom: Connectivity within the central aromatic ring and the benzimidazole moiety of the two tautomeric species is shown to the right.....	105
<b>Figure 4-1.</b> Deconvoluted UV-vis absorption spectra (left) and normalized fluorescence emission spectra (right) of fluorophore: (a) <b>4-1b</b> , (b) <b>4-2b</b> , (c) <b>4-3b</b> , (d) <b>4-4b</b> , and (e) <b>4-5b</b> in aqueous solution (0.1 M KCl, $25^\circ\text{C}$ ). .....	116
<b>Figure 4-2.</b> Normalized UV-vis absorption (left) and fluorescence emission spectra (right, excitation at peak absorption energy) for derivatives (a) <b>4-1a</b> , (b) <b>4-2a</b> , and (c) <b>4-3a</b> , in selected organic solvents illustrating the solvatochromic shift behavior. ....	120
<b>Figure 4-3.</b> Correlation of the peak emission energies of derivative <b>4-1a</b> , <b>4-2a</b> , and <b>4-3a</b> with the solvent polarity parameter $f(\epsilon, n)$ . ....	126

<b>Figure 4-4.</b> Linear regression analysis of the solvatochromic emission shifts according to Reichardt's $E_T^N(30)$ empirical solvent polarity scale. (a) Linear correlation of the peak emission energies of the methoxy-substituted compounds <b>4-2a</b> and <b>4-3a</b> . (b) Linear correlation for compounds <b>4-4a</b> and <b>4-5a</b> . .....	127
<b>Figure 4-5.</b> Energy level diagram for the frontier orbitals of the phototautomer of compounds <b>4-1c-4-3c</b> . A plot of the HOMO and LUMO isosurfaces is also depicted for each compound. ....	134
<b>Figure 5-1:</b> Deconvoluted UV-vis absorption spectra (left) and fluorescence emission spectra (right) of compounds (a) <b>5-4b</b> , (b) <b>5-1b</b> , (c) <b>5-2b</b> , and (d) <b>5-3d</b> in aqueous solution (0.1 M KCl, 25°C). ....	146
<b>Figure 5-2:</b> Two-dimensional fluorescence contour plot for fluorophore <b>5-1b</b> showing the emission profile as a function of excitation wavelength. ....	148
<b>Figure 5-3:</b> Temperature dependent spectra of <b>5-1b</b> in aqueous solution. ....	148
<b>Figure 5-4:</b> Fluorescence decay data of <b>5-1b</b> in aqueous solution: a) in pH 6.5 buffer, 365 nm; b) in pH 6.5 buffer, 600 nm; c) in pH 11 buffer (0.1 M KCl), 480 nm. ....	150
<b>Figure 5-5.</b> UV spectra for the photoreactions of <b>5-2a</b> a) in MeOH; b) in 1mM KOH methanol solution. ....	153
<b>Figure 5-6.</b> Absorbance-time diagrams. a) Azobenzene and <b>5-2a</b> were 50 $\mu$ M solution in methanol. <b>5-2a</b> in base was 50 $\mu$ M in 1 mM KOH methanol solution. b) The absorbance change of 50 $\mu$ M <b>5-2a</b> in 1mM KOH MeOH solution. ....	154
<b>Figure B-1.</b> Linear absorbance difference diagram for the photoreactions of <b>5-2a</b> a) in MeOH; and b) in 1mM KOH methanol solution. ....	175
<b>Figure B-2.</b> Evaluations of the quantum yields ( $\phi^A$ ) of the photoreactions of <b>5-2a</b> b) in MeOH and c) in 1mM KOH methanol solution. a) is curve-fitting graph of azobenzene in methanol. ....	176

## LIST OF SYMBOLS AND ABBREVIATIONS

Å	Angstrom
b	Broad signal
C	Celsius
cm	Centimeter
CT	Charge transfer
d	Doublet
deg	Degree
DNA	Deoxyribonucleic acid
EI	Electron ionization
ESI	Electron spray ionization
ESIPT	Excited-state proton-transfer
ET	Electron transfer
eV	Electron volt
HOMO	Highest occupied molecular orbital
HPLC	High performance liquid chromatography
HRMS	High resolution mass spectrometry
HSAB	Hard and soft acid and base
Hz	Hertz

K	Kelvin
$\lambda$	Wavelength
LE	Local-excited state
LUMO	Lowest unoccupied molecular orbital
m	Multiplet
MHz	Megahertz
mm	Millimeter
MS	Mass spectroscopy
MT	Metallothionein
nm	Nanometer
NMR	Nuclear magnetic resonance
PET	Photoinduced electron transfer
ppm	Part Per Million
PT	Proton-transfer
q	Quartet
s	Singlet
SOD	Superoxide dismutase
t	Triplet
TD-DFT	Time-dependent density functional theory
THF	Tetrahydrofuran

TSQ

6-Methoxy-8-p-toluenesulphonamido-quinoline

UV

Ultraviolet

## SUMMARY

Zinc is an important micronutrient for all living organisms. While most of the cellular zinc is tightly bound to proteins, the rapid exchange kinetics with extracellular ligands indicates the presence of a kinetically labile pool. The biological function and regulation of this labile pool is still poorly understood. Zinc selective fluorescence sensors are ideally suited to gain information about the role of zinc in living systems and are attracting an increasing amount of interest.

The most promising approach comes in the form of ratiometric sensors which undergo a spectral shift upon coordination of the analyte. Unlike sensors based on the switch-on mechanism, ratiometric sensors allow for quantitative analyte measurements independent of the fluorophore concentration. The major challenge in designing this type of sensor lies in the necessity to achieve a spectral-shift upon binding of the metal ion. To develop a new class of ratiometric sensors, the utility of excited-state intramolecular proton transfer (ESIPT) as potential switching mechanism was explored.

In the absence of  $\text{Zn}^{\text{II}}$  at neutral pH, 2-(2'-sulfonamidophenyl)benzimidazole fluorophores undergoes ESIPT to yield a highly Stokes-shifted emission from the proton-transfer tautomer. Coordination of  $\text{Zn}^{\text{II}}$  inhibits the ESIPT process and yields a significant hypsochromic shift of the fluorescence emission maximum. By implementing structural modifications, we were able to gauge free  $\text{Zn}^{\text{II}}$  concentrations in the millimolar to picomolar range.

To tune the peak excitation towards lower energy, a property that is of particular

importance in the light of biological applications, we modified the parent molecule through extension of the conjugated pi-system and through selective introduction of substituents. These studies revealed that the annulation position and the nature of the substituents strongly influenced the photophysical properties of the fluorophores. Several of the target molecules revealed emission ratiometric properties with a large dynamic range combined with a peak absorption beyond 350 nm, thus rendering these probes promising candidates for biological applications.

To gain more insights into the origin of the substituent effects, five derivatives were studied based on solvatochromic shift analysis and quantum chemical calculations. The results showed that the observed negative solvatochromic shift behavior is most pronounced in protic solvents presumably due to specific hydrogen-bonding interactions. The extrapolated gas-phase emission energies correlated qualitatively well with the trends in Stokes shifts, suggesting that solute-solvent interactions do not play a significant role in explaining the emission energy shifts. The quantum chemical calculations confirmed the moderately polarized nature of the ESIPT tautomers and provided a rationale for the observed emission shifts.

The presented work demonstrates the potential of 2-(2'-arylsulfonamidophenyl)-benzimidazoles as ratiometric cation sensors. Notably, the fluorophore platform offers a tunable peak absorption and emission, adjustable zinc affinity with a wide dynamic range, little solvent polarity dependence, and a strong emission ratiometric response. All these properties render the developed probes promising tools to tackle problems in zinc

biology.

# CHAPTER I

## INTRODUCTION

### 1.1. Zinc in Biology

Zinc is an essential trace element and the second most abundant transition metal after iron in the body.<sup>1-3</sup> It supports a healthy immune system<sup>4-10</sup> and is vital for growth and development,<sup>11-13</sup> reproduction<sup>14,15</sup> and neurological functions. Zinc can be found in all tissues and fluids in the form of  $Zn^{2+}$  ions. Interestingly, serum and tissue levels of zinc are typically not correlated with each other.<sup>16</sup> Normally  $Zn^{2+}$  ions are considered nontoxic; however, an overdose of zinc can result in clinical conditions,<sup>17</sup> some of which are similar to those observed with copper deficiency, for example reduced superoxide dismutase (SOD) activity.<sup>18,19</sup> In multicellular organisms, zinc predominately located inside cells. At the cellular level, zinc plays catalytic, structural as well as regulatory roles.

Given its Lewis acidic properties, zinc is utilized by more than 300 enzymes for their catalytic functions and is responsible for stimulating the activity of more than 100 enzymes. Those enzymes include DNA and RNA polymerases,<sup>20</sup> alkaline phosphatases (AP),<sup>21</sup> peptidases,<sup>22</sup> carbonic anhydrases,<sup>23</sup> Alcohol dehydrogenases (ADH),<sup>24</sup> where  $Zn^{2+}$  ion may be directly involved into the bond-making or breaking step, or affects the catalytical reaction by stabilizing the active site conformation. The structure of the

catalytical and co-catalytic zinc motifs has been investigated and proven to be different.<sup>25</sup> About one thousand transcription factors and other proteins contain zinc finger domains, where the  $Zn^{2+}$  is crucial to fold and stabilize the proteins in the correct tertiary structure.<sup>26</sup> Given this abundance of zinc finger domains in transcription factors, zinc may play also a critical role in regulating gene expression. Similarly, alcohol dehydrogenases contain two zinc sites, but only one of them is responsible for their catalytic function, whereas the second  $Zn^{2+}$  ion plays solely a structural role.<sup>23</sup> Furthermore, chromatin and biomembranes appear to be stabilized by  $Zn^{2+}$  ions.<sup>27</sup> Zinc has also been found to modulate neurotransmission,<sup>28-34</sup> and more recently, studies on roles of zinc in apoptosis are growing rapidly.<sup>35-43</sup>

### **1.1.2. Zinc Homeostasis**

The total amount of zinc in the adult body is maintained at an average of 1.4-2.3 gram<sup>44</sup> through intestinal uptake, fecal elimination, renal reabsorption, and distribution to cells.<sup>45</sup> At the cellular level, the total zinc concentration averages 200-300  $\mu M$ ; however, the free intracellular zinc concentration in the cytosol is tightly regulated and presumably extremely low.<sup>46-49</sup> The fact that zinc can be successfully distributed to a myriad of proteins while maintaining such low free zinc concentrations suggests a sophisticated cellular zinc regulatory system.

Studies on the genetic disorder *acrodermatitis enteropathica* revealed that defects in the cellular zinc regulatory system can result in severe zinc deficiency.<sup>50,51</sup> It is also

known that zinc deficiency causes various clinical conditions, such as growth retardation,<sup>52-54</sup> immune system dysfunction,<sup>4-8</sup> anorexia nervosa,<sup>55</sup> and skin lesions<sup>56</sup>. Furthermore, zinc imbalance is related to various neurological diseases including Alzheimer's disease.<sup>32,33,57-61</sup> Understanding zinc homeostasis at the molecular level is pivotal to unravel the mechanisms of these clinical conditions.

### ***1.1.2.1. Zinc Transporters***

A major component of the cellular zinc regulatory system are zinc transporters.<sup>62,63</sup> These are membrane proteins that are responsible for mediating zinc ion import and export into and from the cytoplasm.<sup>62,63</sup> There are two families of zinc transporters: ZIP (zinc-iron related transporter proteins),<sup>64-66</sup> which modulates the zinc ion import into the cytoplasm, and ZnT/CDF (cation diffusion facilitator proteins, only used for yeast), which modulates the zinc ion export from the cytoplasm.<sup>67-75</sup> While the ZIP family of proteins and ZnT1<sup>67-69</sup> locate in the plasma membrane, other ZnT family of proteins locate only in the membranes of the intercellular compartments.<sup>70-75</sup> The ZnT family of proteins share similar structure and membrane topology but many of them have their preferred tissues to be expressed.<sup>62,63</sup> For example, while it's widely distributed, there is more ZnT1 expressed in the tissues involved in zinc acquisition, such as small intestine (villus cells), renal tubular epithelium, and placenta.<sup>76</sup> ZnT2 is expressed in liver, mammary gland, muscle, adipose, thymus, and spleen tissue<sup>70,76</sup> and ZnT3 is found to be expressed in brain and testes.<sup>71</sup> For more details, references 63 and 64 give

comprehensive reviews about zinc transporters.

Since zinc transporters are membrane proteins that are only responsible for zinc trafficking across membranes, they cannot be proper “carriers” to directly deliver zinc to thousands of proteins all over the cell. Considering the extremely low free zinc concentration in the cytoplasm,<sup>46-49</sup> direct insertion of free  $Zn^{2+}$  ion is clearly not a feasible proposal. In this regard, the existence and nature of such  $Zn^{2+}$ -specific “carriers”, also referred to as *metallochaperones*, remains a highly elusive aspect in zinc homeostasis research.

#### ***1.1.2.2 Metallothioneins (MTs)***

Metallothioneins are a family of cysteine-rich, low weight proteins that bind seven equivalent bivalent metal ions (mostly  $Zn^{2+}$ ) with very high affinity.<sup>77</sup> In human hepatocytes, 5%-10% of the total zinc binds to MTs.<sup>78,79</sup> In mammals, four MT isoforms have been found; MT-1 and MT-2 are expressed in all organs, whereas MT-3 and MT-4 are found mainly in the brain and certain stratified tissues, respectively.<sup>80</sup> In the cell, MTs mainly locate in the cytoplasm while some locate in the nuclei and lysosomes.<sup>81-83</sup> One of the major functions of MTS is to detoxify heavy metals and reactive oxygen species (ROS).<sup>84</sup> It's observed that zinc induces the transcription of the MTS gene by activating the transcription factor MTF-1, which is known to activate the promoter of ZnT-1 gene.<sup>85</sup> Interestingly, despite of high zinc binding affinity of MTS, zinc transfer from  $Zn_7$ -MT to apoproteins can be achieved by oxidizing the multiple cysteine residues and *in vivo*

experiment also approved the effective zinc transfer.<sup>86,87</sup> Therefore, it has been proposed that MTs might be the missing piece in the zinc regulatory system;<sup>88,89</sup> however, no direct proof has been established yet.

### ***1.1.2.3. Labile Zinc Pools***

Although the free zinc concentration in the cytoplasm is extremely low, a significant portion of intracellular zinc in eukaryotic cells can be readily removed by an extracellular chelator, suggesting the existence of a kinetically labile zinc pool. Estimates for the zinc concentration in this labile pool are only based on indirect measurements and vary from  $10^{-5}$  to  $10^{-12}$  M.<sup>67,90-93</sup> The intracellular labile zinc pool appears to be located in intracellular vesicles (sometimes referred to as zincosomes), which have been shown to accumulate zinc if the extracellular zinc concentration is increased.<sup>94,95</sup>

Despite the wealth of information available about zinc homeostasis, questions still remain about how zinc ions are delivered to proteins. Hence, it would be very helpful to understand the roles of MTs and labile zinc pools in the zinc regulatory system, a task that can only be solved by developing suitable methods that are capable of tracking zinc in live cells.

## **1.2. Zinc-Selective Fluorescent Sensors**

To measure the total zinc concentration in cells, traditional methods such as atomic absorption spectroscopy (AAS) or inductively coupled plasma mass spectrometry

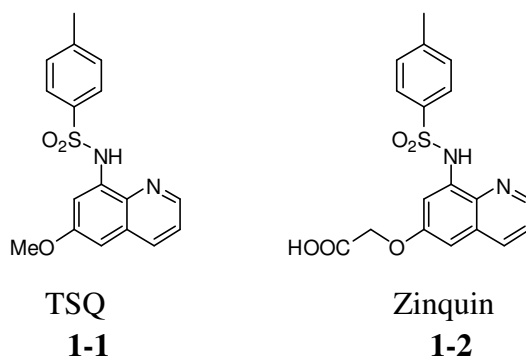
(ICP-MS) would be sufficient. Synchrotron X-ray fluorescence<sup>96</sup> is a powerful technique to visualize the zinc distribution in cells with subcellular resolution; however, this methods requires chemically fixed specimens. For live cell imaging, magnetic resonance imaging (MRI) contrast agents seem to be a viable choice;<sup>97,98</sup> however, the low spatial resolution<sup>99</sup>, typical around 1 mm<sup>3</sup> for commercial medical instruments, renders this approach not suitable for subcellular studies. At present, zinc-responsive fluorescent sensors offer the most promising non-invasive method to visualize zinc trafficking in living cells. Although since the late 80's, research activity in this field dramatically increased,<sup>100-104</sup> there is at present still no probe available that would fulfill all requirements.

To design a suitable zinc-selective fluorescent sensor, the properties of two components must be optimized independently: the fluorophore platform and the zinc binding group. While the fluorophore platform determines the photophysical properties of the sensor, the binding group will determine the zinc binding affinity and selectivity of the probe.

### **1.2.1. First Generation Sensors and Fluorophore Platforms**

Currently, the majority of zinc-responsive sensors function based on any of the following three fundamental photophysical processes: 1) photo-induced electron transfer (PET), 2) photo-induced charge transfer (PCT), and 3) fluorescence resonance energy transfer (FRET).<sup>105</sup> The design approach for the first generation sensors was based on a

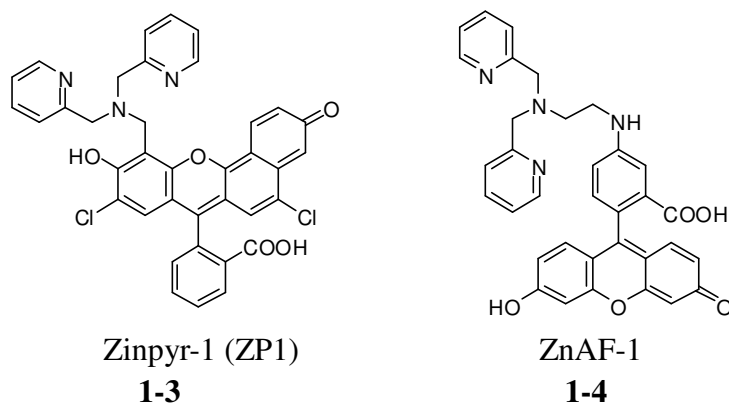
“switch-on” mechanism, which means that the fluorescence emission is quenched in absence and largely enhanced in the presence of  $Zn^{2+}$  ions. As a consequence, the fluorescence intensity is directly proportional to the free  $Zn^{2+}$  concentration available in solution, providing if the sensor is evenly distributed.



**Scheme 1-1.** Selected sensors based on 8-aminoquinoline platform.

One of the very first zinc-selective fluorescent sensors is 6-methoxy-8-*p*-toluenesulfonamide quinoline **1-1** (TSQ).<sup>106</sup> To improve its solubility in water as well as cellular retention, a carboxylic acid group was attached to give Zinquin **1-1** with overall improved performance (Scheme 1-1).<sup>107</sup> The solution chemistry of Zinquin with  $Zn^{2+}$  ions has been fully characterized in aqueous solution<sup>108</sup> and the probe has been successfully applied to live cell imaging of labile zinc pools.<sup>35,37</sup> Zinquin is now commercially available<sup>109</sup> and has become one of the most popular zinc sensors. A few additional sensors have been reported that are based on the 8-aminoquinoline framework, including TFLZn<sup>110</sup> and Danquin<sup>111</sup>. The fluorescein and rhodamine<sup>112</sup> platforms were introduced

later and offered significant improvements with a higher quantum yield and lower energy excitation. Depending on the attachment position of the Zn<sup>2+</sup>-chelating units, the sensors are named ZPs (**1-3**)<sup>113-116</sup> and ZnAFs (**1-4**)<sup>117,118</sup>, respectively. (Scheme 1-2) Both sensors have been applied to live cell imaging studies and revealed similar staining pattern as observed with Zinquin does.<sup>115,119</sup>



**Scheme 1-2.** Selected sensors based on the fluorescein platform.

Besides these two major families of Zn<sup>2+</sup> responsive small molecule sensors, peptides or proteins based probes have been also reported that are based on FRET, including carbonic anhydrase,<sup>120</sup> green fluorescent proteins (GFPs),<sup>121</sup> and engineered copper chaperone domains.<sup>122</sup>

### 1.2.2. Binding Groups

As mentioned above, the concentration of free zinc ions associated with labile pools has been estimated to range from  $10^{-5}$  to  $10^{-12}$  M.<sup>67,90-93</sup> Conclusively, the zinc-responsive sensors should cover a wide dynamic range. Several binding groups (Scheme 1-3) have been already extensively utilized in zinc-selective sensors: 1,4,7,10-tetra-azacyclododecane (cyclen, **1-5**),<sup>123-126</sup> sulfonamide (**1-6**),<sup>108</sup> dipicolylamine (**1-7**)<sup>113-118</sup> and 2,2'-azane-diyl-di-acetate (**1-8**).<sup>112,127</sup>

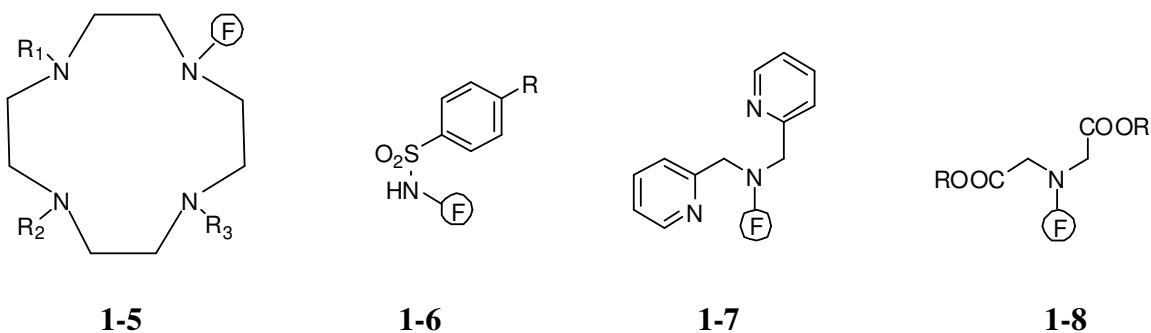
The  $K_d$  of sensors containing chelating group of type **1-5** varies from 0.02 nM<sup>120</sup> to 13.5  $\mu$ M<sup>123</sup>, depending on the substituents  $R_1R_2R_3$ . The sulfonamide **1-6** and quinoline together gives Zinquin a binding affinity of  $\log K = 13.5$ .<sup>108</sup> Group **1-8** gives  $K_d$  around 3  $\mu$ M for two derivatives. Synthetically, the structure of dipicolylamine **1-7** could be easily changed to tune the binding affinity. For example, by changing the length of the carbon linker, Kikuchi and coworkers successfully tuned the  $K_d$  value of their sensors in a very wide range (from 2.7 nM to 0.6 mM).<sup>128</sup>

In Pearson's HSAB Classification System,  $Zn^{2+}$  ion is recognized as a borderline Lewis acid.<sup>129</sup> By selecting borderline Lewis base, such as pyridine, aniline, and sulfonamide as binding groups, the zinc selectivity of the sensor against hard ( $Na^+$ ,  $K^+$ ,  $Mg^{2+}$ ,  $Ca^{2+}$ ,  $Mn^{2+}$ ,  $Cr^{3+}$  and  $Fe^{3+}$ ) and soft ( $Cu^+$ ,  $Ag^+$ ,  $Hg^{2+}$  and  $Cd^{2+}$ ) Lewis acids will be improved. To improve the selectivity against other bio-relevant borderline Lewis acids ( $Fe^{2+}$ ,  $Co^{2+}$ ,  $Ni^{2+}$  and  $Cu^{2+}$ ), designing the right coordination geometry of the zinc-sensor complex should be the way to go.<sup>130</sup> Compared to  $Fe^{2+}$ ,  $Co^{2+}$ ,  $Ni^{2+}$  and  $Cu^{2+}$ ,  $Zn^{2+}$  bears

the special  $d^{10}$  electron configuration and is not subject to ligand field stabilization effects. Therefore, the less ligand field stabilization energy the coordination geometry could induce, the better zinc-selectivity the binding group with this geometry could have. The tetrahedral geometry, which induces less ligand field stabilization energy than other common geometries do, will then be the preferred coordination geometry for zinc sensors.

By evaluating these two points, we can conclude that neither binding group **1-5** nor **1-8** is a good choice for zinc-selective purpose because amines and carboxylic acid groups are hard Lewis bases and the metal-cyclen **1-5** complex prefers the square planar geometry, which offers a large ligand field stabilization energy.

Based on the same consideration, the dipicolylamine **1-7** should very zinc-selective because its zinc complex prefers tetrahedral geometry and pyridines are borderline bases. The sulfonamide group **1-6** is known to be borderline Lewis base. Since it is a monodentate ligand and cannot form a chelator alone, the zinc binding property of the sensor containing the sulfonamide group will also depend on other binding groups.



**Scheme 1-3.** Binding groups used in zinc-selective sensors.

### 1.2.3. Ratiometric Sensors

For the first generation “turn-on” zinc-responsive sensors, the fluorescence intensity is not only dependent on the free metal ion concentration, but also on the total sensor concentration. In biological systems, the sensor concentration is typically not known since it is influenced by many factors, including membrane permeability, incubation time, temperature, and variations in cell size. Therefore, a quantitative interpretation of the fluorescence intensity distribution is complicated or impossible, and the free metal ion concentration cannot be reliably quantified with this type of sensor. To overcome this limitation, a new probe must be designed whose response is independent of the total sensor concentration.

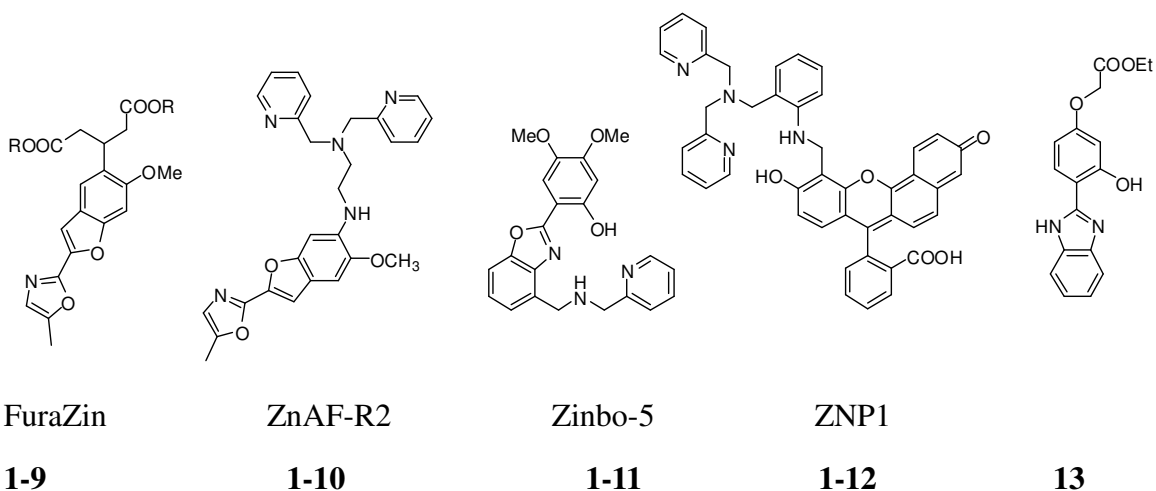
Ratiometric sensors were first proposed by Tsien and coworkers in the late 80’s in context of calcium sensing.<sup>131</sup> If the fluorescence spectra shift upon binding metal ions, the ratio  $R$  of the fluorescence intensities at two different emission or excitation wavelengths  $\lambda_1$  and  $\lambda_2$  is directly related to the free metal ion concentration, according to the following equation shown:

$$[Zn(II)]_{free} = K_d \left( \frac{R - R_{min}}{R_{max} - R} \right) \frac{S_{apo}}{S_{bnd}} \quad \text{Eq. 1-1}$$

where  $R_{min}$  and  $R_{max}$  are the  $R$  values for the free sensor and its metal complex, respectively, both of which can be readily determined from *in vitro* measurements.

Similarly, the calibration procedure will also provide the instrument-dependent parameters  $S_{\text{apo}}$  and  $S_{\text{bnd}}$ . It is worthwhile noting that this equation is only valid for binding sensors that exhibit a 1:1 binding stoichiometry with the metal cation.

The calcium sensor Fura-2 reported by Tsien and coworkers was later modified to a sensor with improved zinc selectivity, FuraZin.<sup>124</sup> Currently, FuraZin (Scheme 1-4) is the only commercially available ratiometric zinc-selective fluorescent sensor.<sup>109</sup> The ratiometric property of FuraZin can only be observed on the excitation side. To apply FuraZin for ratiometric live cell imaging, the microscopy will have to be equipped with two laser sources, which will increase the instrument expense a lot and limit the use of FuraZin. Therefore, an emission ratiometric zinc-selective sensor would be highly desirable.



**Scheme 1-4.** Ratiometric sensors

Some new ideas about ratiometric sensors have been proposed (Scheme 1-4), but none of them solve the problem. ZnAR-Rs **1-10** were designed, synthesized and applied in cultured macrophages to do ratiometric imaging.<sup>132</sup> Benzoxazoles **1-11**<sup>133</sup> and **1-13**<sup>134</sup> were inspired by the same proton transfer mechanism. The fluorescein based ZNP1 was proposed by Lippard.<sup>135</sup>

The study of ZnAR-R2 has revealed the major difficulty that has hampered the development of the emission ratiometric sensor. While the excitation spectra of ZnAR-R2 show large shift upon binding zinc, its peak emission stays almost the same.<sup>132</sup> This fact suggests that the metal ion is ejected from the sensor at the excited state, which has been seen in a lot at sensors that is based on charge transfer and use the donor site for metal ion binding. To tackle this problem, a totally new design will be required.

### **1.3. Thesis Objective**

The objective of this thesis is to find a ratiometric fluorophore platform with tunable affinity and good selectivity towards  $\text{Zn}^{2+}$ . Such a probe would offer a powerful tool for investigating zinc trafficking in living cells. The development of such a sensor would thus help understanding zinc homeostasis and the origin of diseases related to zinc imbalance and deficiency.

To fulfill these objectives, a fluorophore that undergoes emission shift upon binding  $\text{Zn}^{2+}$  must be first developed. Previous studies on benzoxazoles showed that inhibition of

excited-state intramolecular proton-transfer is a promising mechanistic concept to achieve this key feature.<sup>128, 129</sup> The picolylamine group offers good selectivity towards zinc and its binding affinity can be tuned via simple synthetic modifications. Therefore, with careful design, the combination of a benzazole fluorophore with picolylamine as metal chelation moiety should provide a series of emission ratiometric zinc-selective sensors.

#### **1.4. References:**

1. Coleman, J. E. *Annu. Rev. Biochem.* **1992**, *61*, 897.
2. Stefanidou, M. etc. *Arch. Toxicol* **2006**, *80*, 1.
3. Beyersmann. D. *Mat.-wiss. U. Werkstofftech.* **2002**, *33*, 764.
4. Solomons, N. W. *Nutr. Rev.* **1998**, *56*, 27.
5. Prasad, A. S. *Nutrition* **1995**, *11*, 93.
6. Ibs, K. H.; Rink, L. *J. Nutr.* **2003**, *133*, 1452S.
7. Dardenne, M. *Eur. J. Clin. Nutr.* **2002**, *56*, S20.
8. Rink, L.; Gabriel, P., *Proc. Nutr. Soc.* **2000**, *59*, 541.
9. Salgueiro, M. J.; Zubillaga, M.; Lysionek, A.; Cremaschi, G.; Goldman, C. G.; Caro, R.; De Paoli, T.; Hager, A.; Weill, R.; Boccio, J. *Biol.Trace Elem. Res.* **2000**, *76*, 193.
10. Prasad, A. S. *Mol. Cell. Biochem.* **1998**, *188*, 63.
11. Vallee, B.L.; Falchuk, K.H. *Physiol Rev* **1993**, *73*, 79.
12. Simmer, K.; Thompson, R. P. *Acta Paediatr. Scand. Suppl.* **1985**, *319*, 158.
13. Fabris, N.; Mocchegiani, E. *Aging (Milano)* **1995**, *7*, 77.
14. Bedwal, R. S.; Bahuguna, A. *Experientia* **1994**, *50*, 626.
15. Apgar, J. *Ann. Rev. Nutr.* **1985**, *5*, 43.
16. Gorodetsky, R.; Sheskin, J.; Weinreb, A. *Int. J. Dermatol.* **1986**, *25*, 440.
17. Sandstead, H. H. *Nutrition* **1995**, *11*, 87.

18. Yadrick, M. K.; Kenney, M. A.; Winterfelt, E. A. *Am. J. Clin. Nutr.* **1989**, *49*, 145.
19. Barceloux, D. G. *Clin Toxicol* **1999**, *37*, 279.
20. Wu, F. Y. H.; Wu, C. W. *Met. Ions Bio. Sys.* **1984**, *15*, 157.
21. Koike, T.; Kimura, E. *J. Am. Chem. Soc.* **1991**, *113*, 8935.
22. Taylor, A. *FASEB J.* **1993**, *7*, 290.
23. Pastorekova, S.; Parkkila, S.; Pastorek, J.; Supuran, C. T. *J. Enzyme Inh. Med. Chem.* **2004**, *19*, 199.
24. Eid, M. F.; Fewson, C. A. *Crit. Rev. Microbiol.* **1994**, *20*, 13.
25. Vallee, B. L.; Auld, D. S. *Acc. Chem. Res.* **1993**, *26*, 543.
26. Pabo, C. O.; Sauer, R. T. *Ann. Rev. Biochem.* **1992**, *61*, 1053.
27. Tapiero, H.; Tew, K. D. *Biomed. Pharmacotherapy* **2003**, *57*, 399.
28. Hosie, A. M.; Dunne, E. L.; Harvey, R. J.; Smart, T. G. *Nat. Neurosci.* **2003**, *6*, 362.
29. Laube, B., *Eur. J. Neurosci.* **2002**, *16*, 1025.
30. Zhang, D. Q.; Ribelayga, C.; Mangel, S. C.; McMahon, D. G. *J. Neurophysiol.* **2002**, *88*, 1245.
31. Minami, A.; Takeda, A.; Yamaide, R.; Oku, N. *Brain Res.* **2002**, *936*, 91.
32. Brown, C. E.; Dyck, R. H. *J. Neurosci.* **2002**, *22*, 2617.
33. Takeda, A. *Biometals* **2001**, *14*, 343.
34. Frederickson, C. J.; Bush, A. I. *Biometals* **2001**, *14*, 353.
35. Haase, H.; Watjen, W.; Beyersmann, D. *Biol. Chem.* **2001**, *382*, 1227.
36. Vaux, D. L.; Silke, J. *Nat. Rev. Mol. Cell Bio.* **2005**, *6*, 287.

37. Zalewski, P. D.; Forbes, I. J.; Betts, W. H. *Biochem. J.* **1993**, *296*, 403.
38. Truong-Tran, A. Q.; Carter, J.; Ruffin, R. E.; Zalewski, P. D. *Biometals* **2001**, *14*, 315.
39. Sauer, G. R.; Smith, D. M.; Cahalane, M.; Wu, L. N. Y.; Wuthier, R. E. *J. Cell. Biochem.* **2003**, *88*, 954.
40. Truong-Tran, A. Q.; Ruffin, R. E.; Zalewski, P. D. *Am. J. Physiol.-Lung Cell. Mol. Physiol.* **2000**, *279*, L1172.
41. Feng, P.; Liang, J. Y.; Li, T. L.; Guan, Z. X.; Zou, J.; Franklin, R. B.; Costello, L. C. *Mol. Urol.* **2000**, *4*, 31.
42. Chai, F. G.; Truong-Tran, A. Q.; Ho, L. H.; Zalewski, P. D. *Immunol. Cell Biol.* **1999**, *77*, 272.
43. Zalewski, P.; Ratnaike, R. *J. Am. Geriatr. Soc.* **1998**, *46*, A8.
44. Calesnick, B.; Dinan, A. M. *Am. Fam. Physician* **1988**, *37*, 267.
45. Krebs, N. F. *J. Nutr.* **2000**, *130*, S1374.
46. Finney, L. A.; O'Hallorn, T. V. *Science* **2003**, *300*, 931.
47. Outten, C. E.; Tobin, D. A.; Penner-Hahn, J. E.; O'Halloran, T. V. *Biochemistry* **2001**, *40*, 10417.
48. Hitomi, Y.; Outten, C. E.; O'Halloran, T. V. *J. Am. Chem. Soc.* **2001**, *123*, 8614.
49. Benters, J.; Flögel, U.; Schäfer, T.; Leibfritz, D.; Hechtenberg, S.; Beyersmann D. *Biochem. J.* **1997**, *322*, 793.
50. Nakano, A.; Nakano, H.; Nomura, K.; Toyomaki, Y.; Hanada, K. *J. Inv. Dermat.*

**2003**, 120, 963.

51. Dufner-Beattie, J.; Wang, F. D.; Kuo, Y. M.; Gitschier, J.; Eide, D.; Andrews, G. K.  
*J. Biol. Chem.* **2003**, 278, 33474.
52. Rossi, L.; Migliaccio, S.; Corsi, A.; Marzia, M.; Bianco, P.; Teti, A.; Gambelli, L.;  
Cianfarani, S.; Paoletti, F.; Branca, F. *J. Nutr.* **2001**, 131, 1142.
53. McNall, A. D.; Etherton, T. D.; Fosmire, G. J. *J. Nutr.* **1995**, 125, 874.
54. Buzina, R.; Jusic, M.; Sapunar, J.; Milanovic, N. *Am. J. Clin. Nutr.* **1980**, 33, 2262.
55. Salgueiro, M. J.; Zubillaga, M.; Lysionek, A.; Sarabia, M. I.; Caro, R.; De Paoli, T.;  
Hager, A.; Weill, R.; Boccio, J. *Nutrition Research* **2000**, 20, 737.
56. Perafan-Riveros, C.; Franca, L. F. S.; Alves, A. C. F.; Sanches, J. A. *Pediatric  
Dermatology* **2002**, 19, 426.
57. Bush, A. I.; Tanzi, R. E. *Proc. Natl. Acad. Sci. U. S. A.* **2002**, 99, 7317.
58. Robertson, J. D.; Crafford, A. M.; Markesbery, W. R.; Lovell, M. A. *Nuclear  
Instruments & Methods in Physics Research Section B-Beam Interactions with  
Materials and Atoms* **2002**, 189, 454.
59. Bush, A. I.; Moir, R. D.; Rosenkranz, K. M.; Tanzi, R. E. *Science* **1995**, 268, 1921.
60. Cuajungco, M. P.; Faget, K. Y. *Brain Res. Rev.* **2003**, 41, 44.
61. Frederickson, C. J.; Suh, S. W.; Silva, D.; Thompson, R. B. *J. Nutr.* **2000**, 130,  
1471S.
62. Kambe, T.; Yamaguchi-Iwai, Y.; Sasaki, R.; Nagao, M. *Cell. Mol. Life. Sci.* **2004**, 61,  
49.

63. Liuzzi, J. P.; Cousins, R. J. *Annu. Rev. Nutr.* **2004**, *24*, 151.
64. Gaither, L. A.; Eide, D. J. *Biometals* **2001**, *14*, 251
65. McClung, J. P.; Bobilya, D. J. *J. Nutr. Biochem.* **1999**, *10*, 484.
66. Costello, L. C.; Liu, Y.; Zou, J.; Franklin, R. B. *J. Biol. Chem.* **1999**, *274*, 17499.
67. Palmiter, R. D.; Findley, S. D. *EMBO. J.* **1995**, *14*, 639.
68. Tsuda, M.; Imaizumi, K.; Katayama, T.; Kitagawa, K.; Wanaka, A.; Tohyama, M. *J. Neurosci.* **1997**, *17*, 6678.
69. Kim, A. H.; Sheline, C. T.; Tian, M.; Higashi, T.; McMahon, R. J.; Cousins, R. J. *Brain Res.* **2000**, *886*, 99.
70. Palmiter, R. D.; Cole, T. B.; Quaife, C. J.; Findley, S. D. *Proc. Natl. Acad. Sci. U. S. A.* **1996**, *93*, 14934.
71. Palmiter, R. D.; Cole, T. B.; Findley, S. D. *EMBO J.* **1996**, *15*, 1784.
72. Huang, L. P.; Gitschier, J. *Nature Genetics* **1997**, *17*, 292.
73. Huang, L. P.; Kirschke, C. P.; Gitschier, J. *J. Biol. Chem.* **2002**, *277*, 26389.
74. Kirschke, C. P.; Huang, L. P. *J. Biol. Chem.* **2003**, *278*, 4096.
75. Kambe, T.; Narita, H.; Yamaguchi-Iwai, Y.; Hirose, J.; Amano, T.; Sugiura, N.; Sasaki, R.; Mori, K.; Iwanaga, T.; Nagao, M. *J. Biol. Chem.* **2002**, *277*, 19049.
76. Liuzzi, J.P.; Blanchard, R. K.; Cousins, R. J. *J. Nutr.* **2001**, *131*, 46.
77. Kagi, J. H. R. *Methods in Enzymology* **1991**, *205*, 613.
78. Buhler, R. H.; Kagi, J. H. *FEBS Lett.* **1974**, *39*, 229.
79. Maret, W. *J. Nutr.* **2000**, *130*, S1455.

80. Moffatt, P.; Denizeau, F. *Drug Metab. Rev.* **1997**, *29*, 261.
81. Sugiura, T.; Nakamura, H. *Int. Arch. Allergy. Immunol.* **1994**, *103*, 341.
82. Nartey, N. O.; Banerjee, D.; Cherian, M. G. *Pathology* **1987**, *19*, 233.
83. Panemangalore, M.; Banerjee, D.; Onosaka, S.; Cherian, M. G. *Dev. Biol.* **1983**, *97*, 95.
84. Kondoh, M.; Imada, N.; Kamada, K.; Tsukahara, R.; Higashimoto, M.; Takiguchi, M.; Watanabe, Y.; Sato, M. *Toxicol. Lett.* **2003**, *142*, 11.
85. Andrews, G. K. *Biometals.* **2001**, *14*, 223.
86. Jiang, L. J.; Maret, W.; Vallee, B. L. *Proc. Natl. Acad. Sci. USA* **1998**, *95*, 3483.
87. Maret, W.; Vallee, B. L. *Proc. Natl. Acad. Sci. USA* **1998**, *95*, 3478.
88. Vasak, M.; Hasler, D. W. *Curr. Opin. Chem. Biol.* **2000**, *4*, 177.
89. Vasak, M. *J. Trace Elem. Med. Biol.* **2005**, *19*, 13.
90. Sensi, S. L.; Canzoniero, L. M. T.; Yu, S. P.; Ying, H. S.; Koh, J. Y.; Kerchner, G. A.; Choi, D. W. *J. Neurosci.* **1997**, *17*, 9554.
91. Kar, S. R.; Adams, A. C.; Lebowitz, J.; Taylor, K. B.; Hall, L. M. *Biochemistry* **1997**, *36*, 15343.
92. VanZile, M. L.; Cospers, N. J.; Scott, R. A.; Giedroc, D. P. *Biochemistry* **2000**, *39*, 11818.
93. Williams, R. J. P.; Frausto da Silva, J. J. R. *Coord. Chem. Rev.* **2000**, *200-202*, 247.
94. Suhy, D. A.; O'Halloran, T. V. Metal-responsive gene regulation and the zinc metalloregulatory model, **1996**; *Vol. 32*, pp 557.

95. Haase, H.; Beryersmann, D. *BioMetals* **1999**, *12*, 247.
96. McRae, R.; Lai, B.; Vogt, S.; Fahrni C. J. *J. Struct. Biol.* **2006**, *155*, 22.
97. Hanaoka, K.; Kikuchi, K.; Urano, Y.; Narazaki, M.; Yokawa, T.; Sakamoto, S.; Yamaguchi, K.; Nagano, T. *Chem. Biol.* **2002**, *9*, 1027.
98. Trokowski, R.; Ren, J. M.; Kalman, F. K.; Sherry, A. D. *Angew. Chem. Int. Ed.* **2005**, *44*, 6920.
99. Overduin, S. A.; Servos, P. *NeuroImage* **2004**, *23*, 462.
100. De Silva, A. P.; Gunaratne, H. Q.N.; Gunnlaugsson, T.; Huxley, A. J. M.; McCoy, C. P.; Rademacher, J. T.; Rice, T. E. *Chem. Rev.* **1997**, *97*, 1515.
101. Kikuchi, K.; Komatsu, K.; Nagano, T. *Curr. Opin. Chem. Bio.* **2004**, *8*, 182.
102. Thompson, R. B. *Curr. Opin. Chem. Bio.* **2005**, *9*, 526.
103. Lim, N. C.; Freake, H. C.; Bruckner, C. *Chem. Eur. J.* **2005**, *11*, 39.
104. Jiang, P. J.; Guo, Z. J. *Coord. Chem. Rev.* **2004**, *248*, 205.
105. Valeur, B. *Molecular Fluorescence: Principles and Applications*, Wiley-VCH, Weinheim, **2001**.
106. Frederickson, C. J.; Kasarskis, E. J.; Ringo, D.; Frederickson, R. E. *J. Neurosci. Methods* **1987**, *20*, 91.
107. Mahadevan, I.; Kimber, M.; Lincoln, S.; Tiekink, E.; Ward, A.; Betts, W.; Forbes, I.; Zalewski, P., *Aust. J. Chem.* **1996**, *49*, (5), 561
108. Fahrni, C. J.; O'Halloran, T. V. *J. Am. Chem. Soc.* **1999**, *121*, 11448.
109. Haugland, R. P. *Handbook of Fluorescent Probes and Research Products*;

Molecular Probes: Eugene, OR, **2002**.

110. Budde, T.; Minta, A.; White, J.; Kay, A. *Neuroscience* **1997**, *79*, 347.
111. Jiang, P.; Chen, L.; Lin, J.; Liu, Q.; Ding, J.; Gao, X.; Guo, Z. *Chem. Commun.* **2002**, *13*, 1424.
112. Sensi, S. L.; Ton-That, D.; Weiss, J. H.; Rothe, A.; Gee, K. R. *Cell Calcium* **2003**, *34*, 281.
113. Burdette, S.; Walkup, G.; Spingler, B.; Tsien, R.; Lippard, S. *J. Am. Chem. Soc.* **2001**, *123*, 7831.
114. Sjoback, R.; Nygren, J.; Kubista, M. *Spectrochim. Acta, part A* **1995**, *51*, L7.
115. Walkup, G.; Burdette, S.; Lippard, S.; Tsien, R., *J. Am. Chem. Soc.* **2000**, *122*, 5644.
116. Burdette, S.; Frederickson, C.; Bu, W.; Lippard, S., *J. Am. Chem. Soc.* **2003**, *125*, 1778.
117. Hirano, T.; Kikuchi, K.; Urano, Y.; Higuchi, T.; Nagano, T. *Angew. Chem., Int. Ed. Engl.* **2000**, *39*, 1052.
118. Hirano, T.; Kikuchi, K.; Urano, Y.; Nagano, T. *J. Am. Chem. Soc.* **2002**, *124*, 6555.
119. Fahrni, C. J.; Simon, K.; Suhy, D.; Nasir, M.; Dwivedi, R.; O'Halloran, T. *J. Inorg. Biochem.* **1999**, *74*, 125.
120. Thompson, R. B., Cramer, M. L., Bozym, R., Fierke, C. A. *J. Biomed. Opt.* **2002**, *7*, 555.
121. Barondeau, D. P.; Kassmann, C. J.; Tainer, J. A.; Getzoff, E. D. *J. Am. Chem. Soc.*

- 2002**, *124*, 3522.
122. van Dongen, E. M. W. M.; Dekkers, L. M.; Spijker, K.; Meijer, E. W.; Klomp, L. W. J.; Merckx, M. *J. Am. Chem. Soc.* **2006**, *128*, 10754.
123. Aoki, S.; Kaido, S.; Fujioka, H.; Kimura, E. *Inorg. Chem.* **2003**, *42*, 1023.
124. Kimura, E.; Aoki, S.; Kikuta, E.; Koike, T. *Proc. Natl. Acad. Sci. USA* **2003**, *100*, 3731.
125. Lim, N. C.; Yao, L.; Freake, H. C.; Bruckner, C. *Bioorg. Med. Chem. Lett.* **2003**, *13*, 2251.
126. Burdette, S. C.; Lippard, S. J. *Inorg. Chem.* **2002**, *41*, 6816.
127. Gee, K. R.; Zhou, Z. L.; Ton-That, D.; Sensi, S. L.; Weiss, J. H. *Cell Calcium* **2002**, *31*, 245.
128. Komatsu, K.; Kikuchi, K.; Kojima, H.; Urano, Y.; Nagano, T. *J. Am. Chem. Soc.* **2005**, *127*, 10197.
129. Pearson, R. G. *Chemical Hardness: Applications from Molecules to Solids*, Wiley-VCH, New York, **1997**
130. Zumdahl, S. S. *Chemical principles* 5th Edition, Houghton Mifflin, Boston, **2005**.
131. Grynkiewicz, G.; Poenie, M.; Tsien, R. Y. *J. Biol. Chem.* **1985**, *260*, 3440.
132. Maruyama, S.; Kikuchi, K.; Hirano, T.; Urano, Y.; Nagano, T. *J. Am. Chem. Soc.* **2002**, *124*, 10650.
133. Taki, M.; Wolford, J.; O'Halloran, T. V. *J. Am. Chem. Soc.* **2004**, *126*, 712.
134. Henary, M. M.; Fahrni, C. J. *J. Phys. Chem. A* **2002**, *106*, 5210.

135. Chang, C.; Jaworski, J.; Nolan, E.; Sheng, M.; Lippard, S. *Proc. Natl. Acad.*

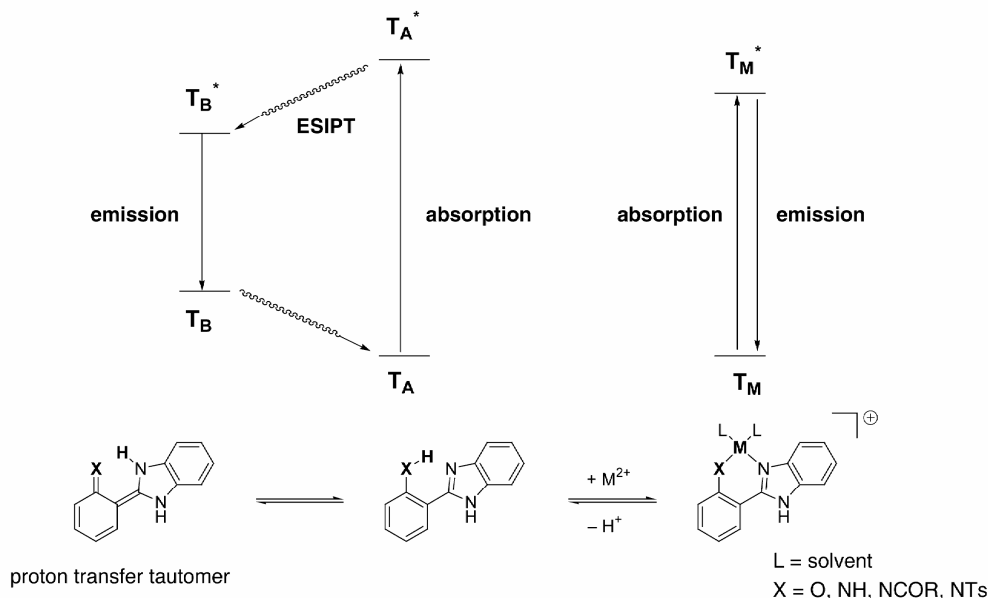
*Sci.U.S.A.* **2004**, *101*, 1129.

## CHAPTER II

# ZINC(II)-SELECTIVE RATIO-METRIC FLUORESCENT SENSORS BASED ON INHIBITION OF EXCITED-STATE INTRAMOLECULAR PROTON TRANSFER

### 2.1. Introduction

Excited-state intramolecular proton transfer (ESIPT) has been observed in various kinds of molecules, such as salicylic acid<sup>1-5</sup>, 2-hydroxy benzophenone<sup>6</sup>, hydroxyflavones<sup>7-10</sup>, 1,5-dihydroxyanthraquinone<sup>11</sup>, 2-hydroxy-4,5-naphthotroponone<sup>12</sup>, benzazoles<sup>13-25</sup> and 2-(2'-hydroxy-5'-methylphenyl) benzotriazole<sup>26-29</sup>, and has a wide range of applications.<sup>30-39</sup> Generally, a pre-existing intramolecular hydrogen bond (between X and N in Scheme 2-1) is required for ESIPT. Upon photoexcitation, the proton covalently attached to the donor group (X) migrates to the acceptor group (N) and forms a more stable phototautomer ( $T_B^*$ ). This phototautomer then gives a highly Stokes' shifted emission and equilibrates back to the original ground state ( $T_A$ ). The excited state proton transfer is essentially barrierless and therefore a very fast process with reaction rates approaching the subpicosecond range.<sup>40-42</sup> ESIPT can be disrupted by deprotonation or coordination of metal ions. The emission from the deprotonated species or metal complex ( $T_M^*$ ) occurs then with normal Stokes shift, thus giving rise to a significant blue-shifted emission relative to the protonated fluorophore.



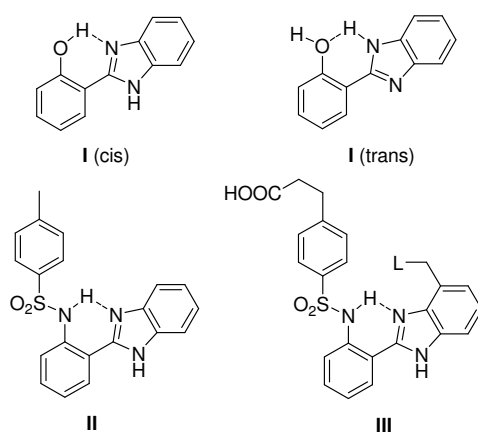
**Scheme 2-1.** Simplified Jablonski diagram illustrating the increase of the emission energy upon metal-cation-induced inhibition of excited-state intramolecular proton transfer.

The interesting photophysical property of ES IPT sparked research in fluorescent sensor design;<sup>37-39</sup> however, its potential for the design of emission ratiometric cation-sensors had not been realized until several years ago.<sup>43, 44</sup>

By measuring the analyte concentration through the ratio of the luminescence intensities at two distinct wavelengths, ratiometric sensors have the advantage that their response is independent of dye concentration, pathlength, or instrument dependent parameters.<sup>45</sup> Since the key photophysical requirement for the design of ratiometric probes relies on a significant spectral shift upon binding of the analyte, ES IPT represents

a promising design principle for developing such sensors.

The photophysics of 2-(2'-hydroxyphenyl)benzazoles (**I**, Scheme 2-2) were already investigated as potential candidates for ratiometric sensors.<sup>43</sup> However, in a polar solvent environment, these fluorophores equilibrate with a *trans*-rotamer that cannot undergo ESIPT. As a consequence, emission occurs mainly with normal Stokes shift in aqueous solution. To overcome this problem, 2-(2'-tosylaminophenyl)benzimidazole (**II**) was proposed because the sulfonamide lacks the electron lone pair to stabilize the *trans*-rotamer.<sup>44</sup> Using this improved fluorophore platform as building block, a series of water soluble benzimidazole derivatives (**III**) were synthesized and characterized as potential ratiometric fluorescent sensors. To tune the binding affinity and optimize the selectivity towards  $Zn^{2+}$  ions, a chelating moiety (L) was introduced through modification of the benzimidazole framework..



**Scheme 2-2**

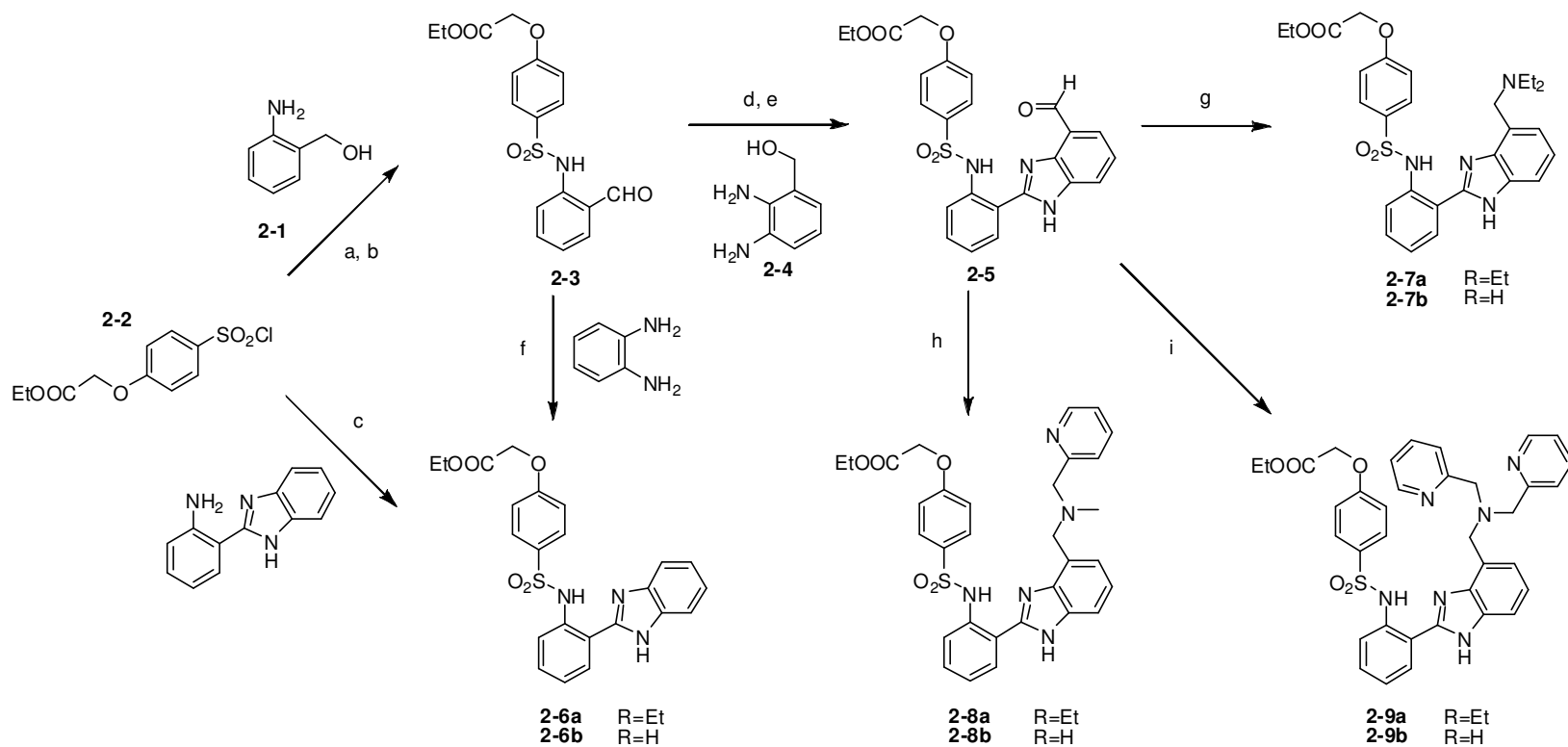
## 2.2. Results and Discussion

### 2.2.1. Synthesis

Using a modular approach, the synthesis of the modified fluorophores was accomplished with three key reactions (Scheme 2-3). Firstly, the condensation of the commercially available amine (**2-1** or 2-(2'-aminophenyl)benzimidazole) with sulfonyl chloride **2-2**<sup>48</sup> gave intermediate **2-3** (after MnO<sub>2</sub> oxidation) or the unsubstituted ligand **2-6a**. Secondly, the copper(II)-mediated oxidative coupling of aldehyde **2-3** with 2,3-diaminobenzyl alcohol<sup>46</sup> **2-4** or 1,2-phenylenediamine provided intermediate **2-5** (after MnO<sub>2</sub> oxidation), or unsubstituted ligand **2-6a** as an alternative pathway. Thirdly, all three substituted ligands **2-7a**, **2-8a** and **2-9a** were synthesized by means of reductive amination of aldehyde **2-5** with the corresponding amines. The water-soluble acids **2-6b**, **2-7b**, **2-8b** and **2-9b** were finally obtained by hydrolysis with LiOH·H<sub>2</sub>O in aqueous methanol.

### 2.2.2. Ground-State Tautomerism

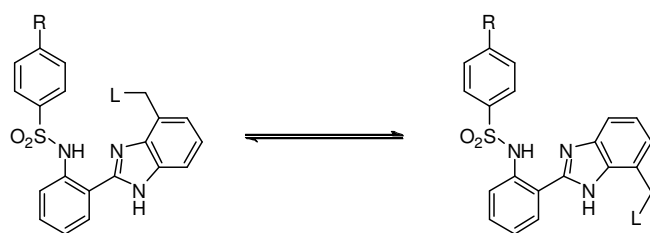
The NH-proton in benzimidazoles undergo fast annular tautomerization.<sup>46</sup> Unlike the unsubstituted ligand **2-6a/b**, ligands **2-7a/b-2-9a/b** are involved in a nondegenerate prototropic equilibrium because the introduced binding moiety renders their tautomer pairs structurally and energetically different (Scheme 2-4). The <sup>1</sup>H NMR spectra of all ligands show only one set of resonances for the benzimidazole protons, suggesting that the tautomerization rate at room temperature is too fast to be observed on the NMR time



**Scheme 2-3.** a) pyridine, 0°C; b) MnO<sub>2</sub>, CH<sub>2</sub>Cl<sub>2</sub>, RT (53%, from **2-1**); c) pyridine, (60%); d) Cu(OAc)<sub>2</sub>, EtOH, reflux (36%); e) MnO<sub>2</sub>, CH<sub>2</sub>Cl<sub>2</sub>, RT (86%); f) Cu(OAc)<sub>2</sub>, EtOH, reflux (20%); g) NaBH(OAc)<sub>3</sub>, Et<sub>2</sub>NH, 1,2-EtCl<sub>2</sub> (76%); h) NaBH(OAc)<sub>3</sub>, N-2-picolyl-N-methylamine, 1,2-EtCl<sub>2</sub> (97%); i) NaBH(OAc)<sub>3</sub>, N,N-2,2'-dipicolylamine, 1,2-EtCl<sub>2</sub> (80%).

scale. For instance, although the proton resonances of ligand **2-7a** in CD<sub>3</sub>OD undergo line broadening when cooled to -60°C (Figure 2-1), the tautomerization rate does not reach the slow-exchange limit that would provide the chemical-shift information for each tautomer and thus their concentration ratio. Therefore, this data set cannot be used to determine the equilibrium constant and activation barrier of the prototropic equilibrium.

According to literature reports, the tautomerization equilibrium constants for 4(7)-substituted benzimidazoles are very close to unity.<sup>47</sup> This indicates that the relative stability of the N1(H) and N3(H) tautomer is almost identical, and that the stability difference between the annular tautomers of ligands **2-6-2-9** is primary controlled through steric factors and presumably very small. Conclusively, both tautomers are expected to be present in significant concentrations. The absorption and emission spectra discussed below correspond therefore to the averaged spectra of both tautomers.



**Scheme 2-4.** Nondegenerate prototropic equilibrium of the tautomer pairs of the substituted ligands **2-7a/b-2-9a/b**.

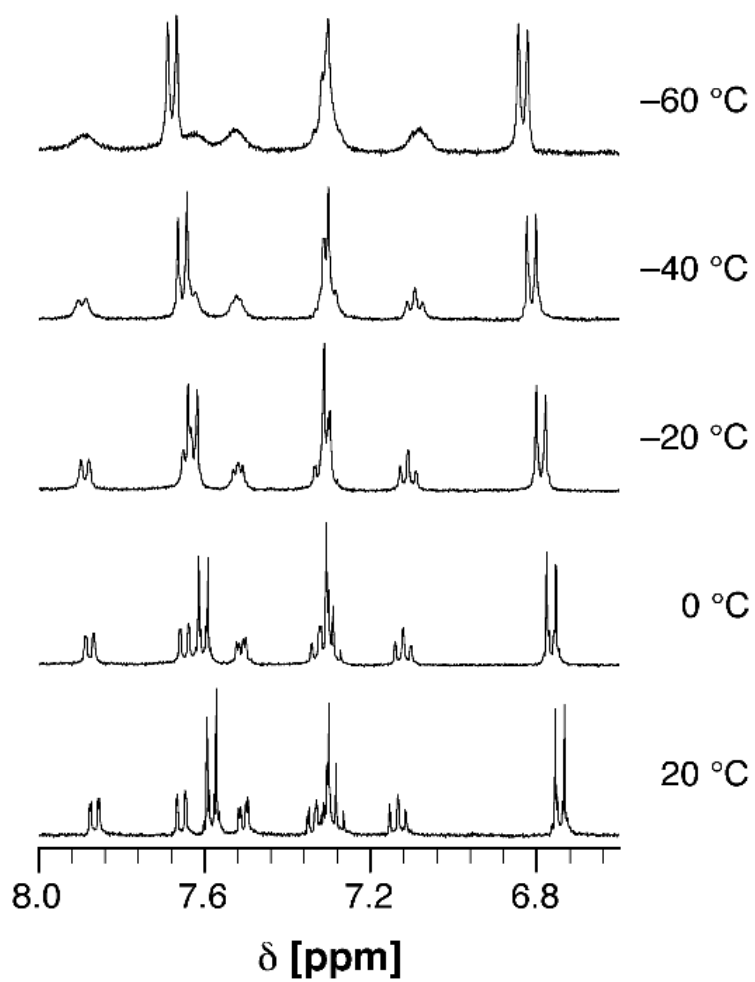


**Figure 2-1.** Variable-temperature <sup>1</sup>H NMR spectra of ligand **2-7a** in CD<sub>3</sub>OD (3 mM).

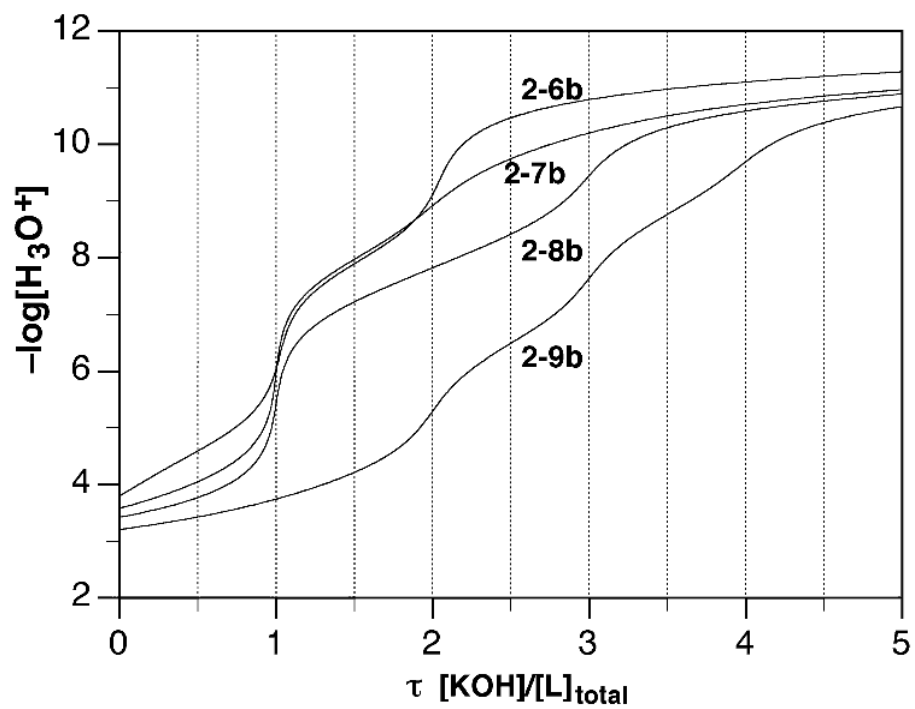


**Figure 2-2.** Potentiometric titration curves for ligands **2-6b-2-9b** in water (0.1 M KCl, 25°C; ligand concentrations (mM): **2-6b** 1.0; **2-7b** 0.47; **2-8b** 0.64; **2-9b** 0.76).

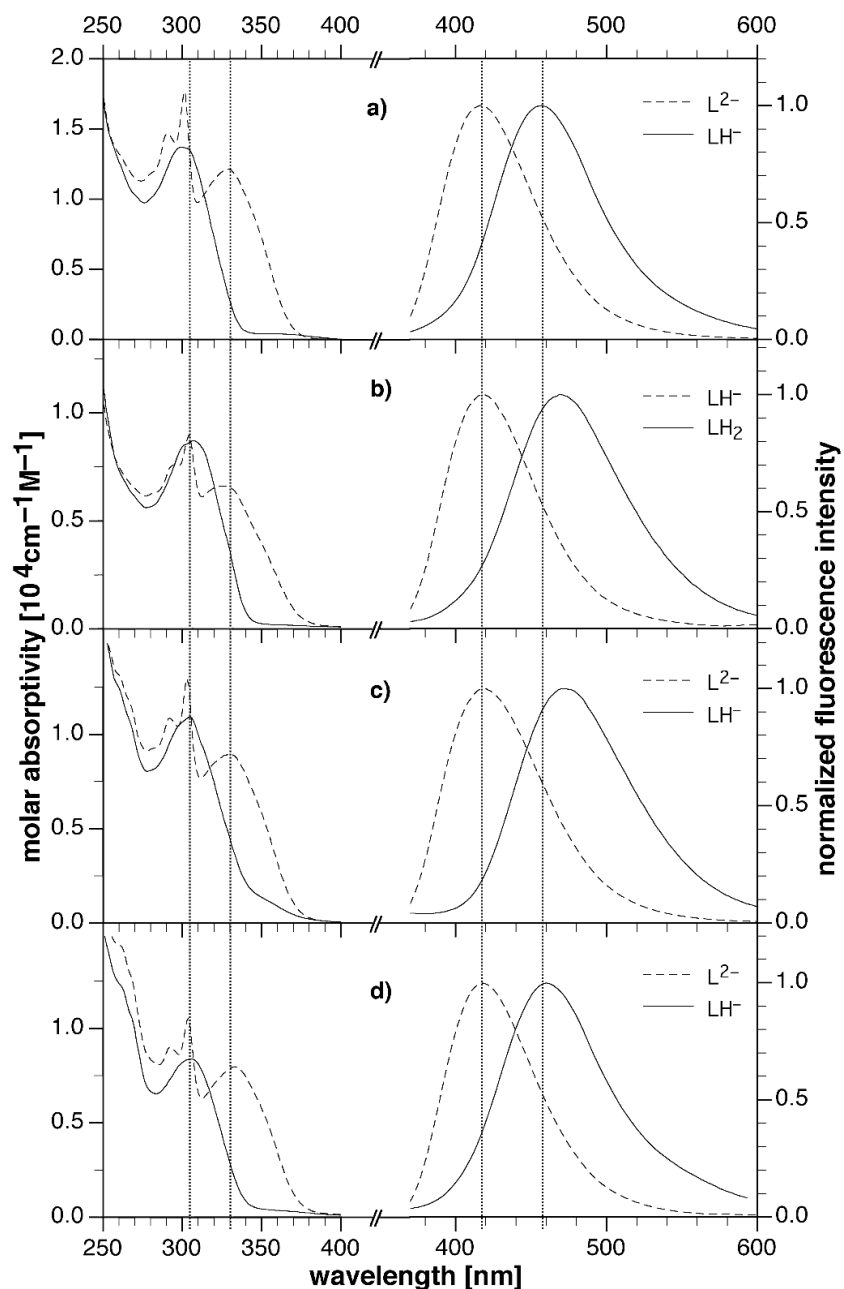


**Figure 2-3.** Comparison of the UV-visible absorption (left) and normalized fluorescence emission spectra (right) of the species with protonated (—) and deprotonated (---) sulfonamide nitrogen atom in aqueous solution (0.1 M KCl, 25°C) for ligands a) **2-6b**, b) **2-7b**, c) **2-8b**, and d) **2-9b**. The emission spectra were recorded at pH 7.2 (—) and 11.0 (---). The UV-visible traces were obtained through deconvolution of a series of spectra with pH range 7-10.

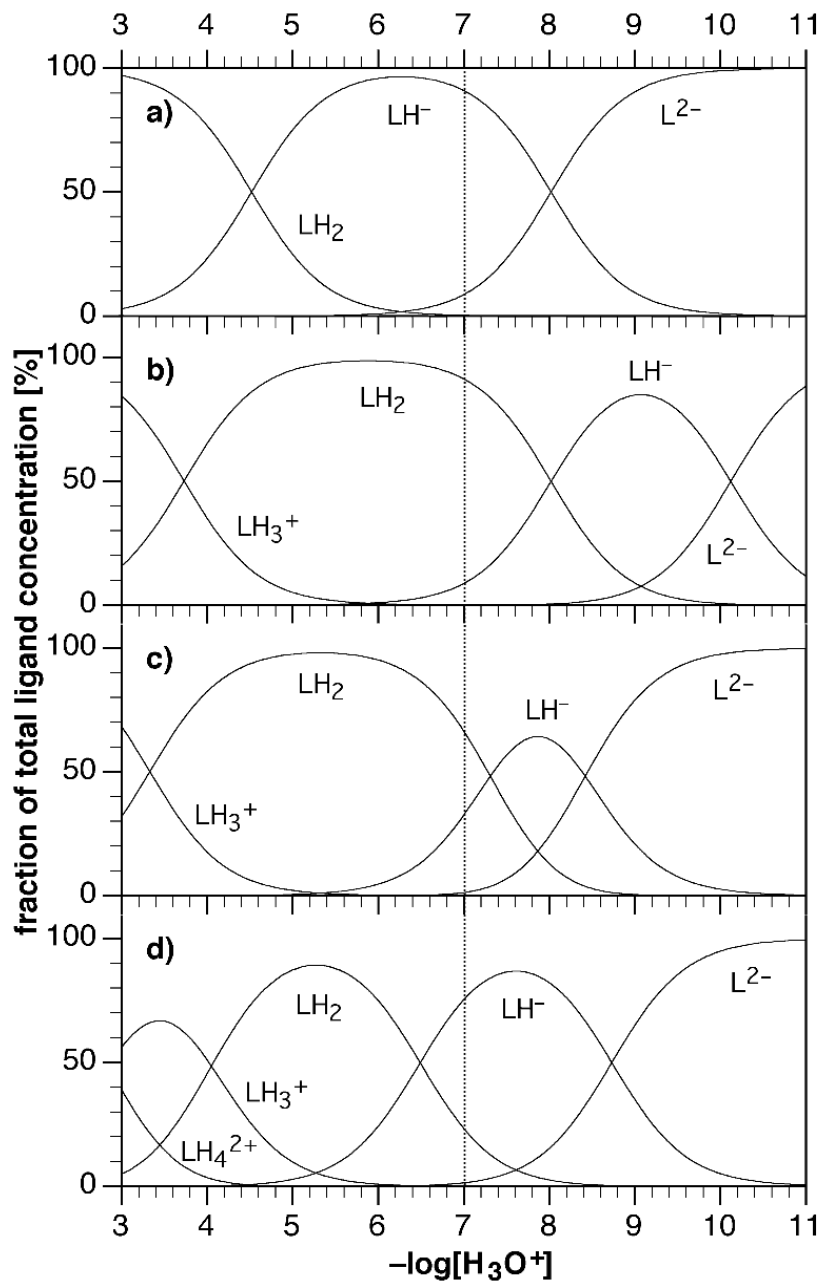


**Figure 2-4.** Calculated species distribution diagrams for ligands a) 2-6b, b) 2-7b, c) 2-8b, and d) 2-9b.

### 2.2.3. Protonation Equilibria

Because the additional binding sites might also act as protonation sites, the protonation equilibria of these four ligands could be very complicated. To clarify possibly ambiguous  $pK_a$  assignment, both potentiometric (Figure 2-2) and spectrophotometric titrations were performed.

For ligand **2-6b** and **2-7b**, potentiometric titrations were sufficient to determine the  $pK_a$  and their assignments. The observed two protonation steps for the titration of ligand **2-6b** ( $pK_a=8.0$  and  $4.5$ ) can be readily assigned to the nitrogen atom of sulfonamide moiety and the carboxylic acid moiety, respectively (Table 2-1). Ligand **2-7b** showed an additional protonation equilibrium with  $pK_a$  10.1 for the tertiary-amine substituent, while the  $pK_a$  for the carboxylic acid moiety was lowered to 3.7, presumably due to the presence of the additional cationic charge. For **2-8b** and **2-9b**, the  $pK_a$  of the picolyl substituent (possibly around 7.3)<sup>48,49</sup> and sulfonamide moiety might fall into the same range and required therefore more careful studies for an unambiguous assignment.

The carboxylic acid and picolyl substituent are decoupled from the fluorophore  $\pi$ -system and deprotonation should therefore not significant influence the absorption spectrum. However, deprotonation of the sulfonamide group is expected to give large spectral changes. Hence, spectrophotometric titrations should be well suited to determine the  $pK_a$  of the sulfonamide group.

The performed UV-vis titrations show that the  $pK_a$  of sulfonamide (8.4 for **2-8b** and

8.7 for **2-9b**) is always higher than that of picolyl substituent (7.3 for **2-8b** and 6.5 for **2-9b**). These titrations also give UV-vis spectra traces (deconvoluted by SPECFIT software package<sup>54</sup>, left in Figure 2-3) and absorption maxima (Table 2-1) of species with deprotonated or protonated sulfonamide moiety.

Based on the information above, a species distribution diagram was calculated for each fluorophore (Figure 2-4). At neutral pH, **2-8b** and **2-9b** undergo very little deprotonation of the sulfonamide species (less than 1%), therefore, spectral interference of the sulfonamide anion on ratiometric  $\text{Zn}^{2+}$  measurements should be negligible. For **2-6b** and **2-7b**, there is about 10% of sulfonamide anion present at neutral pH due to the somewhat lower  $\text{p}K_a$ 's, rendering the optimal pH range for reliable  $\text{Zn}^{2+}$  analysis slightly lower.

Upon excitation, each ligand gives a single clean emission band centered around 460 nm with a quantum yield of 9 to 32% at neutral pH (Figure 2-3, right). These spectra are independent of the excitation wavelength, suggesting the presence of only one emissive species. The large Stokes shifts averaging around  $11,000 \text{ cm}^{-1}$  are clearly due to ESIPT.<sup>44</sup> Upon deprotonation of the sulfonamide moiety, the ESIPT process is disrupted and results in a blueshifted, normal emission around 419 nm. Compared to 2-(2'-hydroxyphenyl)-benzimidazoles, which show multiple emission bands under identical condition,<sup>17, 43</sup> ligands **26b-2-9b** exhibit uniform photophysical properties, thus further demonstrating that formation of the *trans*-rotamer is unfavorable even in aqueous solution.<sup>44</sup>

**Table 2-1.** Protonation constants and photophysical data for ligands **2-6b**, **2-7b**, **2-8b**, and **2-9b** in aqueous solution.<sup>[a]</sup>

Species/Equilibrium	Data	<b>2-6b</b>	<b>2-7b</b>	<b>2-8b</b>	<b>2-9b</b>
$[\text{LH}^-]/[\text{H}^+][\text{L}^{2-}]$	$pK_1$	8.04±0.03	10.12±0.03	8.42±0.03	8.73±0.03
$[\text{LH}_2]/[\text{H}^+][\text{LH}^-]$	$pK_2$	4.50±0.03	8.02±0.03	7.31±0.03	6.49±0.03
$[\text{LH}_3^+]/[\text{H}^+][\text{LH}_2]$	$pK_3$	n/a	3.73±0.05	3.33±0.05	4.05±0.03
$[\text{LH}_4^{2+}]/[\text{H}^+][\text{LH}_3^+]$	$pK_4$	n/a	n/a	n/a	2.84±0.05
$\text{L}^{2-}$	absorption $\lambda_{\text{max}}$ [nm] <sup>[b]</sup>	301 (15870)	304 (10120) <sup>[f]</sup>	303 (15170)	304 (12320)
		329 (10920)	326 (7470) <sup>[f]</sup>	329 (10600)	332 (9220)
	excitation $\lambda_{\text{max}}$ [nm] <sup>[c]</sup>	296	299 <sup>[f]</sup>	297	297
	emission $\lambda_{\text{max}}$ [nm] <sup>[c]</sup>	418	419 <sup>[f]</sup>	419	419
	Stokes' shift (cm <sup>-1</sup> )	6470	6810 <sup>[f]</sup>	6530	6250
$\text{LH}^-$	absorption $\lambda_{\text{max}}$ [nm] <sup>[b]</sup>	299 (12300)	306 (9360) <sup>[g]</sup>	305 (12850)	305 (10100)
	excitation $\lambda_{\text{max}}$ [nm] <sup>[d]</sup>	300	309 <sup>[g]</sup>	309	308
	emission $\lambda_{\text{max}}$ [nm] <sup>[d]</sup>	460	469 <sup>[g]</sup>	471	460
	Stokes' shift (cm <sup>-1</sup> )	11700	11360 <sup>[g]</sup>	11550	11050
	quantum yield <sup>[e]</sup>	0.23	0.32 <sup>[g]</sup>	0.28	0.09

[a] 0.1 M KCl, 25°C; [b] From deconvolution analysis, molar extinction coefficient [L mol<sup>-1</sup>cm<sup>-1</sup>] in parentheses; [c] pH 11.0, 0.1 M KCl; [d] pH 7.00, 10 mM PIPES, 0.1 M KCl; [e] Quinine sulfate in 1 N H<sub>2</sub>SO<sub>4</sub> as standard; [f] Monoprotonated species LH<sup>-</sup>; [g] Diprotonated species LH<sub>2</sub>.

**Table 2-2.** Protonation constants and photophysical data for ligands **2-6b**, **2-7b**, **2-8b**, and **2-9b** in aqueous solution.<sup>[a]</sup>

Data	<b>2-6b</b>	<b>2-7b</b>	<b>2-8b</b>	<b>2-9b</b>
LogK <sup>[b]</sup>	4.50±0.04	3.09±0.04	9.23±0.04	12.10±0.04
absorption $\lambda_{\max}$ [nm] <sup>[c]</sup>	327	318	297	334
excitation $\lambda_{\max}$ [nm]	294	299	300	338
emission $\lambda_{\max}$ [nm]	406	420	415	406
Stokes' shift (cm <sup>-1</sup> )	5950	7640	9570	5310
R <sub>min</sub> F(400/500) <sup>[d]</sup>	0.44	0.15	0.24	0.14
R <sub>max</sub> F(400/500) <sup>[d]</sup>	8.46	3.06	7.34	11.6
R <sub>max</sub> /R <sub>min</sub>	19	20	30	82
quantum yield <sup>[e]</sup>	0.22	0.23	0.17	0.21

[a] 0.1M KClO<sub>4</sub>, 25°C, 10mM PIPES, pH 7.20; [b] Apparent binding constant at pH 7.20; [c] From deconvolution analysis; [d] Ratio R of fluorescence emission intensities at 400 and 500 nm; [e] Quinine sulfate in 1N H<sub>2</sub>SO<sub>4</sub> as standard.

#### 2.2.4. Complexation Studies

All zinc complexes of ligands **2-6b**, **2-7b**, **2-8b**, and **2-9b** yielded bright, blueshifted fluorescence emission in neutral buffer. The interaction of Zn<sup>2+</sup> with each ligand was investigated by spectrophotometric methods (Table 2-2). The selectivity of all four ligands towards biologically important metal cations was also explored. While the coordination of Ca<sup>2+</sup> and Mg<sup>2+</sup> does not give visible changes of fluorescence emission, the coordination of paramagnetic transition-metal cations Mn<sup>2+</sup>, Co<sup>2+</sup>, Fe<sup>2+</sup>, Ni<sup>2+</sup> and Cu<sup>2+</sup> partially or completely quenches the emission.

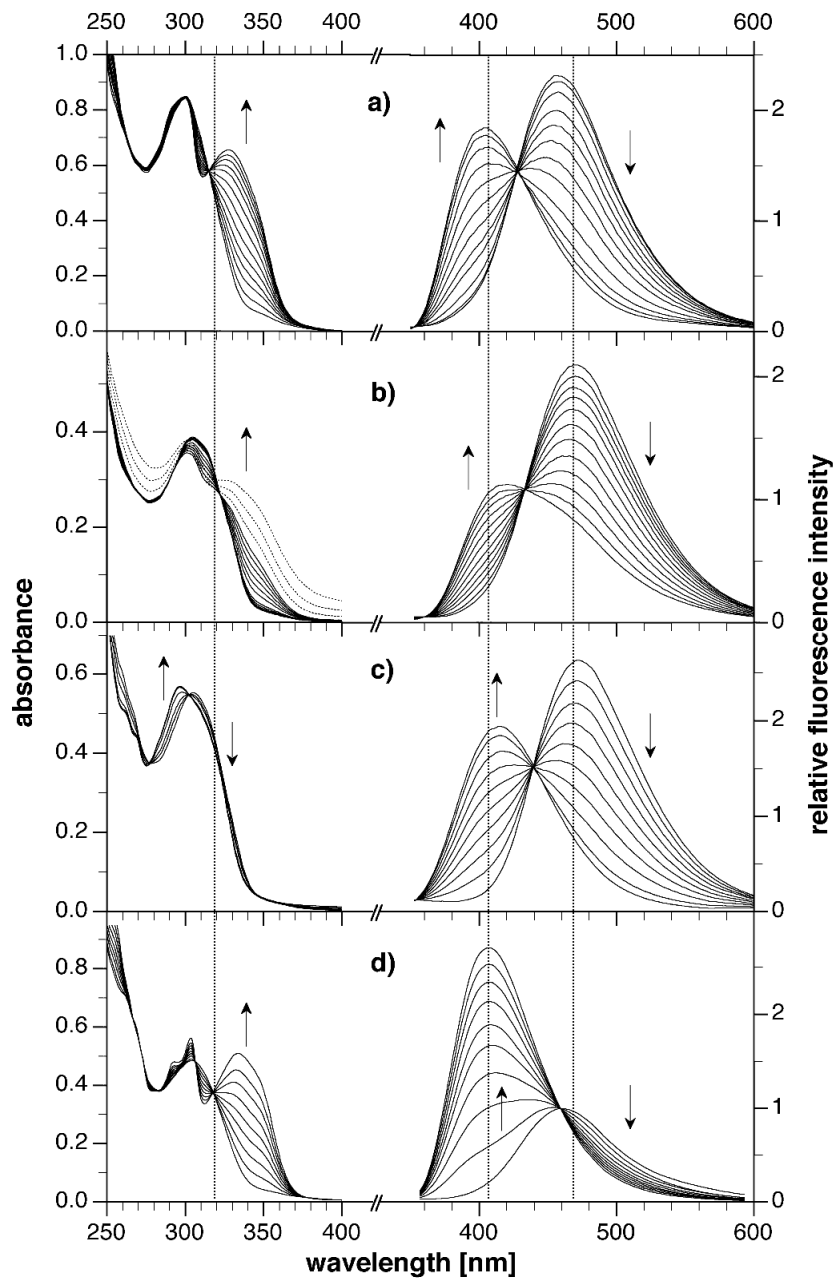


**Figure 2-5.** UV-visible absorbance (left) and fluorescence emission spectra (right) of ligands a) **2-6b**, b) **2-7b**, c) **2-8b**, and d) **2-9b** as a function of added  $Zn^{II}$  (excitation at the isobestic point of the UV-visible traces, pH 7.20, 10 mM PIPES, 0.1 M  $KClO_4$ ).

### 2.2.5. Absorption Spectra

For ligand **2-6b**, **2-7b**, and **2-9b**, the coordination of  $Zn^{2+}$  is associated with deprotonation of the sulfonamide group. Therefore, the UV-vis spectra of their zinc complexes are red-shifted, similar to the deprotonated species measured above. Upon addition of zinc triflate at neutral pH, a single isosbestic point was observed for each UV-vis spectra set (left, Figure 2-5). When  $Zn^{II}$  concentration is above 10mM, ligand **2-7b** behaves differently (Figure 2-5b, dotted lines). The continuous increase of the absorbance over the entire wavelength range contradicts the presence of a stoichiometrically well-defined complex; this is possibly a result of precipitation and/or the formation of a coordination polymer. Interestingly, coordination of  $Zn^{2+}$  with ligand **2-8b** does not give a red-shifted absorption band, thus implying that the sulfonamide nitrogen atom is not deprotonated and presumably not involved in  $Zn^{2+}$  coordination.

### 2.2.6 Emission Spectra

Upon excitation at the wavelength of the absorption isosbestic point, each fluorophore **2-6b**, **2-7b** and **2-9b** gives a set of emission spectra with a clear isosbestic point at various  $Zn^{2+}$  concentrations (Figure 2-5, right), suggesting a well defined equilibrium between free ligand and zinc complex. Interestingly, similar to the other three fluorophores, the zinc complex of ligand **2-8b** gave also a blue-shifted, normal emission upon  $Zn^{2+}$  addition, indicating that ESIPT is still disrupted even without deprotonation of the sulfonamide nitrogen. As discussed in the introduction, the ESIPT process requires

the involvement of both, proton donor (sulfonamide nitrogen) and acceptor (benzimidazole nitrogen with one lone pair). Therefore, coordination of  $Zn^{2+}$  with either group could result in the inhibition of ESIPT. On basis of this understanding, coordination of  $Zn^{2+}$  with the benzimidazole nitrogen alone led to ESIPT inhibition in case of ligand **2-8b**. This hypothesis is further supported by the apparent  $Zn^{2+}$  binding affinity of  $\log K = 9.2$  (Table 2-2), which is much higher than the apparent binding affinity of picolylamine ( $\log K = 3.1$ ).<sup>57</sup>

### 2.2.7. Apparent $Zn^{II}$ Binding Affinities

The emission responses at various  $Zn^{II}$  concentrations were analyzed by nonlinear least-squares fit method to determine the binding affinities. For ligands **2-6b** and **2-7b**, the binding affinities were directly obtained from mol-ratio plots with  $Zn^{II}$  concentrations ranging from  $10\mu M$  to  $50mM$ . It was surprising to find that the affinity of **2-6b** ( $\log K = 4.50$ ) is higher than that of **2-7b** ( $\log K = 3.09$ ), whose diethylamino moiety is a potential additionally zinc binding group. The proton equilibria data give us a hint about this confusing issue. With a relative high  $pK_a$  (10.1), the coordination of the diethylamino group with  $Zn^{2+}$  is prohibited by protonation. The introduced positive charge from the protonation is very close to the binding sites and further lowers the affinity of ligand **2-7b**. Both ligands bind  $Zn^{II}$  with a 1:1 stoichiometry.

For strong  $Zn^{II}$  binding ligands **2-8b** and **2-9b**, metal buffers ( $Zn^{II}/EGTA$  and  $Zn^{II}/HEDTA$ , respectively) were utilized to determine their relatively high affinities. The

affinity of ligand **2-9b** ( $\log K = 12.1$ ) is five log units higher than dipicolylaimie ( $\log K = 7.3^{57}$ ). Combined with the absorption spectra showing the zinc coordination with sulfonamide group, this information convinces us that ligand **2-9b** forms a pentadentate complex involving all five nitrogen-donor atoms.

### 2.2.8. Ratiometric Measurements

Ratiometric sensors determine metal concentration by the ratio  $R$  of the intensities at two different wavelengths  $\lambda_1$  and  $\lambda_2$ .<sup>45</sup> When the binding is 1:1 stoichiometry, Equation (2-4) is valid.

$$[Zn^{II}] = K_d \left( \frac{R - R_{\min}}{R_{\max} - R} \right) \frac{S_{apo}}{S_{bnd}} \quad (2-4)$$

$R_{\min}$  and  $R_{\max}$  are the limiting  $R$  values in the absence and at saturating level of  $Zn^{II}$ , respectively.  $S_{apo}$  and  $S_{bnd}$  are instrument-related factors and can be determined from the measurements of solution with known  $Zn^{II}$  and sensors concentration. The parameter  $R_{\max}/R_{\min}$  reflects the limiting dynamic range and resolution of the measurements.

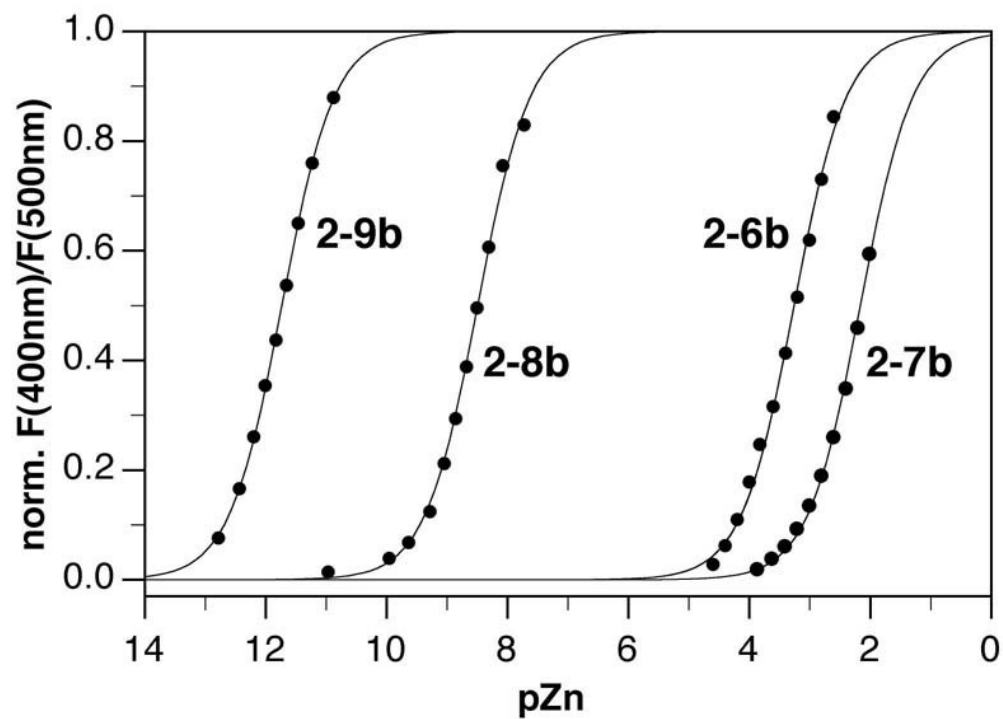


**Figure 2-6.** Change of the emission intensity ratio at 400 and 500 nm ( $\lambda_{\text{ex}} = 320$  nm) for ligands **2-6b-2-9b** as a function of free  $\text{Zn}^{\text{II}}$  ( $\text{pZn} = -\log[\text{Zn}^{\text{II}}_{\text{free}}]$ , pH 7.2, 10 mM PIPES, 0.1 M  $\text{KClO}_4$ ).

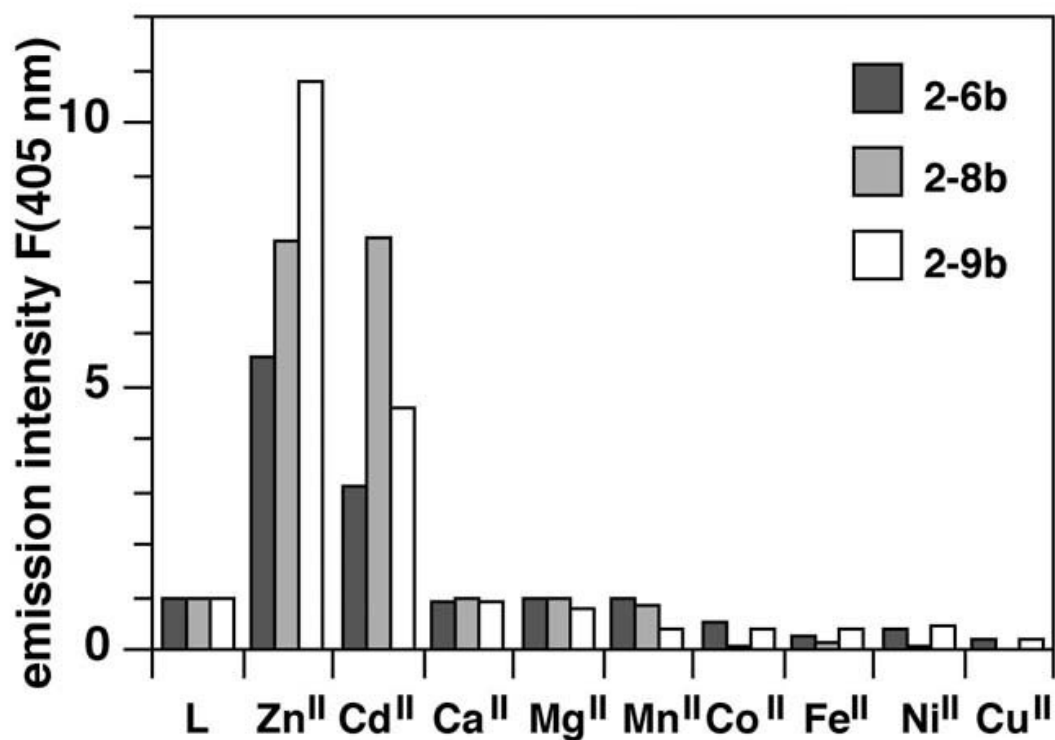


**Figure 2-7.** Emission intensity at 405 nm ( $\lambda_{\text{ex}} = 320$  nm) of ligands **2-6b**, **2-8b**, and **2-9b** in response to various metal cations. Concentrations: **2-6b** 10  $\mu\text{M}$ , all  $\text{M}^{2+}$  1 mM; **2-8b** 10  $\mu\text{M}$ ,  $\text{Ca}^{\text{II}}$ ,  $\text{Mg}^{\text{II}}$  1 mM, all other  $\text{M}^{2+}$  10  $\mu\text{M}$ ; **2-9b** 10  $\mu\text{M}$ ,  $\text{Ca}^{\text{II}}$ ,  $\text{Mg}^{\text{II}}$  1 mM, all other  $\text{M}^{2+}$  10  $\mu\text{M}$  (pH 7.2, 10 mM PIPES, 0.1 M  $\text{KClO}_4$ ).

For ligands **2-6b-2-9b**, the ratios of the emission intensities at 400 and 500 nm were determined at various  $\text{Zn}^{\text{II}}$  concentrations (Figure 2-6, the ratio  $R$  is normalized for a better comparison). Nonlinear least-squares fit analysis using Equation (2-4) gives  $R_{\text{max}}$  and  $R_{\text{min}}$  values (Table 2-2). Compared to the commercial available ratiometric  $\text{Ca}^{\text{II}}$  sensor indo-1 ( $R_{\text{max}}/R_{\text{min}} = 21$ ) and fura-2 ( $R_{\text{max}}/R_{\text{min}} = 45$ ),<sup>45</sup> ligands **2-6b-2-9b** exhibit decent  $R_{\text{max}}/R_{\text{min}}$  ratios (19-82). Because concentration measurements are only reliable between 20-80%,<sup>50</sup> the dynamic range of sensors is restricted to one log units below or above their dissociation constants. Therefore, ligands **2-6b** is suitable to measure free  $\text{Zn}^{\text{II}}$  between 30  $\mu\text{M}$  and 3 mM, and ligands **2-8b** and **2-9b** are good for concentration measurements between 0.1-10 nM and 0.2-20 pM, respectively. The dynamic range of ligand **2-7b** overlaps a lot with that of ligand **2-6b** and its binding stoichiometry is not conserved above 10mM. So this ligand was excluded from further investigation.

### 2.2.9. Selectivity Towards $\text{Zn}^{\text{II}}$

The selectivity of each ligand **2-6b**, **2-8b** and **2-9b** was investigated in two ways. Firstly, the emission intensity at the zinc complex emission maximum 405 nm was used as an indicator for the selectivity of the sensor response (Figure 2-7). While the millimolar concentrations of  $\text{Ca}^{\text{II}}$  and  $\text{Mg}^{\text{II}}$  cannot change the emission spectra, the paramagnetic transition metals  $\text{Mn}^{\text{II}}$ ,  $\text{Co}^{\text{II}}$ ,  $\text{Fe}^{\text{II}}$ ,  $\text{Ni}^{\text{II}}$  and  $\text{Cu}^{\text{II}}$  partially or completely quench the fluorescence. The response of a nonbiological metal  $\text{Cd}^{\text{II}}$  was also explored. Due to its similar coordination property to  $\text{Zn}^{\text{II}}$ ,  $\text{Cd}^{\text{II}}$  gives emission increase at 405 nm

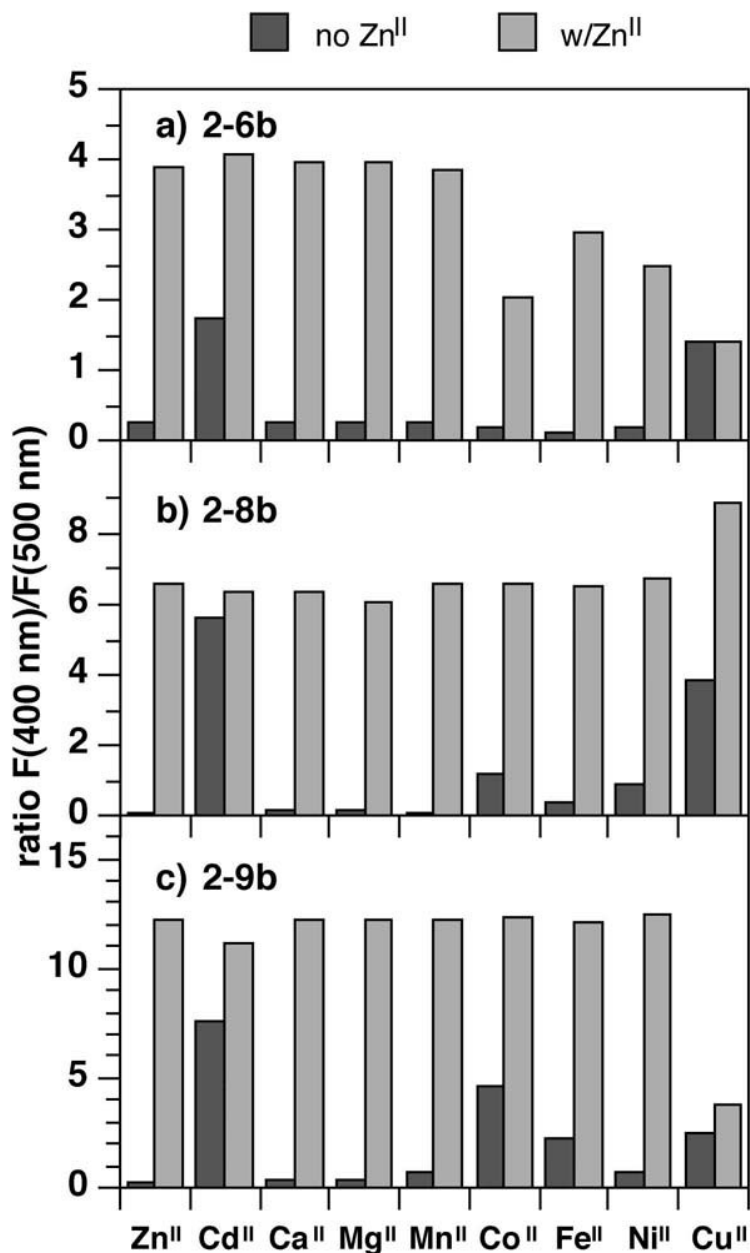


**Figure 2-8.** Emission intensity ratios at 400 and 500 nm in response to various metal cations (pH 7.2, 10 mM PIPES, 0.1 M KClO<sub>4</sub>): a) 10 μM **2-6b**, all M<sup>2+</sup> 1 mM; b) 10 μM **2-8b**, Ca<sup>II</sup>, Mg<sup>II</sup> 1 mM, all other M<sup>2+</sup> 10 μM; c) 10 μM solution of **2-9b**, Ca<sup>II</sup>, Mg<sup>II</sup> 1 mM, all other M<sup>2+</sup> 10 μM. Binding competition measurements were acquired after equilibration for 3h (**2-6b**) and 24h (**2-8b** and **2-9b**) with solutions containing equimolar concentrations of Zn<sup>II</sup> and the respective metal cation.

for each ligand, but only the response of **2-8b** is as strong as that with  $\text{Zn}^{\text{II}}$ .

Secondly, to each metal cation, the ratio  $R$  of the emission intensities at 400 and 500 nm was investigated with or without the presence of an equimolar amount of  $\text{Zn}^{\text{II}}$  (Figure 2-8). Except  $\text{Cu}^{\text{II}}$ , which actually quenches fluorescence completely, all biological metals do not interfere the response of ligand **2-8b** and **2-9b** to  $\text{Zn}^{\text{II}}$  much. Compared to these two strong binding ligands, **2-6b** shows worse selectivity, suggesting that the introduced binding moiety in **2-8b** and **2-9b** helps to increase the selectivity. The response to  $\text{Cd}^{\text{II}}$  is lower than that to  $\text{Zn}^{\text{II}}$ , indicating that binding affinity of  $\text{Cd}^{\text{II}}$  is lower than that of  $\text{Zn}^{\text{II}}$ .

### 2.3. Conclusion

To explore the potential of excited-state intramolecular proton transfer (ESIPT) for  $\text{Zn}^{\text{II}}$ -selective emission ratiometric fluorescent sensors, ligands **2-6b-2-9b** were synthesized and characterized. The ratiometric response was achieved via the spectra shift caused by the inhibition of ESIPT upon binding  $\text{Zn}^{\text{II}}$ . The 2-(2'-arylsulfonamidophenyl)benzimidazole platform allows the introduction of additional binding groups to tune the binding affinity from picomolar to millimolar and improve the  $\text{Zn}^{\text{II}}$  selectivity. However, to gain ratiometric property, these sensors have to be excited in UV range, which limits their application for fluorescence microscopy. Therefore, the future work will focus on tuning the excitation wavelength towards lower energy.

## 2.4. Experimental Section

### 2.4.1. Materials and Reagents

2-Aminobenzyl alcohol (Aldrich, 98%), 2-(2'-aminophenyl)-benzimidazole (Alfa-Aesar, 98%), phenol (Aldrich, 99%), ethyl bromoacetate (Aldrich, 98%), manganese dioxide (Aldrich, 99%), 1,2-phenylenediamine (Aldrich, 99%), copper acetate monohydrate (Aldrich, 98%), thionyl chloride (Aldrich, 99%), 2,2'-dipicolylamine (TCI, 97%), N,N-diisopropylethyl amine (Aldrich, 99%), N-(2-hydroxyethyl)-ethylenediaminetriacetic acid (HEDTA, Aldrich, 99%), ethylenebis(oxyethylenenitrilo)-tetraacetic acid (EGTA, Aldrich, 97%). NMR:  $\delta$  in ppm versus SiMe<sub>4</sub> (0 ppm, <sup>1</sup>H, 400 MHz). MS: selected peaks; m/z. Melting points are uncorrected. Flash chromatography: Merck silica gel (240-400 mesh). TLC: 0.25 mm, Merck silica gel 60 F<sub>254</sub>, visualizing at 254 nm or with 2% KMnO<sub>4</sub> solution.

### 2.4.2. Synthesis

2,3-Diaminobenzyl alcohol<sup>51</sup> **2-4** and ethyl 2-phenoxyacetate<sup>52</sup> were synthesized following the published procedures.

**Ethyl (4-chlorosulfonylphenoxy)acetate (2-2):**<sup>53</sup> Chlorosulfonic acid (7.0 mL) was added dropwise to a solution of ethyl 2-phenoxyacetate (2 g, 11 mmol) in dichloromethane (50 mL) and cooled with ice. After stirring for 3h at RT, the reaction mixture was poured into ice-cold water (20 mL) and extracted two times with diethyl ether (40 mL). The combined organic extracts were dried with anhydrous MgSO<sub>4</sub> and concentrated under reduced pressure to provide the sulfonyl chloride **2-2** as a yellowish

oil (2.40 g, 78% yield).  $^1\text{H}$  NMR ( $\text{CDCl}_3$ , 400 MHz):  $\delta$ =1.32 (t,  $J$ =7.1 Hz, 3H), 4.29 (q,  $J$ =7.1 Hz, 2 H), 4.73(s, 2 H), 7.04 (d,  $J$ =9.3Hz, 2H), 7.97 ppm (d,  $J$ =9.3Hz, 1H); MS (70 eV): m/z (%): 278/280 (39/15) [ $\text{M}^+$ ], 243(100); EI-HRMS: m/z calcd (%) for [ $\text{M}^+$ ]  $\text{C}_{10}\text{H}_{11}\text{ClO}_5\text{S}$ : 278.0016; found: 278.0049.

**Ethyl [4-(2-formylphenylsulfamoyl)phenoxy]acetate (2-3):** A mixture of **2-1** (500 mg, 4.06 mmol), **2** (1.4 g, 5.0 mmol), and pyridine (0.5 mL) in dichloromethane (5 mL) was stirred at RT for 2 h. The reaction mixture was quenched with water (50 mL) and extracted twice with dichloromethane. The combined organic extracts were dried with anhydrous  $\text{MgSO}_4$  and concentrated under reduced pressure to give ethyl [4-(2-hydroxymethylphenylsulfamoyl) phenoxy]acetate as a yellow oil (1.42 g). Without further purification, the product was dissolved in dichloromethane (10 mL) and stirred together with manganese dioxide (4.8 g) at RT overnight. The suspension was filtered through a pad of Celite and concentrated under reduced pressure. Recrystallization from ethyl acetate provided aldehyde **2-3** as a white solid (783mg, 53% yield). M.p. 83-85 °C;  $^1\text{H}$  NMR ( $\text{CDCl}_3$ , 400 MHz):  $\delta$ =1.27 (t,  $J$ =7.1 Hz, 3H), 4.24 (q,  $J$ =7.1 Hz, 2 H), 4.62 (s, 2H), 6.89 (d,  $J$ =8.7 Hz, 2 H), 7.15 (t,  $J$ =7.6 Hz, 1H), 7.49 (t,  $J$ =7.1 Hz, 1H), 7.58 (dd,  $J$ =7.4, 1.4 Hz, 1H), 7.66 (d,  $J$ =8.2 Hz, 1H), 7.81 (d,  $J$ =8.7 Hz, 2H), 9.81 (s, 1H), 10.75 ppm (s, 1H);  $^{13}\text{C}$ NMR ( $\text{CDCl}_3$ , 100 MHz):  $\delta$ =14.6, 62.0, 65.6, 115.1, 118.0, 122.1, 123.2, 129.7, 132.2, 136.0, 136.3, 140.0, 161.5, 167.9, 195.0 ppm; MS (70 eV): m/z (%): 363 (34) [ $\text{M}^+$ ], 243(3 5), 120 (100); EI-HRMS: m/z calcd for [ $\text{M}^+$ ]  $\text{C}_{17}\text{H}_{17}\text{NO}_6\text{S}$ : 363.0776; found: 363.0771; elemental analysis calcd (%) for  $\text{C}_{17}\text{H}_{17}\text{NO}_6\text{S}$  (363.4): C 56.19, H 4.72,

N 3.85; found: C 56.26, H 4.64, N 3.93.

**Ethyl {4-[2-(4-formyl-1H-benzimidazol-2-yl)phenylsulfamoyl]phenoxy}-acetate (2-5):**

Acetic acid (0.280 mL), aldehyde **2-3** (1.11 g, 3.06 mmol) in MeOH (5 mL), and copper(II) acetate monohydrate (610 mg) in water (10 mL) were sequentially added with stirring to a solution of 2,3-diaminobenzyl alcohol **2-4** (300 mg, 2.17 mmol) in EtOH/H<sub>2</sub>O (20 mL, 1:1). The mixture was heated under reflux for 3h, filtered hot, and the residue washed with water. The precipitate was redissolved in a mixture of ethanol (12 mL) and concd HCl (2.2 mL). After addition of Na<sub>2</sub>S·9H<sub>2</sub>O (1.05 g in 8 mL water) the mixture was heated under reflux for 1 h, cooled to RT, and filtered through a pad of Celite to remove the precipitated CuS. The filtrate was neutralized with aqueous NaHCO<sub>3</sub> and extracted three times with dichloromethane. The combined organic extracts were dried with MgSO<sub>4</sub> and concentrated under reduced pressure. The crude product was purified on silica gel (hexanes/ethyl acetate 1:2-1:1) to provide the hydroxymethyl-substituted benzimidazole as a glassy, yellowish solid (378 mg, 36% yield). M.p. 54-56 °C; <sup>1</sup>H NMR (CDCl<sub>3</sub>, 400 MHz) (note: tautomeric proton exchange broadens a few signals): δ=1.30 (t, *J*=7.1 Hz, 3H), 4.26 (q, *J*=7.1 Hz, 2H), 4.50 (s, 2 H), 5.02 (s, 2H), 6.39 (d, *J*=8.7 Hz, 2H), 7.09 (br s, 1 H), 7.15 (t, *J*=7.6 Hz, 2H), 7.22 (d, *J*=7.6 Hz, 1 H), 7.33 (br s, 1 H), 7.32 (t, *J*=7.6 Hz, 2H), 7.49 (d, *J*=7.6 Hz, 1H), 7.67 (br s, 1H), 7.73(d, *J*=7.6 Hz, 1H), 9.80 (br s, 1H), 9.99 ppm (br s, 1H); MS (70 eV): *m/z* (%): 481 (65) [M<sup>+</sup>], 435 (27), 312 (31), 220 (100); EI-HRMS: *m/z* calcd (%) for [M<sup>+</sup>] C<sub>24</sub>H<sub>23</sub>N<sub>3</sub>O<sub>6</sub>S: 481.1308; found: 481.1297.

The above intermediate (482 mg, 1.0 mmol) was dissolved in dichloromethane (15 mL) and stirred with manganese dioxide (1.1 g) at RT overnight. The suspension was filtered through a pad of Celite and concentrated under reduced pressure. Recrystallization from diethylether provided aldehyde **2-5** as a glassy, yellow solid (415 mg, 86% yield). M.p. 65-67 °C; <sup>1</sup>H NMR (CDCl<sub>3</sub>, 400 MHz): δ=1.24 (t, *J*=7.1 Hz, 3H), 4.21 (q, *J*=7.1 Hz, 2 H), 4.52 (s, 2 H), 6.65 (d, *J*=8.8 Hz, 2 H), 7.17 (t, *J*=8.0 Hz, 1H), 7.39 (td, *J*=8.8, 1.7 Hz, 1H), 7.49 (t, *J*=8.0 Hz, 1H), 7.64 (d, *J*=9.3Hz, 2H), 7.68 (dd, *J*=8.8, 1.1 Hz, 1H), 7.79 (dd, *J*=8.5, 1.7 Hz, 2H), 8.11 (d, *J*=7.7 Hz, 1 H), 10.11 (s, 1 H), 10.87 (br s, 1 H), 12.35 ppm (s, 2H); <sup>13</sup>C NMR (CDCl<sub>3</sub>, 100 MHz): δ=14.5, 61.9, 65.3, 114.5, 115.6, 116.4, 121.0, 121.3, 123.0, 123.8, 126.2, 126.9, 127.8, 129.3, 131.7, 132.2, 138.0, 149.0, 151.9, 160.9, 167.9, 192.4 ppm; MS (70 eV): *m/z* (%): 479 (64) [M<sup>+</sup>], 415 (25), 378 (5), 328 (50), 236 (100), 209 (11), 181 (9); EI-HRMS: *m/z* calcd (%) for [M<sup>+</sup>] C<sub>24</sub>H<sub>21</sub>N<sub>3</sub>O<sub>6</sub>S: 479.1151; found: 479.1145; elemental analysis calcd (%) for C<sub>24</sub>H<sub>21</sub>N<sub>3</sub>O<sub>6</sub>S (479.5): C 60.12, H 4.41, N 8.76; found: C 60.24, H 4.49, N 8.66.

**Ethyl {4-[2-(1H-benzimidazol-2-yl)phenylsulfamoyl]phenoxy}acetate (2-6a):** A solution of 2-(2'-aminophenyl)benzimidazole (310 mg, 1.48 mmol) and **2-2** (500 mg, 1.79 mmol) in pyridine (3mL) was stirred for 2 h. The reaction mixture was diluted with water (20 mL) and extracted twice with ethyl acetate (40 mL). The combined organic extracts were dried with MgSO<sub>4</sub> and concentrated under reduced pressure. The crude product was purified by flash chromatography on silica gel (hexanes/ethyl acetate 2:1) to give ligand **2-6a** as a yellowish solid (400 mg, 60% yield). M.p. 134-136 °C; <sup>1</sup>H NMR

([D<sub>6</sub>]DMSO, 400 MHz):  $\delta$ =1.12 (t,  $J$ =6.6 Hz, 3H), 4.08 (q,  $J$ =7.1 Hz, 2H), 4.77 (s, 2 H), 6.92 (d,  $J$ =8.8 Hz, 2H), 7.19 (t,  $J$ =7.7 Hz, 1H), 7.28-7.31 (m, 2 H), 7.40 (t,  $J$ =7.7 Hz, 1 H), 7.60 (d,  $J$ =8.8 Hz, 1 H), 7.64-7.67 (m, 4H), 8.02 (d,  $J$ =8.2 Hz, 1 H), 13.23 ppm (s, 2H); <sup>13</sup>C NMR (CDCl<sub>3</sub>, 100 MHz):  $\delta$ =14.8, 61.5, 65.4, 115.7, 116.4, 119.2, 123.8, 124.0, 128.0, 129.5, 131.5, 131.8, 151.0, 161.5, 168.5, 168.5 ppm; MS (70 eV): m/z (%): 451.1 (44) [M<sup>+</sup>], 387.1 (14), 300.1 (40), 208.1 (100); EI-HRMS: m/z calcd (%) for [M<sup>+</sup>] C<sub>23</sub>H<sub>21</sub>N<sub>3</sub>O<sub>5</sub>S: 451.1202; found: 451.1189; elemental analysis calcd (%) for C<sub>23</sub>H<sub>21</sub>N<sub>3</sub>O<sub>5</sub>S (451.5): C 61.18, H 4.69, N 9.31; found: C 61.09, H 4.72, N 9.36.

**4-[2-(1H-Benzimidazol-2-yl)phenylsulfamoyl]phenoxy}acetic acid (2-6b)**: Ethyl ester **2-6a** (170 mg, 0.38 mmol) was added to a solution of LiOH·H<sub>2</sub>O (350 mg) in a mixture of methanol (1 mL) and water (1 mL). The mixture was stirred at RT for 1 h, and the organic solvent subsequently removed under reduced pressure. The aqueous residue was acidified by the addition of 1M HCl and the product then extracted twice with ethyl acetate. The combined organic extracts were dried with MgSO<sub>4</sub> and concentrated under reduced pressure to provide acid **2-6b** as a yellowish solid (140 mg, 88% yield). For the photophysical studies a sample of the compound (10 mg) was further purified by semipreparative reversed-phase HPLC (10×300 mm C18 column, CH<sub>3</sub>CN/H<sub>2</sub>O (0.01%TFA) 75:25-98:2); M.p. 140 °C (decomp); <sup>1</sup>H NMR ([D<sub>6</sub>]DMSO, 400 MHz):  $\delta$ =4.66 (s, 2H), 6.90 (d,  $J$ =8.8 Hz, 2 H), 7.19 (t,  $J$ =7.7 Hz, 1H), 7.28-7.31 (m, 2H), 7.40 (t,  $J$ =7.7 Hz, 1 H), 7.60 (d,  $J$ =8.8 Hz, 1 H), 7.65-7.67 (m, 4 H), 8.02 (d,  $J$ =8.2 Hz, 1 H), 13.23 ppm (s, 2H); MS (70 eV): m/z (%): 423(20) [M<sup>+</sup>], 300 (17), 208 (100); EI-HRMS:

m/z calcd (%) for  $[M^+]$   $C_{21}H_{17}N_3O_5S$ : 423.0889; found: 423.0863.

**Ethyl {4-{2-[4-[(diethylamino)methyl]-1H-benzimidazol-2-yl]phenylsulfamoyl}phenoxy}acetate (2-7a)**: Diethyl amine (31 mL, 0.292 mmol) and sodium triacetoxyborohydride (66 mg, 0.313 mmol) were added to a solution of aldehyde **2-5** (100 mg, 0.209 mmol) in 1,2-dichloroethane (15 mL). The reaction mixture was allowed to stir for 2.5 h under  $N_2$  and was then quenched by the addition of 1M aqueous  $NH_4OH$  (3mL). The product was extracted twice with dichloromethane and the combined organic extracts were dried with  $MgSO_4$ . The organic solvent was evaporated under reduced pressure and the residue purified by using flash chromatography on silica gel (dichloromethane/methanol/TFA 50:1:0.25-50:1:0.5) to provide ligand **2-7a** as a glassy, pale yellow solid (85 mg, 76% yield). M.p. 54-56°C;  $^1H$  NMR ( $CDCl_3$ , 400 MHz):  $\delta$ =1.15 (t,  $J$ =7.1 Hz, 3H), 1.23 (t,  $J$ =7.1 Hz, 6H), 2.68 (q,  $J$ =6.9 Hz, 4 H), 4.01 (s, 2 H), 4.20 (q,  $J$ =7.1 Hz, 2H), 4.52 (s, 2 H), 6.70 (d,  $J$ =8.8 Hz, 2 H), 7.08-7.13(m, 2 H), 7.20 (t,  $J$ =7.7 Hz, 1H), 7.30 (t,  $J$ =7.7 Hz, 1 H), 7.30 (t,  $J$ =8.2 Hz, 1 H), 7.63(br s, 1H), 7.67 (d,  $J$ =7.7 Hz, 1H), 7.70-7.74 (m, 3H), 9.44 (br s, 1H), 12.52 ppm (br s, 1H);  $^{13}C$  NMR ( $CDCl_3$ , 100 MHz):  $\delta$ =8.1, 10.5, 43.2, 52.2, 57.9, 61.4, 110.6, 112.7, 114.6, 116.3, 118.9, 119.1, 119.6, 120.6, 122.3, 122.6, 125.4, 126.8, 128.6, 129.5, 134.0, 145.7, 156.8, 164.0 ppm; MS (70 eV): m/z (%): 536 (1)  $[M^+]$ , 507 (52), 465 (100), 222 (100), 72 (25); EI-HRMS: m/z calcd (%) for  $[M^+]$   $C_{28}H_{32}N_4O_5S$ : 536.2093; found: 536.2065; elemental analysis calcd (%) for  $C_{28}H_{32}N_4O_5S \cdot 0.5H_2O$  (545.7): C 61.63, H 6.10, N 10.27; found: C 61.83, H 6.13, N 9.93.

**{4-{2-{4-[(Diethylamino)methyl]-1H-benzimidazol-2-yl}phenylsulfamoyl}-phenoxy}**

**acetic acid (2-7b):** Ethyl ester **2-7a** (22 mg, 0.041 mmol) was hydrolyzed as described for acid **2-6b** to provide the free acid **2-7b** (12 mg, 58%). M.p. 225-227 °C; <sup>1</sup>H NMR (CD<sub>3</sub>OD, 400 MHz): δ=1.42 (t, *J*=7.1 Hz, 6H), 3.35 (q, *J*=7.4 Hz, 4H), 3.63 (br s, 1H), 4.34 (s, 2H), 4.74 (s, 2H), 6.61 (d, *J*=8.2 Hz, 2 H), 7.24 (t, *J*=7.4 Hz, 1 H), 7.32 (d, *J*=7.7 Hz, 2H), 7.34-7.45 (m, 3 H), 7.69 (t, *J*=6.9 Hz, 2H), 7.81 ppm (dd, *J*=8.7, 1.1 Hz, 1H); MS (70 eV): *m/z* (%): 509 (100) [M+1]<sup>+</sup>, 435 (5), 338 (15), 295 (44); ESI-TOF-HRMS: *m/z* calcd (%) for [M+1]<sup>+</sup> C<sub>26</sub>H<sub>29</sub>N<sub>4</sub>O<sub>5</sub>S: 509.1859; found: 509.1884.

**Ethyl {4-{2-{4-[(methylpyridin-2-ylmethylamino)methyl]-1H-benzimidazol-2-yl}**

**phenylsulfamoyl}phenoxy}acetate (2-8a):** Prepared as described for **2-7a** by reductive amination of aldehyde **2-5** (100 mg, 0.209 mmol) with methyl picolylamine<sup>54</sup> (100 mg, 0.819 mmol), providing **2-8a** as a glassy, pale yellow solid (119 mg, 97% yield). M.p. 56-58 °C; <sup>1</sup>H NMR (CDCl<sub>3</sub>, 400 MHz): δ=1.22 (t, *J*=7.1 Hz, 3H), 2.29 (s, 3H), 3.74 (s, 2H), 3.89 (s, 2H), 4.18 (q, *J*=7.1 Hz, 2 H), 4.41 (s, 2 H), 6.64 (m, 2 H), 7.03(d, *J*= 7.1 Hz, 1H), 7.14-7.18 (m, 3H), 7.27 (d, *J*=7.7 Hz, 1 H), 7.33 (td, *J*=7.7, 1.7 Hz, 1 H), 7.65 (dd, *J*=7.7, 2.2 Hz, 1 H), 7.68-7.73(m, 3H), 7.78 (dd, *J*=8.2, 1.1 Hz, 1H), 8.18 (d, *J*=7.7 Hz, 1 H), 8.43(d, *J*=4.4 Hz, 1H), 13.48 ppm (br s, 2H); <sup>13</sup>C NMR (CDCl<sub>3</sub>, 100 MHz): δ=14.4, 43.0, 58.8, 61.8, 63.1, 65.3, 114.5, 117.6, 118.2, 120.3, 122.1, 122.5, 122.8, 123.4, 123.6, 123.9, 127.2, 129.4, 130.5, 132.8, 133.1, 137.3, 138.0, 143.0, 149.2, 150.5, 159.0, 160.6, 167.9 ppm; MS (70 eV): *m/z* (%): 586 (100) [M+1]<sup>+</sup>, 344 (13), 293 (27); ESI-TOF-HRMS: *m/z* calcd (%) for [M+1]<sup>+</sup> C<sub>31</sub>H<sub>32</sub>N<sub>5</sub>O<sub>5</sub>S: 586.2124; found: 586.2089;

elemental analysis calcd (%) for C<sub>31</sub>H<sub>31</sub>N<sub>5</sub>O<sub>5</sub>S (585.7): C 63.57, H 5.34, N 11.96; found: C 63.57, H 5.44, N 11.78.

**{4-{2-{4-[(Methylpyridin-2-ylmethylamino)methyl]-1H-benzimidazol-2-yl}phenyl-sulfamoyl}phenoxy}acetic acid (2-8b)**: Ethyl ester **2-8a** (40 mg, 0.068 mmol) was hydrolyzed as described for acid 6b to give free acid **2-8b** (23 mg, 61%). M.p. 133-135°C; <sup>1</sup>H NMR (CDCl<sub>3</sub>, 400 MHz): δ=2.47 (s, 3H), 3.63 (br s, 1H), 4.08 (s, 2H), 4.22 (s, 2 H), 4.36 (s, 2H), 6.40 (d, *J*= 8.3Hz, 2 H), 7.06-7.18 (m, 4H), 7.28 (d, *J*=6.1 Hz, 2 H), 7.31 (d, *J*=7.7 Hz, 4H), 7.69 (d, *J*=6.7 Hz, 2H), 7.75 (d, *J*=7.1 Hz, 2 H), 8.55 ppm (d, *J*=4.4 Hz, 1H); MS (70 eV): *m/z* (%): 558 (100) [M+1]<sup>+</sup>, 344 (5), 279, (19); ESI-TOF-HRMS: *m/z* calcd (%) for [M+1]<sup>+</sup> C<sub>29</sub>H<sub>28</sub>N<sub>5</sub>O<sub>5</sub>S: 558.1811; found: 558.1846.

**Ethyl {4-{2-{4-[(bispyridin-2-ylmethylamino)methyl]-1H-benzimidazol-2-yl}phenylsulfamoyl}phenoxy}acetate (2-9a)**: Prepared as described for **2-7a** by reductive amination of aldehyde **2-5** (40 mg, 0.083mmol) with 2,2'-dipicolylamine (22 mg, 0.11 mmol), providing **2-9a** as a glassy solid (44 mg, 80% yield). M.p. 65-67 8C; <sup>1</sup>H NMR (CDCl<sub>3</sub>, 400 MHz): δ=1.23(t, *J*=7.1 Hz, 3H), 3.89 (s, 2 H), 3.91 (s, 4 H), 4.19 (q, *J*=7.1 Hz, 2 H), 4.41 (s, 2H), 6.66 (d, *J*=9.3Hz, 2 H), 7.09-7.20 (m, 4H), 7.25 (d, *J*=7.6 Hz, 2H), 7.36 (td, *J*=8.5, 1.4 Hz, 1H), 7.54 (td, *J*=7.6, 1.6 Hz, 2H), 7.72-7.77 (m, 3H), 7.81 (dd, *J*=8.2, 1.1 Hz, 1H), 8.17 (dd, *J*=7.9, 1.1 Hz, 1H), 8.40 (d, *J*=3.8 Hz, 2H), 13.20 (br s, 2H), 14.11 ppm (s, 1H); <sup>13</sup>C NMR (CDCl<sub>3</sub>, 400 MHz): δ=14.5, 56.5, 59.9, 61.9, 65.4, 114.6, 118.6, 120.6, 122.3, 122.6, 123.0, 123.3, 123.6, 123.7, 126.9, 129.5, 130.6, 133.0, 133.3, 137.1, 138.1, 143.0, 149.0, 150.6, 159.2, 160.7, 167.9 ppm; MS (70 eV): *m/z* (%): 662 (5)

[M<sup>+</sup>], 570 (100), 465 (13), 222 (40), 198 (53), 93 (78); EI-HRMS: m/z calcd (%) for [M<sup>+</sup>] C<sub>36</sub>H<sub>34</sub>N<sub>6</sub>O<sub>5</sub>S: 662.2311; found: 662.2276; elemental analysis calcd (%) for C<sub>36</sub>H<sub>34</sub>N<sub>6</sub>O<sub>5</sub>S·0.5H<sub>2</sub>O (671.8): C 64.37, H 5.25, N 12.51; found: C 64.76, H 5.13, N 12.16.

**{4-{2-{4-[(Bispyridin-2-ylmethylamino)methyl]-1H-benzimidazol-2-yl}-phenylsulfamoyl}phenoxy}acetic acid (2-9b):** Ethyl ester **2-9a** (22 mg, 0.033 mmol) was hydrolyzed as described for acid **2-6b** to give free acid **2-9b** (16 mg, 76%). For all photophysical studies a sample of the compound (10 mg) was further purified by semipreparative reversed-phase HPLC (10×300 mm C18 column, CH<sub>3</sub>CN/H<sub>2</sub>O (0.01%TFA) 75:25-98:2). M.p. 80-82 °C; <sup>1</sup>H NMR (CDCl<sub>3</sub>, 400 MHz): δ=3.91 (s, 4H), 3.99 (s, 2 H), 4.39 (s, 2 H), 6.50 (d, *J*=8.7 Hz, 2 H), 7.06 (d, *J*=7.1 Hz, 1H), 7.16 (t, *J*=7.6 Hz, 4 H), 7.25 (s, 2H), 7.38 (t, *J*=7.6 Hz, 1H), 7.52 (d, *J*=8.7 Hz, 2H), 7.59 (td, *J*=7.6, 1.4 Hz, 2H), 7.68 (d, *J*=7.6 Hz, 1H), 7.83(d, *J*=8.2 Hz, 1H), 8.00 (d, *J*=7.6 Hz, 1H), 8.40 ppm (d, *J*=4.9 Hz, 2H); FABMS (thioglycerol): m/z (%): 635 (100) [M<sup>+</sup>], 373 (62); FAB-HRMS: m/z calcd (%) for [M+H]<sup>+</sup> C<sub>34</sub>H<sub>31</sub>N<sub>6</sub>O<sub>5</sub>S: 635.2077; found: 635.2119.

### 2.4.3. Steady-state Absorption and Fluorescence Spectroscopy

All sample stock solutions and buffer solutions were filtered through 0.2 mm Nylon membrane filters to remove interfering dust particles or fibers. UV/Vis absorption spectra were recorded at 25 °C by using a Varian Cary Bio50 UV/Vis spectrometer with constant-temperature accessory. Steady-state emission and excitation spectra were

recorded with a PTI fluorimeter and FELIX software. Throughout the titration the sample solution was stirred with a magnetic stirring device. For all titrations the path length was 1 cm with a cell volume of 3.0 mL. All fluorescence spectra have been corrected for the spectral response of the detection system (emission correction file provided by the instrument manufacturer) and for the spectral irradiance of the excitation channel (by using a calibrated photodiode). Quantum yields were determined by using quinine sulfate dihydrate in 1.0 N H<sub>2</sub>SO<sub>4</sub> ( $\Phi_f = 0.54 \pm 0.03$ ) as the fluorescence standard.<sup>55</sup>

#### **2.4.4. Electrode Calibration in Aqueous Solution**

Measurements were performed with an Orion microcombination glass electrode. The electrode was calibrated for  $-\log[\text{H}_3\text{O}^+]$  by titration of a standardized HCl solution (Aldrich, 0.1N volumetric standard) with KOH (Aldrich, 0.1N volumetric standard) at 25 °C and 0.1M ionic strength (KCl). The endpoint, electrode potential, and slope were determined by using Gran's method<sup>56</sup> as implemented in the software GLEE.<sup>57</sup> The calibration procedure was repeated three times prior to each  $\text{p}K_a$  value determination. The electrode potential was measured with the Corning pH/Ion Analyzer 355 and the emf measurements were reproducible with  $\pm 0.1$  mV accuracy.

#### **2.4.5. Potentiometry**

All protonation constants reported in this study were determined from potentiometric titrations and additionally confirmed by spectrophotometric measurements.

Potentiometric titrations were carried out with a motorized burette (Dosimat, Metrohm, Switzerland) by adding a total of 40-100 aliquots of KOH (0.1M) to 10.0 mL of a solution of the corresponding ligand (0.5-1.0 mM) in KCl (0.1M) under a N<sub>2</sub> atmosphere (solvent-vapor-saturated gas). Throughout the titration, the temperature was maintained at 25±0.1 °C by circulating constant-temperature water through the water-jacket of the titration cell. For the potentiometric titration of ligands **2-7b**, **2-8b**, and **2-9b**, the initial solution was further acidified by adding 1-3 molar equivalents of HCl (0.5M). The emf data were converted to  $-\log[\text{H}_3\text{O}^+]$  based on the electrode potential  $E^\circ$  and slope, which were determined as described above prior to each titration. The  $pK_a$  values were obtained from nonlinear least-squares fit analysis of the potentiometric data.<sup>58</sup>

#### **2.4.6. Spectrophotometric Titrations**

The UV/Vis absorption spectra of the ligands were monitored for a series of solutions in which  $-\log[\text{H}_3\text{O}^+]$  was varied between 5 and 11. The emf of each solution was directly measured in the UV quartz cell (electrode diameter 3mm) and converted to  $-\log[\text{H}_3\text{O}^+]$  using the  $E^\circ$  and slope, as obtained from the electrode calibration procedure described above. The raw spectral and emf data were processed with nonlinear least-squares fit analysis using the SPECFIT software package.<sup>59</sup>

#### **2.4.7. Complex stability constants**

All reported stability constants  $K$  were measured at pH 7.2 (PIPES 10 mM, 0.1M

KClO<sub>4</sub> ionic background) and refer to apparent stability constants.<sup>60</sup>

*Determination of the apparent Zn<sup>II</sup> affinity of ligands 2-6b and 2-7b:* UV/Vis spectrophotometric titrations were performed with a 60 μM solution (3.0 mL cell volume) of the corresponding ligand in PIPES buffer (10mM, pH 7.20, 0.1M KClO<sub>4</sub>) over the range of 4 logarithmic units of free Zn<sup>II</sup>. The recorded spectra were processed by nonlinear least-squares fit analysis using the SPECFIT software package.<sup>53</sup> The resulting binding affinities are apparent stability constants, and are defined by Equation (2-1):

$$K' = \frac{[ZnL]}{[Zn]([L] + [LH] + [LH_2] + \dots [LH_m])} \quad (2-1)$$

in which [ZnL]=concentration of zinc-ligand complex, [Zn]=concentration of unbound Zn<sup>II</sup>, ([L]+[LH]+...[LH<sub>m</sub>])=concentration of all ligand species that do not involve Zn<sup>II</sup> (at given conditions of pH 7.2, 0.1M KClO<sub>4</sub>, 25 °C).<sup>54</sup>

*Determination of the apparent Zn<sup>II</sup> affinity of ligand 2-8b and 2-9b:* A series of PIPES-buffered solutions (10mM, pH 7.20, 0.1M KClO<sub>4</sub>) were prepared that contained HEDTA (HEDTA = N-(2-hydroxyethyl)ethylenediaminetriacetic acid, 10mM) or EGTA (EGTA = ethylenebis(oxyethylenenitrilo)tetraacetic acid, 10mM) and between 1-9mM of Zn(OTf)<sub>2</sub>. The concentration of free Zn<sup>II</sup> was calculated using the program Hyss,<sup>61</sup> based on the following published pK<sub>a</sub> and logK values for HEDTA, pK<sub>1</sub> = 9.87, pK<sub>2</sub> = 5.38, pK<sub>3</sub> = 2.62, pK<sub>4</sub> = 1.60, logK(ZnL) = 14.6 (25 °C, μ = 0.1), and EGTA, pK<sub>1</sub> = 9.40, pK<sub>2</sub> =

8.79,  $pK_3 = 2.70$ ,  $\log K(\text{ZnL}) = 12.6$  (25 °C,  $\mu = 0.1$ ).<sup>62</sup> According to Martell and Smith,<sup>56</sup> the tabulated  $pK_a$  data must be corrected upward by 0.11 to account for 0.1M ionic strength. This correction is necessary because the tabulated  $pK_a$  values are determined on the basis of the concentration and not the activity of the hydronium ions. For the calculation of the free  $\text{Zn}^{\text{II}}$  concentrations, the published  $pK_a$  values of HEDTA and EGTA were therefore corrected by 0.11. Ligands **2-8b** or **2-9b** were dissolved in 3.0 mL of the corresponding buffer solutions up to a final concentration of 10  $\mu\text{M}$ . After a 24 h equilibration time, the fluorescence intensity at 400 and 500 nm was determined. The experimental data were analyzed by a nonlinear least-squares fit algorithm with the following formalisms: By assuming a 1:1 metal-to-ligand stoichiometry, the following relationship [Eq. (2-2)] was found between the free  $\text{Zn}^{\text{II}}$  concentration, apparent dissociation constant  $K_d$ , and fluorescence intensity  $F$ :<sup>45</sup>

$$[\text{Zn}] = K_d \frac{F - F_{\min}}{F_{\max} - F} \quad (2-2)$$

in which  $F_{\min}$  = fluorescence intensity of free ligand,  $F_{\max}$  = fluorescence intensity of  $\text{Zn}^{\text{II}}$ -bound ligand.

Using Equation (2-2) the emission intensity  $F$  can be expressed as a function of free  $\text{Zn}^{\text{II}}$  and  $K_d$ , as shown in Equation (2-3):

$$F = \frac{[Zn]F_{\max} + K_d F_{\min}}{K_d + [Zn]} \quad (2-3)$$

Nonlinear least-squares fit analysis of the experimental intensities versus the calculated free Zn<sup>II</sup> concentrations allowed for the determination of  $F_{\max}$ ,  $F_{\min}$ , and  $K_d$ .

## 2.5. References:

1. Weller, A. Z. *Elektrochem.* **1956**, *60*, 1144.
2. Weller, A. *Prog. React. Kinet.* **1961**, *1*, 188.
3. Sandros, K. *Acta Chem. Scand.* **1976**, *A30*, 761.
4. Smith, K. K.; Kaufmann, K. J. *J. Phys. Chem.* **1978**, *82*, 2286.
5. Rodriguez-Santiago, L.; Sodupe, M.; Oliva, A.; Bertran, J. *J. Am. Chem. Soc.* **1999**, *1*, 8882.
6. Lamola, A. A.; Sharp, L. J. *J. Phys. Chem.* **1966**, *60*, 2634.
7. Sengupta, P. K.; Kasha, M. *Chem. Phys. Lett.* **1979**, *68*, 382.
8. McMorow, D.; Kasha, M. *J. Phys. Chem.* **1984**, *88*, 2235.
9. Wolfbeis, O. S.; Leiner, M.; Hochmuth, P.; Geiger, H. *Ber. Bunsen-Ges. Phys. Chem.* **1984**, *88*, 759.
10. Martinez, M. L.; Studer, S. L.; Chou, P. T. *J. Am. Chem. Soc.* **1991**, *113*, 5881.
11. Van Benthem, M. H.; Gillispie, G. D. *J. Phys. Chem.* **1984**, *88*, 2954.
12. Jang, D. J.; Kelley, D. F. *J. Phys. Chem.* **1985**, *89*, 209.
13. Williams, D. L.; Heller, A. *J. Phys. Chem.* **1970**, *74*, 4473.
14. Itoh, M.; Fujiwara, Y. *J. Am. Chem. Soc.* **1985**, *107*, 1561.
15. Frey, W.; Laermer, F.; Elsaesser, T. *J. Phys. Chem.* **1991**, *95*, 10391.
16. Das, K.; Sarkar, N.; Majumdar, D.; Bhattacharyya, K. *Chem. Phys. Lett.* **1992**, *198*, 443.
17. Mosquera, M.; Penedo, J. C.; Ríos Rodríguez, M. C.; Rodríguez-Prieto, F. *J. Phys.*

*Chem.* **1996**, *100*, 5398.

18. Roberts, E. L.; Dey, J.; Warner, I. M. *J. Phys. Chem. A* **1997**, *101*, 5296.
19. Sinha, H. K.; Dogra, S. K. *Chem. Phys.* **1986**, *102*, 337.
20. Grellmann, K. H.; Mordzinski, A.; Heinrich, A. *Chem. Phys.* **1989**, *136*, 201.
21. Itoh, M.; Fujiwara, Y. *J. Am. Chem. Soc.* **1985**, *107*, 1561.
22. Nagaoka, S.; Itoh, A.; Mukai, K.; Hoshimoto, E.; Hirota, N. *Chem. Phys. Lett.* **1992**, *192*, 532.
23. Stephan, J. S.; Grellmann, K. H. *J. Phys. Chem.* **1995**, *99*, 10066.
24. Elsaesser, T.; Schmetzer, B.; Lipp, M.; Baeuerle, R. J. *Chem. Phys. Lett.* **1988**, *148*, 112.
25. Tanaka, K.; Deguchi, M.; Yamaguchi, S.; Yamada, K.; Iwata, S. *J. Heterocycl. Chem.* **2001**, *38*, 131.
26. Otterstedt, J. E. A. *J. Chem. Phys.* **1973**, *58*, 5716.
27. Heller, H. J.; Blattmann, H. R. *Pure Appl. Chem.* **1973**, *36*, 141.
28. Wiechmann, M.; Port, H.; Laermer, F.; Frey, W.; Elsaesser, T. *Chem. Phys. Lett.* **1990**, *165*, 28.
29. Wiechmann, M.; Port, H.; Frey, W.; Laermer, F.; Elsaesser, T. *J. Phys. Chem.* **1991**, *95*, 1918.
30. Parthenopoulos, D. A.; McMorro, D.; Kasha, M. *J. Phys. Chem.* **1991**, *95*, 2668.
31. Chou, P.-T.; Martinez, M. L.; Clements, J. H. *Chem. Phys. Lett.* **1993**, *204*, 395.
32. Sytnik, A.; Kasha, M. *Radiat. Phys. Chem.* **1993**, *41*, 331.

33. Chou, P. T.; Martinez, M. L. *Radiat. Phys. Chem.* **1993**, *41*, 373.
34. Renschler, C. L.; Harrah, L. A. *Nucl. Instrum. Methods Phys. Res. Sect. A* **1985**, *A235*, 41.
35. Keck, J.; Kramer, H. E. A.; Port, H.; Hirsch, T.; Fischer, P.; Rytz, G. *J. Phys. Chem.* **1996**, *100*, 14468.
36. O'Connor, D. B.; Scott, G. W.; Coulter, D. R.; Yavrouian, A. *J. Phys. Chem.* **1991**, *95*, 10252.
37. Sytnik, A.; Kasha, M. *Proc. Natl. Acad. Sci. U.S.A.* **1994**, *91*, 8627.
38. Sytnik, A.; Gormin, D.; Kasha, M. *Proc. Natl. Acad. Sci. U.S.A.* **1994**, *91*, 11968.
39. Sytnik, A.; Del Valle, J. C. *J. Phys. Chem.* **1995**, *99*, 13028.
40. Frey, W.; Elsaesser, T. *Chem. Phys. Lett.* **1992**, *189*, 565.
41. Marks, D.; Proposito, P.; Zhang, H.; Glasbeek, M. *Chem. Phys. Lett.* **1998**, *289*, 535.
42. Barbara, P. F.; Walsh, P. K.; Brus, L. E. *J. Phys. Chem.* **1989**, *93*, 29.
43. Henary, M. M.; Fahrni, C. J. *J. Phys. Chem. A* **2002**, *106*, 5210.
44. Fahrni, C. J.; Henary, M. M.; VanDerveer, D. G. *J. Phys. Chem. A* **2002**, *106*, 7655.
45. Grynkiewicz, G.; Poenie, M.; Tsien, R. Y. *J. Biol. Chem.* **1985**, *260*, 3440.
46. Minkin, V. I.; Garnovskii, A. D.; Elguero, J.; Katritzky, A. R.; Denisko, O. V. *Adv. Heterocycl. Chem.* **2000**, *76*, 157.
47. Elguero, J.; Marzin, C.; Katritzky, A. R.; Linda, P. *Adv. Heterocycl. Chem., Suppl. 1*, 1976.

48. Romary, J. K.; Barger, J. D.; Bunds, J. E. *Inorg. Chem.* **1968**, *7*, 1142.
49. Gruenwedel, D. W. *Inorg. Chem.* **1968**, *7*, 495.
50. Deranleau, D. A. *J. Am. Chem. Soc.* **1969**, *91*, 4044.
51. Kwok, W. H.; Zhang, H.; Payra, P.; Duan, M.; Hung, S.-C.; Johnston, D. H.; Gallucci, J.; Skrzypczak-Jankun, E.; Chan, M. K. *Inorg. Chem.* **2000**, *39*, 2367.
52. Canonne, P.; Belley, M.; Fytas, G.; Plamondon, J. *Can. J. Chem.* **1988**, *66*, 168.
53. Bonnat, M.; Bradley, M.; Kolburn, J. D. *Tetrahedron Lett.* **1996**, *37*, 5409.
54. Holzgrabe, U. *Arch. Pharm.* **1987**, *320*, 647.
55. Demas, J. N.; Crosby, G. A. *J. Phys. Chem.* **1971**, *75*, 991.
56. Gran, G. *Analyst* **1951**, *77*, 661.
57. Gans, P.; O'Sullivan, B. *Talanta* **2000**, *51*, 33.
58. Martell, A. E.; Motekaitis, R. J. *The Determination and Use of Stability Constants*, VCH, New York, **1992**.
59. Binstead, R. A.; Zuberbühler, A. D. SPECFIT Global Analysis System, Spectrum Software Associates, Marlborough MA 01752, **2001**.
60. Schwarzenbach, G. *Complexometric Titrations*, Interscience, New York, **1957**.
61. Alderighi, L.; Gans, P.; Ienco, A.; Peters, D.; Sabatini, A.; Vacca, A. *Coord. Chem. Rev.* **1999**, *184*, 311.
62. Martell, A. E.; Smith, R. M.; NIST Critical Stability Constants of Metal Complexes, NIST Standard Reference Database 46, Version 5.0, **1998**.

## CHAPTER III

### EXCITED STATE INTRAMOLECULAR PROTON TRANSFER IN 2-(2'-ARYLSULFONAMIDOPHENYL)BENZIMIDAZOLE DERIVATIVES: THE EFFECT OF DONOR AND ACCEPTOR SUBSTITUENTS

#### 3.1. Introduction

The study of 2'-(sulfonamidophenyl)benzimidazole derivatives in Chapter 2 revealed their great potential as emission ratiometric zinc(II)-selective fluorescence sensors. However, these fluorophores need to be excited at UV range to gain ratiometric property and the optical setting of standard fluorescence microscopes prohibits the transmission of light at wavelength below 350 nm. Thus, in order to use these sensors for biological imaging applications, their peak absorption has to be shifted toward lower energy, which can be achieved by decreasing the HOMO-LUMO gap of the fluorophore  $\pi$ -system.

In our previous work, the orbital surfaces of the HOMO and LUMO orbitals of 2-(2'-tosylaminophenyl)benzimidazole (TPBI) were calculated by quantum chemical methods (Figure 3-1).<sup>1</sup> These results showed that the LUMO density at position 4' is significantly higher than the HOMO density, and conversely, the HOMO density at position 6(5) is much higher than the LUMO density. On basis of these data it should be possible to decrease HOMO-LUMO energy difference by either introducing an electron

withdrawing group at position 4' (and thus stabilizing the LUMO more than the HOMO) or by introducing an electron donating group at position 6 (thus destabilizing the HOMO more than the LUMO).

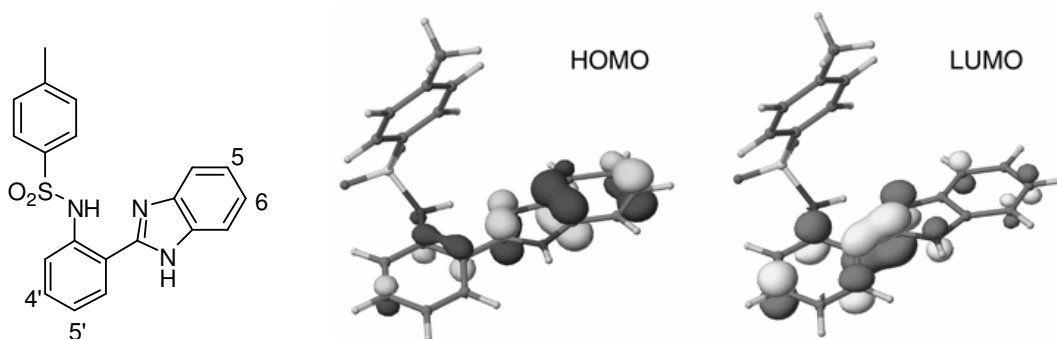


**Figure 3-1.** Molecular orbital surfaces of the HOMO and LUMO responsible for the lowest energy transition in the UV-vis spectrum of 2-(2'-tosylaminophenyl)benzimidazole (TPBI) (CI-ZINDO calculation).<sup>1</sup>

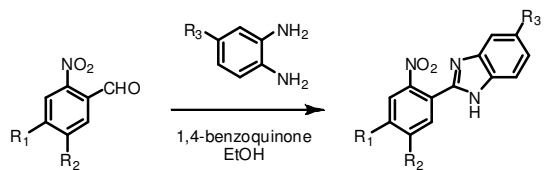
By selecting methoxy and dimethylamino groups as electron-donating substituents and cyano and thiazolyl groups as electron-withdrawing groups, a series of water-soluble 2-(2'-arylsulfonamidophenyl)benzimidazole derivatives were synthesized containing structural modification at the 4', 5' and 6(5) position. Detailed photophysical studies were then performed to experimentally determine the effect of donor and acceptor substituents on the absorption and emission properties of this compound class. Since the corresponding Zn(II) complexes are expected to exhibit similar absorption and emission spectra compared to the fully deprotonated species  $L^{2-}$ , the discussion of the photophysical properties will focus entirely on the deprotonated species as substitute.

## 3.2. Results and Discussion

### 3.2.1. Synthesis

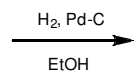
Sulfonyl chloride **3-10** was synthesized as described in Chapter 2 following a modified published procedure.<sup>2</sup> There are two key steps for the synthesis of all derivatives (Scheme 3-1): 1) the condensation reaction of the aniline and sulfonyl chloride to form the sulfonamide moiety, and 2) the oxidative coupling reaction of the corresponding benzaldehyde with phenylenediamine to install the benzimidazole ring system. Depending on the order of these two steps, two distinct routes (A and B) could be principally used for the synthesis of the target fluorophores. Since the nitro-benzaldehyde precursors (**3-1a-e**) are readily accessible or commercially available, fluorophores **3-3a-e** were synthesized according to route A. Thus, in the first step, benzimidazoles **3-2a-e** were synthesized, followed by hydrogenation to form the aniline intermediates **3-3a-e**. Coupling with sulfonyl chloride<sup>2</sup> **3-10** concluded then the synthesis for the products **3-4a-e**. Conversely, the aniline precursors (**3-7i-l**) were the preferred starting materials for route B; therefore, installation of the sulfonamide was performed first (**3-8i-l**), followed by MnO<sub>2</sub> oxidation of the alcohol to the aldehydes **3-9i-l** and the coupling reaction to form the benzimidazoles (**3-4i-l**). In case of fluorophores **3-4f-h**, the nitro-benzaldehydes (**3-1f-g**) were first hydrogenated to anilines (**3-6f-g**, route B), followed by installation of the sulfonamide (**3-9f-g**) and coupling to form the desired benzimidazoles (**3-4f-h**). Hydrolysis of the ethyl esters was performed under mild conditions with lithium hydroxide in MeOH-water-THF.

Route A

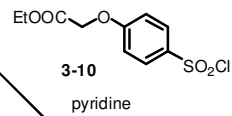


- 3-1a** R<sub>1</sub> = H, R<sub>2</sub> = H  
**3-1b** R<sub>1</sub> = CN, R<sub>2</sub> = H  
**3-1d** R<sub>1</sub> = 2-thiazolyl, R<sub>2</sub> = H  
**3-1e** R<sub>1</sub> = OCH<sub>3</sub>, R<sub>2</sub> = H

**3-2a-e**

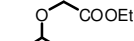


**3-3a-e**

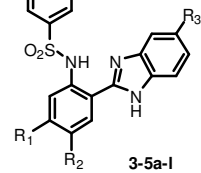
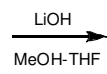


**3-10**

pyridine

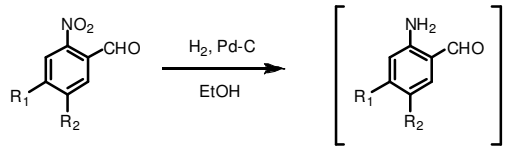


**3-4a-l**



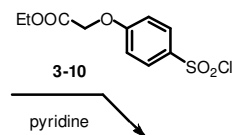
**3-5a-l**

Route B



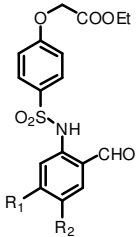
- 3-1f** R<sub>1</sub> = H, R<sub>2</sub> = OCH<sub>3</sub>  
**3-1g** R<sub>1</sub> = H, R<sub>2</sub> = N(CH<sub>3</sub>)<sub>2</sub>

- 3-6f** R<sub>1</sub> = H, R<sub>2</sub> = OCH<sub>3</sub>  
**3-6g** R<sub>1</sub> = H, R<sub>2</sub> = N(CH<sub>3</sub>)<sub>2</sub>

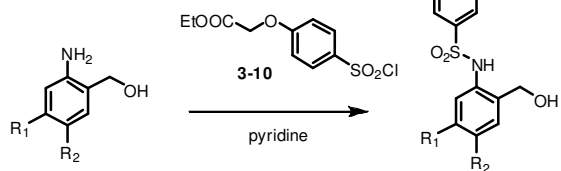


**3-10**

pyridine



- 3-9f** R<sub>1</sub> = H, R<sub>2</sub> = OCH<sub>3</sub>  
**3-9g** R<sub>1</sub> = H, R<sub>2</sub> = N(CH<sub>3</sub>)<sub>2</sub>  
**3-9i** R<sub>1</sub> = H, R<sub>2</sub> = H  
**3-9l** R<sub>1</sub>-R<sub>2</sub> = -OCH<sub>2</sub>O-

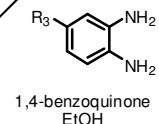


**3-10**

pyridine

- 3-8i** R<sub>1</sub> = H, R<sub>2</sub> = H  
**3-8l** R<sub>1</sub>-R<sub>2</sub> = -OCH<sub>2</sub>O-

- 3-7i** R<sub>1</sub> = H, R<sub>2</sub> = H  
**3-7l** R<sub>1</sub>-R<sub>2</sub> = -OCH<sub>2</sub>O-



**3-10**

EtOH

<b>3-4/5</b>	R <sub>1</sub>	R <sub>2</sub>	R <sub>3</sub>
a	H	H	H
b	CN	H	H
c	CN	H	OCH <sub>3</sub>
d	2-thiazolyl	H	H
e	OCH <sub>3</sub>	H	H
f	H	OCH <sub>3</sub>	H
g	H	N(CH <sub>3</sub> ) <sub>2</sub>	H
h	H	OCH <sub>3</sub>	CN
i	H	H	CN
k	H	H	OCH <sub>3</sub>
l	-OCH <sub>2</sub> O-		H

Scheme 3-1

### 3.2.2. Protonation Equilibria

As previously described in Chapter 2, deprotonation of the sulfonamide group is associated with a bathochromic shift in the absorption spectra and a hypsochromic shift in the fluorescence spectra. To study the effects of substituents without being misled by pH-dependent changes, the UV-vis and fluorescence emission spectra were therefore measured at well-defined protonation states. Hence, the protonation equilibria of each compound were first analyzed by means of spectrochemical UV-vis titrations with  $-\log[\text{H}_3\text{O}^+]$  ranging between 5 and 11. The absorption spectra of the fully deprotonated  $\text{L}^{2-}$  and monoprotinated species  $\text{HL}^-$  were then obtained from deconvolution of the UV-vis traces over the entire spectral range using a non-linear least-squares fitting procedure.

The determined  $\text{p}K_{\text{a}}$  values are shown in Table 3-1 and all spectral data are listed in Table 3-2. The  $\text{p}K_{\text{a}1}$  is associated with a large shift in the absorption spectrum, and thus can be assigned to deprotonation of the sulfonamide group. In contrast,  $\text{p}K_{\text{a}2}$  gives rise to only small absorption change and must be therefore associated with deprotonation of the carboxylic acid group, which is electronically decoupled from the conjugated  $\pi$ -system of the fluorophore. Due to the presence of the dimethylamino substituent, compound **3-5g** has an additional protonation equilibrium with  $\text{p}K_{\text{a}}$  at 8.0, thus resulting in different  $\text{p}K_{\text{a}}$  assignments.

As evident from Table 3-1, the  $\text{p}K_{\text{a}}$  value of the sulfonamide group varies from 6.7

to 9.3 and strongly depends on the nature of the substituent and its attachment position. The explanation of this observation requires careful evaluation of the resonance stabilization and inductive effects of the substituents and can be readily quantified by Hammett's free energy relationship (Figure 3-2).<sup>2</sup> The acidity constant of the derivatives with two substituents (**3-5c** and **3-5h**) show the influence of both groups; however, the substituent on the central benzene ring appears to be more important.

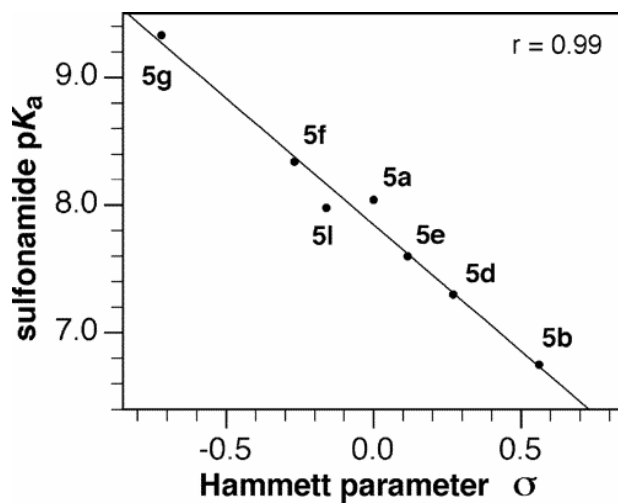


**Figure 3-2** Linear dependence of the sulfonamide acidity ( $pK_{a1}$ ) on Hammett's  $\sigma$  parameters<sup>3</sup> for monosubstituted fluorophores **3-5a**, **3-5b**, **3-5d-3-5g**, and **3-5l** ( $r$  = correlation coefficient).

**Table 3-1.** Protonation Constants of Benzimidazole Derivatives **3-5a-3-5l** in Aqueous Solution<sup>a</sup>

	substituents			$pK_{a1}^b$	$pK_{a2}^c$	$-\log[H_3O^+]^d$	$[L^{2-}]/[L]_{tot}$ [%] <sup>e</sup>
	R <sub>1</sub>	R <sub>2</sub>	R <sub>3</sub>				
<b>3-5a<sup>f</sup></b>	H	H	H	8.04 ± 0.03	4.46 ± 0.08	7.0	4
<b>3-5b</b>	CN	H	H	6.75 ± 0.02	n.d. <sup>g</sup>	5.2	3
<b>3-5c</b>	CN	H	OCH <sub>3</sub>	6.88 ± 0.03	n.d. <sup>g</sup>	5.2	3
<b>3-5d</b>	2-thiazolyl	H	H	7.30 ± 0.01	n.d. <sup>g</sup>	6.0	3
<b>3-5e</b>	OCH <sub>3</sub>	H	H	7.60 ± 0.01	4.79 ± 0.03	6.2	3
<b>3-5f</b>	H	OCH <sub>3</sub>	H	8.34 ± 0.01	4.53 ± 0.06	6.5	<1
<b>3-5g</b>	H	N(CH <sub>3</sub> ) <sub>2</sub>	H	9.33 ± 0.05	8.01 ± 0.02 <sup>h</sup>	6.7	<1
<b>3-5h</b>	H	OCH <sub>3</sub>	CN	7.96 ± 0.02	5.51 ± 0.1	6.7	5
<b>3-5i</b>	H	H	CN	7.63 ± 0.02	5.21 ± 0.1	6.5	6
<b>3-5k</b>	H	H	OCH <sub>3</sub>	7.95 ± 0.02	4.91 ± 0.1	6.5	3
<b>3-5l</b>	-OCH <sub>2</sub> O-		H	7.98 ± 0.01	4.65 ± 0.02	6.3	1

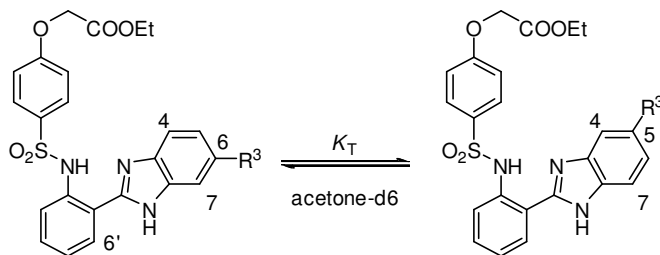
[a] 0.1 M KCl, 25 °C. [b]  $K_{a1} = [L^{2-}][H^+]/[LH^-]$ . [c]  $K_{a2} = [LH^-][H^+]/[LH_2]$ . [d] Proton concentration used for photophysical characterization of  $LH^-$ . [e] Residual concentration of fully deprotonated  $L^{2-}$ . [f] Data from ref 2. [g] Spectral deconvolution insufficient for accurate determination. [h] Protonation of the carboxylate group occurs at  $pK_{a3} = 4.81 \pm 0.05$ .

**Table 3-2.** Photophysical Data of Benzimidazole Derivatives **3-5a-3-5l** in Aqueous Solution<sup>a</sup>

	monoprotonated species (LH <sup>+</sup> )				deprotonated species (L <sup>2-</sup> )				isosbestic point [nm]	emission shift [nm] <sup>e</sup>
	abs $\lambda_{\max}$ [nm] <sup>b</sup>	em $\lambda_{\max}$ [nm] <sup>c</sup>	Stokes shift [cm <sup>-1</sup> ]	$\Phi_F^c$	abs $\lambda_{\max}$ [nm] <sup>b</sup>	em $\lambda_{\max}$ [nm] <sup>d</sup>	Stokes shift [cm <sup>-1</sup> ]	$\Phi_F^d$		
<b>3-5a<sup>f</sup></b>	300	460	11,590	0.23	329	418	6470	0.26	315	42
<b>3-5b</b>	319	483 (404)	10,640	0.37	355	447	5800	0.70	341	36
<b>3-5c</b>	341	481	8540	0.46	362	452	5500	0.34	350	29
<b>3-5d</b>	331	484 (403)	9550	0.41	361	475	6650	0.42	352	9
<b>3-5e</b>	305	432	9640	0.17 <sup>g</sup>	329	396	5140	0.06	314	36
<b>3-5f</b>	298	497	13,440	0.14	334	444	7420	0.27	322	53
<b>3-5g</b>	273	568 (448)	14,760 <sup>h</sup>	<0.01	348	505	8930	0.08	296	63
<b>3-5h</b>	306	534	13,950	0.03	340	480	8580	0.02	326	54
<b>3-5i</b>	307	489	12,120	0.25	333	452	7910	0.29	320	37
<b>3-5k</b>	316	452	9520	0.13	333	416	5990	0.29	320	36
<b>3-5l</b>	314	459	10,060	0.04	340	423	5770	0.04	326	36

[a] 0.1 M KCl, 25 °C. [b] From deconvolution analysis. [c] At the proton concentration as indicated in Table 3-1; excitation at isosbestic point. [d] pH 10.8, 0.1 M KCl. [e] Difference of peak emission wavelength of species LH<sup>+</sup> and L<sup>2-</sup>. [f] Data from ref 2. [g] Excitation at 370 nm increases the quantum yield to 0.35. [h] Based on excitation spectrum acquired at 650 nm.

### 3.2.3. Ground-State Tautomerism



**Scheme 3-2**

It is known that 1*H*-benzimidazole derivatives undergo rapid annular tautomerization in solution.<sup>2,4</sup> With the introduction of substituent R<sup>3</sup>, the N1(H)/N3(H) prototropic equilibrium will lead to a nondegenerate tautomer pair (Scheme 3-2). The equilibrium constant  $K_T$  is directly related to the concentration ratio of two tautomers and can be used to calculate their stability difference ( $\Delta G_T = -RT \ln K_T$ ).

Temperature dependent <sup>1</sup>H NMR spectroscopy was used to investigate the effect of the electron-withdrawing group 5(6)-cyano (**3-4i**, Figure 3-3) and the electron-donating group 5(6)-methoxy (**3-4k**) on the energy difference of the two tautomers. While the tautomerization rate does not reach the slow-exchange limit in protic solvents<sup>2</sup>, the solution in acetone-*d*<sub>6</sub> gives two-sets of well-resolved signals at -60°C. For compound **3-4i**, the equilibrium constant ( $K_T = 1.43 \pm 0.008$ ) of two tautomers can be calculated through the integration intensity ratio of C4(H) and C7(H) resonances at 8.43 and 8.11 ppm, which also gives the free energy difference of two tautomers ( $\Delta G_T = 0.63 \pm 0.01$  kJ mol<sup>-1</sup>)

To find out which of the two tautomers is more stable in solution, 2D NOESY NMR experiments were performed at  $-80^{\circ}$  in acetone- $d_6$  (Figure 3-4). This temperature is sufficiently low to slow down the exchange kinetics and thus to yield two well-separated benzimidazole NH resonances. Since the N1(H) proton is in NOE contact with the proton C7(H), it is straight forward to assign the corresponding singlet of the proton C7(H) to the 6-substituted species. By comparing the integrations of the proton C7(H) of 6-substituted species and the proton C4(H) of 5-substituted species, the concentration ratio of two tautomers was calculated. As shown in Figure 3-4a, for the cyano-substituted derivative **3-4i**, the 5-substituted species is more stable, a finding that is consistent with recent quantum chemical calculation results.<sup>5</sup> For the methoxy-substituted derivative **3-4k**, unlike **3-4i**, the 6-substituted species is actually more stable ( $K_T = 0.66 \pm 0.01$ ,  $\Delta G_T = 0.66 \pm 0.01$  KJ mol<sup>-1</sup>), indicating that the resonance effect of the substituent is the major reason for the stability difference of two tautomers.

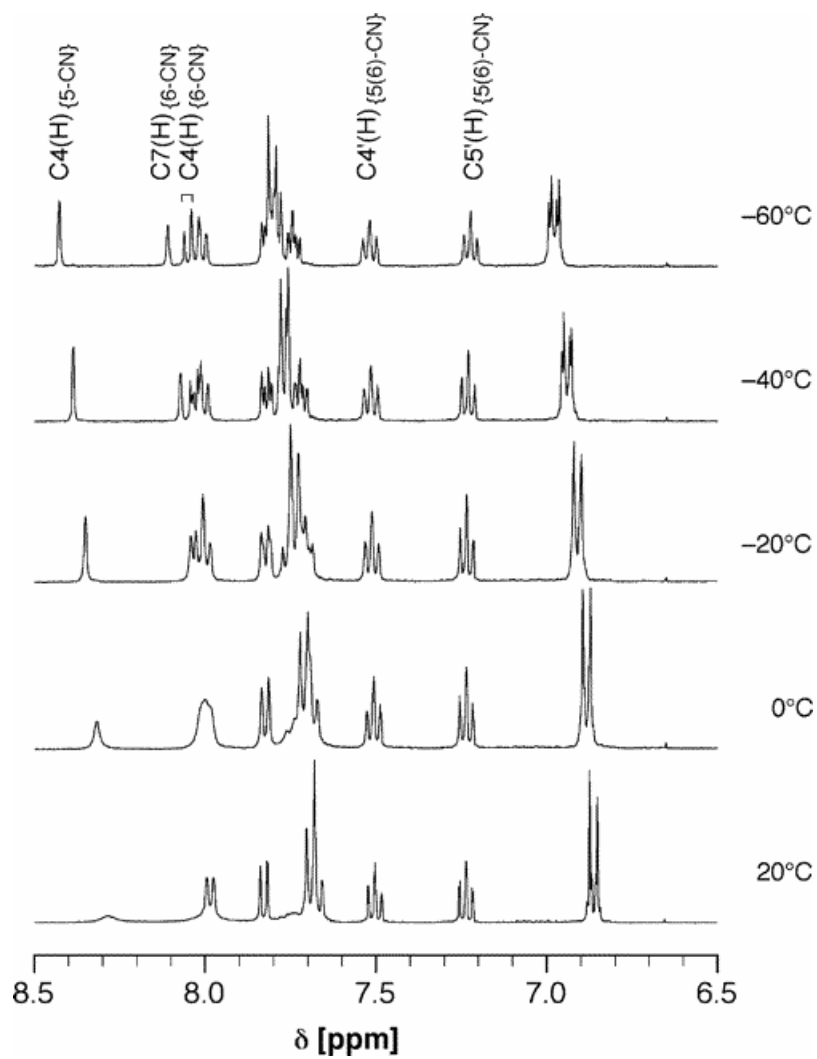


**Figure 3-3.** Variable temperature <sup>1</sup>H NMR spectra 5(6)-cyano-substituted benzimidazole derivative **3-4i** in aceton-*d*<sub>6</sub> (20 mM).

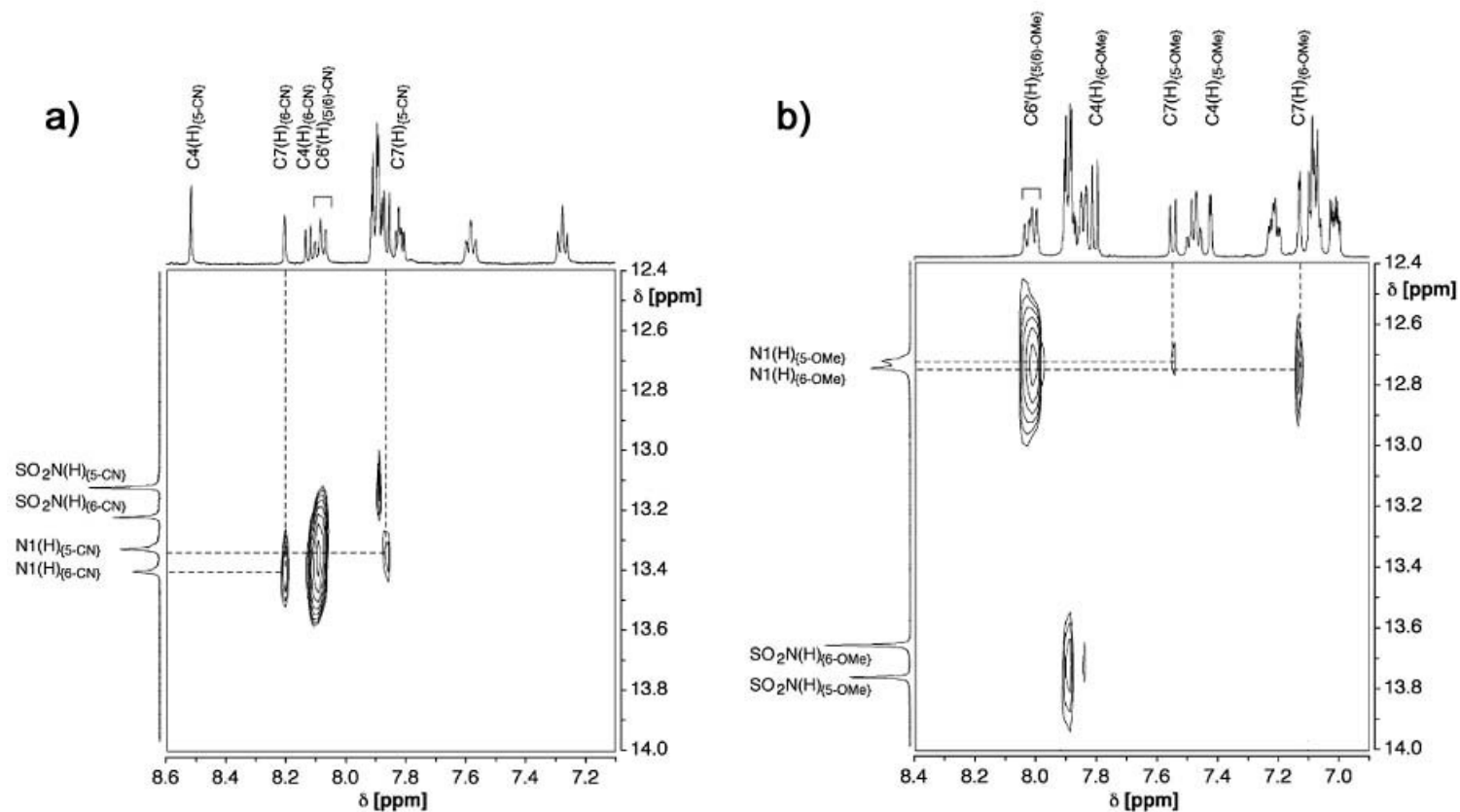


**Figure 3-4.** Two-dimensional 500 MHz  $^1\text{H}$ - $^1\text{H}$  NOESY spectra of (a) **3-4i** (left) and (b) **3-4k** (right) in acetone- $d_6$  at  $-80^\circ\text{C}$ . The dashed lines indicate the correlation signals for the benzimidazole proton N1(H) of each tautomer. For both derivatives, N1(H) shows NOE contact with the C7(H) singlet of the 6-substituted tautomer, while the 5-substituted tautomer shows an NOE contact with C(7)H appearing as a doublet (atom numbering shown in Scheme 3-2).

### 3.2.4. Substituent Effects on Photophysical Properties

#### 3.2.4.1 Effect of Donor Substitution

The deconvoluted UV-vis spectra and measured emission spectra of the three methoxy-substituted derivatives are shown on Figure 3-5. For all three derivatives, the deprotonation of the sulfonamide group is associated with a bathochromic shift in the absorption spectra. The structural modification did not significantly affect the absorption spectrum of the fully deprotonated species  $L^{2-}$ ; however, more significant changes were observed for the monoprotonated species  $HL^-$ . In this case, the absorption spectrum is stronger influenced by substitution on the benzimidazole ring (**3-5k**), resulting in a ( $\lambda_{max}$  16 nm red-shifted absorption maximum compared to the unsubstituted parent fluorophore **3-5a**, while substitution on the central benzene ring resulted only in small shifts ( $\lambda_{max}$  red-shifted 5 nm for **3-5e**, blue-shifted 2nm for **3-5f**).

For all derivatives, the deprotonation of the sulfonamide group is associated with a hypsochromic shift in the emission spectra due to the disruption of the ESIPT process. Interestingly, the emission maxima of these fluorophores strongly depended on the substituent position, with the deprotonated species  $L^{2-}$  being equally affected compared to the monoprotonated species  $HL^-$ . While the emission spectra of the 6-substituted derivative **3-5k** are similar to the parent fluorophore **3-5a**, the 4'- and 5'-substituted derivatives **3-5e** and **3-5f** give significantly red- (28nm) and blue-shifted (37nm) emissions. The origin of this unexpected divergent spectral shift will be further discussed

in detail in Chapter 4.

#### *3.2.4.1.1. Ground-State Proton Transfer*

For 4'-substituted derivative **3-5e**, an additional low-energy absorption band at 360 nm was observed, which is most likely due to formation of a prototropic imino tautomer present in the ground-state equilibrium.<sup>6</sup> Excitation spectra acquired over the entire emission energy range consistently showed a similar low-energy band, thus supporting this hypothesis. The emission spectrum measured with excitation at 350 nm were also similar to those acquired with excitation below 350 nm. These data further support that the low-energy absorption band originates from a ground-state intramolecular proton transfer species.

#### *3.2.4.1.2. Effect of Donor Strength*

Stronger donors including 5'-dimethylamino (**5-3g**) and 4',5'-methylenedioxy (**5-3l**) were introduced on the central benzene ring of the fluorophore. Compared to 5'-methoxy derivative **3-5f**, fluorophore **5-3g** showed largely red-shifted emissions (Table 3-2) for both monoprotonated HL<sup>-</sup> (71 nm shift) and deprotonated L<sup>2-</sup> species (62 nm shift). Considering that 4'-methoxy (**3-5e**) and 5'-methoxy (**3-5f**) showed opposite effects on the emission maxima, it's not very surprising that 4',5'-methylenedioxy group does not change the peak emission wavelength much. Interestingly, both **5-3g** and **5-3l** showed very low quantum yield (<0.01 and 0.04, respectively), indicating that the strong donor may offer additional nonradiative deactivation pathways.

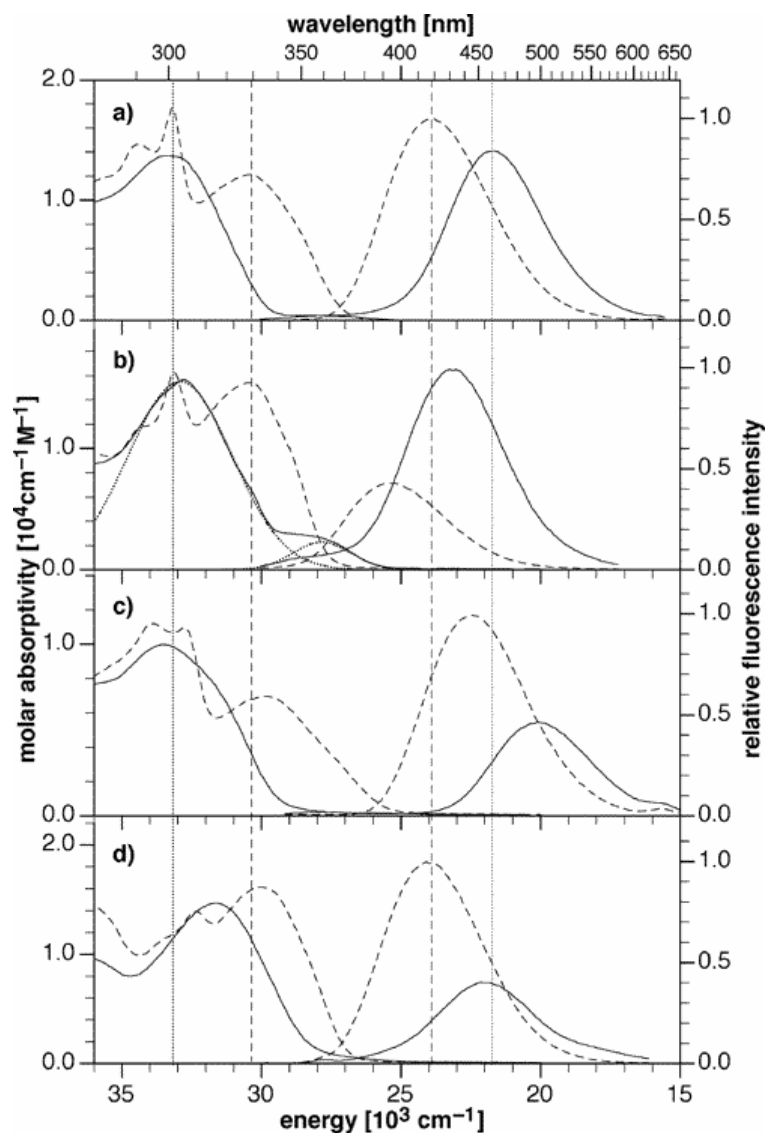


**Figure 3-5.** Effect of donor substituents: deconvoluted UV-vis absorption spectra (left) and fluorescence emission spectra (right) of compounds (a) **3-5a**, (b) **3-5e**, (c) **3-5f**, and (d) **3-5k** in aqueous solution (0.1 M KCl, 25 °C). UV-vis traces for the species with protonated (-) and deprotonated (- - -) sulfonamide group were obtained through deconvolution analysis of a series of spectra with  $-\log[\text{H}_3\text{O}^+]$  ranging between 6 and 10. Emission spectra were acquired with excitation at the isosbestic point and were recorded near neutral pH as specified in Table 3-1 (-) and at pH 11 (- - -) without further deconvolution. The four vertical grid lines are added as a guide to the eye indicating the position of the peak absorption and emission of parent compound **3-5a**.

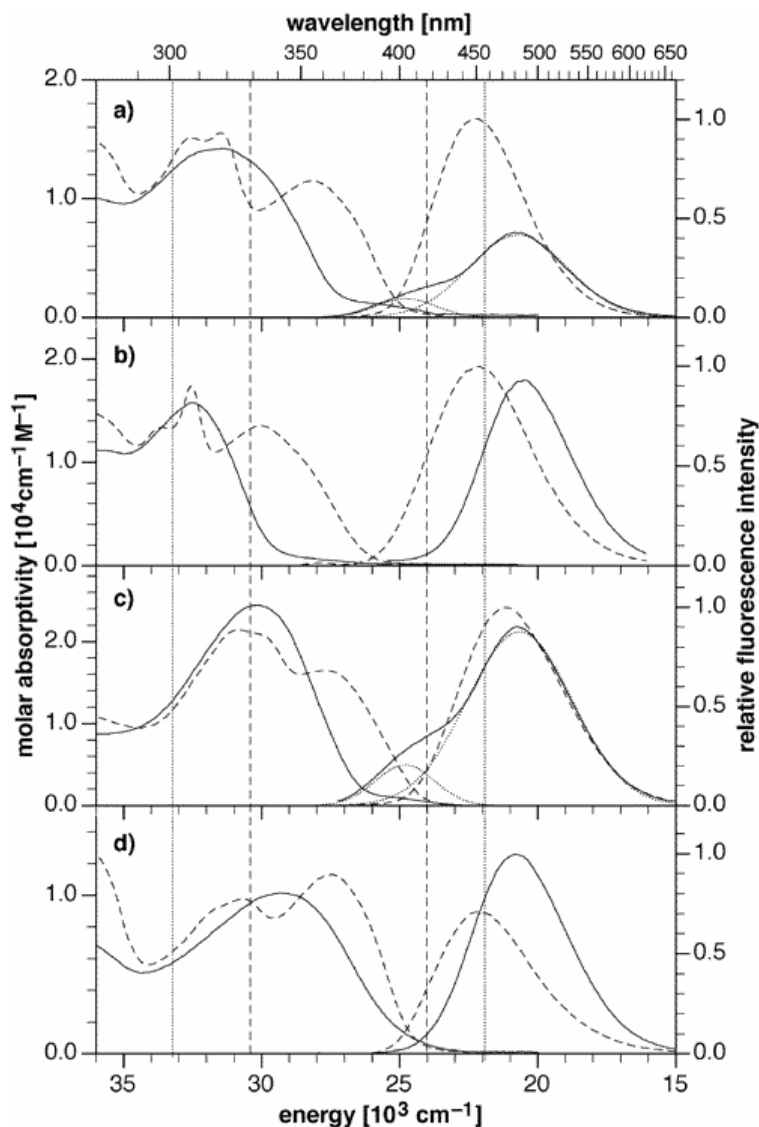
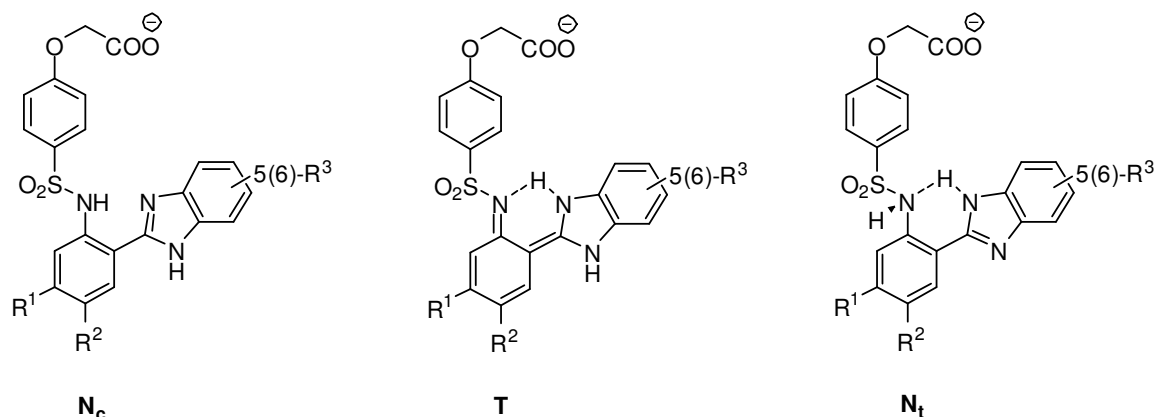


**Figure 3-6.** Effect of acceptor substituents: deconvoluted UV-vis absorption spectra (left) and fluorescence emission spectra (right) of compounds (a) **3-5b**, (b) **3-5i**, (c) **3-5d**, and (d) **3-5c** in aqueous solution (0.1 M KCl, 25 °C). UV-vis traces for the species with protonated (-) and deprotonated (- - -) sulfonamide group were obtained through deconvolution analysis of a series of spectra with  $-\log[\text{H}_3\text{O}^+]$  ranging between 6 and 10. Emission spectra were acquired with excitation at the isosbestic point and were recorded near neutral pH as specified in Table 1 (-) and at pH 11 (- - -) without further deconvolution. The four vertical grid lines are intended as a guide to the eye indicating the position of the peak absorption and emission of parent compound **3-5a**.

### 3.2.4.2. Effect of Acceptor Substitution



**Scheme 3-3**

As shown in Figure 3-6, the introduction of the electron-withdrawing group resulted in red-shifted absorption and emission spectra. For example, compared to the parent compound **3-5a**, fluorophore **3-5b** revealed a 19 nm and 26 nm shift in the absorption spectra for HL<sup>-</sup> and L<sup>2-</sup>, respectively, and a 23 nm and 29 nm shift in the emission spectra. Since the thiazolyl ring extends the fluorophore  $\pi$ -system, the absorption and emission spectra are even more red-shifted for derivative **3-5d**.

Interestingly, a high-energy emission band (404 nm and 403 nm, respectively) is observed for the monoprotonated species of derivative **3-5b** and **3-5d**. Dual fluorescence emission is not unusual for ESIPT fluorophores, and could be principally due to the presence of a rotamer (Scheme 3-3, **N<sub>t</sub>**) that cannot undergo ESIPT,<sup>7</sup> or radiative decay from a polarized, local excited state<sup>8</sup>. Detailed photophysical studies revealed uniform excitation spectra regardless of the emission wavelength, suggesting that only one species gives rise to both emission peaks. Furthermore, quantum chemical calculation suggested that the cis-rotamer **N<sub>c</sub>** is strongly favored over the trans-rotamer **N<sub>t</sub>** in case of

2'-sulfonamidophenyl-substituted benzimidazoles.<sup>1</sup> Therefore, the dual emission is most likely not due to the existence of a additional ground-state rotamer, but might originate from competition between radiative relaxation of a local excited state and formation of the proton-transfer phototautomer.

#### ***3.2.4.3. Effect of Donor-Acceptor Double Substitutions***

As discussed in the introductory paragraph, 4'-cyano-6-methoxy-derivative **3-5c** was expected to yield further red-shifted absorption and emission spectra, a prediction that was indeed confirmed by photophysical studies (Figure 3-6d). Compared to the parent fluorophore **3-5a**, the compound **3-5c** revealed a strongly red-shift absorption (41 nm shift for HL<sup>-</sup>; 33 nm shift for L<sup>2-</sup>) and emission maximum (21 nm for HL<sup>-</sup>; 34 nm for L<sup>2-</sup>). The spectral blue-shift caused by deprotonation of the sulfonamide group is 29 nm. This change should be sufficient for reliable ratiometric concentration measurements. The quantum yield of **3-5c** (0.46 for HL<sup>-</sup>; 0.34 for L<sup>2-</sup>) is also much higher than that of **3-5a** (0.23 for HL<sup>-</sup>; 0.26 for L<sup>2-</sup>).

An additional double substituted derivative **3-5h** was also synthesized and characterized (Table 3-2). The 5'-methoxy-6-cyano substituents led to a largely red-shifted emission spectra, but yielded a very low quantum yield with no substantial changes in the absorption maxima.

### 3.3 Conclusion

In this chapter, the substituent effects on 2-(2'-arylsulfonamidophenyl)-benzimidazole platform was systematically investigated. Both the nature of substituents and the substitution positions showed very strong influence on the photophysical and protonation properties of the derivatives. While differences in the protonation equilibria were readily explained using Hammett's free energy relationship, the substituents effects on their photophysical properties appeared more complicated. For some derivatives, a ground-state proton-transfer species was found to cause an additional band in the absorption spectrum. Also, the radiative relaxation of the local excited state was believed to be the reason of the additional emission peak in some derivatives' spectra. Most importantly, the absorption and emission maximums strongly depend on the substituents. This effect was utilized to achieve the red-shifted absorption. As predicted by theoretical calculations, fluorophore **3-5c** was found to have decent absorbance beyond 350 nm. Although its  $pK_a$  value of the sulfonamide group is still low (6.88), it should be possible to further adjust it by introducing suitable substituents on the arylsulfonamido moiety. Furthermore, the substituent effects on emission spectra shift will be investigated in details in chapter 4.

## 3.4. Experimental Section

### 3.4.1. Synthesis

Benzimidazole derivatives **3-4a** and **3-5a**, (4-chlorosulfonyl-phenoxy)acetic acid ethyl ester **3-10**, and 2-(4-(*N*-(2-formylphenyl) sulfamoyl)phenoxy)acetic acid ethyl ester **3-9i** were synthesized as previously describe.<sup>9</sup> Compounds 4-cyano-2-nitrobenzaldehyde<sup>10</sup> (**3-1b**), 5-methoxy-2-nitrobenzaldehyde<sup>11</sup> (**3-1f**), 4-methoxy-2-nitrobenzaldehyde<sup>12</sup> (**3-1e**), and 4-bromo-2-nitrobenzaldehyde<sup>13</sup> were synthesized according to published procedures. NMR:  $\delta$  in ppm versus SiMe<sub>4</sub> (0 ppm, <sup>1</sup>H, 400 MHz; 0 ppm, <sup>13</sup>C, 100 MHz). Note: due to the presence of prototropic exchange equilibria, benzimidazole hydrogens are in many cases broadened (indicated as “br”) or not resolved. Similarly, <sup>13</sup>C resonances for C3a(7a), C4(7), and C5(6) of the benzimidazole ring were either broadened or absent. For variable temperature NMR experiments, the actual sample temperature was determined by means of a calibration curve using neat methanol as chemical-shift thermometer.<sup>14</sup> Two-dimensional NOESY <sup>1</sup>H-<sup>1</sup>H NMR spectra were acquired in acetone-d<sub>6</sub> at 193 K with a 500 MHz spectrometer (300 ms mixing time). Structural assignments were confirmed with 2D COSY experiments acquired at the same temperature (Figure 3-7 and Figure 3-8). MS: selected peaks; m/z. Melting points are uncorrected. Flash chromatography (FC): silica gel (240-400 mesh).

**2-Nitro-4-(thiazol-2-yl)benzaldehyde (3-1d).** A solution of 4-bromo-2-nitrobenzalde-

hyde<sup>6</sup> (310 mg, 1.3 mmol), 2-(tributylstannyl)-thiazole (500 mg, 410  $\mu\text{L}$ , 1.3 mmol), and Pd(PPh<sub>3</sub>)<sub>4</sub> (50 mg, 0.043 mmol) in DMF (10 mL) was degassed and then heated at 80°C overnight. After cooling to room temperature, the reaction mixture was diluted with CH<sub>2</sub>Cl<sub>2</sub>, washed with deionized water, and concentrated under reduced pressure. The residual crude product was purified on silica gel (FC, EtOAc/hexanes, 1:3) providing 340 mg (1.45 mmol, quantitative yield) of thiazole **3-1d** as a yellow solid. Mp 101-103 °C; <sup>1</sup>H NMR (CDCl<sub>3</sub>, 400 MHz)  $\delta$  7.55 (d, *J* = 3.1 Hz, 1H), 8.01 (d, *J* = 3.2 Hz, 1H), 8.06 (d, *J* = 8.0 Hz, 1H), 8.34 (dd, *J* = 8.0 Hz, 1.7 Hz, 1H), 8.71 (d, *J* = 1.7 Hz, 1H), 10.45 (s, 1H); <sup>13</sup>C NMR (CDCl<sub>3</sub>, 100 MHz)  $\delta$  121.6, 122.0, 130.4, 130.87, 130.91, 138.6, 144.8, 150.1, 163.8, 187.3; IR (KBr) 3121, 3106, 2926, 1691, 1526, 1506, 1348, 1141, 824, 770, 736 cm<sup>-1</sup>; MS (70 eV) *m/z* 234 ([M<sup>+</sup>], 11), 204 (100), 176 (25), 159 (27); EI-HRMS calcd for C<sub>10</sub>H<sub>6</sub>N<sub>2</sub>O<sub>3</sub>S 234.0099, found 234.0078.

**5-(Dimethylamino)-2-nitrobenzaldehyde (3-1g).** A mixture of 5-fluoro-2-nitrobenzaldehyde (100 mg, 0.59 mmol), dimethylamine hydrochloride (77 mg), and anhydrous K<sub>2</sub>CO<sub>3</sub> (245 mg) in DMSO (2 mL) was heated at 105°C for 2 h. After cooling to room temperature, the reaction mixture was diluted with water, and the precipitated product was extracted twice with diethylether (40 mL). The combined organic extracts were dried with anhydrous MgSO<sub>4</sub>, filtered, and concentrated under reduced pressure, providing 92 mg (0.47 mmol, 80% yield) of compound **3-1g** as a yellow solid. Mp 124-126 °C; <sup>1</sup>H NMR (CDCl<sub>3</sub>, 400 MHz)  $\delta$  3.16 (s, 6H), 6.72 (dd, *J* = 9.3, 3.0 Hz, 1H), 6.91 (d, *J* = 3.0 Hz, 1H), 8.11 (d, *J* = 9.3 Hz, 1H), 10.51 (s, 1H); <sup>13</sup>C NMR (CDCl<sub>3</sub>, 100 MHz)  $\delta$  40.3,

110.0, 112.7, 127.4, 135.0, 136.2, 153.3, 190.0; IR (KBr) 2902, 1701, 1600, 1573, 1295, 1261, 1231, 1198, 886, 811  $\text{cm}^{-1}$ ; MS (70 eV)  $m/z$  194.1 ( $[\text{M}^+]$ , 100), 164.1 (18), 136.3 (100), 119.1 (32), 105.1 (18); EI-HRMS calcd for  $[\text{M}^+]$   $\text{C}_9\text{H}_{10}\text{N}_2\text{O}_3$  194.0691, found 194.0674.

**General Procedure A: Synthesis of Benzimidazole Derivatives through Oxidative Coupling with Benzoquinone.** An equimolar solution of the corresponding aldehyde and phenylenediamine (0.5 mmol) in EtOH (2 mL) was heated under reflux until all starting material was converted to the imine intermediate (ca. 1.5 h). After addition of 1,4-benzoquinone (119 mg, 1.10 mmol) the reaction mixture was heated at reflux until the imine intermediate was completely converted to the benzimidazole product (typically 30-60 min). The reaction mixture was then cooled to room temperature, diluted with saturated aqueous  $\text{NaHCO}_3$ , and the product was extracted twice with ethyl acetate. The combined organic extracts were dried with anhydrous  $\text{MgSO}_4$ , filtered, and concentrated under reduced pressure. The crude product was purified by FC on silica to give the analytically pure benzimidazole.

**4-(1*H*-Benzimidazol-2-yl)-3-nitrobenzotrile (3-2b).** Starting from 200 mg of aldehyde **3-1b** (0.12 mmol) and 1,2-phenylenediamine (129 mg, 1.19 mmol), benzimidazole derivative **3-2b** was obtained in 43% yield (FC, EtOAc/hexanes, gradient 1:2 to 1:1). Mp 209-211 °C;  $^1\text{H}$  NMR ( $\text{CD}_3\text{OD}$ , 400 MHz)  $\delta$  7.33 (m, 2H), 7.64 (br, 2H), 8.06 (d,  $J = 8.2$  Hz, 1H), 8.20 (dd,  $J = 8.2, 1.6$  Hz, 1H), 8.53 (d,  $J = 1.6$  Hz, 1H);  $^{13}\text{C}$  NMR (acetone- $d_6$ , 100 MHz)  $\delta$  115.7, 117.2, 124.5 (br), 129.5, 130.1, 133.7, 137.1, 147.5,

150.0; IR (KBr) 3198, 3097, 3072, 2236, 1560, 1535, 1425, 1354, 787, 747  $\text{cm}^{-1}$ ; MS (70 eV)  $m/z$  264.1 ( $[\text{M}^+]$ , 100), 247.1 (65), 234.1 (26); EI-HRMS calcd for  $[\text{M}^+]$   $\text{C}_{14}\text{H}_8\text{N}_4\text{O}_2$  264.06473, found 264.06592.

**4-(5(6)-Methoxy-1H-benzimidazol-2-yl)-3-nitrobenzotrile (3-2c).** Starting from 200 mg of aldehyde **3-1b** (0.12 mmol) and 4-methoxybenzene-1,2-diamine (165 mg, 1.19 mmol), benzimidazole derivative **3-2c** was obtained in 30% yield (FC, EtOAc/hexanes, gradient 1:2 to 1:1). Mp 75-77  $^{\circ}\text{C}$ ;  $^1\text{H}$  NMR ( $\text{CD}_3\text{OD}$ , 400 MHz)  $\delta$  3.86 (s, 3H), 6.95 (dd,  $J = 8.9, 2.4$  Hz, 1H), 7.09 (br, 1H), 7.52 (d,  $J = 8.7$  Hz, 1H), 8.02 (d,  $J = 8.0$  Hz, 1H), 8.16 (dd,  $J = 8.0, 1.6$  Hz, 1H), 8.49 (d,  $J = 1.6$  Hz, 1H);  $^{13}\text{C}$  NMR (acetone- $d_6$ , 100 MHz)  $\delta$  55.9, 114.0, 114.2, 117.1, 128.5, 128.7, 131.9, 136.0, 145.3, 149.6, 157.9; IR (KBr) 3074, 2946, 2234, 1617, 1540, 1269, 1198, 1157, 1025, 1001, 831  $\text{cm}^{-1}$ ; MS (70 eV)  $m/z$  294.1 ( $[\text{M}^+]$ , 100); EI-HRMS calcd for  $[\text{M}^+]$   $\text{C}_{15}\text{H}_{10}\text{N}_4\text{O}_3$  294.07529, found 294.07582.

**2-(2-Nitro-4-thiazol-2-yl-phenyl)-1H-benzimidazole (3-2d).** Starting from 28 mg of aldehyde **3-1d** (0.12 mmol) and 1,2-phenylenediamine (15 mg, 0.14 mmol), benzimidazole derivative **3-2d** was obtained in 31% yield (FC, EtOAc/hexanes, 1:1). Mp 120-122  $^{\circ}\text{C}$ ;  $^1\text{H}$  NMR ( $\text{CD}_3\text{OD}/\text{CDCl}_3$  1:1, 400 MHz)  $\delta$  7.29-7.35 (m, 2H), 7.61-7.68 (br, 2H), 7.69 (d,  $J = 3.2$  Hz, 1H), 7.96 (d,  $J = 8.1$  Hz, 1H), 8.00 (d,  $J = 3.2$  Hz, 1H), 8.33 (dd,  $J = 8.1, 1.8$  Hz, 1H), 8.65 (d,  $J = 1.8$  Hz, 1H);  $^{13}\text{C}$  NMR ( $\text{CD}_3\text{OD}/\text{CDCl}_3$ , 100 MHz)  $\delta$  122.1, 123.0, 123.9 (br), 126.9, 130.8, 133.5, 136.5, 144.9, 148.2, 150.0, 165.6; IR (KBr) 3120, 3091, 1534, 1518, 1474, 1448, 1433, 1369, 1354, 1276, 771, 746  $\text{cm}^{-1}$ ; MS (70 eV)  $m/z$  322 ( $[\text{M}^+]$ , 50), 292 (100), 129 (57), 57(52), 40.9 (37); EI-HRMS calcd for  $[\text{M}^+]$

C<sub>16</sub>H<sub>10</sub>N<sub>4</sub>O<sub>2</sub>S 322.0525, found 322.0496.

**2-(4-Methoxy-2-nitro-phenyl)-1H-benzimidazole (3-2e).** Starting from 410 mg of aldehyde **3-1e** (2.26 mmol) and 1,2-phenylenediamine (257 mg, 2.37 mmol), benzimidazole derivative **3-2e** was obtained in 82% yield (FC, EtOAc/hexanes, gradient 1:4 to 1:2). Mp 178-180 °C; <sup>1</sup>H NMR (CD<sub>3</sub>OD, 400 MHz) δ 3.96 (s, 3H), 7.25-7.29 (m, 2H), 7.38 (dd, *J* = 8.6, 2.6 Hz, 1H), 7.58 (br, 2H), 7.65 (d, *J* = 2.6 Hz, 1H), 7.74 (d, *J* = 8.6 Hz, 1H); <sup>13</sup>C NMR (DMSO-*d*<sub>6</sub>, 100 MHz) δ 56.3, 109.6, 115.9, 117.8, 122.1 (br), 131.6, 147.1, 149.7, 160.1; IR (KBr) 2844, 1628, 1531, 1500, 1449, 1430, 1304, 1272, 1238, 1027, 755 cm<sup>-1</sup>; MS (70 eV) *m/z* 269 ([M<sup>+</sup>], 90), 239.1 (100), 196 (32), 110.1 (77); EI-HRMS calcd for [M<sup>+</sup>] C<sub>14</sub>H<sub>11</sub>N<sub>3</sub>O<sub>3</sub> 269.0800, found 269.0816.

**3-Amino-4-(1H-benzimidazol-2-yl)benzonitrile (3-3b).** A solution of nitro-substituted benzimidazole intermediate **3-2b** (102 mg, 0.39 mmol) in 5 mL of methanol was hydrogenated at room temperature under ambient pressure in the presence of Pd on activated carbon as catalyst (25 mg, 5 wt % Pd). After completion of the reaction (TLC), the catalyst was filtered off through a pad of Celite, and the filtrate was concentrated under reduced pressure providing 85 mg (0.36 mmol, 94% yield) of amine **3-3b** as a yellow solid. Mp 88-90 °C; <sup>1</sup>H NMR (CD<sub>3</sub>OD, 400 MHz) δ 6.92 (dd, *J* = 8.2, 1.6 Hz, 1H), 7.12 (d, *J* = 1.6 Hz, 1H), 7.22-7.25 (m, 2H), 7.58 (br, 2H), 7.79 (d, *J* = 8.2 Hz, 1H); <sup>13</sup>C NMR (CD<sub>3</sub>OD, 100 MHz) δ 114.0, 116.0, 119.1, 119.7, 120.1, 129.0, 149.2, 151.9; IR (KBr) 3305 (br), 3060, 2228, 1617, 1586, 1577, 1454, 1437, 1334, 1267, 766, 741 cm<sup>-1</sup>; MS (70 eV) *m/z* 234.1 ([M<sup>+</sup>], 100); EI-HRMS calcd for [M<sup>+</sup>] C<sub>14</sub>H<sub>10</sub>N<sub>4</sub> 234.0906, found

234.0907.

**3-Amino-4-(1H-benzimidazol-2-yl)benzonitrile (3-3c).** Synthesized from **3-2c** as described for **3-3b**, 53% yield. Mp 193-195 °C; <sup>1</sup>H NMR (CD<sub>3</sub>OD, 400 MHz) δ 3.83 (s, 3H), 6.87 (dd, *J* = 8.8, 2.7 Hz, 1H), 6.93 (dd, *J* = 8.2, 1.6 Hz, 1H), 7.07 (d, *J* = 2.2 Hz, 1H), 7.12 (d, *J* = 1.6 Hz, 1H), 7.49 (d, *J* = 8.8 Hz, 1H), 7.79 (d, *J* = 8.2 Hz, 1H); <sup>13</sup>C NMR (CD<sub>3</sub>OD, 100 MHz) δ 56.2, 97.6, 113.3, 113.5, 116.2, 117.3, 119.0, 119.9, 128.7, 135.4, 139.3, 148.9, 151.6, 157.9; IR (KBr) 3296, 2224, 1631, 1610, 1590, 1453, 1434, 1338, 1263, 1199, 1158, 832 cm<sup>-1</sup>; MS (70 eV) *m/z* 264 ([M<sup>+</sup>], 100), 249.1 (52), 167 (28), 147.9 (78), 129 (90); EI-HRMS calcd for [M<sup>+</sup>] C<sub>15</sub>H<sub>12</sub>N<sub>4</sub>O 264.1011, found 264.1014.

**2-(1H-Benzimidazol-2-yl)-5-thiazol-2-yl-phenylamine (3-3d).** Synthesized from **3-2d** as described for **3-3b**, 88% yield. Mp dec>230 °C; <sup>1</sup>H NMR (CD<sub>3</sub>OD, 400 MHz) δ 7.12-7.16 (m, 2H), 7.21 (dd, *J* = 8.2, 1.8 Hz, 1H), 7.37 (d, *J* = 1.8 Hz, 1H), 7.47- 7.52 (m, 2H), 7.53 (d, *J* = 3.3 Hz, 1H), 7.73 (d, *J* = 8.2 Hz, 1H), 7.79 (d, *J* = 3.3 Hz, 1H); <sup>13</sup>C NMR (CD<sub>3</sub>OD, 100 MHz) δ 114.2, 114.7, 115.1 (br), 115.3, 120.1, 123.0, 128.9, 135.1, 139.9 (br), 143.6, 148.3, 152.3, 169.4; IR (KBr) 3321, 2500, 1617, 1452, 1286, 1262, 1138, 1060, 868, 806, 730, 658 cm<sup>-1</sup>; FAB-MS (thioglycerol) *m/z* 293 ([M<sup>+</sup>], 100), 237 (13); FAB-HRMS calcd for [M<sup>+</sup>] C<sub>16</sub>H<sub>13</sub>N<sub>4</sub>S 293.0861, found 293.0876.

**2-(4-Methoxy-2-amino-phenyl)-1H-benzimidazole (3-3e).** Synthesized from **3-2e** as described for **3-3b**, 99% yield (FC, hexanes/EtOAc, gradient 3:1 to 2:1). Mp 140-143 °C; <sup>1</sup>H NMR (DMSO<sub>d</sub><sub>6</sub>, 400 MHz) δ 3.74 (s, 3H), 6.27 (dd, *J* = 8.7, 2.4 Hz, 1H), 6.37 (d, *J* = 2.4 Hz, 1H), 7.11-7.18 (m, 2H), 7.32 (br, 2H), 7.45 (d, *J* = 7.3 Hz, 1H), 7.59 (d, *J* = 7.3

Hz, 1H), 7.76 (d,  $J = 8.7$  Hz, 1H), 12.47 (s, 1H);  $^{13}\text{C}$  NMR (DMSO- $d_6$ , 100 MHz)  $\delta$  54.8, 99.2, 102.7, 103.7, 110.3, 117.6, 121.0, 121.7, 128.4, 133.2, 142.8, 149.6, 149.7, 152.4, 160.9; IR (KBr) 3201, 1627, 1614, 1502, 1447, 1431, 1251, 1214, 1026, 735  $\text{cm}^{-1}$ ; MS (70 eV)  $m/z$  239 ( $[\text{M}^+]$ , 100), 210 (7), 196 (32); EI-HRMS calcd for  $[\text{M}^+]$   $\text{C}_{14}\text{H}_{13}\text{N}_3\text{O}$  239.1058, found 239.1056.

**2-(4-(*N*-(2-(1*H*-Benzimidazol-2-yl)-5-cyanophenyl)sulfamoyl)-phenoxy)acetic Acid Ethyl Ester (3-4b).** To a solution of amine **3-3b** (35 mg, 0.149 mmol) in anhydrous pyridine (2 mL) was added (4-chlorosulfonyl-phenoxy)-acetic acid ethyl ester<sup>2</sup> **3-10** (50 mg, 0.179 mmol). After stirring at room temperature for 18 h, the reaction mixture was poured into aqueous 1 M HCl (20 mL), and the product was extracted twice with ethyl acetate. The combined organic extracts were dried with anhydrous  $\text{MgSO}_4$ , filtered, and concentrated under reduced pressure. The crude product was purified on silica gel (EtOAc/hexanes, gradient 1:3 to 1:1) providing 25 mg (0.053 mmol, 35%) of sulfonamide **3-4b** as a tan solid. Mp 208-210  $^\circ\text{C}$ ;  $^1\text{H}$  NMR ( $\text{CDCl}_3$ , 400 MHz)  $\delta$  1.34 (t,  $J = 7.1$  Hz, 3H), 4.31 (q,  $J = 7.1$  Hz, 2H), 4.65 (s, 2H), 6.45 (d,  $J = 9.0$  Hz, 2H), 7.34-7.40 (m, 4H), 7.43 (dd,  $J = 8.1$  Hz, 1.6 Hz, 1H), 7.50 (br, 1H), 7.58 (d,  $J = 8.0$  Hz, 1H), 7.83 (br, 1H), 8.05 (d,  $J = 1.5$  Hz, 1H), 9.93 (s, 1H), 12.18 (s, 1H);  $^{13}\text{C}$  NMR ( $\text{CDCl}_3/\text{acetone-}d_6$ , 100 MHz)  $\delta$  13.7, 61.2, 64.7, 112.9, 114.2, 117.4, 119.9, 122.3, 123.3 (br), 125.9, 126.9, 128.7, 131.2, 137.6, 147.9, 160.6, 167.4; IR (KBr) 3313, 3068, 2983, 2232, 1757, 1595, 1497, 1403, 1277, 1226, 1155, 1095, 555  $\text{cm}^{-1}$ ; MS (70 eV)  $m/z$  476.1 ( $[\text{M}^+]$ , 39), 412.1 (35), 325.1 (37), 233.1(100); EI-HRMS calcd for  $[\text{M}^+]$   $\text{C}_{24}\text{H}_{20}\text{N}_4\text{O}_5\text{S}$

476.1154, found 476.1156.

**2-(4-(N-(5-Cyano-2-(5(6)-methoxy-1H-benzimidazol-2-yl)phenyl)sulfamoyl)-**

**phenoxy)acetic Acid Ethyl Ester (3-4c).** Synthesized from amine **3-3c** as described for **3-4b**, 43% yield. Mp 83-85 °C; <sup>1</sup>H NMR (CD<sub>3</sub>OD) δ 1.20 (t, *J* = 7.1 Hz, 3H), 3.87 (s, 3H), 4.17 (q, *J* = 7.1 Hz, 2H), 4.65 (s, 2H), 6.81 (d, *J* = 9.0 Hz, 2H), 6.97 (dd, *J* = 8.9, 2.4 Hz, 1H), 7.11 (d, *J* = 2.3 Hz, 1H), 7.49 (dd, *J* = 8.2, 1.6 Hz, 1H), 7.57 (d, *J* = 8.9 Hz, 1H), 7.64 (d, *J* = 9.0 Hz, 2H), 7.92 (d, *J* = 8.2 Hz, 1H), 7.98 (d, *J* = 1.5 Hz, 1H); <sup>13</sup>C NMR (DMSO-*d*<sub>6</sub>/CDCl<sub>3</sub>, 100 MHz) δ 13.6, 55.1, 60.7, 64.5, 111.9, 113.1 (br), 114.2, 117.4, 119.6, 121.2, 125.5, 127.0, 128.3, 130.9, 137.0, 147.4, 156.4, 160.4, 166.9; IR (KBr) 3400, 2980, 2231, 1759, 1595, 1496, 1400, 1273, 1200, 1158, 1095, 828, 554 cm<sup>-1</sup>; MS (70 eV) 506.1 ([M<sup>+</sup>], 47), 263.1 (100); EI-HRMS *m/z* calcd for [M<sup>+</sup>] C<sub>25</sub>H<sub>22</sub>N<sub>4</sub>O<sub>6</sub>S 506.1260, found 506.1281.

**(4-(2-(1H-Benzimidazol-2-yl)-5-thiazol-2-yl-phenylsulfamoyl)-phenoxy)acetic Acid Ethyl Ester (3-4d).** Synthesized from amine **3-3d** as described for **3-4b**, yield 68% (FC, EtOAc/hexanes, 1:1). Mp 202-204 °C; <sup>1</sup>H NMR (CD<sub>3</sub>OD/CDCl<sub>3</sub> 1:1, 400 MHz) δ 1.23 (t, *J* = 7.1 Hz, 3H), 4.20 (q, *J* = 7.1 Hz, 2H), 4.59 (s, 2H), 6.76 (d, *J* = 9.0 Hz, 2H), 7.30-7.36 (m, 2H), 7.57 (d, *J* = 3.3 Hz, 1H), 7.64-7.71 (m, 2H), 7.74 (d, *J* = 9.0 Hz, 2H), 7.77 (dd, *J* = 8.3, 1.8 Hz, 1H), 7.91 (d, *J* = 3.3 Hz, 1H), 7.93 (d, *J* = 8.3 Hz, 1H), 8.29 (d, *J* = 1.7 Hz, 1H); <sup>13</sup>C NMR (CD<sub>3</sub>OD/CDCl<sub>3</sub> 1:1, 100 MHz) δ 14.2, 62.2, 65.5, 115.1, 119.0, 119.3, 120.8, 121.9, 123.8, 128.1, 129.9, 132.2, 135.3, 138.6, 144.2, 150.3, 161.7, 168.0, 169.1; IR (KBr) 2923, 2852, 2265, 1775, 1758, 1594, 1577, 1497, 1406, 1330, 1151, 654, 573,

555 cm<sup>-1</sup>; MS (70 eV) *m/z* 534 ([M<sup>+</sup>], 48), 470 (13), 383 (24), 291 (100); EI-HRMS calcd for [M<sup>+</sup>] C<sub>26</sub>H<sub>22</sub>N<sub>4</sub>O<sub>5</sub>S<sub>2</sub> 534.1032, found 534.1023.

**(4-(2-(1*H*-Benzimidazol-2-yl)-5-methoxy-phenylsulfamoyl)-phenoxy)acetic Acid**

**Ethyl Ester (3-4e).** Synthesized from amine **3-3e** as described for **3-4b**, 36% yield (FC, hexanes/EtOAc, gradient 2:1 to 1:1). Mp 75-77 °C; <sup>1</sup>H NMR (CDCl<sub>3</sub>, 400 MHz) δ 1.28 (t, *J* = 7.1 Hz, 3H), 3.71 (s, 3H), 4.25 (q, *J* = 7.1 Hz, 2H), 4.57 (s, 2H), 6.53 (d, *J* = 8.9 Hz, 2H), 6.57 (d, *J* = 2.5 Hz, 1H), 7.20 (d, *J* = 2.5 Hz, 1H), 7.22-7.26 (m, 2H), 7.42 (d, *J* = 8.7 Hz, 1H), 7.50 (br, 2H), 7.52 (d, *J* = 8.9 Hz, 2H), 7.75 (br, 1H), 9.88 (br, 1H); <sup>13</sup>C NMR (CDCl<sub>3</sub>, 100 MHz) δ 14.2, 29.8, 55.5, 61.9, 64.8, 106.8, 110.5, 110.7 (br), 111.0, 114.0, 118.9 (br), 122.9 (br), 127.4, 128.9, 131.3, 132.8 (br), 138.7, 142.2 (br), 149.8, 160.4, 161.0, 168.2; IR (KBr) 3367, 2925, 1754, 1596, 1582, 1497, 1409, 1274, 1200, 1143, 1094, 1082, 585 cm<sup>-1</sup>; MS (70 eV) *m/z* 481 ([M<sup>+</sup>], 46), 330 (21), 238 (100); EI-HRMS calcd for [M<sup>+</sup>] C<sub>24</sub>H<sub>23</sub>N<sub>3</sub>O<sub>6</sub>S 481.1308, found 481.1297.

Imidazole derivatives **3-4f-l** were synthesized according to procedure A.

**4-(2(1*H*-Benzimidazol-2-yl)-4-methoxy-phenylsulfamoyl)-phenoxy-acetic Acid Ethyl**

**Ester (3-4f).** Starting from 50 mg of aldehyde **3-9f** (0.13 mmol) and 1,2-phenylenediamine (15 mg, 0.13 mmol), benzimidazole **3-4f** was obtained in 74% yield (FC, EtOAc/hexanes, gradient 1:4 to 1:2). Mp 76-78 °C; <sup>1</sup>H NMR (CDCl<sub>3</sub>, 400 MHz) δ 1.38 (t, *J* = 7.1 Hz, 3H), 3.83 (s, 3H), 4.36 (q, *J* = 7.1 Hz, 2H), 4.65 (s, 2H), 6.13 (d, *J* = 8.9, 2H), 6.89 (d, *J* = 2.9 Hz, 1H), 6.95 (d, *J* = 8.9 Hz, 2H), 6.97 (dd, *J* = 8.9, 2.9 Hz, 1H), 7.29-7.34 (m, 2H), 7.43 (br, 1H), 7.71 (d, *J* = 8.9, 1H), 7.78 (br, 1H), 9.76 (s,

1H), 10.68 (s, 1H);  $^{13}\text{C}$  NMR ( $\text{CDCl}_3$ , 100 MHz)  $\delta$  14.2, 55.6, 62.0, 64.4, 111.2 (br), 112.0, 113.3, 115.6, 119.1 (br), 122.4, 122.6 (br), 123.5 (br), 126.8, 128.5, 129.4, 130.0, 133.2 (br), 133.6, 149.1, 157.0, 160.0, 168.7; IR (KBr) 3338, 2936, 1757, 1735, 1595, 1502, 1325, 1279, 1214, 1158, 1094, 831, 566  $\text{cm}^{-1}$ ; MS (70 eV)  $m/z$  481 ( $[\text{M}^+]$ , 38), 238 (100); EI-HRMS calcd for  $[\text{M}^+]$   $\text{C}_{24}\text{H}_{23}\text{N}_3\text{O}_6\text{S}$  481.1307, found 481.1320.

**2-(4-(N-(2-(1H-Benzimidazol-2-yl)-4-(dimethylamino)phenyl)sulfamoyl)phenoxy)acetic Acid Ethyl Ester (3-4g).** Starting from 131 mg of aldehyde **3-9g** (0.32 mmol) and 1,2-phenylenediamine (26 mg, 0.20 mmol), benzimidazole **3-4g** was obtained in 50% yield (FC, EtOAc/hexanes, gradient 1:3 to 1:1). Mp 82-84 °C;  $^1\text{H}$  NMR ( $\text{CD}_3\text{OD}$ , 400 MHz)  $\delta$  1.17 (t,  $J = 7.1$  Hz, 3H), 2.89 (s, 6H), 4.13 (q,  $J = 7.1$  Hz, 2H), 4.43 (s, 2H), 6.40 (d,  $J = 8.8$  Hz, 2H), 6.73 (dd,  $J = 9.3, 2.7$  Hz, 1H), 6.97 (d,  $J = 3.3$  Hz, 1H), 7.20-7.26 (m, 4H), 7.48 (d,  $J = 9.3$  Hz, 1H), 7.55 (br, 2H);  $^{13}\text{C}$  NMR ( $\text{CDCl}_3$ , 100 MHz)  $\delta$  14.2, 40.4, 61.8, 64.3, 109.7, 113.2, 114.1, 122.5, 122.6 (br), 125.1, 126.8, 128.5, 130.0, 148.1, 150.1, 159.8, 168.6; IR (KBr) 3318, 2981, 2904, 2806, 1752, 1735, 1595, 1510, 1497, 1279, 1215, 1158, 1094  $\text{cm}^{-1}$ ; MS (70 eV)  $m/z$  494.2 ( $[\text{M}^+]$ , 18), 251.2 (100); EI-HRMS calcd for  $[\text{M}^+]$   $\text{C}_{25}\text{H}_{26}\text{N}_4\text{O}_5\text{S}$  494.1624, found 494.1615.

**2-(4-(N-(2-(5(6)-Cyano-1H-benzimidazol-2-yl)-4-methoxyphenyl)sulfamoyl)phenoxy)acetic Acid Ethyl Ester (3-4h).** Starting from 72 mg of aldehyde **3-9f** (0.183mmol) and 3,4-diaminobenzonitrile (26 mg, 0.20 mmol), benzimidazole **3-4h** was obtained in 53% yield (FC, EtOAc/hexanes, gradient 1:3 to 1:1). Mp 72-74 °C;  $^1\text{H}$  NMR ( $\text{CD}_3\text{OD}$ , 400 MHz)  $\delta$  1.23 (t,  $J = 7.1$  Hz, 3H), 3.85 (s, 3H), 4.19 (q,  $J = 7.1$  Hz, 2H),

4.57 (s, 2H), 6.57 (d,  $J = 9.0$  Hz, 2H), 7.07 (dd,  $J = 9.0, 2.9$  Hz, 1H), 7.29-7.34 (m, 3H), 7.60 (dd,  $J = 8.3, 1.5$  Hz, 1H), 7.65 (d,  $J = 9.0$  Hz, 1H), 7.72 (br, 1H), 8.06 (br, 1H);  $^{13}\text{C}$  NMR (acetone- $d_6$ , 400 MHz) mixture of two tautomers (ratio 2:3)  $\delta$  14.4, 56.0, 61.6, 65.5, 106.5, 107.0, 112.6, 113.4, 114.9, 116.8, 118.2, 118.5, 119.3, 119.9, 120.6, 124.3, 124.8, 126.7, 127.5, 129.5, 129.6, 131.5, 131.6, 132.1, 132.2, 133.8, 137.0, 142.6, 145.8, 153.4, 154.1, 157.2, 161.7, 168.3; IR (KBr) 3283, 2936, 2223, 1752, 1735, 1594, 1503, 1318, 1293, 1214, 1159, 1094, 832  $\text{cm}^{-1}$ ; MS (70 eV)  $m/z$  506.1 ( $[\text{M}^+]$ , 47), 263.1 (100); EI-HRMS calcd for  $[\text{M}^+]$   $\text{C}_{25}\text{H}_{22}\text{N}_4\text{O}_6\text{S}$  506.1260, found 506.1251.

**2-(4-(*N*-(2-(5(6)-Cyano-1*H*-benzimidazol-2-yl)phenyl)sulfamoyl)-phenoxy)acetic**

**Acid Ethyl Ester (3-4i).** Starting from 150 mg of aldehyde **3-9i** (0.41 mmol) and 3,4-diaminobenzonitrile (60 mg, 0.41 mmol), benzimidazole **3-4i** was obtained in 50% yield (FC, EtOAc/hexanes, gradient 1:2 to 1:1). Mp 169-171  $^{\circ}\text{C}$ ;  $^1\text{H}$  NMR ( $\text{CD}_3\text{OD}$ , 400 MHz)  $\delta$  1.21 (t,  $J = 7.1$  Hz, 3H), 4.17 (q,  $J = 7.1$  Hz, 2H), 4.61 (s, 2H), 6.72 (d,  $J = 9.0$  Hz, 2H), 7.22 (ddd,  $J = 8.5, 7.5, 1.1$  Hz, 1H), 7.44 (ddd,  $J = 8.5, 7.5, 1.5$  Hz, 1H), 7.54 (d,  $J = 9.0$  Hz, 2H), 7.58 (dd,  $J = 8.4, 1.5$  Hz, 1H), 7.73 (br, 1H), 7.75 (dd,  $J = 8.3, 1.0$  Hz, 1H), 7.82 (d,  $J = 7.9, 1.4$  Hz, 1H), 8.02 (br, 1H);  $^{13}\text{C}$  NMR ( $\text{CD}_3\text{OD}$ , 100 MHz)  $\delta$  14.1, 61.1, 64.9, 105.1 (br), 113.2 (br), 115.7, 119.5, 119.9, 124.0, 127.0 (br), 128.2, 129.2, 131.2, 132.0, 136.7 (br), 137.5, 141.4 (br), 144.5 (br), 153.4 (br), 161.2, 168.2; IR (KBr) 3332, 2985, 2220, 1758, 1740, 1594, 1496, 1315, 1154, 1095, 921, 572  $\text{cm}^{-1}$ ; MS (70 eV)  $m/z$  476.2 ( $[\text{M}^+]$ , 36), 412.1 (32), 325.1 (34), 233.1 (100); EI-HRMS calcd for  $[\text{M}^+]$   $\text{C}_{24}\text{H}_{20}\text{N}_4\text{O}_5\text{S}$  476.1154, found 476.1135.

**2-(4-(N-(2-(5(6)-Methoxy-1H-benzimidazol-2-yl)phenyl)sulfamoyl)phenoxy)acetic**

**Acid Ethyl Ester (3-4k).** Starting from 200 mg of aldehyde **3-9i** (0.55 mmol) and 1,2-diamino-4-methoxybenzene (80 mg, 0.58 mmol), benzimidazole **3-4k** was obtained in 60% yield (FC, EtOAc/hexanes, gradient 1:3 to 1:1). Mp 72-74 °C; <sup>1</sup>H NMR (CD<sub>3</sub>OD, 400 MHz) δ 1.19 (t, *J* = 7.1 Hz, 3H), 3.85 (s, 3H), 4.16 (q, *J* = 7.1 Hz, 2H), 4.58 (s, 2H), 6.69 (d, *J* = 9.0 Hz, 2H), 6.91 (dd, *J* = 8.8, 2.4 Hz, 1H), 7.09 (d, *J* = 2.2 Hz, 1H), 7.16 (ddd, *J* = 8.5, 7.8, 1.2 Hz, 1H), 7.33 (ddd, *J* = 8.3, 7.4, 1.5 Hz, 1H), 7.49-7.54 (m, 3H), 7.69-7.75 (m, 2H); <sup>13</sup>C NMR (CDCl<sub>3</sub>, 100 MHz) δ 14.0, 55.6, 61.8, 64.7, 113.0 (br), 114.1, 116.1, 118.2, 121.5, 124.1, 126.2, 128.9, 130.2, 131.2, 136.8, 149.4 (br), 156.8 (br), 160.6, 168.4; IR (KBr) 3325, 2938, 1752, 1497, 1333, 1283, 1200, 1160, 1148, 1094, 570 cm<sup>-1</sup>; MS (70 eV) *m/z* 481.2 ([M<sup>+</sup>], 38), 238 (100); EI-HRMS calcd for [M<sup>+</sup>] C<sub>24</sub>H<sub>23</sub>N<sub>3</sub>O<sub>6</sub>S 481.13076, found 481.13063.

**2-(4-(N-(6-(1H-Benzimidazol-2-yl)benzo[1,3]dioxol-5-yl)sulfamoyl)phenoxy)acetic**

**Acid Ethyl Ester (3-4l).** Starting from 51 mg of aldehyde **3-9l** (0.12 mmol) and 1,2-phenylenediamine (14 mg, 0.12 mmol), benzimidazole **3-4l** was obtained in 44% yield (FC, EtOAc/hexanes, gradient 1:3 to 1:1). Mp 168-170 °C; <sup>1</sup>H NMR (acetone-*d*<sub>6</sub>, 400 MHz) δ 1.17 (t, *J* = 7.1, 3H), 4.15 (q, *J* = 7.1 Hz, 2H), 4.70 (s, 2H), 6.09 (s, 2H), 6.80 (d, *J* = 8.6 Hz, 2H), 7.28-7.31 (m, 2H), 7.32 (s, 1H), 7.40 (s, 1H), 7.50 (br, 1H), 7.60 (d, *J* = 8.6 Hz, 2H), 7.76 (br, 1H), 11.78 (br, 1H); <sup>13</sup>C NMR (acetone-*d*<sub>6</sub>, 100 MHz) δ 14.4, 61.7, 65.7, 102.8, 103.2, 106.6, 111.2, 112.0, 115.4, 119.4, 123.4, 124.3, 129.9, 132.0, 132.8, 134.7, 143.1, 145.4, 150.5, 151.6, 162.1, 168.7; IR (KBr) 3372, 2922, 1731, 1597,

1499, 1482, 1429, 1328, 1279, 1250, 1161, 1098, 1037, 916, 769  $\text{cm}^{-1}$ ; MS (70 eV)  $m/z$  495 ( $[\text{M}^+]$ , 32), 252 (100); EI-HRMS calcd for  $[\text{M}^+]$   $\text{C}_{24}\text{H}_{21}\text{N}_3\text{O}_7\text{S}$  495.1100, found 495.1089.

**General Procedure B: Hydrolysis of Esters 3-4 to Acids 3-5.** A solution of the corresponding ester (0.085 mmol) and  $\text{LiOH} \cdot \text{H}_2\text{O}$  (87 mg) in 1.5 mL of  $\text{MeOH}/\text{water}/\text{THF}$  (1:1:2) was heated at reflux for 3 h. After removing the organic solvents under reduced pressure, the residue was acidified with aqueous  $\text{HCl}$  (1 M) until the acid precipitated. The product was filtered off, washed with water, and dried in vacuum to give the free acid.

**2-(4-(*N*-(2-(1*H*-Benzimidazol-2-yl)-5-cyanophenyl)sulfamoyl)-phenoxy)acetic Acid (3-5b).** From **3-4b**, 92% yield. Mp  $>210$  °C (dec);  $^1\text{H}$  NMR ( $\text{CD}_3\text{OD}$ , 400 MHz)  $\delta$  4.60 (s, 2H), 6.80 (d,  $J = 8.9$  Hz, 2H), 7.33-7.38 (m, 2H), 7.51 (dd,  $J = 8.2$  Hz, 1.3 Hz, 1H), 7.62 (d,  $J = 8.9$  Hz, 2H), 7.65-7.69 (m, 2H), 7.97 (d,  $J = 8.2$  Hz, 1H), 8.00 (d,  $J = 1.4$  Hz, 1H);  $^{13}\text{C}$  NMR ( $\text{DMSO}-d_6$ , 100 MHz)  $\delta$  65.7, 111.7, 114.5, 115.1, 118.7, 121.0, 121.5, 122.6, 128.1, 128.5, 131.3, 133.6, 137.5, 143.0, 150.2, 160.4, 170.2; IR (KBr) 3071, 2922, 2851, 2233, 1735, 1594, 1581, 1570, 1497, 1401, 1333, 1274, 1155, 1094, 566, 552  $\text{cm}^{-1}$ ; ESI-MS  $m/z$  449.0918 ( $[\text{M} + \text{H}]^+$ ); ESIHRMS calcd for  $[\text{M} + \text{H}]^+$   $\text{C}_{22}\text{H}_{17}\text{N}_4\text{O}_5\text{S}$  449.0914, found 449.0913.

**2-(4-(*N*-(5(6)-Cyano-2-(5-methoxy-1*H*-benzimidazol-2-yl)-phenyl)sulfamoyl)phenoxy)acetic Acid (3-5c).** From **3-4c**, 85% yield. Mp 112-115 °C;  $^1\text{H}$  NMR ( $\text{CD}_3\text{OD}$ , 400 MHz)  $\delta$  3.89 (s, 3H), 4.61 (s, 2H), 6.82 (d,  $J = 9.0$  Hz, 2H), 6.98 (dd,  $J = 8.9$  Hz, 2.4 Hz,

1H), 7.12 (d,  $J = 2.4$  Hz, 1H), 7.51 (dd,  $J = 8.2$  Hz, 1.6 Hz, 1H), 7.58 (d,  $J = 9.1$ , 1H), 7.62 (d,  $J = 9.0$  Hz, 2H), 7.92 (d,  $J = 8.2$  Hz, 1H), 8.00 (d,  $J = 1.3$  Hz, 1H);  $^{13}\text{C}$  NMR (DMSO- $d_6$ , 100 MHz)  $\delta$  55.6, 64.9, 96.7, 111.8, 113.6, 114.9, 118.1, 120.1, 121.2, 126.0, 128.0, 128.6, 130.8, 137.9, 148.1, 156.6, 161.1, 169.3; IR (KBr) 2924, 2851, 2231, 1735, 1636, 1594, 1570, 1496, 1405, 1272, 1157, 1094, 833, 554  $\text{cm}^{-1}$ ; MS (70 eV)  $m/z$  478 ( $[\text{M}^+]$ , 8), 263.1 (100); EI-HRMS calcd for  $[\text{M}^+]$   $\text{C}_{23}\text{H}_{18}\text{N}_4\text{O}_6\text{S}$  478.0947, found 478.0946.

**(4-(2-(1H-Benzimidazol-2-yl)-5-thiazol-2-yl-phenylsulfamoyl)-phenoxy)acetic Acid (3-5d).** From **3-4d**, 71% yield. Mp  $>300$  °C;  $^1\text{H}$  NMR ( $\text{CD}_3\text{OD}$ , 400 MHz)  $\delta$  4.43 (s, 2H), 6.73 (d,  $J = 9.0$  Hz, 2H), 7.30-7.36 (m, 2H), 7.58 (d,  $J = 9.0$  Hz, 2H), 7.64-7.71 (m, 3H), 7.78 (dd,  $J = 8.1$ , 1.8 Hz, 1H), 7.89-7.95 (m, 2H), 8.33 (d,  $J = 1.7$  Hz, 1H);  $^{13}\text{C}$  NMR (DMSO- $d_6$ , 100 MHz)  $\delta$  66.0, 114.9, 115.9, 117.5, 121.5, 123.1, 128.6, 130.9, 134.4, 139.0, 144.3, 150.2, 161.7, 166.0, 169.6; IR (KBr) 3401 (br), 1612, 1595, 1577, 1496, 1426, 1324, 1247, 1162, 1095, 1065, 576  $\text{cm}^{-1}$ ; FAB-MS (thioglycerol)  $m/z$  507 ( $[\text{M}^+]$ , 24), 349.1 (26), 327 (28), 311 (62), 279 (58), 237 (100); FAB-HRMS calcd for  $[\text{M}^+]$   $\text{C}_{24}\text{H}_{19}\text{N}_4\text{O}_5\text{S}_2$  507.0797, found 507.0835.

**(4-[2-(1H-Benzimidazol-2-yl)-5-methoxy-phenylsulfamoyl]-phenoxy)acetic Acid (3-5e).** From **3-4e**, 88% yield. Mp 128-131 °C;  $^1\text{H}$  NMR ( $\text{CD}_3\text{OD}$ , 400 MHz)  $\delta$  3.72 (s, 3H), 4.52 (s, 2H), 6.67 (dd,  $J = 8.8$ , 2.5 Hz, 1H), 6.73 (d,  $J = 8.9$  Hz, 2H), 7.09 (d,  $J = 2.5$  Hz, 1H), 7.22-7.26 (m, 2H), 7.54-7.58 (m, 4H), 7.67 (d,  $J = 8.8$  Hz, 1H);  $^{13}\text{C}$  NMR ( $\text{CD}_3\text{OD}$ , 100 MHz)  $\delta$  56.0, 65.9, 107.8, 111.3, 111.8, 115.35, 115.42, 124.1, 129.8,

130.0, 132.2, 137.9, 139.8, 151.5, 162.5, 162.6, 171.9; IR (KBr) 2934, 1735, 1629, 1611, 1594, 1581, 1497, 1302, 1261, 1230, 1155, 1092 cm<sup>-1</sup>; MS (70 eV) *m/z* 454 ([M + H<sup>+</sup>] 100); ESI-TOF-HRMS calcd for [M + H<sup>+</sup>] C<sub>22</sub>H<sub>20</sub>N<sub>3</sub>O<sub>6</sub>S 454.1067, found 454.1097.

**2-(4-(N-(2-(1H-Benzimidazol-2-yl)-4-methoxyphenyl)sulfamoyl)-phenoxy)acetic**

**Acid (3-5f).** From **3-4f**, 96% yield. Mp 187-190 °C; <sup>1</sup>H NMR (DMSO-*d*<sub>6</sub>, 400 MHz)  $\delta$  3.81 (s, 3H), 4.64 (s, 2H), 6.82 (d, *J* = 8.9 Hz, 2H), 7.06 (dd, *J* = 9.0, 2.8 Hz, 1H), 7.29-7.34 (m, 2H), 7.54 (d, *J* = 8.9 Hz, 2H), 7.59 (d, *J* = 8.9 Hz, 1H), 7.59 (d, *J* = 2.9 Hz, 1H), 7.68 (br, 2H); <sup>13</sup>C NMR (DMSO-*d*<sub>6</sub>, 100 MHz)  $\delta$  55.6, 64.5, 109.4, 111.9, 114.5, 114.6, 116.8, 117.6, 121.4, 123.3 (br), 128.5, 130.0, 130.6, 149.9, 155.2, 160.6, 169.1; IR (KBr) 3067, 2928, 2853, 2736, 1735, 1594, 1582, 1500, 1330, 1233, 1159, 1095, 835 cm<sup>-1</sup>; MS (70 eV) *m/z* 453 ([M<sup>+</sup>], 18), 238 (100); EI-HRMS calcd for [M<sup>+</sup>] C<sub>22</sub>H<sub>19</sub>N<sub>3</sub>O<sub>6</sub>S<sub>4</sub> 53.0994, found 453.1009.

**2-(4-(N-(2-(1H-Benzimidazol-2-yl)-4-(dimethylamino)phenyl)-sulfamoyl)phenoxy)acetic**

**Acid (3-5g).** From **3-4g**, 67% yield. Mp >230 °C; <sup>1</sup>H NMR (CD<sub>3</sub>OD, 400 MHz)  $\delta$  2.93 (s, 6H), 4.28 (s, 2H), 6.58 (d, *J* = 9.3 Hz, 2H), 6.81 (d, *J* = 7.7 Hz, 1H), 7.23-7.32 (m, 5H), 7.43 (d, *J* = 8.8 Hz, 1H), 7.59-7.63 (m, 2H); <sup>13</sup>C NMR (DMSO-*d*<sub>6</sub>, 100 MHz)  $\delta$  41.4, 67.6, 112.0, 113.8, 116.7, 118.2, 120.5, 121.0, 127.6, 128.6, 143.1, 153.8, 159.7, 171.0; IR (KBr) 3436, 1686, 1648, 1444, 1384, 1212, 1140, 846, 804, 726 cm<sup>-1</sup>; MS (70 eV) *m/z* 466.1 ([M<sup>+</sup>], 9), 252.2 (100), 238.1 (100), 184 (44), 125 (46); EI-HRMS calcd for [M<sup>+</sup>] C<sub>23</sub>H<sub>22</sub>N<sub>4</sub>O<sub>5</sub>S 466.1311, found 466.1326.

**2-(4-(N-(2-(5(6)-Cyano-1H-benzimidazol-2-yl)-4-methoxyphenyl)sulfamoyl)- phen-**

**oxy)acetic Acid (3-5h).** From **3-4h**, 49% yield. Mp 236-239 °C; <sup>1</sup>H NMR (DMSO-*d*<sub>6</sub>, 400 MHz) δ 3.85 (s, 3H), 4.54 (s, 2H), 6.57 (d, *J* = 9.0 Hz, 2H), 7.08 (dd, *J* = 9.0, 2.9 Hz, 1H), 7.30 (d, *J* = 9.0 Hz, 2H), 7.32 (d, *J* = 2.9 Hz, 1H), 7.61 (dd, *J* = 8.4, 1.5 Hz, 1H), 7.65 (d, *J* = 9.0 Hz, 1H), 7.73 (br, 1H), 8.05 (br, 1H); <sup>13</sup>C NMR (DMSO-*d*<sub>6</sub>, 100 MHz) δ 55.6, 64.6, 104.8, 112.4, 114.4, 117.6, 119.5, 122.5, 126.3, 128.5, 130.0, 130.2, 152.8, 155.5, 160.7, 169.1; IR (KBr) 3293 (br), 3078, 2927, 2224, 1735, 1592, 1502, 1339, 1240, 1158, 1095, 835, 570 cm<sup>-1</sup>; ESI-MS *m/z* 479.10 ([M + H<sup>+</sup>]); ESI-HRMS calcd for [M + H<sup>+</sup>] C<sub>23</sub>H<sub>19</sub>N<sub>4</sub>O<sub>6</sub>S 479.1020, found 479.1053.

**2-(4-(N-(2-(5(6)-Cyano-1H-benzimidazol-2-yl)phenyl)sulfamoyl)-phenoxy)acetic**

**Acid (3-5i).** From **3-4i**, 68% yield. Mp 279-281 °C; <sup>1</sup>H NMR (DMSO-*d*<sub>6</sub>, 400 MHz) δ 4.69 (s, 2H), 6.92 (d, *J* = 8.9 Hz, 2H), 7.26 (td, *J* = 7.4, 1.0 Hz, 1H), 7.50 (td, *J* = 7.4, 1.4 Hz, 1H), 7.63-7.62 (m, 4H), 7.81 (br, 1H), 8.05 (d, *J* = 7.8 Hz, 1H), 8.24 (br, 1H), 12.71 (br, 1H); <sup>13</sup>C NMR (DMSO-*d*<sub>6</sub>, 100 MHz) δ 64.6, 104.8, 114.8, 115.3, 119.0, 119.5, 123.5, 126.3, 126.4, 127.9, 128.8, 130.5, 131.6, 137.1, 153.0, 161.0, 169.2; IR (KBr) 3300, 2923, 2220, 1741, 1594, 1581, 1492, 1339, 1251, 1160, 1095, 576 cm<sup>-1</sup>; MS (70 eV) *m/z* 448 ([M<sup>+</sup>], 10), 234.1 (100); EI-HRMS calcd for [M<sup>+</sup>] C<sub>22</sub>H<sub>16</sub>N<sub>4</sub>O<sub>5</sub>S 448.0841, found 448.0867.

**2-(4-(N-(2-(5(6)-Methoxy-1H-benzimidazol-2-yl)phenyl)sulfamoyl)phenoxy)acetic**

**Acid (3-5k).** From **3-4k**, 90% yield. Mp 133-135 °C; <sup>1</sup>H NMR (CD<sub>3</sub>OD, 400 MHz) δ 3.83 (s, 3H), 4.53 (s, 2H), 6.68 (d, *J* = 9.0 Hz, 2H), 6.91 (dd, *J* = 8.8, 2.4 Hz, 1H), 7.08 (d, *J* = 2.3, 1H), 7.17 (td, *J* = 7.6, 1.2 Hz, 1H), 7.33 (td, *J* = 7.5, 1.5 Hz, 1H), 7.46-7.51 (m,

3H), 7.61 (dd,  $J = 9.2, 1.0$  Hz, 1H), 7.71 (dd,  $J = 7.9, 1.4$  Hz, 1H);  $^{13}\text{C}$  NMR ( $\text{CD}_3\text{OD}$ , 100 MHz)  $\delta$  56.2, 65.9, 97.5, 114.2, 115.3, 116.9, 119.9, 123.1, 125.6, 128.1, 130.0, 131.3, 132.2, 133.6, 137.8, 138.3, 150.6, 158.3, 162.4, 171.8; IR (KBr) 3068, 2943, 1636, 1595, 1492, 1403, 1332, 1302, 1274, 1233, 1155, 824, 573  $\text{cm}^{-1}$ ; MS (70 eV)  $m/z$  453.2 ( $[\text{M}^+]$ , 26), 238 (100); EI-HRMS calcd for  $[\text{M}^+]$   $\text{C}_{22}\text{H}_{19}\text{N}_3\text{O}_6\text{S}$  453.0995, found 453.1032.

**2-(4-(*N*-(6-(1*H*-Benzimidazol-2-yl)benzo[1,3]dioxol-5-yl)sulfamoyl)phenoxy)acetic**

**Acid (3-5l).** From **3-4l**, 81% yield. Mp >128 °C (dec);  $^1\text{H}$  NMR ( $\text{CD}_3\text{OD}$ , 400 MHz)  $\delta$  4.34 (s, 2H), 6.00 (s, 2H), 6.57 (d,  $J = 9.0$  Hz, 2H), 7.18 (s, 1H), 7.22 (s, 1H), 7.23-7.28 (m, 2H), 7.35 (d,  $J = 9.0$  Hz, 2H), 7.55-7.58 (m, 2H);  $^{13}\text{C}$  NMR ( $\text{DMSO}-d_6$ , 100 MHz)  $\delta$  67.0, 101.6, 102.6, 106.6, 110.6, 114.9, 115.0, 123.2, 128.8, 130.0, 133.5, 144.3, 149.5, 151.0, 162.3, 171.1; IR (KBr) 3068, 2923, 1595, 1503, 1484, 1256, 1226, 1157, 1037  $\text{cm}^{-1}$ ; MS (70 eV) 467 ( $[\text{M}^+]$ , 18), 252.1 (100); EI-HRMS  $m/z$  calcd for  $[\text{M}^+]$   $\text{C}_{22}\text{H}_{17}\text{N}_3\text{O}_7\text{S}$  467.0787, found 467.0791.

**4-(2-Formyl-4-methoxy-phenylsulfamoyl)-phenoxy]acetic Acid Ethyl Ester (3-9f).** A

solution of 5-methoxy-2-nitrobenzaldehyde<sup>4</sup> **3-1f** (250 mg, 1.38 mmol) in methanol (15 mL) was hydrogenated at atmospheric pressure in the presence of Pd on activated carbon (10 wt %, 50 mg) as catalyst. After completion of the reaction (3 h) the reaction mixture was filtered through a pad of Celite and concentrated under reduced pressure. The crude amine **3-6f** was immediately dissolved in anhydrous pyridine (4 mL), and ethyl (4-chlorosulfonyl-phenoxy)-acetate<sup>2</sup> **3-10** (770 mg, 2.76 mmol) was added. The mixture was stirred at room temperature for 3 h, diluted with water (10 mL), and extracted twice

with ethyl acetate (20 mL). The combined organic extracts were dried with MgSO<sub>4</sub> and concentrated under reduced pressure. The residue was purified on silica gel (FC, gradient hexanes/EtOAc, 2:1 to 1:1) providing 243 mg of aldehyde **3-9f** as a tan solid (0.62 mmol, 45%). Mp 133-135 °C; <sup>1</sup>H NMR (CDCl<sub>3</sub>, 400 MHz) δ 1.28 (t, *J* = 7.1 Hz, 3H), 3.81 (s, 3H), 4.25 (q, *J* = 7.1 Hz, 2H), 4.62 (s, 2H), 6.87 (d, *J* = 8.9 Hz, 2H), 7.05 (d, *J* = 3.0 Hz, 1H), 7.09 (dd, *J* = 9.0, 3.3 Hz, 1H), 7.67 (d, *J* = 9.0 Hz, 1H), 7.73 (d, *J* = 8.9, 2H), 9.73 (s, 1H), 10.19 (s, 1H); <sup>13</sup>C NMR (CDCl<sub>3</sub>, 100 MHz) δ 14.2, 55.7, 61.7, 65.2, 114.6, 119.2, 121.0, 121.9, 123.4, 129.2, 131.7, 132.6, 155.5, 160.9, 167.6, 194.3; IR (KBr) 2924, 1735, 1654, 1593, 1580, 1497, 1271, 1163, 1149, 1095 cm<sup>-1</sup>; MS (70 eV) *m/z* 393 ([M<sup>+</sup>], 5), 241 (11), 129 (100); EI-HRMS calcd for [M<sup>+</sup>] C<sub>18</sub>H<sub>19</sub>NO<sub>7</sub>S 393.0882, found 393.0869.

**2-(4-(*N*-(4-(Dimethylamino)-2-formylphenyl)sulfamoyl)phenoxy)acetic Acid Ethyl Ester (3-9g).** A solution of 2-nitro-5-dimethylamino-benzaldehyde **3-1g** (255 mg, 1.3 mmol) in methanol (50 mL) was hydrogenated at room temperature and ambient pressure in the presence of Pd on activated carbon as catalyst (60 mg, 5 wt % Pd). After completion of the reaction (TLC), the catalyst was filtered off through a pad of Celite, and the solvent was evaporated under reduced pressure. The crude amine (227 mg) was immediately dissolved in pyridine (3 mL), and (4-chlorosulfonylphenoxy)-acetic acid ethyl ester **10** (462 mg, 1.66 mmol) was added. After stirring for 2 h at room temperature, the reaction mixture was poured into 1 M aqueous HCl (10 mL), and the product was extracted twice with ethyl acetate. The combined organic extracts were dried with MgSO<sub>4</sub>, filtered, and concentrated under reduced pressure. The crude product was

recrystallized from diethyl ether to give 146 mg (0.36 mmol) of aldehyde **3-9g** as a tan solid (28% total yield). Mp 85-87 °C; <sup>1</sup>H NMR (CDCl<sub>3</sub>, 400 MHz) δ 1.27 (t, *J* = 7.1 Hz, 3H), 2.94 (s, 6H), 4.25 (q, *J* = 7.1 Hz, 2H), 4.61 (s, 2H), 6.80 (d, *J* = 3.3 Hz, 1H), 6.84 (d, *J* = 9.3 Hz, 2H), 6.88 (dd, *J* = 8.8, 3.3 Hz, 1H), 7.57 (d, *J* = 8.8 Hz, 1H), 7.67 (d, *J* = 8.8 Hz, 2H), 9.70 (s, 1H), 9.85 (s, 1H); <sup>13</sup>C NMR (CDCl<sub>3</sub>, 100 MHz) δ 14.1, 40.5, 61.6, 65.1, 114.4, 118.1, 119.0, 121.7, 124.1, 128.1, 129.1, 131.8, 147.1, 160.7, 167.6, 195.1; IR (KBr) 3206, 2987, 2812, 1762, 1663, 1591, 1507, 1364, 1204, 1152, 1094, 921, 563 cm<sup>-1</sup>; MS (70 eV) *m/z* 406.2 ([M<sup>+</sup>], 68), 163.1 (100), 135.1 (100); EI-HRMS calcd for [M<sup>+</sup>] C<sub>19</sub>H<sub>22</sub>N<sub>2</sub>O<sub>6</sub>S 406.1199, found 406.1197.

**2-(4-(N-(6-Formylbenzo[1,3]dioxol-5-yl)sulfamoyl)phenoxy)acetic Acid Ethyl Ester (3-9I).** A solution of 6-nitropiperonal (1.0 g, 5.12 mmol) in ethanol (30 mL) was hydrogenated at room temperature and ambient pressure in the presence of Pd on activated carbon (200 mg, 5% Pd) as catalyst. After completion of the reaction (2 h), the catalyst was filtered through a pad of Celite, and the filtrate was concentrated under reduced pressure providing 885 mg of crude **3-7I** as a yellow solid. A solution of crude amine **3-7I** (885 mg) and (4-chlorosulfonyl-phenoxy)acetic acid ethyl ester<sup>2</sup> **3-10** (1.79 g, 6.4 mmol) in 22 mL of pyridine was stirred at room temperature for 48 h. The mixture was poured into 1 N HCl and extracted twice with ethyl acetate. The combined organic extracts were dried with anhydrous MgSO<sub>4</sub>, filtered, and concentrated under reduced pressure. The crude product was purified by silica FC (EtOAc/hexanes, gradient 1:2 to 1:1) to give 584 mg of intermediate **3-8I** as a yellowish solid. A mixture of intermediate

**8I** (576 mg, 1.41 mmol) and MnO<sub>2</sub> (1.6 g, 18.4 mmol) in 5 mL of CH<sub>2</sub>Cl<sub>2</sub> was stirred overnight at room temperature. The reaction mixture was filtered through a pad of Celite and concentrated under reduced pressure to give aldehyde **3-9I** as a pale yellow solid (378 mg, 0.928 mmol, 18% yield over three steps). Mp 166-168 °C; <sup>1</sup>H NMR (CDCl<sub>3</sub>, 400 MHz) δ 1.28 (t, *J* = 7.1 Hz, 3H), 4.26 (q, *J* = 7.1 Hz, 2H), 4.64 (s, 2H), 6.04 (s, 2H), 6.90 (d, *J* = 9.0 Hz, 2H), 6.91 (s, 1H), 7.27 (s, 1H), 7.79 (d, *J* = 9.0 Hz, 2H), 9.57 (s, 1H), 11.07 (s, 1H); <sup>13</sup>C NMR (CDCl<sub>3</sub>, 100 MHz) δ 14.3, 61.8, 65.2, 99.6, 102.5, 112.8, 114.8, 115.9, 129.3, 131.8, 137.9, 143.5, 153.7, 161.1, 167.7, 192.2; IR (KBr) 2913, 1735, 1641, 1594, 1487, 1361, 1283, 1245, 1225, 1151, 1093, 1038, 574 cm<sup>-1</sup>; MS (70 eV) 407 ([M<sup>+</sup>], 37), 164 (100); EI-HRMS *m/z* calcd for [M<sup>+</sup>] C<sub>18</sub>H<sub>17</sub>NO<sub>8</sub>S 407.0675, found 407.0662.

### 3.4.2 Structural Assignments on the Basis of 2D <sup>1</sup>H-<sup>1</sup>H COSY experiments

See Figure 3-7 and 3-8.

### 3.4.3. Electrode Calibration in Aqueous Solution

Measurements were performed with an Orion microcombination glass electrode. The electrode was calibrated for -log[H<sub>3</sub>O<sup>+</sup>] by titration of a standardized HCl solution (Aldrich, 0.1 N volumetric standard) with KOH (Aldrich, 0.1 N volumetric standard) at 25 °C and 0.1M ionic strength (KCl). The endpoint, electrode potential, and slope were determined by using Gran's method<sup>15</sup> as implemented in the software GLEE.<sup>16</sup> The calibration procedure was repeated three times prior to each p*K<sub>a</sub>* value determination. The electrode potential was measured with the Corning pH/Ion Analyzer 355 and the emf

measurements were reproducible with  $\pm 0.1$  mV accuracy.

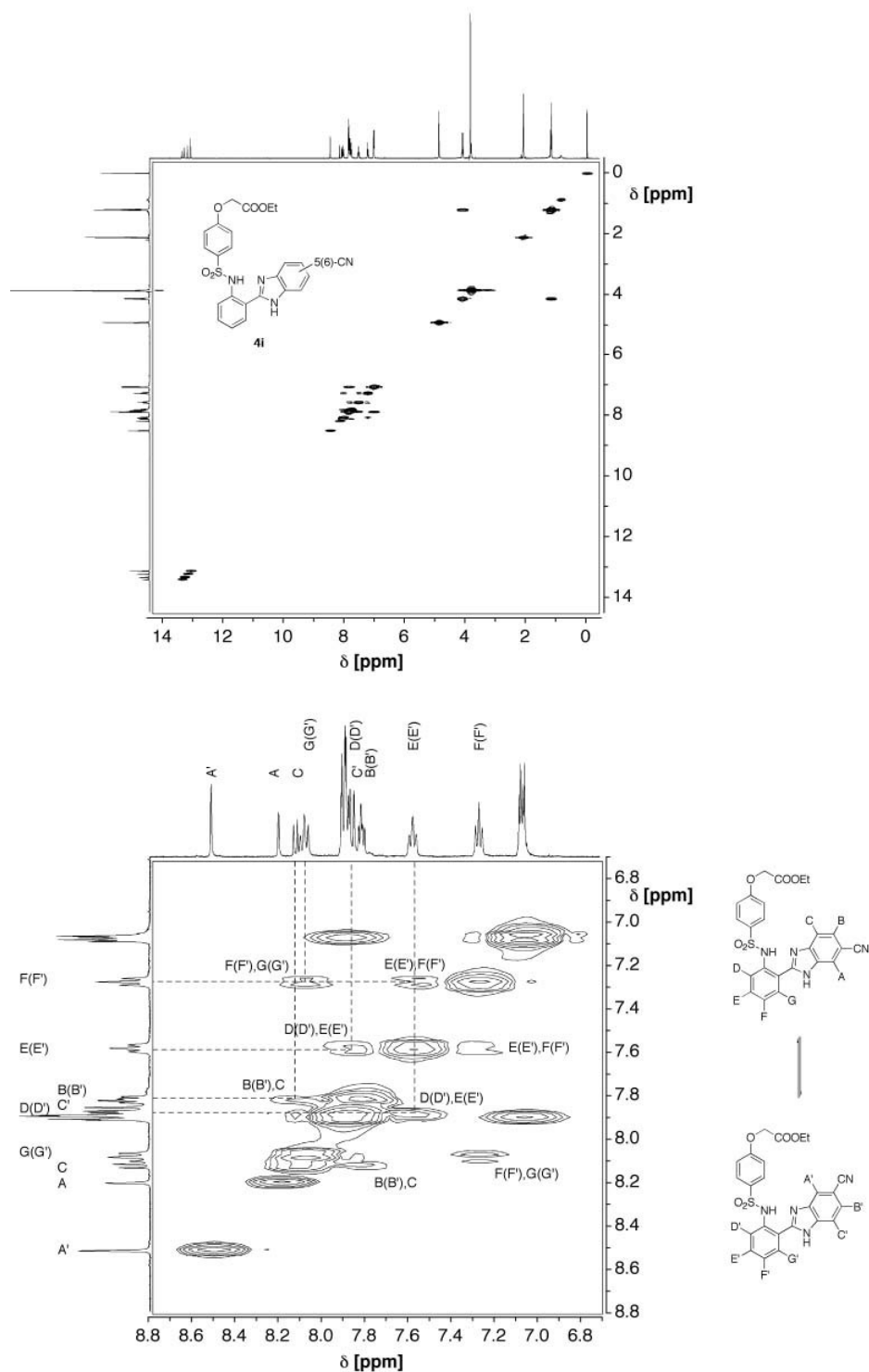


**Figure 3-7.** 2D  $^1\text{H}$ - $^1\text{H}$  COSY NMR spectrum of **3-4i** at  $-80^\circ\text{C}$  in acetone- $d_6$ . Top: overview spectrum. Bottom: Connectivity within the central aromatic ring and the benzimidazole moiety of the two tautomeric species is shown to the right.

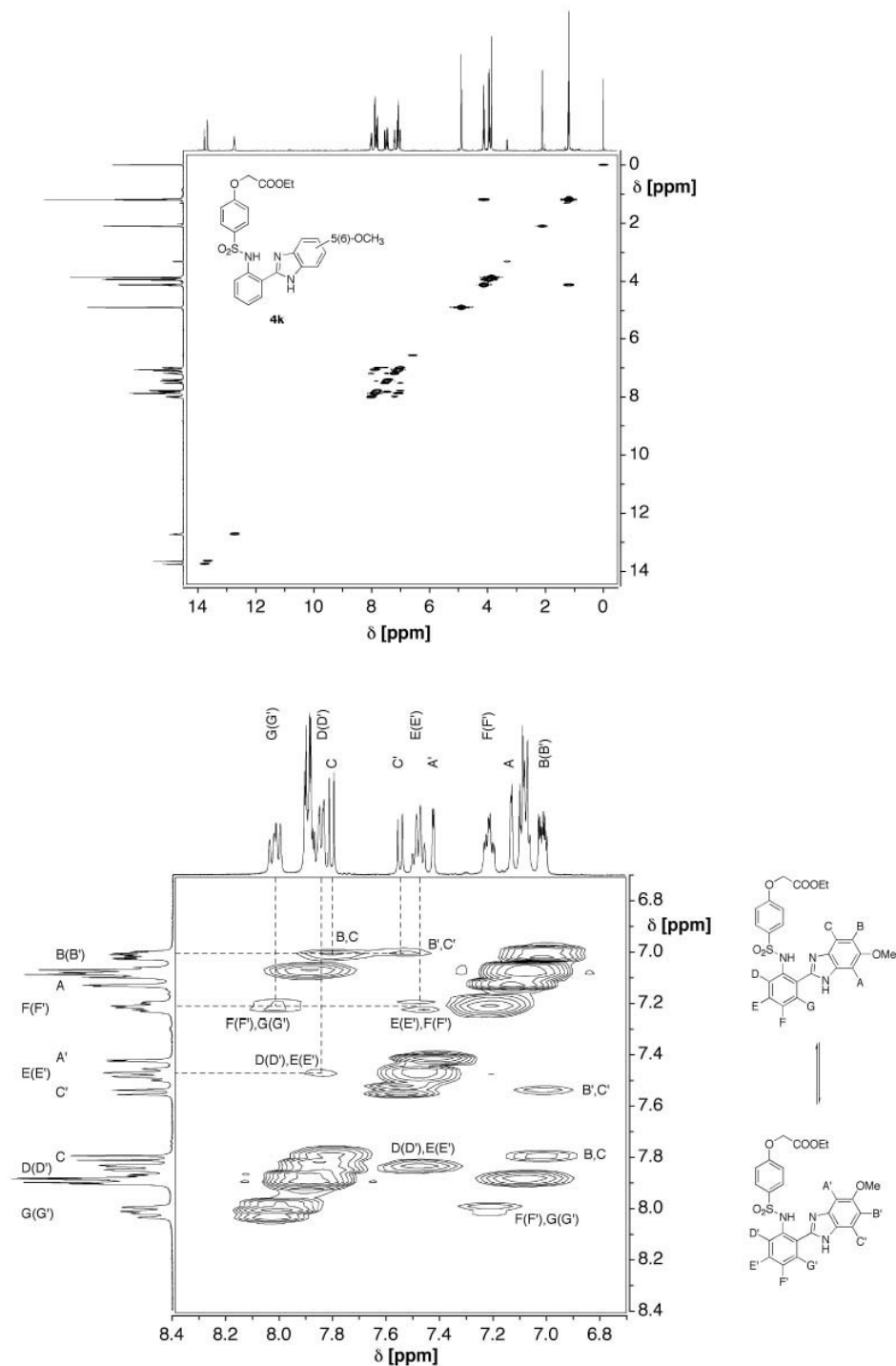


**Figure 3-8.** 2D  $^1\text{H}$ - $^1\text{H}$  COSY NMR spectrum of **3-4k** at  $-80^\circ\text{C}$  in acetone- $d_6$ . Top: overview spectrum. Bottom: Connectivity within the central aromatic ring and the benzimidazole moiety of the two tautomeric species is shown to the right.

#### 3.4.4. Spectrophotometric Titrations

The UV/Vis absorption spectra of the ligands were monitored for a series of solutions in which  $-\log[\text{H}_3\text{O}^+]$  was varied between 5 and 11. The emf of each solution was directly measured in the UV quartz cell (electrode diameter 3mm) and converted to  $-\log[\text{H}_3\text{O}^+]$  using the  $E^\circ$  and slope, as obtained from the electrode calibration procedure described above. The raw spectral and emf data were processed with nonlinear least-squares fit analysis using the SPECFIT software package.<sup>17</sup>

#### 3.4.5. Steady-state Absorption and Fluorescence Spectroscopy

All sample stock solutions and buffer solutions were filtered through 0.2 mm Nylon membrane filters to remove interfering dust particles or fibers. UV/Vis absorption spectra were recorded at 25 °C by using a Varian Cary Bio50 UV/Vis spectrometer with constant-temperature accessory. Steady-state emission and excitation spectra were recorded with a PTI fluorimeter and FELIX software. Throughout the titration the sample solution was stirred with a magnetic stirring device. For all titrations the path length was 1 cm with a cell volume of 3.0 mL. All fluorescence spectra have been corrected for the spectral response of the detection system (emission correction file provided by the instrument manufacturer) and for the spectral irradiance of the excitation channel (by using a calibrated photodiode). Quantum yields were determined by using quinine sulfate dihydrate in 1.0 N  $\text{H}_2\text{SO}_4$  ( $\Phi_f = 0.54 \pm 0.05$ ) as the fluorescence standard.<sup>18</sup>

### 3.5. References:

1. Fahrni, C. J.; Henary, M. M.; VanDerveer, D. G. *J. Phys. Chem. A* **2002**, *106*, 7655.
2. Hammett, L. P. *J. Am. Chem. Soc.* **1937**, *59*, 96.
3. Hansch, C.; Leo, A.; Taft, R. W. *Chem. Rev.* **1991**, *91*, 165.
4. Minkin, V. I.; Garnovskii, A. D.; Elguero, J.; Katritzky, A. R.; Denisko, O. V. In *Advances in Heterocyclic Chemistry*; Vol, 76, 157.
5. Raczynska, E. D. *J. Chem. Res. Synop.* 1998, 704.
6. Mosquera, M.; Penedo, J. C.; Rios Rodriguez, M. C.; Rodriguez-Prieto, F. *J. Phys. Chem.* **1996**, *100*, 5398.
7. Henary, M. M.; Fahrni, C. J. *J. Phys. Chem. A* **2002**, *106*, 5210.
8. Cheng, Y. M.; Pu, S. C.; Hsu, C. J.; Lai, C. H.; Chou, P. T. *ChemPhysChem* **2006**, *7*, 1372.
9. Henary, M. M.; Wu, Y.; Fahrni, C. J. *Chem. Eur. J.* **2004**, *10*, 3015.
10. Dann, O.; Ruff, J.; Wolff, H. P.; Griessmeier, H. *Liebigs Ann. Chem.* **1984**, 409.
11. Manetsch, R.; Zheng, L.; Reymond, M. T.; Woggon, W.-D.; Reymond, J.-L. *Chem. Eur. J.* **2004**, *10*, 2487.
12. Katritzky, A. R.; Xu, Y.-J.; Vakulenko, A. V.; Wilcox, A. L.; Bley, K. R. *J. Org. Chem.* **2003**, *68*, 9100.
13. Jung, M. E.; Dansereau, S. M. K. *Heterocycles* **1994**, *39*, 767.
14. Amman, C.; Meier, P.; Merbach, A. E. *J. Magn. Reson.* **1982**, *46*, 319.
15. Gran, G. *Analyst* **1951**, *77*, 661.

16. Gans, P.; O'Sullivan, B. *Talanta* **2000**, *51*, 33.
17. Binstead, R. A.; Zuberbühler, A. D. SPECFIT Global Analysis System, Spectrum Software Associates, Marlborough MA 01752, **2001**.
18. Demas, J. N.; Crosby, G. A. *J. Phys. Chem.* **1971**, *75*, 991.

## CHAPTER IV

# EXCITED STATE INTRAMOLECULAR PROTON TRANSFER IN 2-(2'-ARYLSULFONAMIDOPHENYL)BENZIMIDAZOLE DERIVATIVES: INSIGHTS INTO THE ORIGIN OF DONOR SUBSTITUENT-INDUCED EMISSION ENERGY SHIFTS

### 4.1. Introduction

The systematic studies on substituent effects on the photophysical properties of 2-(2'-arylsulfonamidophenyl)benzimidazole fluorophores described in Chapter 3 revealed that the peak emission energies of the methoxy substituted derivatives **4-2** and **4-3** (Chart 4-1) strongly depended on the substituent attachment position while their absorption spectra show very little shift. This observation implies that the substituent might influence the fluorescence emission properties of this compound class with unexpected complexity. Since the peak emission energy represents a key property of fluorescence sensors, it would be worthwhile investigating the origin of this effect to gain further insights for rationally tuning and ultimately optimizing the ESIPT sensor properties.

Principally, the observed substituent effects on the fluorescence emission energy could be due different polarization of the excited state, specific solute-solvent interactions, or perhaps a differential stabilization of the frontier orbital energies depending on the

attachment position of the substituents. Solute-solvent interactions could be based on simple isotropic dielectric effects, or alternatively, non-isotropic hydrogen-bonding interactions with the fluorophore. The latter may be of particular importance since all photophysical measurements were performed in aqueous buffer solution, a very polar solvent environment that offers potentially strong hydrogen-bonding interactions. For example, methoxy and sulfonyl groups may undergo hydrogen bonding interactions through their oxygen lone-pair electrons. In addition, because an intramolecular proton-transfer process is the key photophysical feature of the investigated systems, hydrogen-bonding interactions might play a central role in understanding the observed substituent effects.

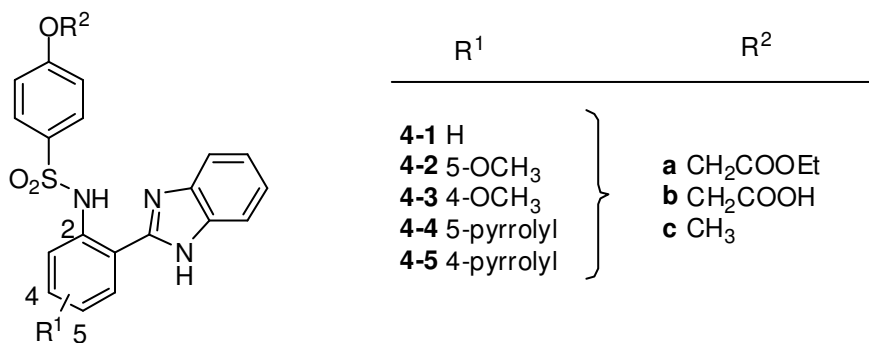
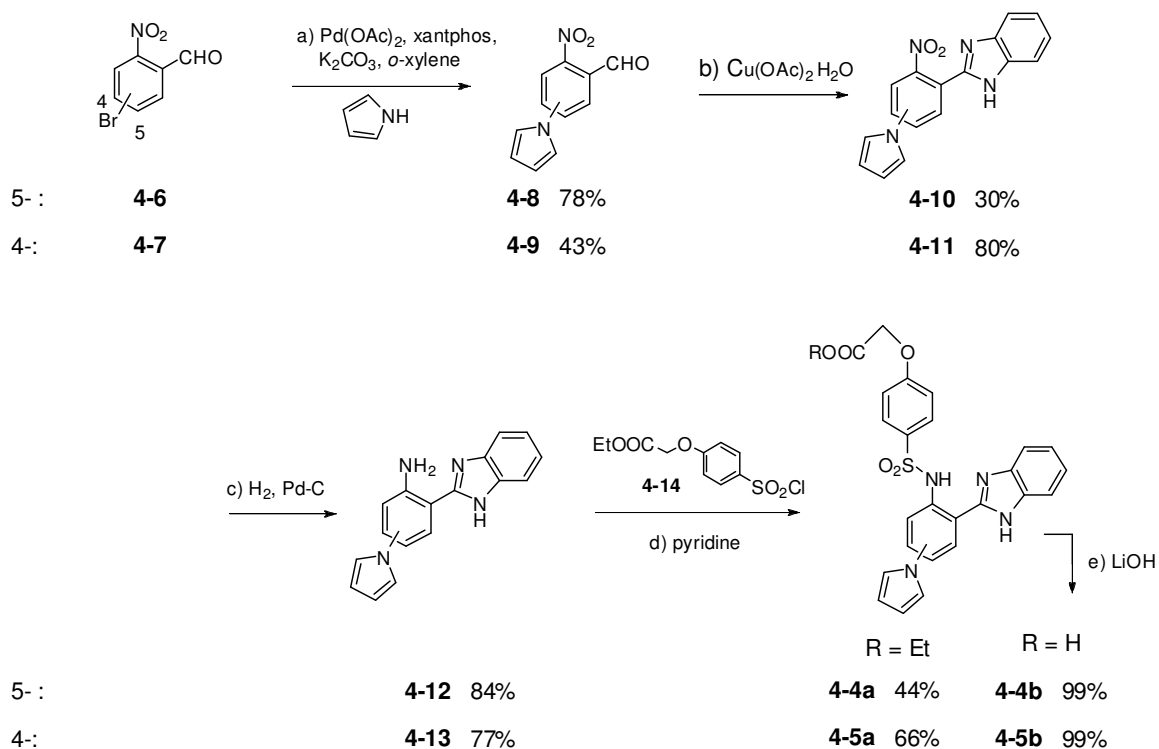


**Chart 4-1**

In order to evaluate the importance of these factors, detailed solvatochromic studies were performed with the methoxy-substituted **4-2** and **4-3**. Furthermore, to explore whether the hydrogen-bonding of the methoxy substituent is important to the photophysical properties of **4-2** and **4-3**, two additional derivatives of 2-(2'-arylsulfonamidophenyl)benzimidazoles with a pyrrole rather than methoxy substituent as donor group (**4-4** and **4-5**) were synthesized and characterized. In pyrrole, the nitrogen lone-pair electrons are integral part of an aromatic ring-system and therefore not readily available for hydrogen-bonding interactions with the solvent.

## 4.2. Results and Discussion

### 4.2.1. Synthesis



**Scheme 4-1**

The procedures for the synthesis of parent compound **4-1**, sulfonyl chloride **4-14**, and the methoxy-substituted derivatives **4-2** and **4-3** were already described in Chapters 2 and 3, respectively.<sup>1,2</sup> The pyrrole-substituted derivatives **4-4** and **4-5** were synthesized using a similar approach, which included copper-mediated oxidative coupling of the corresponding nitro-benzaldehydes (**4-8** and **4-9**) with *o*-phenylenediamine to form benzimidazoles **4-10** and **4-11**, respectively, followed by reduction of the nitro group and

**Table 4-1:** Protonation Constants and Photophysical Data of Benzimidazole Derivatives **4-1b-4-5b** in Aqueous Solution<sup>a</sup>

Species	Data	<b>4-1b</b> <sup>b</sup>	<b>4-2b</b>	<b>4-3b</b>	<b>4-4b</b>	<b>4-5b</b>
pK <sub>a1</sub>	[L <sup>2-</sup> ][H <sup>+</sup> ]/[LH <sup>-</sup> ]	8.04 ± 0.03	8.34 ± 0.02	7.60 ± 0.01	7.69 ± 0.01	7.28 ± 0.01
pK <sub>a2</sub>	[LH <sup>-</sup> ][H <sup>+</sup> ]/[LH <sub>2</sub> ]	4.50 ± 0.04	4.54 ± 0.05	4.79 ± 0.01	4.32 ± 0.05	4.44 ± 0.02
L <sup>2-</sup>	absorption <sup>c</sup> λ <sub>max</sub> (nm)	301 (1.59)	305 (1.10)	302 (1.62)	277 (2.28)	310 (1.61)
		329 (1.09)	334 (0.70)	329 (1.54)	339 (0.76)	340 (1.43)
	excitation <sup>d</sup> λ <sub>max</sub> (nm)	296	297	330	337 (sh)	310
	emission <sup>d</sup> λ <sub>max</sub> (nm)	418	444	396	438	404
	quantum yield <sup>e</sup>	0.26	0.27	0.06	0.32	0.32
	Stokes shift (cm <sup>-1</sup> )	6470	7420	5140	6660	4660
LH <sup>-</sup>	absorption <sup>c</sup> λ <sub>max</sub> (nm)	299 (1.23)	298 (1.00)	305 (1.57)	270 (2.36)	316 (1.72)
					303 (sh)	
	excitation λ <sub>max</sub> (nm)	300	295	308	<i>n/a</i>	321
	emission λ <sub>max</sub> (nm)	460	497	437	485	444
	Stokes shift (cm <sup>-1</sup> )	11,700	13,430	9640	12,380	9120
	quantum yield <sup>e</sup>	0.23	0.14	0.17	0.16	0.13
LH <sub>2</sub>	absorption <sup>c</sup> λ <sub>max</sub> (nm)	290 (1.31)	292 (1.07)	303 (1.69)	272 (2.35)	316 (1.79)

[a] 0.1 M KCl, 25 °C. [b] Data from ref 1. [c] From deconvolution analysis, molar extinction coefficient [10<sup>4</sup> L mol<sup>-1</sup> cm<sup>-1</sup>] in parentheses. [d] pH 11.20, 0.1 M KCl. [e] Quinine sulfate in 1 N H<sub>2</sub>SO<sub>4</sub> as standard.

reaction of the anilines **4-12** and **4-13** with sulfonyl chloride<sup>1</sup> **4-14** to give the final fluorophores **4-4** and **4-5**. The precursors **4-8** and **4-9** were synthesized via palladium-catalyzed amination of bromo-benzene **4-6** and **4-7**, respectively. The ethyl esters **4-1a** through **4-5a** were used for solvatochromic studies in organic solvents, while the corresponding carboxylic acids **4-1b** through **4-5b** were used for the photophysical characterization in aqueous solution. The hydrolysis of the corresponding ethyl esters was accomplished under mild conditions with lithium hydroxide in a methanol-water-THF solvent mixture.

#### **4.2.2. Protonation Equilibria**

The protonation equilibria of each compound was investigated by UV-vis titration with  $-\log[\text{H}_3\text{O}^+]$  ranging between 5 to 11. The absorption spectra of deprotonated species  $\text{L}^{2-}$  and monoprotated species  $\text{HL}^-$  were deconvoluted from UV-vis traces obtained from the spectrophotometric titrations. The  $\text{p}K_{\text{a}}$  values obtained from non-linear least squares fitting procedures and all spectral data are listed in Table 4-1. The  $\text{p}K_{\text{a}1}$  is associated with a large bathochromic shift of the absorption maximum, and can be therefore readily assigned to deprotonation of the sulfonamide group. In contrast,  $\text{p}K_{\text{a}2}$  results only in small absorption changes and can be therefore assigned to deprotonation of the carboxylic acid group, which is electronically decoupled from conjugated  $\pi$ -system of the fluorophore.

As evident from Table 4-1, the  $pK_a$  values of the derivatives containing the electron donating substituent in the *para*-position relative to the sulfonamide group (**4-2b**: 8.34, **4-4b**: 7.69) are higher than those of the *meta*-substituted derivatives (**4-3b**: 7.60, **4-5b**: 7.28). This observation can be readily rationalized by weighing the contributions of substituent resonance stabilization and inductive effects as already discussed in Chapter 3. Furthermore, the  $pK_a$  values of the pyrrole-substituted derivatives **4-4b** and **4-5b** are significantly lower compared to their methoxy-substituted analogs, suggesting that the pyrrole ring acts primarily as  $\sigma$ -acceptor rather than  $\pi$ -donor moiety in the ground state.

### 4.2.3. UV-vis Spectra

While the methoxy substituents have no significant effect on the absorption spectra, the 4-pyrrolyl-substituted derivative **4-4b** revealed an additional strong absorption band centered around 270 nm (Figure 4-1), thus indicating significant electronic interactions between pyrrole ring and fluorophore  $\pi$ -system. For 5-pyrrolyl-substituted derivative **4-5b**, the peak absorptions are significantly red-shifted (HL<sup>-</sup>: 316 nm, L<sup>2-</sup>: 340 nm) compared to the parent compound **4-1b** (HL<sup>-</sup>: 299 nm, L<sup>2-</sup>: 329 nm), but the shape of the absorption spectra are qualitatively quite similar. Interestingly, an additional low-energy band centered around 365 nm was observed for both **4-3b** and **4-5b**, which is presumably due to the presence of a ground-state tautomeric equilibrium as discussed in Chapter 3.

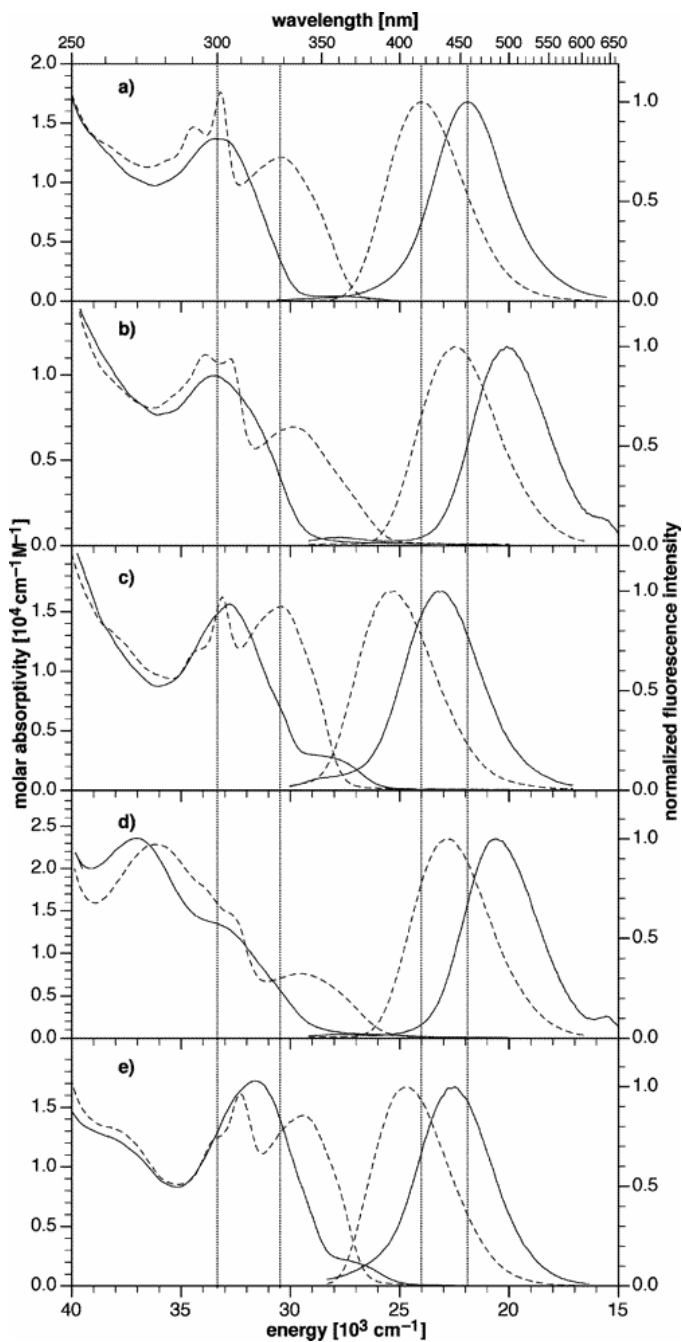


**Figure 4-1.** Deconvoluted UV-vis absorption spectra (left) and normalized fluorescence emission spectra (right) of fluorophore: (a) **4-1b**, (b) **4-2b**, (c) **4-3b**, (d) **4-4b**, and (e) **4-5b** in aqueous solution (0.1 M KCl, 25 °C). UV-vis traces for the species with protonated (-) and deprotonated (---) sulfonamide group were obtained through deconvolution of a series of spectra with pH ranging between 6 and 10. The emission spectra were directly recorded at pH 6.0 (-) and 11.0 (---) without deconvolution analysis (excitation at the isosbestic point).

#### 4.2.4. Fluorescence Spectra

For all derivatives, deprotonation of the sulfonamide group is associated with a hypsochromic shift in the emission spectra due to disruption of the ESIPT process. However, compared to parent compound **4-1b**, the peak emissions of the 5-substituted derivatives **4-2b** and **4-4b** are red-shifted while those of the 4-substituted derivatives **4-3b** and **4-5b** were blue-shifted.

As outlined in Section 4.1, differences in the strength of hydrogen-bonding interactions of the methoxy substituents might be a key contributor to the divergent peak emission shifts. If the methoxy group would act primarily as a strong  $\pi$ -donor, one of the two oxygen lone pairs would be involved in  $\pi$ -conjugation with the fluorophore ring system, while the other lone pair would be available for hydrogen bonding interactions with the solvent. However, if hydrogen-bonding interaction with the second lone pair outweighs resonance stabilization, the methoxy group would rotate out of plane and thus acting solely as  $\sigma$ -acceptor. As discussed above, the pyrrole-substituted derivatives **4-4b** and **4-5b** showed qualitatively the same trends in the emission spectra compared to the methoxy-substituted analogs **4-2b** and **4-3b**. Because the pyrrolyl group does not have a lone pair available for hydrogen bonding, these data strongly suggest that hydrogen-bonding interactions of the methoxy group are not critical for the interpretation of the divergent emission energy shifts. Having excluded this possibility, detailed solvatochromic shift studies were performed to further explore the origin of the peculiar substituent effects on the fluorescence emission.

#### 4.2.5. Solvatochromic Shift Studies

Solvatochromic shift measurements in a set of solvents with varying polarity represent a powerful approach to probe the extent and nature of solvent-solute interactions. The technique has been widely used as a major tool to investigate the photophysical properties of fluorophores, and is particularly suitable to determine changes in dipole moments between ground and excited state, and to probe the importance of ground and excited state hydrogen bonding interactions with solvent molecules.<sup>3</sup> Several theoretical and empirical approaches have already been established to explore these complex interactions, including the Onsager's reaction field model,<sup>4</sup> Reichardt's empirical solvent polarity scale  $E_T(30)$ ,<sup>9</sup> and Kamlet-Taft's empirical solvent index.<sup>5</sup>

For the following solvatochromic shift studies, the absorption and emission spectra of the ethyl ester derivatives of all five fluorophores were recorded in a set of 14 organic solvents. In aqueous buffer, the corresponding carboxylic acid derivatives were used. At neutral pH, the acid moiety is fully dissociated, thus significantly increasing the solubility of the fluorophores in aqueous solution. A compilation of all solvent parameters and peak energies is provided in Appendix A.

The normalized absorption and emission spectra shown Figure 4-2 illustrate the trends in solvatochromic shifts for the methoxy-substituted derivatives **4-2** and **4-3**, as well as the unsubstituted parent compound **4-1**. All fluorophores showed minor changes in their peak absorption, suggesting very small dipole moment changes between the

ground and Frank-Condon excited state. Furthermore, with increasing solvent polarity, the peak absorption energy underwent a small blue-shift, an observation that is consistent with a decrease of the molecular dipole moment upon photoexcitation. Interestingly, protic solvents revealed a stronger solvatochromic shift than would be expected solely based on their polarity (dielectric constant), suggesting that hydrogen-bonding interactions are at least partially responsible for the degree of emission shift and cannot be entirely ignored in this system. For a more detailed solvatochromic shift analysis, all three approaches mentioned above were utilized to further investigate the origin of the divergent donor-substituent induced emission shifts.

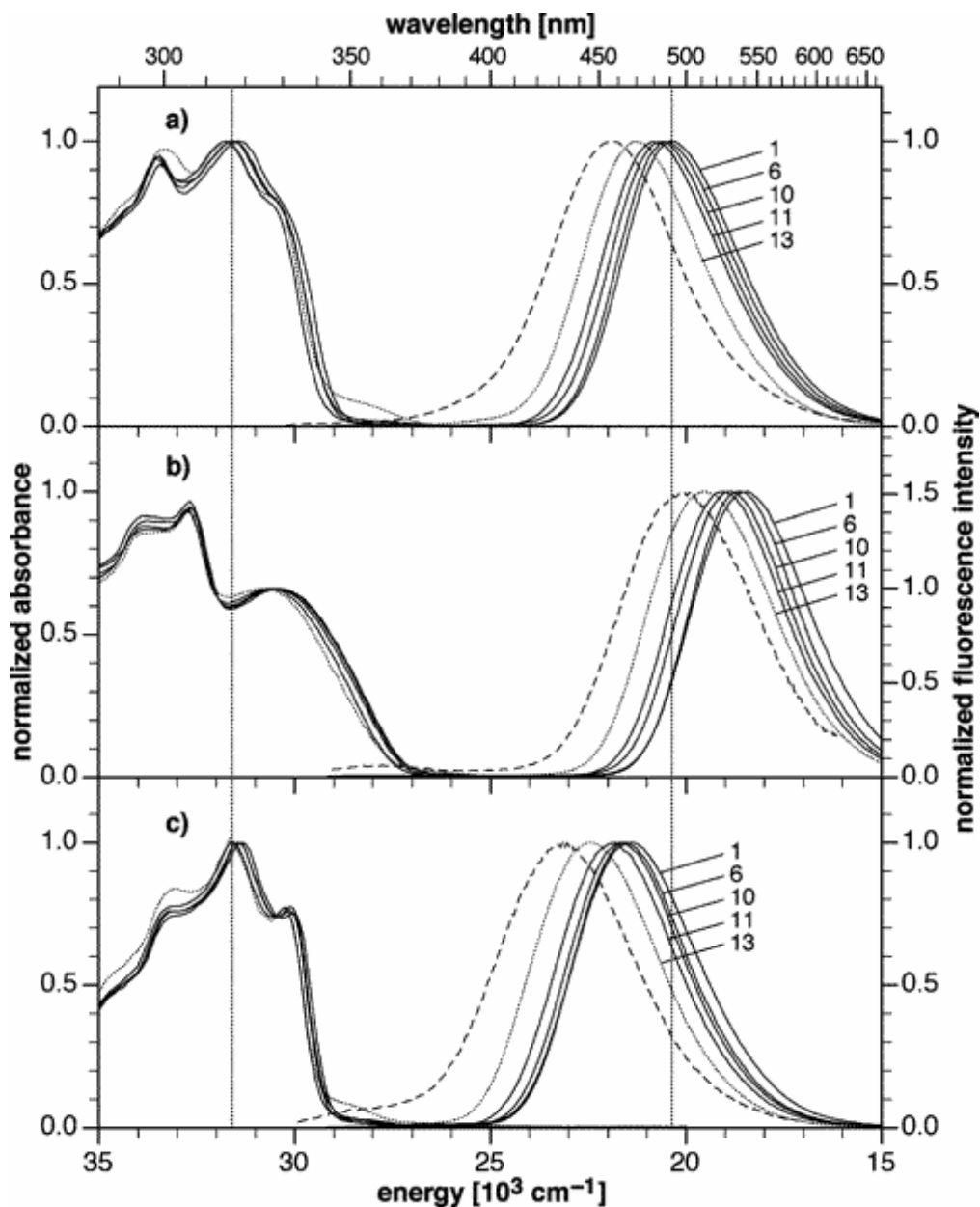


**Figure 4-2.** Normalized UV-vis absorption (left) and fluorescence emission spectra (right, excitation at peak absorption energy) for derivatives (a) **4-1a**, (b) **4-2a**, and (c) **4-3a**, in selected organic solvents illustrating the solvatochromic shift behavior (solvent legend : no. 1 1,4-dioxane, no. 6 ethylacetate, no. 10 butyronitrile, no. 11 acetonitrile, no. 13 ethanol). For comparison, the fluorescence emission spectra of the water-soluble compounds **4-1b**, **4-2b**, and **4-3b** in aqueous buffer (pH 6.0, 0.1 M KCl) have been also included (dashed traces).

#### 4.2.5.1. Onsager's Reaction Field Model

This model treats the solvent as homogeneous, polarizable medium and assumes the solute is located in a cavity of defined size surrounded by solvent molecules. The permanent dipole moment of the solute will then polarize the solvent molecules in close proximity and thus induce an opposing dipole moment that will electrostatically interact with the solute, thus resulting in a net stabilization.<sup>10</sup> If the dipole moment of the solute changes upon photoexcitation, the ground and excited state will be differently stabilized, which gives rise to the solvatochromic shift behavior. Therefore, this model is used to analyze the solvatochromic shift mainly caused by isotropic electrostatic solute-solvent interactions based on equation 4-1.<sup>6</sup>

$$v = mf(\epsilon_r, n) + const \qquad \text{Eq. 4-1}$$

with

$$f(\epsilon_r, n) = \frac{\epsilon_r - 1}{2\epsilon_r + 1} - \frac{n^2 - 1}{2n^2 + 1}$$

As shown in Figure 4-3, for derivatives **4-1**, **4-2** and **4-3**, linear regression analysis of peak emission energies versus Onsager's solvent polarity parameters  $f$  yielded a good correlation in case of all nonprotic solvents, while protic solvents, such as butanol,

ethanol, methanol and water revealed emission energies significantly outside of the linear regression range. Most importantly, all derivatives showed a similar pattern, suggesting that the substituent attachment position is not responsible for the deviation observed in protic solvents. If only nonprotic solvents are considered, a relatively flat slope is obtained from the regression analysis, indicating very little dipole moment changes between the ground and excited-states of all three derivatives. Conclusively, given the lack of significant solvatochromic shifts, dipole moment changes upon photoexcitation are not the primary reason for the divergent emission shifts observed in donor-substituted derivatives. Nevertheless, it is noteworthy that hydrogen-bonding interactions appear to promote some of the solvatochromic shift behavior; however, the overall influence is significantly smaller compared to the emission energy shift observed for the *para* vs *meta*-substituted derivative and the trend follows qualitatively for both derivatives the same direction.

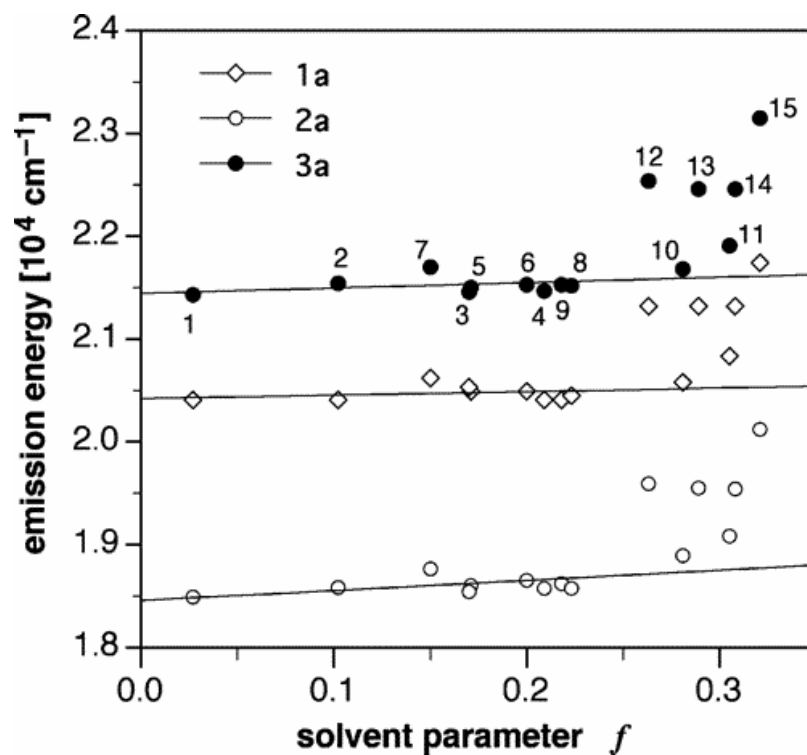


**Figure 4-3.** Correlation of the peak emission energies of derivative **4-1a**, **4-2a**, and **4-3a** with the solvent polarity parameter  $f$  ( $\epsilon, n$ ). The plotted linear regression line does not include acetonitrile (no. 11) and any protic solvents (nos. 12-15). The solvent numbering scheme and values for  $f$  ( $\epsilon, n$ ) are given in Table A-1 provided with the Appendix A.

#### 4.2.5.2. Reichardt's $E_T(30)$ Solvent Scale

This is an empirical approach based on the negative solvatochromism of an N-phenolate betaine dye.<sup>9</sup> Because the betaine dye is known to exhibit stronger spectral shifts in solvents with hydrogen-bonding donor properties, Reichardt's  $E_T^N(30)$  solvent scale already includes specific solvent acidity effects, which can be directly interpreted as the hydrogen-bond donating property of the solvent. As illustrated with Figure 4-4 and the data compiled in Table 4-2, for all derivatives, linear regression analysis with peak emission energies versus Reichardt's  $E_T^N(30)$  solvent scale gives a good correlation over the entire range of solvents, including the carboxylic acids **4-1b-4-5b** measured in aqueous buffer. This result further confirmed that the hydrogen-bond interaction with solvent molecules plays an important role in the solvatochromic shift behavior of this fluorophore system. Interestingly, the calculated slopes for all derivatives are similar, indicating again that the substituent attachment position is not important for the observed solvatochromic shift. However, the calculated intercepts from the linear regression of the 4-substituted derivatives **4-3** and **4-5** are larger than that of the parent compound **4-1**, while those of the 5-substituted derivatives **4-2** and **4-4** are smaller, suggesting that the origin of the divergent emission shift might be due to differences in the electronic structures of the fluorophores caused by attaching substituents at different positions.

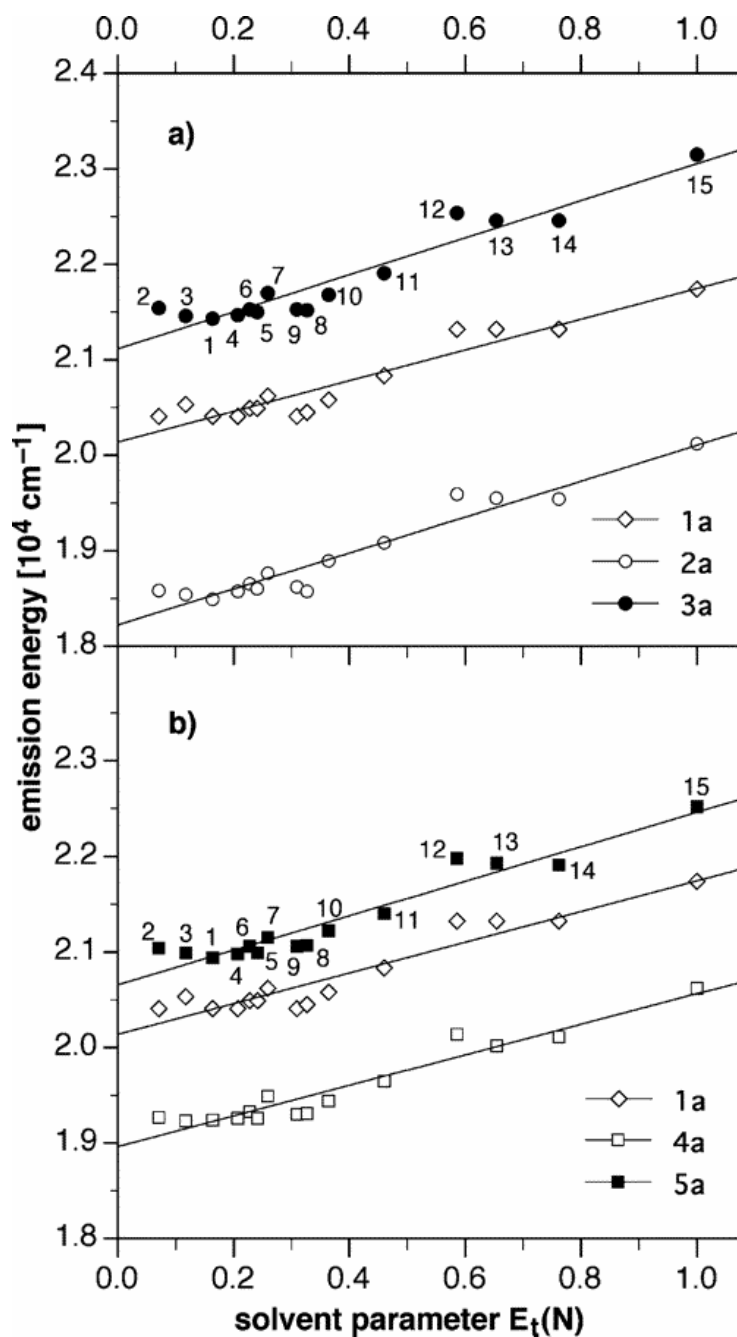


**Figure 4-4.** Linear regression analysis of the solvatochromic emission shifts according to Reichardt's  $E_T^N(30)$  empirical solvent polarity scale. (a) Linear correlation of the peak emission energies of the methoxy-substituted compounds **4-2a** and **4-3a**. (b) Linear correlation for compounds **4-4a** and **4-5a**. For ease of comparison, the data for the unsubstituted parent compound **4-1a** are included in both graphs.

**Table 4-2:** Fitted Parameters for the Regression Analysis of the Solvatochromic Peak Fluorescence Emission Shifts According to the  $E_T(30)$  Empirical Solvent Model<sup>a</sup>

parameter	<b>4-1a</b>	<b>4-2a</b>	<b>4-3a</b>	<b>4-4a</b>	<b>4-5a</b>
slope [ $\text{cm}^{-1}$ ]	1605 $\pm$ 148	1882 $\pm$ 147	1941 $\pm$ 166	1597 $\pm$ 127	1803 $\pm$ 145
intercept [ $\text{cm}^{-1}$ ]	20,140 $\pm$ 68	18,222 $\pm$ 68	21,114 $\pm$ 76	18,966 $\pm$ 58	20,658 $\pm$ 67
correlation coeff	0.949	0.962	0.956	0.961	0.960

[a] Linear regression includes all 15 solvents listed in Appendix A.

**Table 4-3:** Fitted Parameters for the Multiple Regression Analysis of the Solvatochromic Peak Fluorescence Emission Shifts According to the Kamlet-Abboud-Taft Empirical Solvent Model

parameter	<b>4-1a</b>	<b>4-2a</b>	<b>4-3a</b>	<b>4-4a</b>	<b>4-5a</b>
dielectric interactions (s, [ $\text{cm}^{-1}$ ])	369 $\pm$ 198	580 $\pm$ 262	386 $\pm$ 208	304 $\pm$ 182	388 $\pm$ 212
H-bonding donor (a, [ $\text{cm}^{-1}$ ])	842 $\pm$ 91	910 $\pm$ 121	977 $\pm$ 96	824 $\pm$ 84	904 $\pm$ 98
H-bonding acceptor (b, [ $\text{cm}^{-1}$ ])	224 $\pm$ 199	540 $\pm$ 263	322 $\pm$ 209	349 $\pm$ 183	330 $\pm$ 214
$\nu_0$ [ $\text{cm}^{-1}$ ]	20,221 $\pm$ 163	18,131 $\pm$ 216	21,215 $\pm$ 171	19,010 $\pm$ 150	20,727 $\pm$ 175
correlation coeff $r$	0.976	0.968	0.980	0.977	0.976

#### 4.2.5.3. Kamlet-Abboud-Taft's Solvent Index (KAT)

KAT solvent index is a comprehensive empirical approach, which covers a wide range of solvent properties, such as dielectric effects, hydrogen-bonding properties, acidity and basicity as shown expressed by equation 4-2.

$$\nu = \nu_0 + s \cdot \pi^* + a \cdot \alpha + b \cdot \beta \quad \text{Eq. 4-2}$$

where  $\pi^*$  is a measure for the dipolarity and polarizability of the solvent,  $\alpha$  and  $\beta$  refer to the solvent's ability to act as hydrogen-bond donor and acceptor, respectively. A multiple linear regression analysis of the emission energy ( $\nu$ ) versus three parameters  $\pi^*$ ,  $\alpha$  and  $\beta$  will give  $s$ ,  $a$ , and  $b$  as the corresponding fitted parameters as well as the absorption or emission energy in vacuum ( $\nu_0$ ). A compilation of the corresponding solvent parameters for each of the 15 solvents used in the regression analysis is provided in Appendix A Table A-1.<sup>7</sup>

As evident from the data listed in Table 4-3, multiple linear regression analysis yielded good correlations for all the derivatives. It is immediately apparent, that the fitted parameter  $a$  is significantly larger than the other two solvent parameters, thus indicating that hydrogen-bonding interactions of the solvent dominate the solvatochromic shift behavior of this compound class. Interestingly, the emission energies in vacuum of 4-substituted derivatives **4-3** and **4-5** are higher than that of the parent compound **4-1** while those of the 5-substituted derivatives **4-2** and **4-4** are lower. This result further

confirms that the origin of donor substituent-induced emission energy shifts is most likely due to differences in their electronic structure induced by the different attachment positions of the donor substituents.

There are principally several hydrogen-bonding acceptors on the fluorophore framework available: the oxygen atoms of the sulfonamide moiety, the  $sp^2$  hybridized benzimidazole nitrogen, as well as the oxygen atom of  $-OR^2$  moiety and the methoxy substituent (Chart 4-1). Above studies already demonstrated that hydrogen-bonding interactions with the methoxy group have little influence on the solvatochromic shift behavior. Because the benzimidazole nitrogen is already occupied with formation of the intramolecular sulfonamide hydrogen-bond, possible moieties that may undergo hydrogen bonding interactions with solvent molecules and thus cause the observed solvatochromic shifts are reduced to the oxygen atoms of the sulfonamide group or the oxygen atom of the  $-OR^2$  substituent. Moreover, previous studies on 2-(2'-tosylaminophenyl)benzimidazole revealed a similar solvatochromic shift behavior as observed for above derivatives.<sup>8</sup> Therefore, potential hydrogen bonding candidates of the fluorophore framework are further reduced to the oxygen atoms of the sulfonamide moiety, which, due to its close proximity, would be expected to have some influence on the excited state proton transfer process.

**Table 4-4:** Experimental and Calculated Vertical Excitation and Emission Energies (eV) for **4-1c-4-3c**.

Parameter	<b>4-1c</b>	<b>4-2c</b>	<b>4-3c</b>
Excitation [eV]			
INDO-SCI	4.12	4.11	4.09
$f^a$	0.355	0.360	0.492
$M_{ge}$ [D] <sup>b</sup>	4.8	4.8	5.6
expt <sup>c</sup>	4.13	4.20	4.07
Emission [eV]			
INDO-SCI	2.61	2.52	2.66
$f^a$	0.447	0.462	0.429
$M_{ge}$ [D] <sup>b</sup>	6.7	6.9	6.5
expt <sup>c</sup>	2.70	2.49	2.84
gas-phase fit <sup>d</sup>	2.51	2.25	2.63

[a] Oscillator strength. [b] Transition dipole moment. [c] Measured in aqueous solution, 0.1 M ionic strength (KCl). [d] Extrapolated gas-phase values from Kamlet-Abboud-Taft empirical solvent model.

**Table 4-5:** HFCIS/3-21+G(d,p)//INDO-SCI Computed Ground and Excited State Dipole Moments and Their Differences for **4-1c-4-3c**.

Parameter	<b>4-1c</b>	<b>4-2c</b>	<b>4-3c</b>
Gas Phase			
$\mu_g$ [D]	13.4	14.4	15.2
$\mu_e$ [D]	11.1	12.8	12.7
$\mu\Delta$ [D]	-2.2	-1.6	-2.5
Solution Phase (MeOH)			
$\mu_g$ [D]	15.6	16.9	17.4
$\mu_e$ [D]	13.2	15.0	15.1
$\mu\Delta$ [D]	-2.4	-1.9	-2.4

### 4.3. Quantum Chemical Calculations

Quantum chemical calculations were carried out to investigate the substituent effects on emission shifts. In this case, methoxy-substituted compounds were preferred since they show more pronounced emission shifts than the corresponding pyrrole-substituted compounds. To simplify the calculations, the carboxymethyl substituent ( $\text{OCH}_2\text{-COOR}'$ ) was replaced by a methoxy group. Therefore, the molecules used in all calculations were **4-1c**, **4-2c** and **4-3c** (Chart 4-1).

The calculated photophysical data are shown in Table **4-4** and **4-5**. Consistent with the solvatochromic analysis, the dipole moment change upon excitation is small for all derivatives. The HOMO and LUMO isosurface diagram (Figure 4-5) shows that while the 5-position on the central benzene ring contributes strongly to the HOMO but weakly to the LUMO, the 4-position contributes strongly to the LUMO but weakly to the HOMO. Therefore, the electron-donating group methoxy on 5-position increases the HOMO energy and does not affect LUMO energy, thus decreasing the HOMO-LUMO gap and resulting in a red-shifted emission. The methoxy group in the 4-position results therefore in a blue-shifted emission. These two results are fully consistent with experimental data.

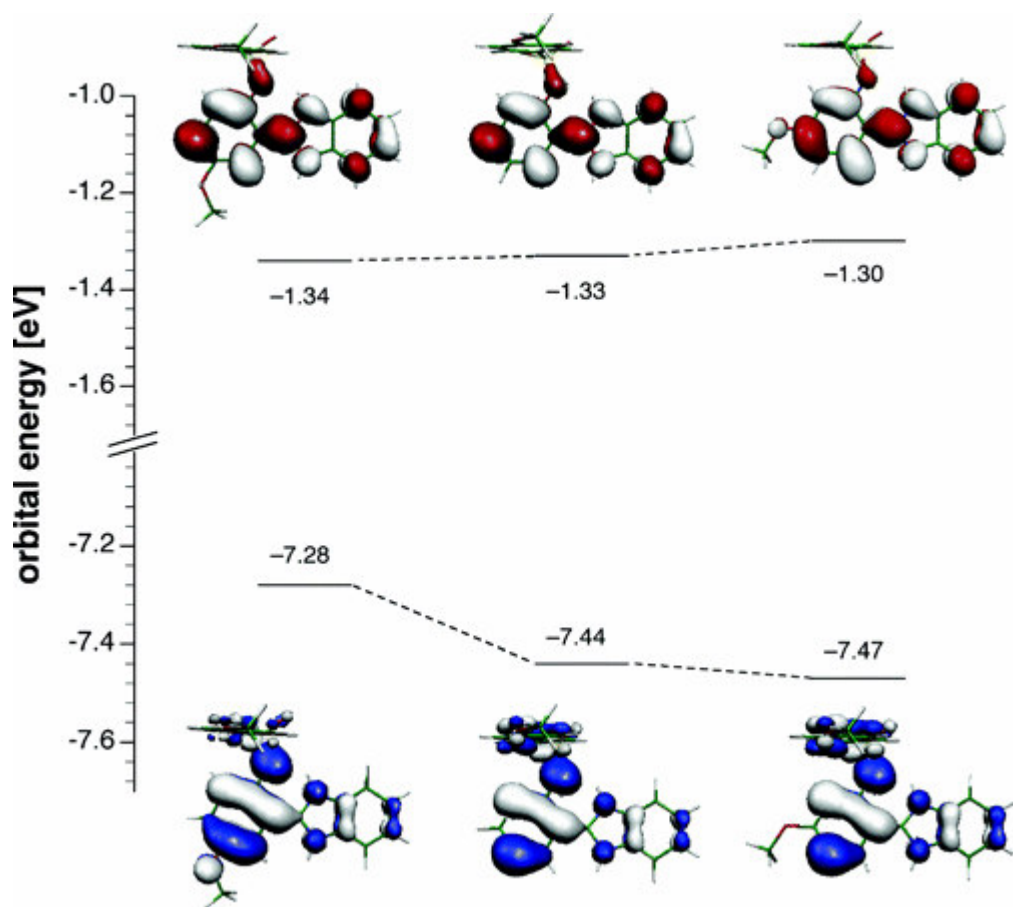


**Figure 4-5.** Energy level diagram for the frontier orbitals of the phototautomer of compounds **4-1c-4-3c**. A plot of the HOMO and LUMO isosurfaces is also depicted for each compound.

## 4.4. Conclusions

In this chapter, solvatochromic shift analysis and theoretical calculations were performed to investigate the photophysical properties of the ESIPT fluorophores, in particular the effect of substituents on the fluorescence emission. Both, experimental and theoretical studies showed that the dipole moment change upon excitation is small for 2-(2'-arylsulfonamidophenyl)benzimidazole fluorophores. The observed negative solvatochromic shift is dominated by hydrogen-bonding in protic solvents through the oxygen atoms of the sulfonamide moiety. The origin of the substituent effects on the emission shift is solely due to the HOMO-LUMO energy difference, whereas different hydrogen-bonding modes of methoxy group on central benzene ring can be excluded. These studies provide a detailed understanding of the photophysical properties of ESIPT fluorophores and may also offer further guidelines for rationally tuning their properties.

## 4.5. Experimental Section

### 4.5.1. Synthesis.

Sulfonyl chloride **4-14** and fluorophores **4-1a/b**, **4-2a/b**, and **4-3a/b** were synthesized following published procedures.<sup>2</sup> NMR:  $\delta$  in ppm vs SiMe<sub>4</sub> (0 ppm, <sup>1</sup>H, 400 MHz), br = exchange broadened signal. MS: selected peaks; m/z. Melting points are uncorrected. Flash chromatography (FC): Merck silica gel (240-400 mesh). TLC: 0.25 mm, Merck silica gel 60 F<sub>254</sub>, visualizing at 254 nm or with 2% KMnO<sub>4</sub> solution.

**2-Nitro-5-pyrrol-1-yl-benzaldehyde (4-8).** In a Schlenk tube 2-nitro-5-bromobenz-

aldehyde<sup>9</sup> (**4-6**, 500 mg, 2.17 mmol), freshly distilled pyrrole (133 mg, 1.97 mmol, 0.137 mL), palladium acetate (4.4 mg, 0.02 mmol), xantphos (34 mg, 0.059 mmol), and potassium carbonate (817 mg, 5.91 mmol) were mixed in 5 mL of *o*-xylene. The mixture was degassed and the tube refilled with argon. After heating at 120 °C overnight, the mixture was cooled to room temperature, washed with water, and extracted with EtOAc. The combined organic extracts were dried over anhydrous MgSO<sub>4</sub> and concentrated under reduced pressure. The residue was purified on silica gel (FC, EtOA-hexanes, 2:9) providing 367 mg (1.7 mmol, 78% yield) of **4-8** as a yellow solid: mp 74-76 °C. *R<sub>f</sub>* 0.47 (EtOAc-hexanes, 2:9); <sup>1</sup>H NMR (CDCl<sub>3</sub>, 400 MHz) δ 6.46 (t, *J* = 2.2 Hz, 2H), 7.22 (t, *J* = 2.2 Hz, 2H), 7.69 (dd, *J* = 8.9, 2.6 Hz, 1H), 7.89 (d, *J* = 2.6 Hz, 1H), 8.27 (d, *J* = 8.9 Hz, 1H), 10.53 (s, 1H); MS (70 eV) *m/z* 216 ([*M*<sup>+</sup>], 100), 186 (31), 158.1 (23), 141.1 (52), 130 (30), 115.1 (38); EI-HRMS calculated for [*M*<sup>+</sup>] C<sub>11</sub>H<sub>8</sub>N<sub>2</sub>O<sub>3</sub> 216.05349, found 216.05407.

**2-(2-Nitro-5-pyrrol-1-yl-phenyl)-1*H*-benzimidazole (4-10).** A mixture of aldehyde **4-8** (200 mg, 0.925 mmol), *o*-phenylenediamine (120 mg, 1.11 mmol), acetic acid (0.08 mL, 1.4 mmol), and copper(II) acetate monohydrate (183 mg, 0.92 mmol) in 20 mL of ethanol-water (1:1) was refluxed overnight. The reaction mixture was cooled to room temperature and quenched by addition of 10 mL of concentrated aqueous NH<sub>4</sub>OH. The mixture was extracted with EtOAc, and the combined organic extracts were dried (MgSO<sub>4</sub>) and concentrated under reduced pressure. The residue was purified on silica gel

(FC, EtOAc:hexanes, 1:3), affording 85 mg (0.28 mmol, 30% yield) of benzimidazole derivative **4-10** as a tan solid: mp >210 °C dec;  $R_f$  0.18 (EtOAc-hexanes, 1:3);  $^1\text{H}$  NMR (DMSO- $d_6$ , 400 MHz)  $\delta$  6.39 (t,  $J = 2.2$  Hz, 2H), 7.27 (br, 2H), 7.64 (br, 2H), 7.64 (t,  $J = 2.2$  Hz, 2H), 7.97 (dd,  $J = 8.9, 2.5$  Hz, 1H), 8.150 (d,  $J = 8.9$  Hz, 1H), 8.154 (d,  $J = 2.5$  Hz, 1H), 13.02 (s, 1H); MS (70 eV)  $m/z$  304.1 ( $[M^+]$ , 100), 287.1 (83), 262.1 (23), 257 (12), 155.1 (15), 141 (15); EI-HRMS calculated for  $[M^+]$   $\text{C}_{17}\text{H}_{12}\text{N}_4\text{O}_2$  304.0960, found 304.1004.

**2-(1H-Benzimidazol-2-yl)-4-pyrrol-1-ylphenylamine (4-12)**. A solution of **4-10** (80 mg, 0.26 mmol) in 8 mL of ethanol was hydrogenated at atmospheric pressure in the presence of Pd on activated carbon (5 wt %, 13 mg) as catalyst. Upon completion of the reaction (TLC) the mixture was filtered through a pad of Celite and concentrated under reduced pressure, affording 60 mg (0.22 mmol, 84% yield) of amine **4-12** as a tan solid: mp 163-165 °C;  $R_f$  0.65 (EtOAc-hexanes, 1:2);  $^1\text{H}$  NMR (DMSO- $d_6$ , 400 MHz)  $\delta$  6.24 (t,  $J = 2.2$  Hz, 2H), 6.91 (d,  $J = 8.7$  Hz, 1H), 7.21-7.23 (m, 2H), 7.25 (t,  $J = 2.2$  Hz, 2H), 7.37 (dd,  $J = 8.7, 2.5$  Hz, 1H), 7.56-7.64 (m, br, 2H), 8.00 (d,  $J = 2.5$  Hz, 1H); MS (70 eV)  $m/z$  274.1 ( $[M^+]$ , 100), 246.1 (8), 137 (9); EI-HRMS calculated for  $[M^+]$   $\text{C}_{17}\text{H}_{14}\text{N}_4$  274.1219, found 274.1208.

**{4-[2-(1H-Benzimidazol-2-yl)-4-pyrrol-1-ylphenylsulfamoyl]phenoxy}acetic acid ethyl ester (4-4a)**. A solution of amine **4-12** (54 mg, 0.20 mmol) and ethyl (4-chloro-sulfonylphenoxy) acetate<sup>1</sup> (**4-14**, 66 mg, 0.24 mmol) in anhydrous pyridine (1 mL) was stirred for 2 h at room temperature. The reaction mixture was diluted with aqueous HCl

(1 M, 5 mL) and extracted twice with EtOAc (10 mL). The combined organic extracts were dried with MgSO<sub>4</sub> and concentrated under reduced pressure. The crude product was purified on silica gel (FC, EtOAc-hexanes, 1:2), providing 45 mg (0.087 mmol, 44% yield) of **4-4a** as a tan solid: mp >106 °C dec; *R<sub>f</sub>* 0.25 (EtOAc-hexanes, 1:2); <sup>1</sup>H NMR (CDCl<sub>3</sub>, 400 MHz) δ 1.23 (t, *J* = 7.1 Hz, 3H), 4.17 (q, *J* = 7.1 Hz, 2H), 4.65 (s, 2H), 6.21 (d, *J* = 8.9 Hz, 2H), 6.36 (t, *J* = 2.1 Hz, 2H), 7.06-7.12 (m, 4H), 7.32-7.37 (m, 2H), 7.40-7.47 (m, 3H), 7.81 (br, 1H), 7.83 (d, *J* = 9.5 Hz, 1H), 9.98 (s, br, 1H), 11.20 (s, br, 1H); MS (70 eV) *m/z* 516.1 ([*M*<sup>+</sup>], 48), 273.1 (100); EI-HRMS calculated for [*M*<sup>+</sup>] C<sub>27</sub>H<sub>24</sub>N<sub>4</sub>O<sub>5</sub>S 516.1467, found 516.1417.

**{4-[2-(1*H*-Benzimidazol-2-yl)-4-pyrrol-1-ylphenylsulfamoyl]phenoxy}acetic Acid (4-4b).** Ester **4-4a** (40 mg, 0.077 mmol) was dissolved in THF (1.5 mL), and a solution of LiOH·H<sub>2</sub>O (97 mg) in MeOH-water (1:1, 3 mL) was added. The resulting mixture was heated under reflux for 4 h and then cooled to room temperature. After removal of the organic solvent under reduced pressure, the reaction mixture was diluted with water (2 mL). Aqueous HCl (1 M) was added until the product started to precipitate. The product was filtered off, washed with little water, and dried in vacuum, affording 38 mg (0.082 mmol, 99%) of acid **4-4b** as a tan solid: mp >130 °C dec; *R<sub>f</sub>* 0.44 (MeOH-CH<sub>2</sub>Cl<sub>2</sub>, 1:3); <sup>1</sup>H NMR (DMSO-*d*<sub>6</sub>, 400 MHz) δ 4.68 (s, 2H), 6.31 (t, *J* = 2.2 Hz, 2H), 6.92 (d, *J* = 9.0 Hz, 2H), 7.33-7.37 (m, 2H), 7.41 (t, *J* = 2.2 Hz, 2H), 7.67-7.70 (m, 4H), 7.72 (br, 2H), 8.26 (s, 1H), 13.22 (br, 2H); MS (70 eV) *m/z* 488.1 ([*M*<sup>+</sup>], 23), 273.1 (100), 299 (79); EIHRMS calculated for [*M*<sup>+</sup>] C<sub>25</sub>H<sub>20</sub>N<sub>4</sub>O<sub>5</sub>S 488.1154, found 488.1141.

**2-Nitro-4-pyrrol-1-yl-benzaldehyde (4-9).** 2-Nitro-4-bromobenzaldehyde<sup>10</sup> (**4-7**, 250 mg, 1.09 mmol) was converted to pyrrole derivative **4-9** as described for the synthesis of **4-8**, yielding 102 mg (0.47 mmol, 43% yield) of **4-9** as a yellow solid: mp 113-115 °C;  $R_f$  0.18 (EtOAc-hexanes, 1:9);  $^1\text{H NMR}$  ( $\text{CDCl}_3$ , 400 MHz)  $\delta$  6.47 (t,  $J = 2.0$  Hz, 2H), 7.22 (t,  $J = 2.0$  Hz, 2H), 7.76 (dd,  $J = 8.5, 2.2$  Hz, 1H), 8.07 (d,  $J = 2.2$  Hz, 1H), 8.09 (d,  $J = 8.5$  Hz, 1H), 10.40 (s, 1H); MS (70 eV)  $m/z$  216.1 ( $[M^+]$ , 100), 186.1 (64), 141 (78), 130.1 (50), 115.1 (42); EI-HRMS calculated for  $[M^+]$   $\text{C}_{11}\text{H}_8\text{N}_2\text{O}_3$  216.0535, found 216.0544.

**2-(2-Nitro-4-pyrrol-1-yl-phenyl)-1H-benzimidazole (4-11).** Aldehyde **4-9** (102 mg, 0.47 mmol) was converted to benzimidazole derivative **4-11** as described for **4-10**, providing 114 mg (0.37 mmol, 80% yield) of **4-11** as a yellow solid: mp >200 °C (dec);  $R_f$  0.26 (EtOAc-hexanes, 1:2);  $^1\text{H NMR}$  ( $\text{DMSO}-d_6$ , 400 MHz)  $\delta$  6.37 (t,  $J = 2.0$  Hz, 2H), 7.23-7.26 (m, 2H), 7.58-7.62 (m, 2H), 7.65 (t,  $J = 2.0$  Hz, 2H), 8.07 (d,  $J = 8.5$  Hz, 1H), 8.13 (dd,  $J = 8.5, 2.4$  Hz, 1H), 8.31 (d,  $J = 2.4$  Hz, 1H), 13.06 (s, br, 1H); MS (70 eV)  $m/z$  304.1 ( $[M^+]$ , 100), 287.1 (18), 141 (15). EI-HRMS calculated for  $[M^+]$   $\text{C}_{17}\text{H}_{12}\text{N}_4\text{O}_2$  304.0960, observed 304.0937.

**2-(1H-Benzimidazol-2-yl)-5-pyrrol-1-yl-phenylamine (4-13).** Nitrocompound **4-11** (110 mg, 0.36 mmol) was reduced to amine **4-13** as described for the synthesis of **4-12**, yielding 76 mg of **4-13** (0.28 mmol, 77% yield) as a tan solid: mp 253-255 °C;  $R_f$  0.67 (EtOAc-hexanes, 1:1);  $^1\text{H NMR}$  ( $\text{DMSO}-d_6$ , 400 MHz)  $\delta$  6.28 (t,  $J = 2.1$  Hz, 2H), 6.90 (dd,  $J = 8.5$  Hz, 2.4 Hz, 1H), 6.98 (d,  $J = 2.4$  Hz, 1H), 7.16-7.23 (m, 2H), 7.34 (t,  $J = 2.1$

Hz, 2H), 7.45 (s, br, 2H), 7.50 (d, br,  $J = 7.6$  Hz, 1H), 7.64 (d, br,  $J = 7.6$  Hz, 1H), 7.92 (d,  $J = 8.6$  Hz, 1H), 12.69 (s, 1H); MS (70 eV)  $m/z$  274.1 ( $[M^+]$ , 100), 246.1 (12); EI-HRMS calculated for  $[M^+]$  C<sub>17</sub>H<sub>14</sub>N<sub>4</sub> 274.1219, found 274.1211.

**{4-[2-(1*H*-Benzimidazol-2-yl)-5-pyrrol-1-yl-phenylsulfamoyl]phenoxy}acetic Acid Ethyl Ester (4-5a).** Amine **4-13** (20 mg, 0.073mmol) was reacted with ethyl (4-chlorosulfonylphenoxy)acetate<sup>3</sup> **4-14** as described above for the synthesis of **4-4a**, affording 25 mg (0.048 mmol, 66% yield) of **4-5a** as a tan solid: mp 193-195 °C;  $R_f$  0.55 (EtOAc-hexanes, 3:2); <sup>1</sup>H NMR (CDCl<sub>3</sub>, 400 MHz)  $\delta$  1.30 (t,  $J = 7.1$  Hz, 3H), 4.27 (q,  $J = 7.1$  Hz, 2H), 4.60 (s, 2H), 6.32 (t,  $J = 2.1$  Hz, 2H), 6.62 (d,  $J = 8.9$  Hz, 2H), 6.88 (t,  $J = 2.1$  Hz, 2H), 7.05 (dd,  $J = 8.5, 2.1$  Hz, 1H), 7.18 (d,  $J = 2.1$  Hz, 1H), 7.23-7.26 (m, 2H), 7.50 (d,  $J = 8.9$  Hz, 2H), 7.52-7.55 (m, 2H), 7.65 (d,  $J = 8.6$  Hz, 1H); MS (70 eV)  $m/z$  516.1 ( $[M^+]$ , 28), 365.1 (9), 274.1 (100), 273 (50), 212.1 (28); EI-HRMS calculated for  $[M^+]$  C<sub>27</sub>H<sub>24</sub>N<sub>4</sub>O<sub>5</sub>S 516.1467, found 516.1460.

**{4-[2-(1*H*-Benzimidazol-2-yl)-5-pyrrol-1-ylphenyl-sulfamoyl]phenoxy}acetic Acid (4-5b).** Ethyl ester **4-5a** (10 mg, 0.019 mmol) was hydrolyzed as described for the synthesis of **4-4b**, yielding 10 mg (0.082 mmol, 99% yield) of acid **4-5b** as a tan solid: mp >190 °C (dec);  $R_f$  0.53 (MeOH-CH<sub>2</sub>Cl<sub>2</sub>, 1:3); <sup>1</sup>H NMR (DMSO-d<sub>6</sub>, 400 MHz)  $\delta$  4.69 (s, 2H), 6.35 (t,  $J = 2.1$  Hz, 2H), 6.96 (d,  $J = 9.0$  Hz, 2H), 7.31-7.37 (m, 4H), 7.51 (dd,  $J = 8.3, 1.6$  Hz, 1H), 7.65-7.73 (m, 3H), 7.75 (d,  $J = 8.9$  Hz, 2H), 8.13 (d,  $J = 8.8$  Hz, 1H), 13.40 (s, br, 2H); FAB-MS (thioglycerol)  $m/z$  489 ( $[M^+]$ , 13), 327 (25), 274.1 (18), 273 (17), 237 (100); EI-HRMS calculated for  $[M^+]$  C<sub>25</sub>H<sub>21</sub>N<sub>4</sub>O<sub>5</sub>S 489.1233, found 489.1268.

#### 4.5.2. Electrode Calibration in Aqueous Solution

Measurements were performed with an Orion microcombination glass electrode. The electrode was calibrated for  $-\log[\text{H}_3\text{O}^+]$  by titration of a standardized HCl solution (Aldrich, 0.1 N volumetric standard) with KOH (Aldrich, 0.1 N volumetric standard) at 25°C and 0.1M ionic strength (KCl). The endpoint, electrode potential, and slope were determined by using Gran's method<sup>11</sup> as implemented in the software GLEE.<sup>12</sup> The calibration procedure was repeated three times prior to each  $\text{p}K_a$  value determination. The electrode potential was measured with the Corning pH/Ion Analyzer 355 and the emf measurements were reproducible with  $\pm 0.1$  mV accuracy.

#### 4.5.3. Spectrophotometric Titrations

The UV/Vis absorption spectra of the ligands were monitored for a series of solutions in which  $-\log[\text{H}_3\text{O}^+]$  was varied between 5 and 11. The emf of each solution was directly measured in the UV quartz cell (electrode diameter 3mm) and converted to  $-\log[\text{H}_3\text{O}^+]$  using the  $E^\circ$  and slope, as obtained from the electrode calibration procedure described above. The raw spectral and emf data were processed with nonlinear least-squares fit analysis using the SPECFIT software package.<sup>13</sup>

#### 4.5.4. Steady-state Absorption and Fluorescence Spectroscopy

All sample stock solutions and buffer solutions were filtered through 0.2  $\mu\text{m}$  Nylon

membrane filters to remove interfering dust particles or fibers. UV/Vis absorption spectra were recorded at 25°C by using a Varian Cary Bio50 UV/Vis spectrometer with constant-temperature accessory. Steady-state emission and excitation spectra were recorded with a PTI fluorimeter and FELIX software. Throughout the titration the sample solution was stirred with a magnetic stirring device. For all titrations the path length was 1 cm with a cell volume of 3.0 mL. All fluorescence spectra have been corrected for the spectral response of the detection system (emission correction file provided by the instrument manufacturer) and for the spectral irradiance of the excitation channel (by using a calibrated photodiode). Quantum yields were determined by using quinine sulfate dihydrate in 1.0 N H<sub>2</sub>SO<sub>4</sub> ( $\Phi_f = 0.54 \pm 0.05$ ) as the fluorescence standard.<sup>14</sup>

#### 4.6. References:

1. Henary, M. M.; Wu, Y.; Fahrni, C. J. *Chem. Eur. J.* **2004**, *10*, 3015.
2. Henary, M. M.; Wu, Y. G.; Cody, J.; Sumalekshmy, S.; Li, J.; Mandal, S.; Fahrni, C. *J. J. Org. Chem.* **2007**, *72*, 4784.
3. Reichardt, C. *Chem. Rev.* **1994**, *94*, 2319.
4. Onsager, L. *J. Am. Chem. Soc.* **1936**, *58*, 1486.
5. Kamlet, M. J.; Abboud, J. L.; Taft, R. W. *J. Am. Chem. Soc.* **1977**, *99*, 6027.
6. Lippert, E. *Z. Elektrochem.* **1957**, *61*, 962.
7. Kamlet, M. J.; Abboud, J. L.; Abraham, M. H.; Taft, R. W. *J. Org. Chem.* **1983**, *48*, 2877.
8. Fahrni, C. J.; Henary, M. M.; VanDerveer, D. G. *J. Phys. Chem. A* **2002**, *106*, 7655.
9. Jung, M. E.; Dansereau, S. M. K. *Heterocycles* **1994**, *39*, 767.
10. Hu, Y.-Z.; Zhang, G.; Thummel, R. P. *Org. Lett.* **2003**, *5*, 2251.
11. Gran, G. *Analyst* **1951**, *77*, 661.
12. Gans, P.; O'Sullivan, B. *Talanta* **2000**, *51*, 33.
13. Binstead, R. A.; Zuberbühler, A. D. SPECFIT Global Analysis System, Spectrum Software Associates, Marlborough MA 01752, **2001**.
14. Demas, J. N.; Crosby, G. A. *J. Phys. Chem.* **1971**, *75*, 991.

## CHAPTER V

### EXCITED STATE INTRAMOLECULAR PROTON TRANSFER (ESIPT) IN 2-(2'-SULFONAMIDOPHENYL)BENZIMIDAZOLE DERIVATIVES: IMPACT OF EXTENDED $\pi$ -CONJUGATION

#### 5.1. Introduction

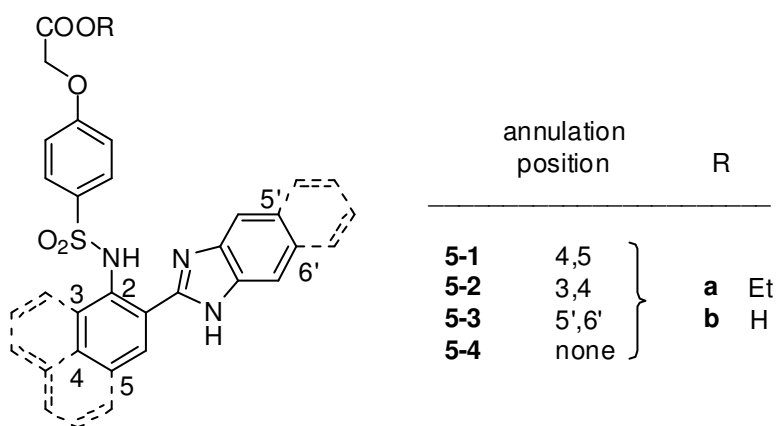
As outlined in Chapter 3, in order to utilize ESIPT sensors for biological imaging applications, the peak absorption wavelength should be greater than 350 nm. Besides taking advantage of substituent-induced absorption shifts as discussed in Chapter 3, extension of the  $\pi$ -conjugated aromatic system of the fluorophore might serve as promising alternative approach.

In principle, the more p-orbitals are participating in a  $\pi$ -conjugated system, the more discrete  $\pi$ -orbitals are involved in bonding.<sup>1</sup> As a consequence, the HOMO-LUMO energy gap generally decreases with increasing size of a conjugated  $\pi$ -system, an effect that has utilized on structurally related 2-(*o*-hydroxyaryl)benzazole ESIPT systems.<sup>2</sup> More interestingly, it was found that in these systems, the photophysical properties depended not only on the size of the  $\pi$ -conjugated system, but also on the relative position of the annulated ring-extension.

To explore the effect of extended  $\pi$ -conjugation on the photophysical properties of

2-(2'-sulfonamidophenyl)benzimidazoles fluorophores, three derivatives **5-1**, **5-2** and **5-3** were synthesized which contained a ring extension annulated to three different positions of the parent structure (Chart 5-1).

**Chart 5-1**



## 5.2. Results and Discussion

### 5.2.1. Synthesis

The precursors **5-4**<sup>3</sup>, **5-5**<sup>4</sup> and **5-15**<sup>3</sup> were synthesized following published procedures. The individual synthetic routes were chosen based on the commercial availability of the starting materials. Since the synthesis of derivative **5-1** was best started from naphthylamine **5-5**, the aryl-sulfonamide moiety was installed prior to the formation of the benzimidazole ring. The alcohol **5-6** was obtained through reduction of **5-5** with lithium aluminum hydride, and then reacted with sulfonylchloride **5-15** to form the sulfonamide intermediate **5-7**. After mild oxidation of the primary alcohol with MnO<sub>2</sub>, the resulting aldehyde **5-8** was subjected to copper-mediated condensation with *o*-phenylenediamine, providing the final product **5-1a** with 6% yield. The disappointingly low yield of the coupling step is presumably due to the significant stability but low solubility of the formed copper complex in the workup process. For compound **5-2a** and **5-3a**, the corresponding nitro-substituted arylaldehyde precursors are commercially available. Hence, the benzimidazole ring was installed prior to formation of the aryl-sulfonamide moiety. The yield for the copper-mediated coupling reaction could be markedly improved by using ammonium hydroxide to remove the copper salts during the work up procedure. Finally, the hydrolysis of the carboxylate esters was accomplished under mild conditions with lithium hydroxide in a methanol-water-THF solvent mixture.

### Scheme 5-1

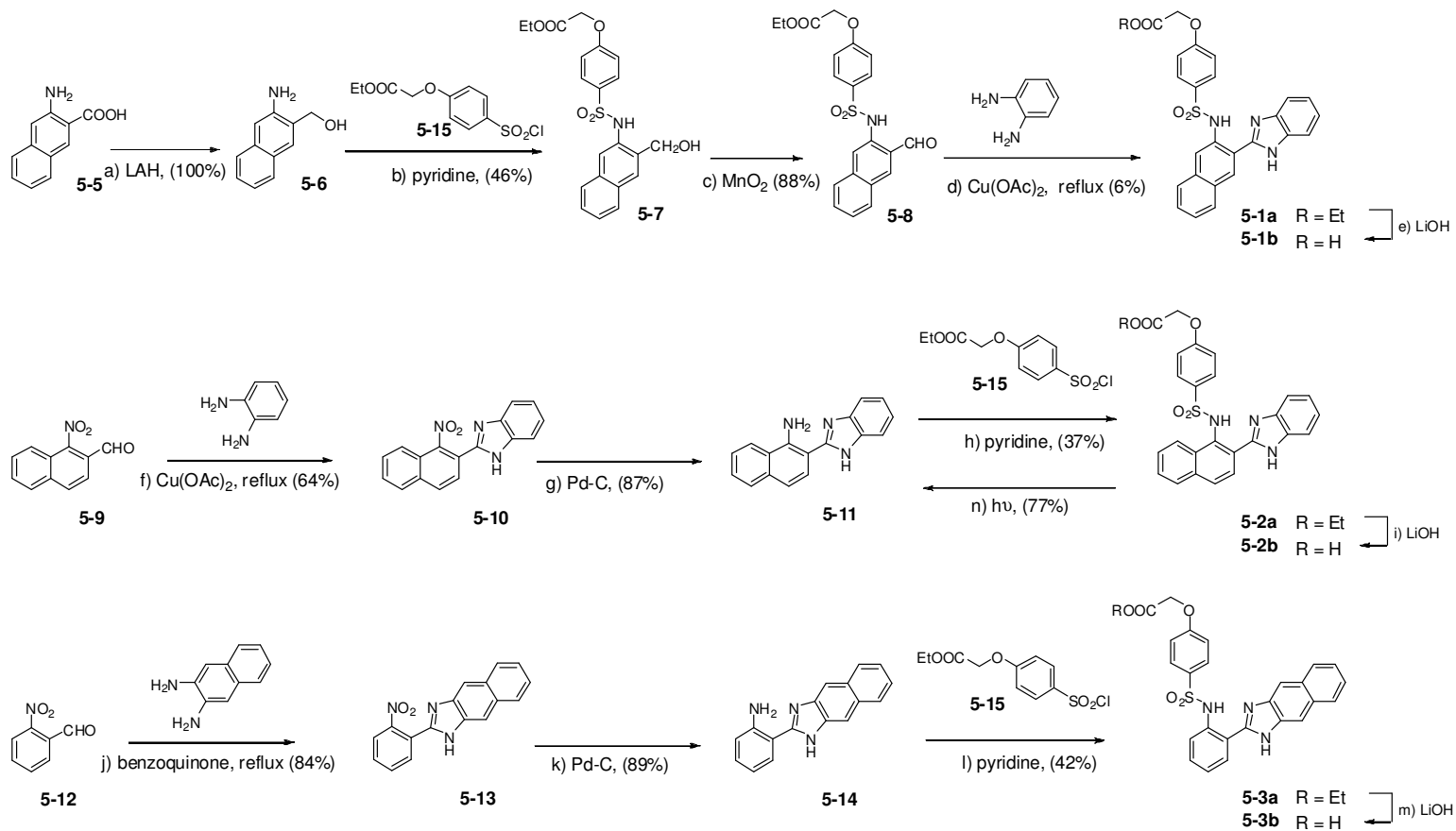


**Table 5-1:** Protonation Constants and Photophysical Data.<sup>[a]</sup>

Species/equilibrium	Data	<b>5-1b</b>	<b>5-2b</b> <sup>[f]</sup>	<b>5-3b</b>	<b>5-4b</b> <sup>[g]</sup>
[H <sup>+</sup> ][LH <sup>-</sup> ]/[LH <sub>2</sub> ]	pK <sub>a</sub> <sup>1</sup>	4.73±0.05	4.75±0.03	n.d. <sup>[h]</sup>	4.46±0.03
[H <sup>+</sup> ][L <sup>2-</sup> ]/[LH <sup>-</sup> ]	pK <sub>a</sub> <sup>2</sup>	8.06±0.005	7.62±0.06	7.94±0.005	8.04±0.03
L <sup>2-</sup>	absorption λ <sub>max</sub> (nm) <sup>[b]</sup>	290 (28050)	328 (11280)	347 (6379)	301 (15870)
		322 (19780)	355 (7140) (sh)		329 (10920)
	excitation λ <sub>max</sub> (nm) <sup>[c]</sup>	319	294	346	296
	emission λ <sub>max</sub> (nm) <sup>[c]</sup>	480	436	456	418
	Stokes shift (cm <sup>-1</sup> )	10223	7552	6889	6470
	quantum yield <sup>[e]</sup>	0.30	0.12	0.35	0.26
LH <sup>-</sup>	absorption λ <sub>max</sub> (nm) <sup>[b]</sup>	286 (19910)	321 (11772)	336 (5358)	299 (12300)
		314 (18000)			
	excitation λ <sub>max</sub> (nm) <sup>[d]</sup>	304	292	334	300
	emission λ <sub>max</sub> (nm) <sup>[d]</sup>	394	471	487	460
		554			
	Stokes' Shift (cm <sup>-1</sup> )	6466, 13797	9921	9228	11700
	quantum Yield <sup>[e]</sup>	0.09	0.10	0.29	0.23
brightness (εφ, Lmol <sup>-1</sup> cm <sup>-1</sup> )	1620	1177	1340	2829	

<sup>[a]</sup> 0.1M KCl, 25°C. <sup>[b]</sup> from deconvolution analysis; molar extinction coefficient [Lmol<sup>-1</sup>cm<sup>-1</sup>] in parentheses; <sup>[c]</sup> pH = 11.0, 0.1M KCl; <sup>[d]</sup> pH = 6.5 (**5-1b**), 6.2 (**5-2b**), or 6.3 (**5-3b**), 10 mM PIPES, 0.1 M KCl; <sup>[e]</sup> quinine sulfate in 1 N H<sub>2</sub>SO<sub>4</sub> as standard; <sup>[f]</sup> contaminated by photoreaction products; <sup>[g]</sup> data taken from reference 2; <sup>[h]</sup> spectral deconvolution insufficient for accurate determination.

### 5.2.2. Protonation Equilibria

As already discussed in chapter 3 and 4, deprotonation of the sulfonamide group is typically associated with a bathochromic shift in the peak absorption and a hypsochromic shift in the fluorescence emission. To study the impact of the extended  $\pi$ -conjugated system without being misled by pH-dependent absorption changes, the UV-vis and fluorescence emission spectra were therefore acquired at well-defined protonation states. Hence, the protonation equilibria of each compound were analyzed by means of spectrochemical UV-vis titrations with  $-\log[\text{H}_3\text{O}^+]$  ranging between 5 and 11. The absorption spectra of the fully deprotonated  $\text{L}^{2-}$  and monoprotonated species  $\text{HL}^-$  were then obtained by means of deconvolution based on non-linear least-squares fitting of the UV-vis traces over the entire spectral range (Figure 5-1).

As evident from Table 5-1, the  $\text{p}K_{\text{a}}$  values of the sulfonamide group depended strongly on the annulation position of the  $\pi$ -system extension. While derivative **5-1b** (8.06) and **5-3b** (7.94) gave a surprisingly similar  $\text{p}K_{\text{a}}$  compared to the unsubstituted parent molecule **5-4b** (8.04), derivative **5-2b** revealed significantly lower  $\text{p}K_{\text{a}}$  of 7.62, thus indicating a different degree of ground state resonance stabilization by the extended conjugated system.

### 5.2.3. Photophysical Studies in Aqueous Solution.

#### 5.2.3.1. UV-vis Spectra.

For the monoprotonated species  $HL^-$ , extension of  $\pi$ -conjugated system led to red-shifted absorption for all derivatives. The bathochromic shift was strongest for derivative **5-3b** (37 nm), followed by **5-2b** (22 nm) and **5-1b** (15 nm). The absorption band shifts of **5-1b** and **5-2b** are consistent with the results previously observed for 2-(*o*-hydroxyaryl)benzazoles.<sup>2</sup> For the deprotonated species  $L^{2-}$ , the absorption maxima follow the same trend (**5-3b**: 347 nm, **5-2b**: 328 nm, **5-1b**: 322 nm); however, compared to parent compound **5-4b** (329nm), the absorption spectra of **5-1b** and **5-2b**  $L^{2-}$  are actually slightly blue-shifted. The extinction coefficient of **5-1b**  $HL^-$  is the highest (18,000  $Lmol^{-1}cm^{-1}$ ), followed by **5-4b** (12,300  $Lmol^{-1}cm^{-1}$ ), **5-2b** (11,800  $Lmol^{-1}cm^{-1}$ ), and **5-3b** (5,360  $Lmol^{-1}cm^{-1}$ ).

#### 5.2.3.2. Fluorescence Steady-State Spectra.

Compared to parent compound **5-4b** (460nm), the ESIPT emission band of the monoprotonated species  $HL^-$  is red-shifted for all three derivatives. While the emission shift of **5-2b** (471 nm) and **5-3b** (487 nm) follow the same order as observed in their absorption spectra, the peak emission of derivative **5-1b** is significantly more red-shifted to 554 nm, an observation that is consistent with what the nodal-plane model recently proposed in the literature.<sup>2</sup> Since the deprotonation of the sulfonamide nitrogen disrupts the proton transfer process, the emission of the deprotonated species  $L^{2-}$  is blue shifted for

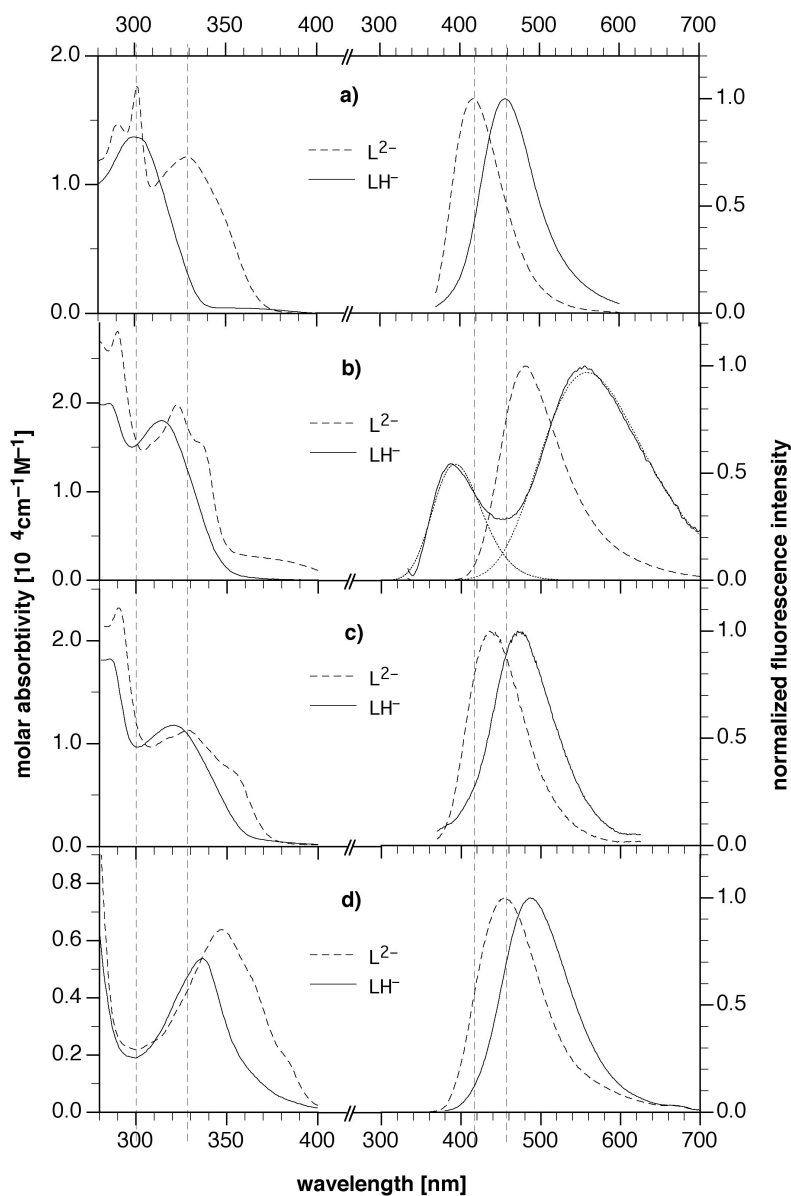


**Figure 5-1:** Deconvoluted UV-vis absorption spectra (left) and fluorescence emission spectra (right) of compounds (a) **5-4b**, (b) **5-1b**, (c) **5-2b**, and (d) **5-3d** in aqueous solution (0.1 M KCl, 25°C). UV-vis traces for the species with monoprotonated (—) and deprotonated (---) sulfonamide group were obtained through deconvolution analysis of a series spectra with  $-\log[\text{H}_3\text{O}^+]$  ranging between 5-11. Emission spectra were acquired with excitation at the isosbestic point and were recorded near pH as specified in Table 5-1 and at pH 11 without further deconvolution. The four vertical grid lines are intended as a guide to the eye indicating the position of the peak absorption and emission of platform compound **5-4b**.

all derivatives. The emission maxima still follow the same trend (**5-4b**: 418 nm, **5-2b**: 436 nm, **5-3b**: 456 nm, **5-1b**: 480 nm) as observed for the corresponding ESIPT emission bands.

Interestingly, the mono-protonated species of **5-1b** revealed an additional high-energy emission band centered around 394 nm. As discussed in chapter 3, dual emission is not uncommon in ESIPT fluorophores, and can be attributed either to a rotamer that cannot undergo excited state proton transfer<sup>5,6</sup> or a competing radiative decay from a polarized local excited state<sup>7</sup>. A contour plot of the emission intensities revealed uniform excitation spectra regardless of the emission wavelength, suggesting that only one species is responsible for both emission bands (Figure 5-2). Furthermore, the quantum chemical calculation indicated that the cis-rotamer is thermodynamically favored in case of 2'-sulfonamidophenyl-substituted benzimidazoles.<sup>8</sup> Therefore, the dual emission is most likely not due to the presence of an additional ground-state rotamer, but might originate from competition between radiative relaxation of the local excited state and formation of the proton-transfer phototautomer. To further investigate this hypothesis, a set of absorption and emission spectra were acquired over an extended temperature range. As shown in Figure 5-3, the absorption spectra changed very little as a function of the temperature changes; however, the ratio of the intensity of the higher energy emission vs. ESIPT emission gradually decreased as the temperature increased, an observation that is consistent with an increased efficiency of the intramolecular proton transfer with

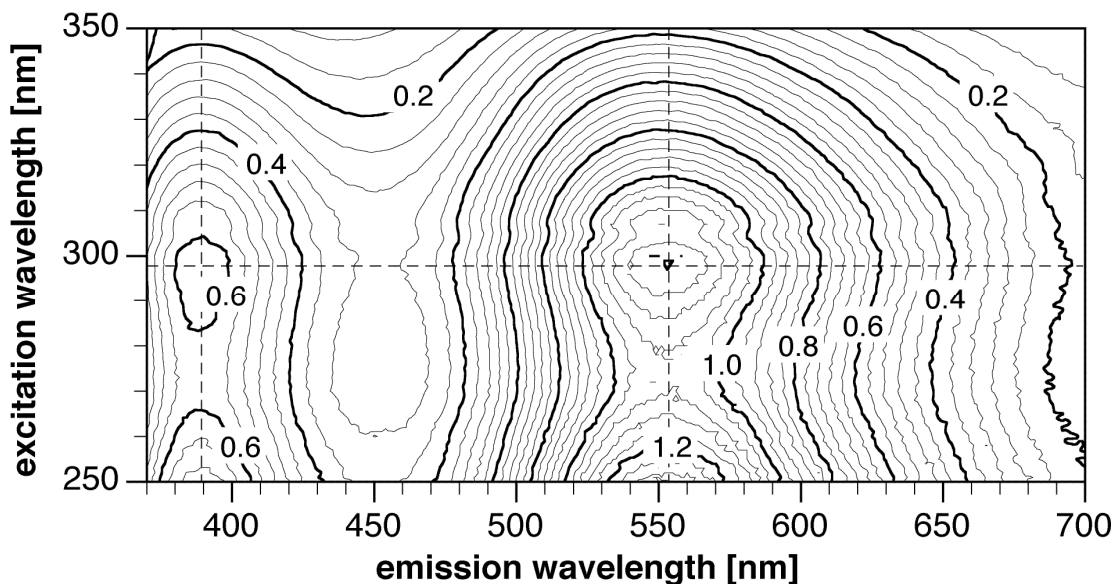


**Figure 5-2:** Two-dimensional fluorescence contour plot for fluorophore **5-1b** showing the emission profile as a function of excitation wavelength.

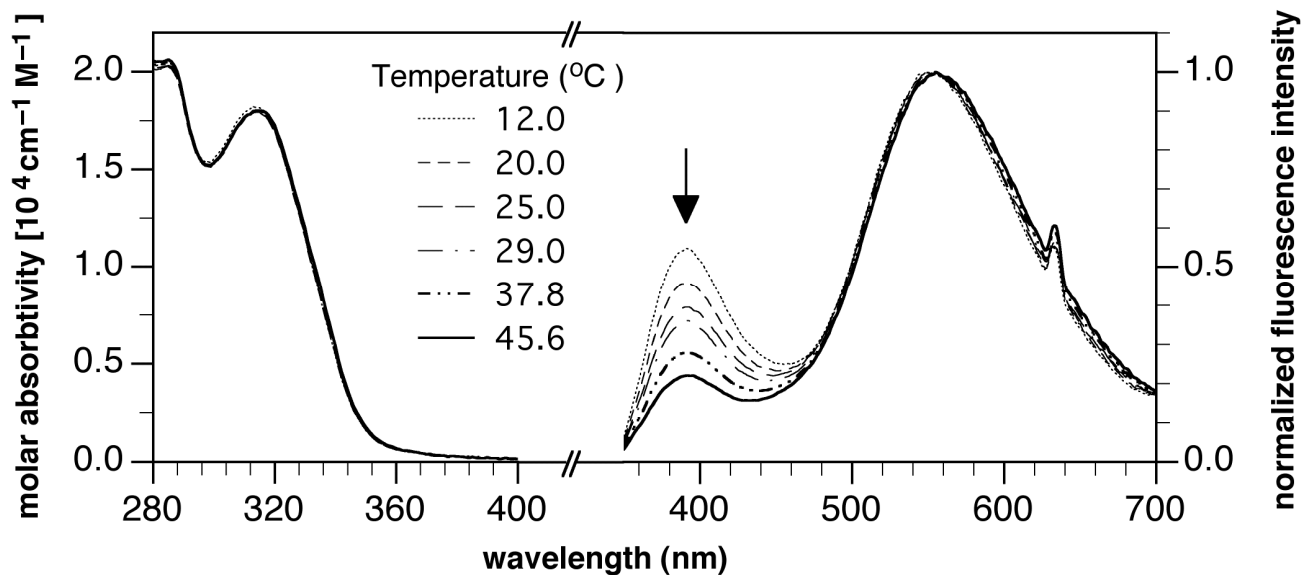


**Figure 5-3:** Temperature dependent spectra of **5-1b** in aqueous solution (pH = 6.5, 10 mM PIPES, 0.1 M KCl).

increasing temperature. Hence, these data suggest that the proton transfer process is associated with an energy barrier, which would imply a reduced proton transfer rate and thus more effective competition between emission from a local excited state (LE) and the proton transfer tautomer. In conclusion, the temperature dependent measurements further support that the higher energy band originates from a local excited state.

### ***5.2.3.3. Time Resolved Spectroscopy.***

If the emission bands of **5-1b** HL<sup>-1</sup> originate from two distinct excited-states, the fluorescence life time measured at the two wavelengths is expected to be different. Indeed, the fluorescence lifetime of **5-1b** was determined to be 1.7 ns for the LE emission band, 3.9 ns for the ESIPT band, and 6.6 ns for emission of the deprotonated species L<sup>2-</sup> (Figure 5-4). Again, the shorter lifetime of the LE emission band compared to the ESIPT band is consistent with the hypothesized competition between radiative deactivation of the local excited state (LE) and the proton transfer process. By Gaussian fitting of the fluorescence spectrum of the monoprotinated species of **5-1b** (Figure 5-1), the quantum yield of the two emission processes was estimated to be 0.06 (for ESIPT emission) and 0.03 (for LE). Combined with the fluorescence lifetime data, the radiative decay rates were calculated to be  $1.9 \times 10^7 \text{ s}^{-1}$  for LE emission,  $1.5 \times 10^7 \text{ s}^{-1}$  for ESIPT emission,  $4.1 \times 10^7 \text{ s}^{-1}$  for L<sup>2-</sup> emission.

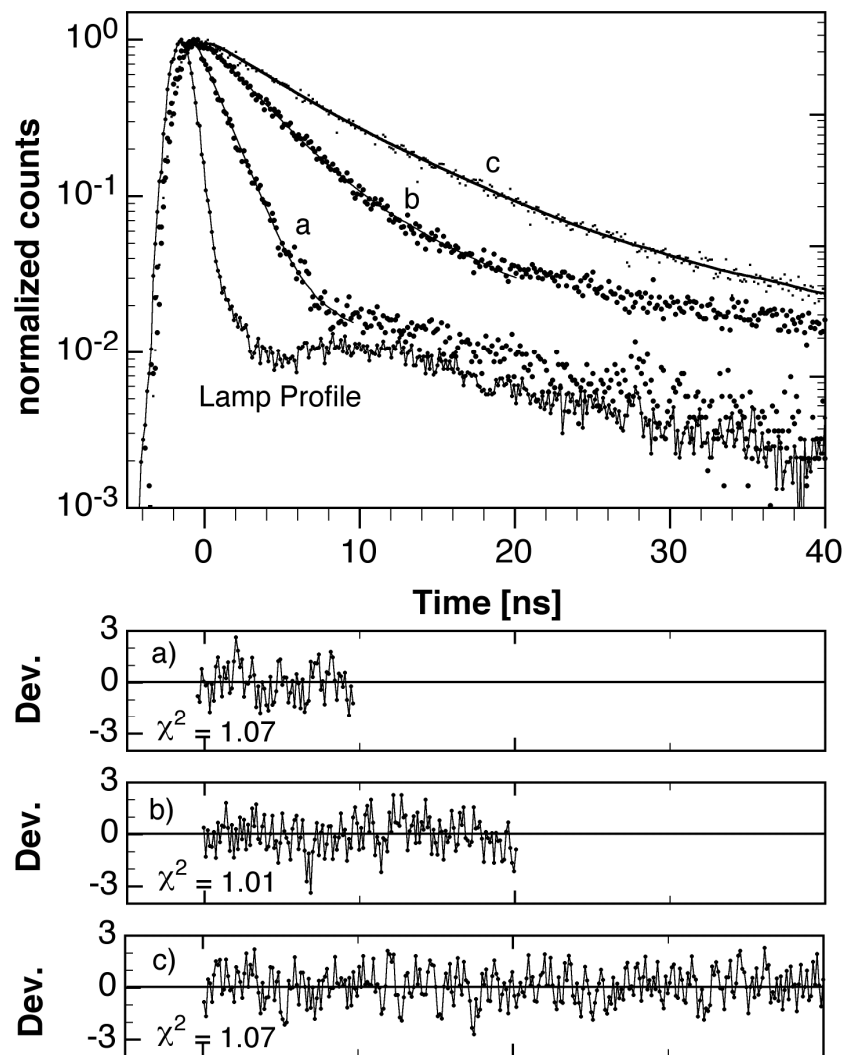


**Figure 5-4:** Fluorescence decay data of **5-1b** in aqueous solution: a) in pH 6.5 buffer (10 mM PIPES, 0.1 M KCl), 365 nm; b) in pH 6.5 buffer, 600 nm; c) in pH 11 buffer (0.1 M KCl), 480 nm. The curve fit is based on a monoexponential decay law (for monoprotated species  $HL^-$ : at 365 nm:  $\tau = 1.7$  ns,  $\chi^2 = 1.07$ ; at 600 nm:  $\tau = 3.9$  ns,  $\chi^2 = 1.01$ ; for deprotonated species  $L^{2-}$ :  $\tau = 6.6$  ns,  $\chi^2 = 1.07$ )

#### 5.2.3.4. Fluorescence Quantum Yield and Brightness.

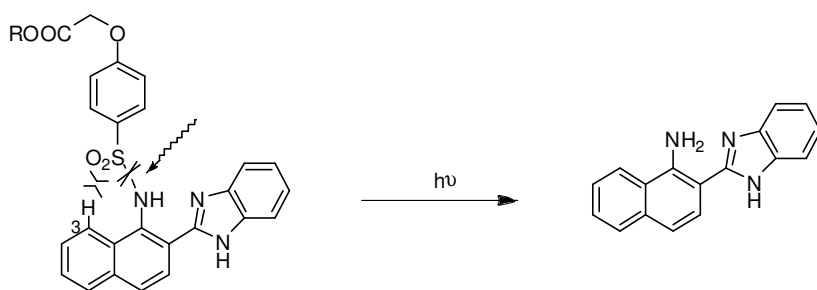
The quantum yield of the deprotonated species  $L^{2-}$  was found to be consistently higher compared to the monoprotonated species  $HL^-$ , an observation that is presumably due to the intrinsically larger Stokes' shift of the ESIPT emission. Derivative **5-3b** has the highest quantum yield ( $L^{2-}$ : 0.34,  $HL^-$ : 0.25), followed by the parent compound **5-4b** ( $L^{2-}$ : 0.26,  $HL^-$ : 0.23). The quantum yield of **5-2b** is relatively low ( $L^{2-}$ : 0.13,  $HL^-$ : 0.10), which is consistent with the fact that there is the photochemical decomposition as an alternative deactivation pathway. For the monoprotonated species  $HL^-$  of **5-1b**, the slow proton transfer rate could result in more irradiative relaxation of the excited state which might be responsible for the lower quantum yield (0.09). The brightness of all fluorophores is best compared by combining the corresponding quantum yield and extinction coefficients ( $\epsilon\phi$ ). According to these data, the parent compound is significantly brighter ( $2829 \text{ Lmol}^{-1}\text{cm}^{-1}$ ) compared to the derivatives with extended conjugated system, whose brightness follows the order of **5-1b** ( $1620 \text{ Lmol}^{-1}\text{cm}^{-1}$ ), **5-3b** ( $1340 \text{ Lmol}^{-1}\text{cm}^{-1}$ ), **5-2b** ( $1177 \text{ Lmol}^{-1}\text{cm}^{-1}$ ).

#### 5.2.4. Photochemical Studies

Unlike all other derivatives, compound **5-2b** undergoes photodecomposition under irradiation of UV light. The photodecomposition is associated with the absorption spectra blue shift. (Figure 5-5). One of the photoproducts is the naphthylamine derivative (**5-11**) as determined by NMR and mass spectrometry (Scheme 5-1). The photo-cleavage of the weakened sulfur-nitrogen bond that is presumably due to steric effects imposed through

the hydrogen in position 3 of the naphthyl ring (Scheme 5-2). Since this photoreaction results in a blue-shifted absorption spectrum, its efficiency could be determined by actinometry. By using azobenzene as the actinometric standard, the quantum yield of the photoreaction was determined to be  $\phi^A=0.40$ . Furthermore, measurements at high pH revealed that deprotonation of the sulfonamide nitrogen significantly reduced photodecomposition (Figure 5-6,  $\phi^A=0.04$ ). The uniformity of the reaction was demonstrated by linear absorbance difference methods.

### Scheme 5-2



### 5.3. Conclusions

In this chapter, the impact of the extension of  $\pi$ -conjugated system on 2-(2'-sulfonamidophenyl)benzimidazoles fluorophores was investigated in detail. The annulation position of the additional benzene ring strongly influences the photophysical properties and photochemical stability. Similar to what was observed in chapter 3, the radiative relaxation of the local excited state causes dual emission for derivative **5-1**. Presumably due to the introduced steric strain, compound **5-2** was rendered photolabile. More importantly, the absorption maxima depended on the annulation position, thus

leading to fluorophore **5-3** with good ratiometric properties combined with a substantial absorption cross section beyond 350 nm. Unlike the fluorophores obtained by substituent engineering, the sulfonamide nitrogen of **5-3b** has a  $pK_a$  value as 7.94, and is almost unaffected by the structural modifications. Hence, fluorophore **5-3** represents a promising candidate for biological imaging applications.

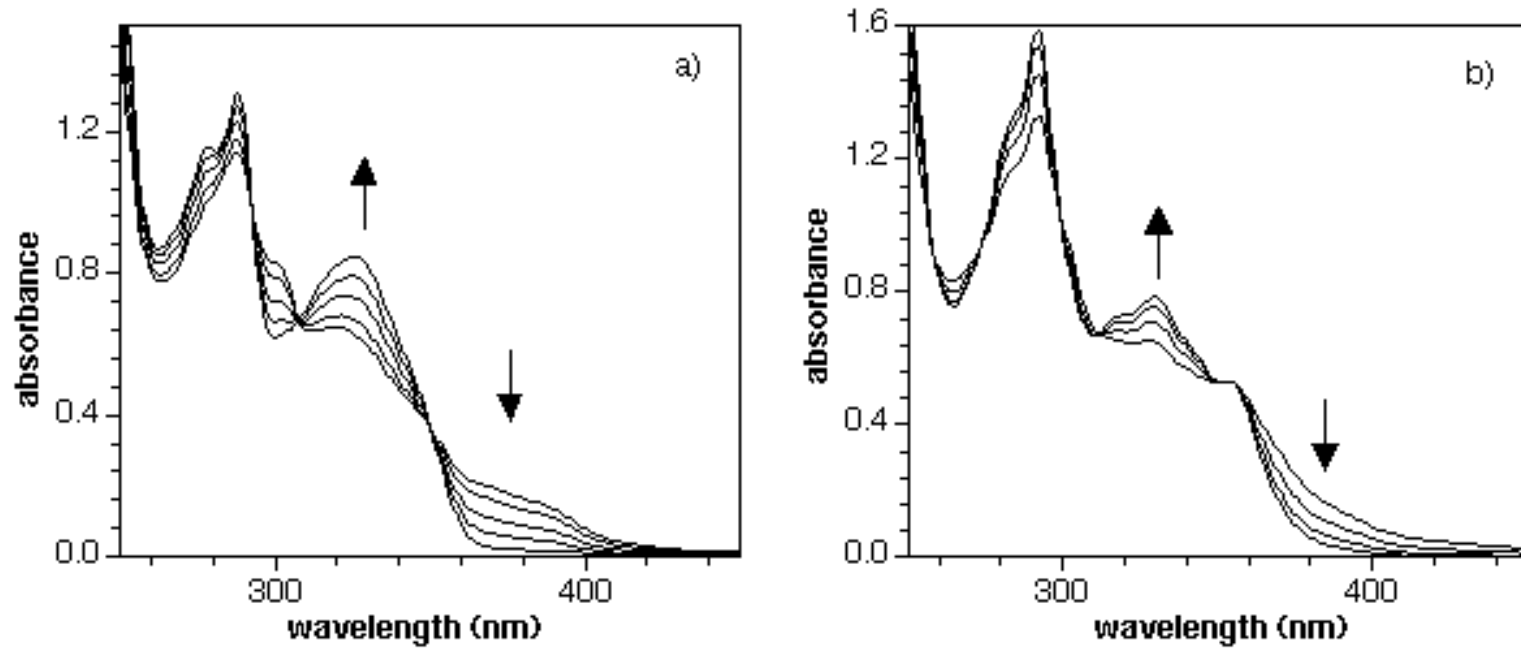


**Figure 5-5.** UV spectra for the photoreactions of **5-2a** a) in MeOH; b) in 1mM KOH methanol solution.

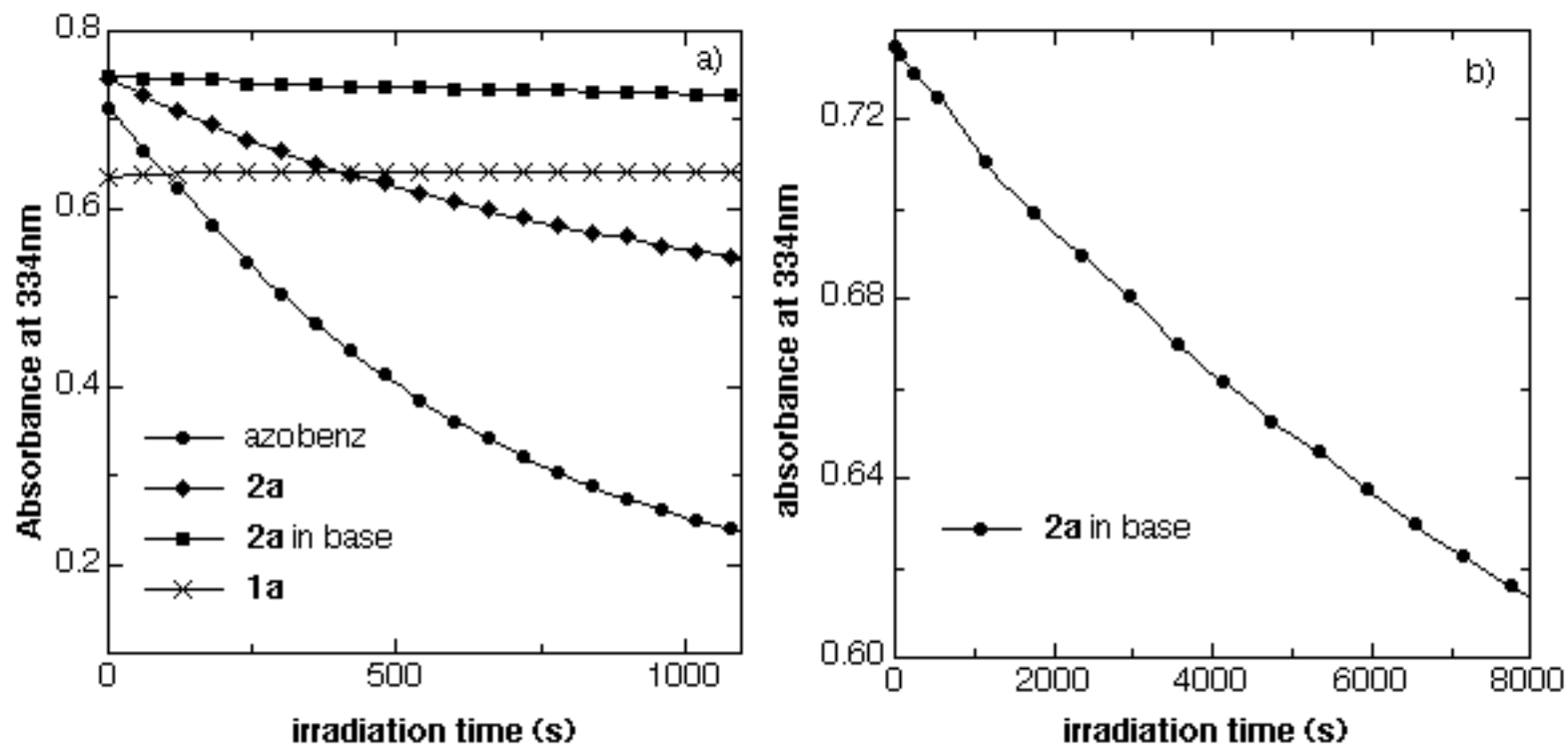


**Figure 5-6.** Absorbance-time diagrams. a) Azobenzene and **5-2a** were 50  $\mu\text{M}$  solution in methanol. **5-2a** in base was 50  $\mu\text{M}$  in 1 mM KOH methanol solution. And **5-1a** was 30 $\mu\text{M}$  solution in methanol. The absorbance change was measured at 334 nm following every one minute's irradiation at 334 nm. b) The absorbance change of 50  $\mu\text{M}$  **5-2a** in 1mM KOH MeOH solution.

## 5.4. Experimental Section

### 5.4.1. Synthesis.

Fluorophores **5-4a** and **b** were synthesized following published procedures.<sup>2</sup> NMR:  $\delta$  in ppm vs SiMe<sub>4</sub> (0 ppm, <sup>1</sup>H, 400 MHz). MS: selected peaks; m/z. Melting points are uncorrected. Flash chromatography (FC): Merck silica gel (240-400 mesh). TLC: 0.25 mm, Merck silica gel 60 F<sub>254</sub>, visualizing at 254 nm or with 2% KMnO<sub>4</sub> solution.

**(a) (3-Amino-naphthalen-2-yl)-methanol (5-6).** Acid **5-5** (200 mg, 1.0 mmol) was suspended in dry THF (10 ml) and the mixture cooled to 0°C. Then solid lithium aluminum hydride (120 mg, 3.2 mmol) was added in portions with stirring. After the gas evolution subsided, the mixture was heated under reflux for 1 hour. After cooling to room temperature, the reaction mixture was quenched with ice-cold water (4 eqv. to LAH). Silica gel was added to absorb the precipitate, all solid material was filtered off and washed by EtOAc. The combined organic solutions were dried over anhydrous MgSO<sub>4</sub>, filtered, and concentrated under reduced pressure, providing 175.5 mg yellow solid (1.0 mmol, 100% yield). Mp > 150°C (dec.); *R<sub>f</sub>* 0.50 (1:1 EtOAc:Hexane). <sup>1</sup>H-NMR (CDCl<sub>3</sub>, 400 MHz)  $\delta$  4.36 (s, 2H), 4.84 (s, 2H), 7.02 (s, 1H), 7.22 (t, *J* = 7.8 Hz, 1H), 7.36 (t, *J* = 7.9 Hz, 1H), 7.57 (s, 1H), 7.58 (d, *J* = 10 Hz, 1H), 7.67 (d, *J* = 8.0 Hz, 1H). MS (70 eV) 173 (M<sup>+</sup>, 58), 155 (72), 128(100). EI-HRMS *m/e* calculated for (M<sup>+</sup>) C<sub>11</sub>H<sub>11</sub>NO 173.08406, observed 173.08422.

**(b) [4-(3-Hydroxymethyl-naphthalen-2-ylsulfamoyl)-phenoxy]-acetic acid ethyl**

**ester (5-7).** Amine **5-6** (90 mg, 0.52 mmol) and **5-15** (180 mg, 0.65 mmol) were dissolved in pyridine (1 ml) and stirred overnight. The mixture was then poured into 1 N HCl, extracted with EtOAc, dried with anhydrous MgSO<sub>4</sub>, and evaporated to dryness. The crude product was purified on silica gel (1:1.5 EtOAc/hexanes), providing 100 mg of a beige solid (0.24 mmol, 46% yield). Mp 149-151°C; *R<sub>f</sub>* 0.42 (1:1 EtOAc:Hexane). <sup>1</sup>H-NMR (CDCl<sub>3</sub>, 400 MHz) δ 1.23 (t, *J* = 7.1 Hz, 3H), 4.20 (q, *J* = 7.1 Hz, 2H), 4.46 (s, 2H), 4.54 (s, 2H), 6.77 (d, *J* = 8.9 Hz, 2H), 7.39 (t, *J* = 7.9 Hz, 1H), 7.44 (t, *J* = 8.2 Hz, 1H), 7.47 (s, 1H), 7.63-7.70 (m, 3H), 7.73 (d, *J* = 8.0 Hz, 1H), 7.85 (s, 1H), 8.22 (s, 1H). MS (70 eV) 415 (M<sup>+</sup>, 4), 155 (50), 106 (77), 41 (100). EI-HRMS *m/e* calculated for (M<sup>+</sup>) C<sub>21</sub>H<sub>21</sub>NO<sub>6</sub>S 415.10896, observed 415.10668.

(c) **[4-(3-Formyl-naphthalen-2-ylsulfamoyl)-phenoxy]-acetic acid ethyl ester (5-8).** Alcohol **5-7** (100 mg, 0.24 mmol) was dissolved in CHCl<sub>3</sub> (20 ml), then MnO<sub>2</sub> (200 mg, 2.3 mmol) was added. The mixture was stirred overnight at room temperature, and subsequently filter through Celite. The filtrate was evaporated to dryness providing 87 mg of a yellow solid (0.21 mmol, 88% yield). Mp 155-157°C; *R<sub>f</sub>* 0.63 (1:1 EtOAc:hexanes). <sup>1</sup>H-NMR (CDCl<sub>3</sub>, 400 MHz) δ 1.23 (t, *J* = 7.1 Hz, 3H), 4.22 (q, *J* = 7.1 Hz, 2H), 4.58 (s, 2H), 6.85 (d, *J* = 9.0 Hz, 2H), 7.48 (t, *J* = 8.0 Hz, 1H), 7.63 (t, *J* = 8.0 Hz, 1H), 7.80-7.88 (m, 4H), 8.04 (s, 1H), 8.14 (s, 1H), 9.96 (s, 1H), 10.40 (s, 1H). MS (70 eV) 413 (M<sup>+</sup>, 58), 170 (100), 142(23), 115(28). EI-HRMS *m/e* calculated for (M<sup>+</sup>) C<sub>21</sub>H<sub>19</sub>NO<sub>6</sub>S 413.09331, observed 413.09352.

(d) **{4-[3-(1*H*-Benzoimidazol-2-yl)-naphthalen-2-ylsulfamoyl]-phenoxy}-acetic acid ethyl ester (5-1a)**. Phenylenediamine (28 mg, 0.26 mmol) was dissolved in EtOH/H<sub>2</sub>O (1:1, 4 ml), and then acetic acid (22  $\mu$ l), aldehyde **5-6** (90 mg, 0.22 mmol) in EtOH (2 ml), and Cu(OAc)<sub>2</sub> H<sub>2</sub>O (52.7 mg, 0.26 mmol) in water (2 ml) were added. The mixture was refluxed overnight, the formed precipitate was filtered off and redissolved in EtOH/conc. HCl (10:1). Saturated Na<sub>2</sub>S 9H<sub>2</sub>O in water was added and the mixture was refluxed for 1 hour. After filtering off the black residue, the filtrate was neutralized with saturated aqueous NaHCO<sub>3</sub>. The remaining EtOH was distilled off under reduced pressure, and the aqueous solution was extracted with EtOAc. The combined organic layer were dried with anhydrous MgSO<sub>4</sub> and concentrated under reduced pressure, providing 7 mg of a yellow solid (0.014 mmol, 6% yield). Mp 88-90°C; *R<sub>f</sub>* 0.13 (1:2 EtOAc:hexanes). <sup>1</sup>H-NMR (CDCl<sub>3</sub>, 400 MHz)  $\delta$  1.32 (t, *J* = 7.1 Hz, 3H), 4.31 (q, *J* = 7.1 Hz, 2H), 4.59 (s, 2H), 6.20 (d, *J* = 9.0 Hz, 2H), 7.11(d, *J* = 9.0 Hz, 2H), 7.28-7.35 (m, 2H), 7.44-7.50 (m, 2H), 7.54 (t, *J* = 6.9 Hz, 1H), 7.76 (d, *J* = 8.3 Hz, 1H), 7.82 (s, 1H), 7.86 (d, *J* = 8.2 Hz, 1H), 7.93 (s, 1H), 8.18 (s, 1H), 9.94 (s, 1H), 11.42 (s, 1H). MS (70 eV) 501 (M<sup>+</sup>, 14), 259 (49), 44 (100). EI-HRMS *m/e* calculated for (M<sup>+</sup>) C<sub>27</sub>H<sub>23</sub>N<sub>3</sub>O<sub>5</sub>S 501.14842, observed 501.13590.

(e) **{4-[3-(1*H*-Benzoimidazol-2-yl)-naphthalen-2-ylsulfamoyl]-phenoxy}-acetic acid (5-1b)**. To a solution of LiOH H<sub>2</sub>O (50 mg, 1.2 mmol) in MeOH/H<sub>2</sub>O (1:1, 0.6 ml), **1a** (30 mg, 0.060 mmol) in THF (500  $\mu$ l) was added, and the resulting mixture was stirred at room temperature for 1 hour. The organic solvent was removed under reduced pressure.

The residue was diluted with water and the solution neutralized with 1 N HCl until the product started to precipitate. The yellow solid was filtered off, washed with water, and dried *in vacuo*, affording 22 mg of a yellow solid. Yield 77%. Mp > 175°C (dec.); *R<sub>f</sub>* 0.10 (1:9 MeOH: CH<sub>2</sub>Cl<sub>2</sub>). <sup>1</sup>H-NMR (DMSO, 400 MHz) δ 4.62 (s, 1H), 6.85 (d, *J* = 7.4 Hz, 2H), 7.30-7.38 (m, 2H), 7.48 (t, *J* = 7.6 Hz, 1H), 7.56 (t, *J* = 8.0 Hz, 1H), 7.65-7.72 (m, 4H), 7.84-7.90 (m, 2H), 7.98 (s, 1H), 8.62 (s, 1H), 13.36 (s, 2H). MS (70 eV) 473 (M<sup>+</sup>, 8), 415 (25), 299 (79), 269 (60), 259 (100), 209 (83), 44 (44). EI-HRMS *m/e* calculated for (M<sup>+</sup>) C<sub>25</sub>H<sub>19</sub>N<sub>3</sub>O<sub>5</sub>S 473.09262, observed 473.10435.

**(f) 2-(1-Nitro-naphthalen-2-yl)-1H-benzimidazole (5-10).** A solution of *o*-phenylenediamine (64.5 mg, 0.60 mmol), 1-nitro-2-naphthaldehyde **5-9** (100 mg, 0.50 mmol), Cu(OAc)<sub>2</sub>·H<sub>2</sub>O (120 mg, 0.60 mmol) and acetic acid (50 μL) in 10 mL of MeOH/H<sub>2</sub>O (1:1) was reflux overnight. After all starting materials had been consumed (TLC), the organic solvent was removed under reduced pressure. After addition of 10 mL aqueous ammonium hydroxide (28%), the mixture was extracted twice with dichloromethane. The combined organic layers were dried over anhydrous MgSO<sub>4</sub>, and concentrated under reduced pressure. The crude product was purified on silica gel (FC, 1:1.5 EtOAc : Hexane) affording 93 mg of a yellow solid (0.32 mmol, 64% yield). Mp > 230°C (dec.); *R<sub>f</sub>* 0.37 (1:1 EtOAc : Hexane). <sup>1</sup>H-NMR (DMSO, 400 MHz) δ 7.23-7.29 (m, 2H), 7.63-7.68 (m, 2H), 7.70-7.75 (m, 1H), 7.77-7.82 (m, 2H), 8.15-8.24 (m, 2H), 8.40 (d, *J* = 8.7 Hz, 1H), 13.30 (s, 1H). EI-MS (70 eV) 289.1 (M<sup>+</sup>, 100), 272.1 (90), 247.1 (62), 231.1 (25), 126.1 (30). EI-HRMS *m/e* calculated for (M<sup>+</sup>) C<sub>17</sub>H<sub>11</sub>N<sub>3</sub>O<sub>2</sub> 289.08513,

observed 289.08563.

**(g) 2-(1*H*-Benzoimidazol-2-yl)-naphthalen-1-ylamine (5-11).** Compound **5-10** (90 mg, 0.31 mmol) was suspended in 10 mL ethanol and hydrogenated at ambient pressure in the presence of Pd/C (3% wt, 20 mg) as catalyst. Upon completion of the reaction (TLC), the solution was filtered through celite and concentrated under reduced pressure, providing 70mg of a yellow solid (0.27mmol, 87% yield). Mp > 232°C (dec.); *R<sub>f</sub>* 0.53 (1:2 EtOAc : Hexane). <sup>1</sup>H-NMR (CDCl<sub>3</sub>, 400 MHz) δ 7.22-7.28 (m, 2H), 7.25-7.30 (m, 2H), 7.50-7.55 (m, 2H), 7.61 (d, *J* = 8.7 Hz, 2H), 7.77-7.83 (m, 1H), 7.96-8.01 (m, 1H). EI-MS (70eV) 259.1 (M<sup>+</sup>, 100). EI-HRMS *m/e* calculated for (M<sup>+</sup>) C<sub>17</sub>H<sub>13</sub>N<sub>3</sub> 259.11095, observed 259.11043.

**(h) {4-[2-(1*H*-Benzoimidazol-2-yl)-naphthalen-1-ylsulfamoyl]-phenoxy}-acetic acid ethyl ester (5-2a).** A solution of amine **5-11** (70 mg, 0.27 mmol) and sulfonyl chloride **5-15** (97 mg, 0.34 mmol) in 2 ml pyridine was stirred at room temperature overnight. The resulting mixture was poured in 20 ml 1 N HCl and extracted twice with EtOAc. The combined organic extracts were dried with anhydrous MgSO<sub>4</sub> and evaporated under reduced pressure. The crude product was recrystallized from CH<sub>2</sub>Cl<sub>2</sub>/hexane and further purified on a short silica gel column (EtOAc:hexanes, 1:1), providing 50 mg of a yellow solid (0.10 mmol, 37%). Mp 216-218°C; *R<sub>f</sub>* 0.41 (1:1 hexanes:EtOAc). <sup>1</sup>H-NMR (CDCl<sub>3</sub>, 400 MHz) □ δ 1.44 (t, *J* = 7.1 Hz, 3H), 4.44 (q, *J* = 7.1 Hz, 2H), 4.69 (s, 1H), 5.98 (d, *J* = 8.7 Hz, 2H), 6.67 (d, *J* = 8.6 Hz, 2H), 7.30-7.35 (m, 2H), 7.39 (d, *J* = 8.4 Hz, 1H), 7.61-7.66 (m, 3H), 7.77 (d, *J* = 8.4 Hz, 1H), 7.82 (d, *J* = 8.4

Hz, 1H), 8.85 (d,  $J = 8.2$  Hz, 1H). MS (70 eV) 501.2(M<sup>+</sup>, 19), 437.2 (5), 350.1 (5), 258.1 (100), 231.1 (13). EI-HRMS  $m/e$  calculated for (M<sup>+</sup>) C<sub>27</sub>H<sub>23</sub>N<sub>3</sub>O<sub>5</sub>S 501.13519, observed 501.13463.

(i) **{4-[2-(1*H*-Benzoimidazol-2-yl)-naphthalen-1-ylsulfamoyl]-phenoxy}-acetic acid (5-2b)**. A mixture of LiOH H<sub>2</sub>O (20 mg, 0.48 mmol) and **5-2a** (10 mg, 0.020 mmol) in MeOH/H<sub>2</sub>O/THF (0.1 mL/0.1 mL/0.3 mL) was stirred overnight at room temperature. The organic solvent was removed under reduced pressure. The residue was diluted with water and the solution neutralized with 1 N HCl until the product started to precipitate. The yellow solid was filtered off, washed with water, and dried *in vacuo* (9 mg, 0.019 mmol, 95%). Mp > 245°C(dec.);  $R_f$  0.42 (1:6 MeOH : CH<sub>2</sub>Cl<sub>2</sub>). <sup>1</sup>H-NMR (DMSO, 400 MHz)  $\delta$  4.56 (s, 2H), 6.53-6.60 (m, 2H), 7.08-7.13 (m, 2H), 7.48-7.56 (m, 3H), 7.66 (t,  $J = 7.6$  Hz, 1H), 7.74-7.79 (m, 2H), 7.89 (d,  $J = 8.6$  Hz, 1H), 8.04 (d,  $J = 8.1$  Hz, 1H), 8.14 (d,  $J = 8.8$  Hz, 2H). MS (70 eV) 473.1 (M<sup>+</sup>, 8), 259.1 (100). EI-HRMS  $m/e$  calculated for (M<sup>+</sup>) C<sub>25</sub>H<sub>19</sub>N<sub>3</sub>O<sub>5</sub>S 423.08889, observed 473.10506.

(j) **2-(2-Nitrophenyl)-1*H*-naphtho[2,3-*d*]imidazole (5-13)**. A mixture of naphthalene-2,3-diamine (625 mg, 4.0 mmol) and 2-nitrobenzaldehyde (500 mg, 3.3 mmol) in 100 mL of ethanol was heated under reflux overnight. After addition of 1, 4-benzoquinone (715 mg, 6.6 mmol), the solution was refluxed for an additional hour and then the solvent was removed under reduced pressure. The residue was redissolved in EtOAc and washed with 5% NaOH. The combined organic layers were dried with

anhydrous  $\text{MgSO}_4$  and *concentrated in vacuo*. The crude product was purified by silica gel flash chromatography (1:1, EtOAc:hexanes), providing 800 mg of a beige solid (2.8mmol, 84% yield.). Mp > 280°C (dec.); R<sub>f</sub> 0.28 (1:1 EtOAc:Hexane). <sup>1</sup>H-NMR (CDCl<sub>3</sub>, 400 MHz) δ 7.40-7.48 (m, 2H), 7.70 (t, *J* = 7.6 Hz, 1H), 7.79 (t, *J* = 7.6 Hz, 1H), 7.91-7.98 (m, 2H), 8.02 (d, *J* = 8.1 Hz, 2H), 8.18 (d, *J* = 7.6 Hz, 1H), 8.32 (s, 1H), 9.63 (s, 1H). MS (70 eV) 289.1 (M<sup>+</sup>, 78), 256.1 (100), 243.1 (28), 140.1 (65). EI-HRMS *m/e* calculated for (M<sup>+</sup>) C<sub>17</sub>H<sub>11</sub>N<sub>3</sub>O<sub>2</sub> 289.08513, observed 289.08519.

**(k) 2-(1*H*-Naphtho[2,3-*d*]imidazol-2-yl)aniline (5-14).** A suspension of compound **5-13** (800 mg, 2.8 mmol) in 300 mL ethanol was hydrogenated at ambient pressure in the presence of Pd/C (3% wt, 120 mg) as catalyst. The reaction mixture was filtered through celite and concentrated under reduced pressure, providing 660 mg of a brown solid (2.5 mmol, 89% yield). Mp > 250°C (dec); R<sub>f</sub> 0.67 (1:1 EtOAc : Hexane). <sup>1</sup>H-NMR (CDCl<sub>3</sub>, 400 MHz) 6.47 (br, 2H), 6.79 (t, *J* = 8.0 Hz, 1H), 6.84 (d, *J* = 8.3 Hz, 1H), 7.37-7.45 (m, 2H), 7.59 (d, *J* = 8.0 Hz, 1H), 7.84 (s, 1H), 7.91 (d, *J* = 7.5 Hz, 1H), 7.99 (d, *J* = 7.5 Hz, 1H), 8.21 (s, 1H), 9.18 (br, 1H). EI-MS (70eV) 259.1 (M<sup>+</sup>, 100). EI-HRMS *m/e* calculated for (M<sup>+</sup>) C<sub>17</sub>H<sub>13</sub>N<sub>3</sub> 259.11095, observed 259.11034.

**(l) Ethyl 2-(4-(N-(2-(1*H*-naphtho[2,3-*d*]imidazol-2-yl)phenyl)sulfamoyl)-phenoxy)acetate (5-3a).** A solution of amine **5-14** (440 mg, 1.7 mmol) and sulfonyl chloride **5-15** (800 mg, 2.8 mmol) in 10 ml pyridine was stirred at room temperature overnight. Then the mixture was poured into 100 ml 1 N HCl, extracted twice with EtOAc, dried by anhydrous  $\text{MgSO}_4$  and evaporated. The crude product was purified by a short silica gel

column (EtOAc:hexanes, 1:2-1:1), affording 360 mg of a yellow solid (0.72 mmol, 42%). Mp 235-237°C; *R<sub>f</sub>* 0.32 (1:1 hexane:EtOAc). <sup>1</sup>H-NMR (CDCl<sub>3</sub>, 400 MHz) δ 1.11 (t, *J* = 7.1 Hz, 3H), 4.08 (q, *J* = 7.1 Hz, 2H), 4.77 (s, 2H), 6.94 (d, *J* = 9.0 Hz, 2H), 7.26 (t, *J* = 7.7 Hz, 1H), 7.41-7.46 (m, 2H), 7.49 (t, *J* = 7.7 Hz, 1H), 7.67 (d, *J* = 8.4 Hz, 1H), 7.72 (d, *J* = 9.0 Hz, 2H), 8.05-8.11 (m, 2H), 8.15 (dd, *J* = 7.8, 1.2 Hz, 1H), 8.21 (br, 2H), 13.34 (br, 1H). EI-HRMS *m/e* calculated for (M<sup>+</sup>) C<sub>27</sub>H<sub>23</sub>N<sub>3</sub>O<sub>5</sub>S 501.13584, observed 501.13411.

(m) **2-(4-(N-(2-(1*H*-naphtho[2,3-*d*]imidazol-2-yl)phenyl)sulfamoyl)phenoxy)-acetic acid (5-3b)**. A mixture of LiOH H<sub>2</sub>O (150 mg, 3.6 mmol) and **5-3a** (65 mg, 0.13 mmol) in MeOH/H<sub>2</sub>O/THF (0.9 mL/0.9 mL/2 mL) was stirred at room temperature overnight. The organic solvent was removed under reduced pressure. The residue was diluted with water and the solution neutralized with 1 N HCl until the product started to precipitate. The solid was collected by filtration, washed with water, and dried *in vacuo*, (50 mg, 0.11 mmol, 85%). Mp > 112°C (dec.); *R<sub>f</sub>* 0.18 (2:9 MeOH:CH<sub>2</sub>Cl<sub>2</sub>). <sup>1</sup>H-NMR (DMSO, 400 MHz) δ 4.47 (s, 2H), 6.80 (d, *J* = 8.8 Hz, 2H), 7.23 (t, *J* = 7.4 Hz, 1H), 7.39-7.44 (m, 2H), 7.47 (t, *J* = 7.4 Hz, 1H), 7.60 (d, *J* = 8.8 Hz, 2H), 7.63 (d, *J* = 8.0 Hz, 1H), 8.04-8.09 (m, 2H), 8.13 (d, *J* = 8.0 Hz, 1H), 8.29 (br, 2H). ESI-HRMS *m/e* calculated for (M<sup>-</sup>) C<sub>25</sub>H<sub>18</sub>N<sub>3</sub>O<sub>5</sub>S 472.097266, observed 472.0979.

(n) **2-(1*H*-Benzoimidazol-2-yl)-naphthalen-1-ylamine (5-11)**. Compound **5-2a** (5.09 mg, 0.010 mmol) was dissolved in 0.5 mL DMSO, and exposed to 250 nm UV light irradiation from a mercury lamp. The decomposition reaction was monitored by TLC

until starting material was completely consumed. After purification on a short silica gel column (EtOAc : Hexane 1:1), 2 mg of a yellow solid were obtained (0.0077 mmol, 77%). Mp 216-218°C;  $R_f$  0.41 (1:1 hexane:EtOAc).  $^1\text{H-NMR}$  ( $\text{CDCl}_3$ , 400 MHz)  $\delta$  1.44 (t,  $J = 7.1$  Hz, 3H), 4.44 (q,  $J = 7.1$  Hz, 2H), 4.69 (s, 1H), 5.98 (d,  $J = 8.7$  Hz, 2H), 6.67 (d,  $J = 8.6$  Hz, 2H), 7.30-7.38 (m, 2H), 7.39 (d,  $J = 8.4$  Hz, 1H), 7.61-7.67 (m, 3H), 7.77 (d,  $J = 8.4$  Hz, 1H), 7.82 (d,  $J = 8.4$  Hz, 1H), 8.85 (d,  $J = 8.2$  Hz, 1H). MS (70 eV) 501.2 ( $\text{M}^+$ , 19), 437.2 (5), 350.1 (5), 258.1 (100), 231.1 (13). EI-HRMS  $m/e$  calculated for ( $\text{M}^+$ )  $\text{C}_{19}\text{H}_{27}\text{N}_5\text{O}_7\text{S}_2$  501.13519, observed 501.13463.

#### 5.4.2. Steady-state Absorption and Fluorescence Spectroscopy.

All spectroscopic measurements were carried out in a quartz cuvette with 3.0 mL volume and 1cm path length. For spectrophotometric titrations the sample solution was continuously stirred. Steady-state UV-vis spectra were recorded on a Varian Cary Bio50 UV-vis spectrometer at 25°C, maintained by a temperature control accessory. Fluorescence emission and excitation spectra were recorded on a PTI fluorimeter with FELIX software. All fluorescence spectra were corrected by the correction file provided by the instrument manufacturer. Quinine sulfate in 1.0 N  $\text{H}_2\text{SO}_4$  ( $\Phi = 0.54$ ) was used as the standard for quantum yield measurements.<sup>9</sup>

#### 5.4.3. Electrode Calibration in Aqueous Solution.

A Ross ultra semimicro pH glass electrode (Orion No. 8103BNUMP) was used for

all measurements. The electrode was calibrated for  $-\log[\text{H}_3\text{O}^+]$  by titration of 0.1 N volumetric standard HCl with 0.1 N volumetric standard KOH under 0.1 M ionic strength (KCl). The software GLEE was used to determine the end point  $E^o$  and slope.<sup>10</sup> A Corning pH/Ion Analyzer 355 was used to measure the electron potential.

#### 5.4.4. Determination of $pK_a$ Values.

To determine  $pK_a$  values, the UV-vis spectra of the sample solution in 0.1 M KCl were monitored from  $-\log[\text{H}_3\text{O}^+]$  5 to 11. The emf was converted to  $-\log[\text{H}_3\text{O}^+]$  by  $E^o$  and slope determined from the electrode calibration. All data were processed by non-linear least-squares fit analysis using the SPECFIT software package.<sup>11</sup>

#### 5.4.5. Actinometry.

The Xenon arc-lamp of a PTI fluorimeter was used as the light source for actinometric measurements. The wavelength of the incident beam was set to 334 nm. UV-vis absorption spectra were recorded with a Varian Cary Bio50 UV-vis spectrometer. All solutions were measured in a 3.0 mL volume cell with stirring at 23°C.

#### 5.4.6. Determination of Quantum Yield ( $\phi$ ) of Photochemical Reactions.

The *trans-cis* photoisomerisation ( $A \xrightarrow{h\nu} B$ ) of azobenzene was used as the chemical actinometer to determine the incident irradiance intensity. In this investigation, the UV absorbance of 50  $\mu\text{M}$  azobenzene in pure methanol was measured at 334 nm

multiple times following one minute of irradiation at 334 nm. The relationship of the absorbance and time will be as following:<sup>12-14</sup>

$$\frac{dE}{dt} = 1000 \cdot I_0 \cdot (\Phi_2^{cis} \cdot \epsilon_{cis} + \Phi_1^{trans} \cdot \epsilon_{trans}) \cdot (E_{\lambda\infty} - E) \cdot F(t), \quad \text{Eq. 5-1}$$

which can be simplified to

$$\frac{dE}{dt} = (z_{\lambda 1} + z_{\lambda 2} E_{\lambda}) \cdot F(t). \quad \text{Eq. 5-2}$$

The parameters are defined as

$$\begin{aligned} z_{\lambda 1} &= I_0 \cdot Q \cdot E_{\lambda\infty} \\ z_{\lambda 2} &= -I_0 \cdot Q \\ Q &= 1000 \cdot (\Phi_2^{cis} \cdot \epsilon_{cis} + \Phi_1^{trans} \cdot \epsilon_{trans}) \end{aligned} \quad \text{Eq. 5-3}$$

and  $F(t) = \frac{1 - 10^{-E'(t)}}{E'(t)}$  is the photokinetic factor in decadic units. If the UV

absorbance is measured at the irradiation wavelength (in this investigation, it is 334 nm),

then  $E'(t) = E(t)$ .

To evaluate Eq. 5-2, formal integration can be used:<sup>8</sup>

$$\frac{\Delta E}{\int_{t_1}^{t_n} \frac{1 - 10^{-E(t_n)}}{E(t_n)} dt} = z_{\lambda 1} + z_{\lambda 2} \frac{\int_{t_1}^{t_n} E_{\lambda}(t_n) \frac{1 - 10^{-E(t_n)}}{E(t_n)} dt}{\int_{t_1}^{t_n} \frac{1 - 10^{-E(t_n)}}{E(t_n)} dt} \quad \text{Eq. 5-4}$$

$$Y = z_{\lambda 1} + z_{\lambda 2} X$$

This is a linear equation with  $z_{\lambda 1}$  and  $z_{\lambda 2}$  corresponding to the intercept and slope of the fitted line, respectively.  $Q$  was obtained from ref. 8. Hence, the irradiance intensity  $I_0$  and  $E_{\lambda\infty}$  can be calculated from Eq. 5-3.

For a uniform photoreaction  $A \xrightarrow{h\nu} B$  (in this investigation, the uniformity of the photoreaction is demonstrated by E-diagram and ED-diagram shown in Appendix B), Eq. 5-4 is still valid with modified definitions of  $z_{\lambda 1}$  and  $z_{\lambda 2}$ :<sup>8</sup>

$$\begin{aligned} z_{\lambda 1} &= 1000 \varepsilon'_A \varphi^A I_0 E_{\lambda\infty} \\ z_{\lambda 2} &= -1000 \varepsilon'_A \varphi^A I_0 \end{aligned} \qquad \text{Eq. 5-5}$$

With  $I_0$  obtained from above, the quantum yield  $\varphi^A$  and  $E_{\lambda\infty}$  can then be calculated with Eq. 5-5.

#### 5.4.7. Time-Resolved Measurements.

Time resolved measurements were done with a Photon Technology International (PTI) fluorescence lifetime instrument. The light source was a nitrogen laser (model GL-3300). All samples were excited at 337 nm with a repetition rate of 10 Hz (pulse width 3.5 ns), and the fluorescence signal was analyzed after passing through a monochromator set at the peak emission of the corresponding sample. The fluorescence decay data were fitted with the TimeMaster Pro software package (provided with the

spectrometer).

#### 5.4.8. 2D Fluorescence Spectra.

40  $\mu$ M solution of **5-1b** in pH 6.50 buffer was prepared. A set of 101 emission spectra (350-700 nm) were collected with a PTI fluorimeter and FELIX software. The excitation wavelength was programmed by the macro of FELIX as 1 nm interval from 250-350 nm. The data were processed with proFit software to get a contour plot.

#### 5.5. References:

1. Birks, J. B. *Organic molecular photophysics* J. Wiley, New York, **1973**.
2. Nagaoka, S.; Kusunoki, J.; Fujibuchi, T.; Hatakenaka, S.; Mukai, K.; Nagashima, U. *J. Photochem. Photobio. A: Chem.* **1999**, *122*, 151.
3. Henary, M. M.; Wu, Y. G.; Fahrni, C. J. *Chem. Eur. J.* **2004**, *10*, 3015.
4. Taffarel, E.; Emmanuelle, C.; Chirayil, S.; Thummel, R. P. *J. Org. Chem.* **1994**, *59*, 823.
5. Mosquera, M.; Penedo, J. C.; Rios Rodriguez, M. C.; Rodriguez-Prieto, F. *J. Phys. Chem.* **1996**, *100*, 5398.
6. Henary, M. M.; Fahrni, C. J. *J. Phys. Chem. A* **2002**, *106*, 5210.
7. Cheng, Y. M.; Pu, S. C.; Hsu, C. J.; Lai, C. H.; Chou, P. T. *ChemPhysChem* **2006**, *7*, 1372.
8. Fahrni, C. J.; Henary, M. M.; VanDerveer, D. G. *J. Phys. Chem. A* **2002**, *106*, 7655.
9. Demas, J. N.; Crosby, G. A. *J. Phys. Chem.* **1971**, *75*, 991.

10. Grans, P.; O'Sullivan, B. *Talanta* **2000**, *51*, 33.
11. Binstead, R. A.; Zuberbühler, A. D. SPECFIT Global Analysis System; 3.0.27 ed.; SpectrumSoftware Associate, Marlborough MA 01752, **2001**
12. Gauglitz, G. J. *Photochem.* 1976, *5*, 41.
13. Gauglitz, G.; Hubig., S. J. *Photochem.* 1981, *15*, 255.
14. Mauser, H.; Gauglitz, G. "Photokinetics-Theoretical Fundamentals and Applications", 1998, 36, *Chemical Kinetics*, Edited by Compton, R. G.; Phil, D.; Hancock, G., Elsevier,.

APPENDIX A

SPECTROSCOPIC DATA

**Table A-1:** Selected solvent parameters utilized in the solvatochromic shift analyses in Chapter 4.

No.	Solvent	$\epsilon_r$	$n$	$E_T N$	$\pi^*$	$\alpha$	$\beta$
1	1,4-dioxane	2.27	1.422	0.164	0.490	0.000	0.370
2	di- <i>n</i> -butylether	3.18	1.398	0.071	0.180	0.000	0.460
3	diethylether	4.42	1.352	0.117	0.240	0.000	0.470
4	tetrahydrofuran	7.47	1.406	0.207	0.550	0.000	0.550
5	<i>n</i> -butylacetate	5.01	1.394	0.241	0.529343	0.000	0.450
6	ethylacetate	6.053	1.372	0.228	0.450	0.000	0.450
7	chloroform	4.89	1.446	0.259	0.690	0.200	0.100
8	1,2-dichloroethane	10.74	1.445	0.327	0.730	0.000	0.100
9	dichloromethane	24.56	1.424	0.309	0.730	0.130	0.100
10	<i>n</i> -butanenitrile	24.56	1.383	0.364	0.630	0.000	0.400
11	acetonitrile	35.94	1.344	0.460	0.660	0.190	0.400
12	<i>n</i> -butanol	17.51	1.3993	0.586	0.36173	0.840	0.840
13	ethanol	24.55	1.36143	0.654	0.340535	0.860	0.750
14	methanol	32.04	1.3284	0.762	0.345582	0.980	0.660
15	water	78	1.33	1.000	1.09	1.100	0.180

**Summary of Spectroscopic Data (Tables A-2-A-6)**

The reported absorption energies refer to the peak of the lowest energy band. Fluorescence peak emission energies are corrected as described in the experimental section of Chapter 4. All spectra were acquired at 298 K.

**Table A-2:** Peak absorption and emission energies of compound **4-1a**

No.	Solvent	$\nu_A$ [cm <sup>-1</sup> ]	$\nu_F$ [cm <sup>-1</sup> ]
1	1,4-dioxane	31443	20408
2	di- <i>n</i> -butylether	31443	20408
3	diethyl ether	31552	20534
4	Tetrahydrofuran	31443	20408
5	<i>n</i> -butylacetate	31443	20492
6	Ethylacetate	31552	20492
7	Chloroform	33327	20619
8	1,2-dichloroethane	33449	20450
9	Dichloromethane	33327	20408
10	<i>n</i> -butanenitrile	31552	20576
11	Acetonitrile	31739	20833
12	<i>n</i> -butanol	31645	21322
13	Ethanol	31739	21322
14	Methanol	31850	21322

**Table A-3:** Peak absorption and emission energies of compound **4-2a**

No.	Solvent	$\nu_A$ [cm <sup>-1</sup> ]	$\nu_F$ [cm <sup>-1</sup> ]
1	1,4-dioxane	33650	18490
2	di- <i>n</i> -butylether	33270	18580
3	diethyl ether	33400	18540
4	tetrahydrofuran	33120	18570
5	<i>n</i> -butylacetate	33340	18600
6	ethylacetate	33400	18650
7	chloroform	33610	18760
8	1,2-dichloroethane	33530	18570
9	dichloromethane	33380	18620
10	<i>n</i> -butanenitrile	33170	18890
11	acetonitrile	33350	19080
12	<i>n</i> -butanol	33630	19590
13	ethanol	33660	19550
14	methanol	33670	19540

**Table A-4:** Peak absorption and emission energies of compound **4-3a**

No.	Solvent	$\nu_A$ [cm <sup>-1</sup> ]	$\nu_F$ [cm <sup>-1</sup> ]
1	1,4-dioxane	31800	21430
2	di- <i>n</i> -butylether	31360	21540
3	diethyl ether	31530	21460
4	tetrahydrofuran	31630	21470
5	<i>n</i> -butylacetate	31480	21500
6	ethylacetate	31570	21530
7	chloroform	31890	21700
8	1,2-dichloroethane	31850	21520
9	dichloromethane	31310	21530
10	<i>n</i> -butanenitrile	31490	21680
11	acetonitrile	31670	21910
12	<i>n</i> -butanol	31840	22540
13	ethanol	31995	22460
14	methanol	32060	22460

**Table A-5:** Peak absorption and emission energies of compound **4-4a**

No.	Solvent	$\nu_A$ [cm <sup>-1</sup> ]	$\nu_F$ [cm <sup>-1</sup> ]
1	1,4-dioxane	19240	
2	di- <i>n</i> -butylether	33340	19270
3	diethyl ether	33450	19230
4	tetrahydrofuran	19260	
5	<i>n</i> -butylacetate	33410	19260
6	ethylacetate	33520	19330
7	chloroform	19490	
8	1,2-dichloroethane	19310	
9	dichloromethane	33340	19300
10	<i>n</i> -butanenitrile	33280	19440
11	acetonitrile	33400	19650
12	<i>n</i> -butanol	20140	
13	ethanol	20020	
14	methanol	20110	

**Table A-6:** Peak absorption and emission energies of compound **4-5a**

No.	Solvent	$\nu_A$ [cm <sup>-1</sup> ]	$\nu_F$ [cm <sup>-1</sup> ]
1	1,4-dioxane	30400	20940
2	di- <i>n</i> -butylether	30165	21040
3	diethyl ether	30310	20990
4	tetrahydrofuran	30580	20980
5	<i>n</i> -butylacetate	30260	20990
6	ethylacetate	30320	21060
7	chloroform	31270	21150
8	1,2-dichloroethane	30790	21070
9	dichloromethane	30490	21060
10	<i>n</i> -butanenitrile	30270	21220
11	acetonitrile	30500	21400
12	<i>n</i> -butanol	30670	21980
13	ethanol	30590	21930
14	methanol	30830	21910

## APPENDIX B

### PHOTOCHEMICAL DATA

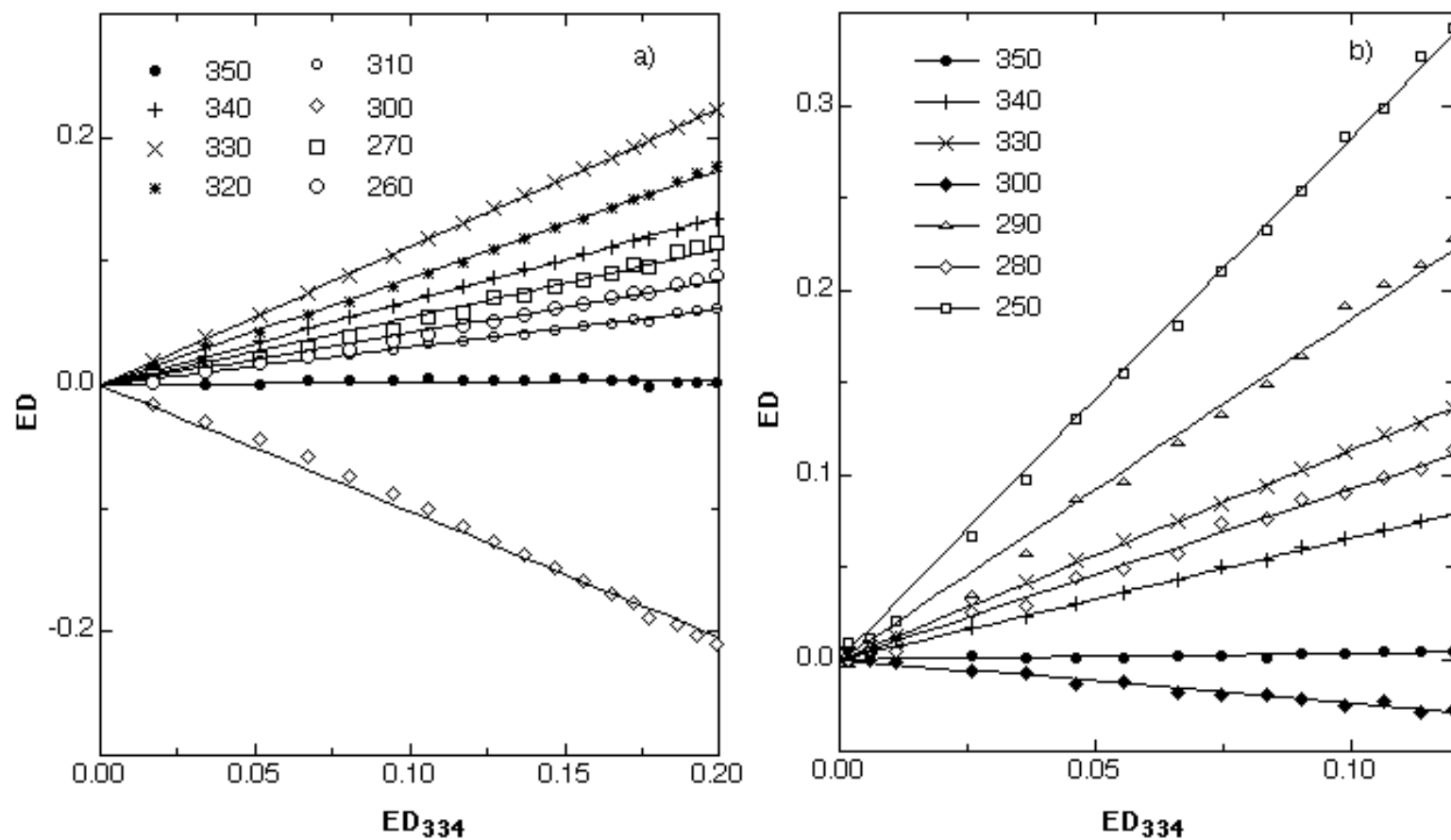


**Figure B-1.** Linear absorbance difference diagram for the photoreactions of **5-2a** a) in MeOH; and b) in 1mM KOH methanol solution.

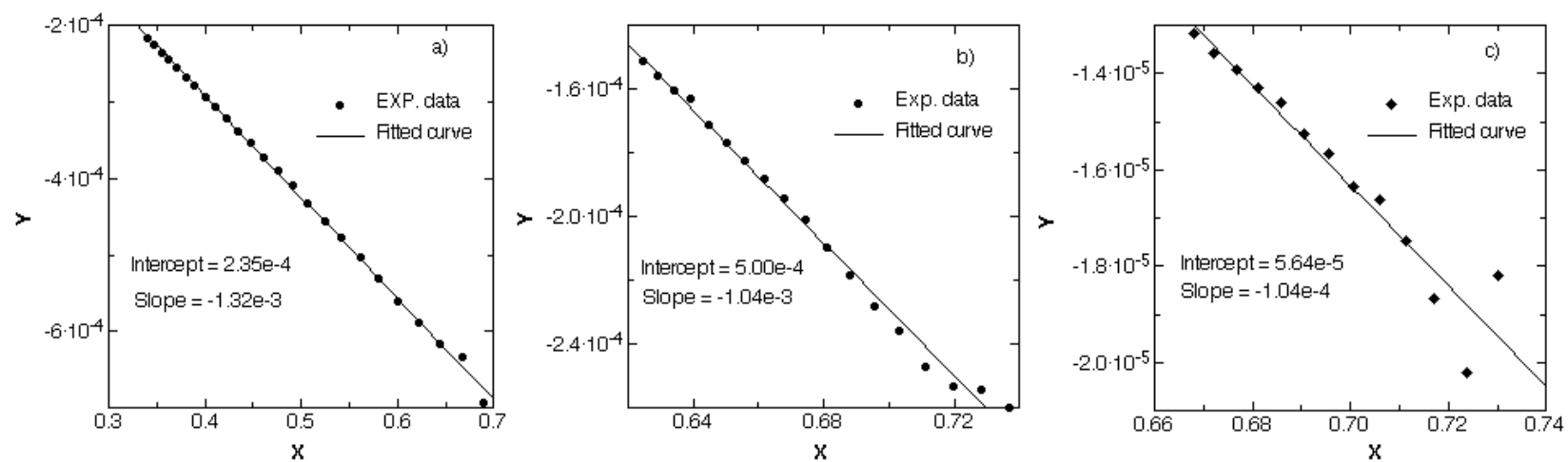


**Figure B-2.** Evaluations of the quantum yields ( $\phi^A$ ) of the photoreactions of **5-2a** b) in MeOH and c) in 1mM KOH methanol solution. a) is curve-fitting graph of azobenzene in methanol.